Using Sap Flow Sensors to Measure Water Uptake in Trees: Challenges and Opportunities

by

Morgane Merlin

A thesis submitted in partial fulfillment of the requirements for the degree of

Doctor of Philosophy

in

Forest Ecology and Management

Department of Renewable Resources

University of Alberta

Abstract

Water is a resource crucial for the survival and growth of trees. Understanding water relations and how changes in water availability may affect the growth and survival of trees across spatial and temporal scales is critical to gain insights in the future of forests. Sap flow sensors allow estimating tree water flow *in vivo* using heat as a tracer. The relative simplicity of the various sap flow methods and the affordability of the associate sensors and their easy deployment has made them the most widely used approach to estimate tree-level water fluxes. Together with other measurements of tree biomass, leaf area. and growth, sap flow sensors can provide data with a high spatial and temporal real time resolution, vital to assessing the impacts of edaphic and climatic conditions on the establishment, survival and productivity of trees and associated forest ecosystems. In a first study, I evaluated and quantified the impact of changes in soil water availability, modulated by rooting depth and topography on leaf area and sap flow of 15-year-old trembling aspen and white spruce trees planted on a reclaimed site. Results indicate that scaling water fluxes from an individual tree to the stand-level is complex and require a deeper understanding of trees' physiological responses to variation in edaphic conditions. Another variable often ignored is the role of ontogeny in tree sap flow and its extrapolation to larger scales. Obtaining an accurate quantification of water flow in large trees is critical, but we currently lack direct calibrations of sap flow methods for large trees. In a second study, I quantified the uncertainty associated with the use of sap flow sensors in a large tree by directly comparing sap flow rates to gravimetric measurements using the cut-tree method on a large mature trembling aspen tree. Also, estimating canopy transpiration using sap flow sensors inserted at the base of the stem is operationally efficient, but can fail to incorporate spatial variability of sap flow, especially for large and tall trees The oversight of within-tree variability

in wood hydraulic properties along with neglecting to incorporate the role of stem water storage and radial exchanges of water between tissues might produce biased estimates of short-term tree-level water fluxes. In a third study, I assessed the spatial partitioning of sap flux density and rate across azimuths and within the crown of a large tree and estimated the contribution of stem water storage to daily transpiration fluxes.

Overall, this PhD work highlights that sap flow sensors are a crucial tool that can help to improve our understanding of the spatial and temporal dynamics of trees' water relations in connection with edaphic and climatic conditions, however they should be used with caution particularly for large trees where significant circumferential and height-related spatial partitioning of sap flow might produce erroneous data that when extrapolated to larger scales could lead to is more likely than in young trees. Furthermore, sap flow sensors alone may not be sufficient to map and quantify the temporal and spatial relationships between sap flow, stem water storage and water exchanges with neighboring tissues in large trees, but best employed in combination with other methods.

Preface

This thesis is an original work from Morgane Merlin.

Chapter 2 of this thesis has been published as Merlin M., Landhäusser SM (2019) Rooting space characteristics influence seasonal pattern of water uptake in *Populus tremuloides* and *Picea glauca* on a reclaimed site in the boreal forest. Plant and Soil (439), 487-504. doi: 10.1007/s11104-019-04029-6. S.M. Landhäusser conceived the idea and developed the experiment, M. Merlin partially collected the field data and analyzed the data. M. Merlin and S.M. Landhäusser wrote the manuscript.

Chapter 3 of this thesis has been submitted for publication to Agricultural and Forest Meterology as Merlin M, Solarik K, Landhäusser SM: Quantification of the uncertainties introduced by data-processing procedures of the heat ratio method sap flow measurements using the cut-tree method on a large mature tree. M. Merlin, K. Solarik and S.M. Landhäusser designed and executed the study, M. Merlin analyzed the data, M. Merlin and S.M. Landhäusser wrote the manuscript, and K. Solarik contributed to revisions. The manuscript is currently under review.

Chapter 4 of this thesis is ready for submission for publication to Tree Physiology as Merlin M, Landhäusser SM: Insights into the spatial partitioning of sap fluxes and the importance of stem water storage in a large diffuse-porous tree. M. Merlin and S.M. Landhäusser designed and executed the study, M. Merlin analyzed the data, M. Merlin and S.M. Landhäusser wrote the manuscript.

Acknowledgments

I would like to start by thanking my supervisor, Dr. Simon Landhäusser. Thank you for taking me on first as a summer research intern in May 2015, and then as a PhD student in the following fall semester. Thank you for your support and guidance these past 4 ½ years, for your advice and constructive criticism. Working with you on all those diverse projects has allowed me to expand my horizons beyond the fundamental aspect of research and tackle challenging questions in the field of tree ecophysiology. You have always encouraged me to surpass myself and think outside the box, and it has made my PhD experience enriching and special.

I would also like to thank Drs. Sean Carey and Sylvie Quideau for being part of my supervisory committee and all their questions and comments during my PhD.

The research would not have been possible without the financial support from the Natural Science and Engineering Research Council (NSERC), the Canadian Oil Sands Innovation Alliance (COSIA, Syncrude Canada Ltd., Canadian Natural Resources Ltd., Suncor Energy, Imperial Oil Ltd.), the Faculty of Graduate Studies and Research and the Graduate Student Association at the University of Alberta.

Lastly, I would like to thank my labmates, friends and family for all their help and support in the past 4 ½ years.

Table of Contents

List of Tables

CHAPTER 2

CHAPTER 3

CHAPTER 4

List of Figures

CHAPTER 1

CHAPTER 2

CHAPTER 3

CHAPTER 4

CHAPTER 1: General introduction

Forested landscapes cover approximately 30 % of the total terrestrial landscapes on the globe (FAO, 2018) and exert a large influence on local and global water cycles (Ellison et al., 2017). Trees' survival and productivity require the uptake and transport of large amounts of water from the soil to the leaves (from less than 300 to more than 1000 mm per year; Calder 1998), where it is released to the atmosphere in the form of water vapor through transpiration. Hence, forests play an important and complex role in the belowground dynamics of water infiltration, streamflow, and groundwater recharge (Andréassian, 2004; Li et al., 2018; Liu, 2011; Prieto et al., 2012; Sun and Liu, 2013), as well as in climatic dynamics (rainfall and temperature forcing; (Bonan, 2008) Bonan 2008, Notaro and Liu 2008, Li et al. 2016, Prevedello et al. 2019). Both climatic and anthropogenic changes have contributed to changes in forest distribution, cover, and productivity. Forest cover has decreased due to anthropogenic land-use changes such as agricultural and urban conversions, logging and mining (FAO, 2018). Climatic changes (Hanes et al., 2019; IPCC, 2014) have contributed to decreasing productivity (Lee et al., 2013; Rita et al., 2019), triggering large-scale forest mortality events (Allen et al., 2015; Anderegg et al., 2013; Peng et al., 2011) and ecosystem shifts of varying magnitudes (Allen and Breshears, 1998; Beck et al., 2011; Martínez-Vilalta and Lloret, 2016). Conversely, increased forest productivity and cover has been observed in some ecosystems, favored by warmer, wetter climates and CO_2 fertilization (Buma and Barrett, 2015; Norby et al., 2005), along with increases in forest cover due to changes in land use, management and restoration efforts (Bolte et al., 2009; Gonçalves et al., 2017; Holmgren et al., 2015; Macdonald et al., 2015; Rosan et al., 2019; Stanturf et al., 2014). Overall, these changes in forested landscapes are tightly linked with changes in water flow and availability, with important consequences for several aspects of ecosystem functioning and hydroclimate dynamics (Liu et al.,

2008) from the local to the global scale. To be able to understand, prepare for and potentially mitigate the current changes in forested landscapes, it is imperative to have a detailed understanding of the water dynamics in trees.

Water transport in trees

Water is essential for survival and supports various physiological processes such as growth and transport of nutrients, hormones and sugars. The large volume of water taken up by trees to support leaf transpiration (more than 95 % of total water uptake, Lambers et al. 2008) is a necessity for photosynthesis, which converts the sun energy, CO_2 and water into sugars, essential for growth, survival and reproduction. The question of how water moves through trees from the roots to the canopy more than dozens of meters away has long fascinated scientists throughout history. Research has shown that most of the water transport is a passive mechanism, driven by differences in water potential along the soil - plant - atmosphere transport continuum (Dixon and Joly, 1895; Tyree and Zimmermann, 2002).

Water potential and cohesion-tension theory

Water can passively move along a gradient from higher to lower water potentials Ψ (Pa). The water potential represents the combined effects of pressure potential Ψ_p (based on mechanical pressure when membranes are present), the negative matrix potential Ψ_m (associated with the adhesion of water molecules to solid particles such as cell walls components), the negative osmotic potential Ψ_o (proportional to the solute concentration) and the positive gravitational potential Ψ_g:

$$\Psi = \Psi_p + \Psi_m + \Psi_o + \Psi_g$$

Within the soil - plant - atmosphere continuum, the water potential of the different components may vary, and the cohesion-tension theory (Dixon and Joly, 1895) describes how water can move following water potential gradients. The theory, developed in the late 19th century, is today the most widely accepted explanation of the mechanism of the ascent of sap. It states that the water present in the apoplast of the trees - *i.e.* the cell wall continuum of a plant - forms a continuous cohesive string of water molecules thanks to weak hydrogen bonds. At the leaf level where transpiration occurs, water adhesion to the cell walls and evaporation creates a negative water potential in the sap directly behind the cell wall surface. This applies tension, propagated throughout the water column. The tension and cohesion between water molecules drives water movement from the roots to the leaves. Other processes leading to changes in water potential (such osmotic adjustment) can contribute to multi-directional water movement within the tree. While this theory has been subject to criticism throughout the years (see Meinzer et al. 2001), it is widely supported by a large amount of data on water transport in plants.

Transport of water along the soil-plant-atmosphere continuum

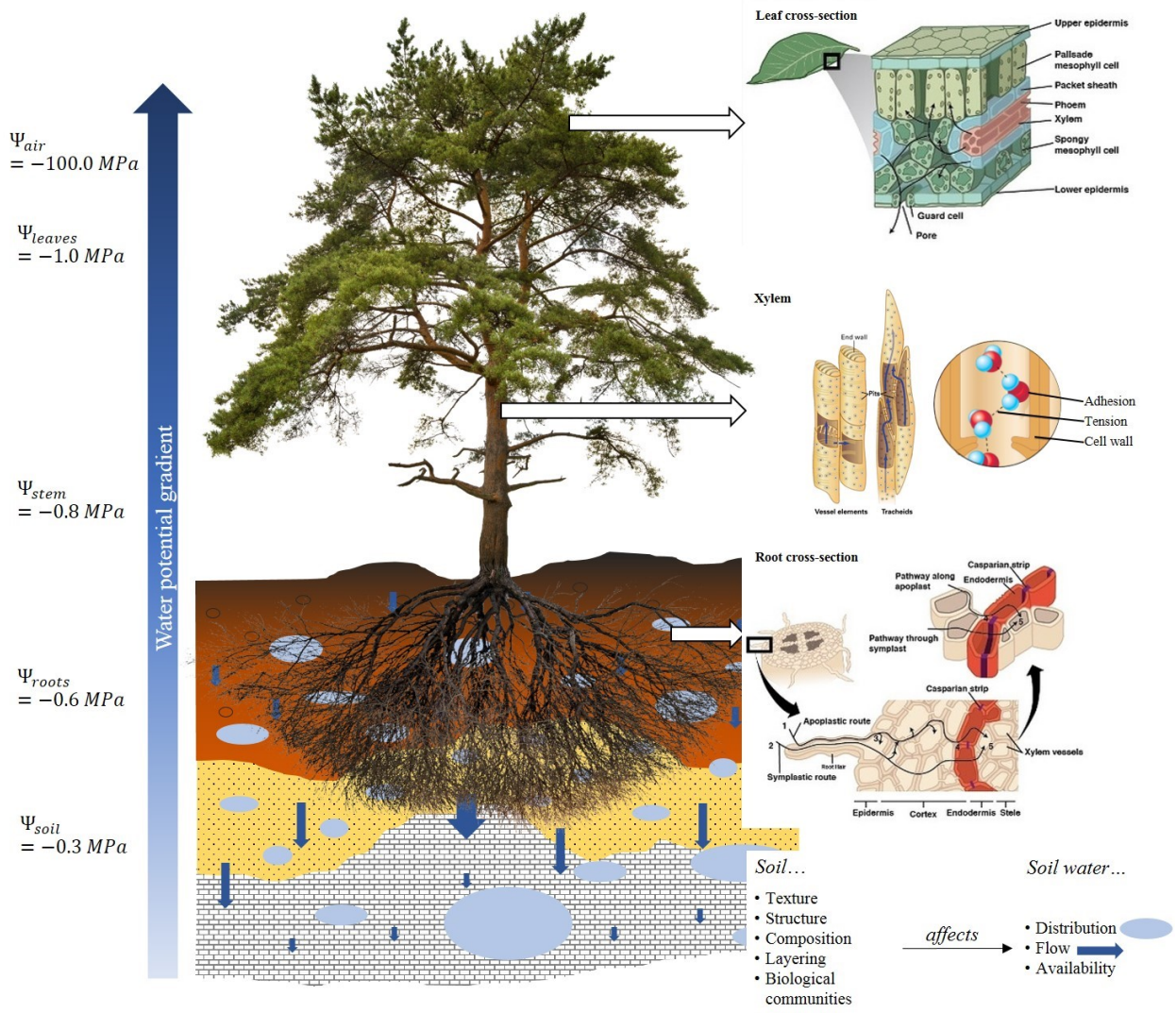

Figure 1. 1. Schematic representation of water movement along the soil-plant-atmosphere continuum following a gradient in water potential Ψ created according to the cohesion-tension theory. Transpiration from the leaves drives the upwards movement of water through the xylem elements from the roots, responsible for the water uptake from the soil, where water can be heterogeneously distributed (adapted from Campbell et al. 2004 and McElrone et al. 2013).

From the soil to the roots

The tension generated by leaf transpiration in the water column attracts water from the soil through the root system following the difference in water potential. Soil water potential describes the degree to which water is bound to the soil, and thus its availability to plants. It varies both temporally and spatially, depending on the soil hydraulic properties. Soil composition, texture and structure play an important role in determining the soil permeability, infiltration and drainage properties (Salas et al., 2014). The spatial organization of soil layers can lead to an uneven distribution of the water resource within a soil profile, due to changes in physical and chemical properties (Bakker et al., 2006; Doerr et al., 2000; Sakai et al., 2007) limiting water flow as well as root exploration (Bathke et al., 1992) and water uptake. Other factors such as topography, climate and disturbance regime further contribute to a spatially and temporally heterogeneous distribution of soil water (Figure 1. 1). These factors are decisive in determining root system architecture and the potential for tree establishment, survival and growth. Trees species have developed rooting strategies allowing for variations in root architecture and distribution (Jackson et al., 1996; Schenk and Jackson, 2002; Strong and LaRoi, 1983), temporal plasticity of root growth and water uptake with environmental conditions (Nepstad et al., 1994) and physiological adjustments (Prieto et al., 2012) to overcome limitations in soil water availability and competition (Casper and Jackson, 1997). As a result, the source of water utilized by trees can vary temporally and spatially with soil conditions, depth, climate and surrounding vegetation (Bertrand et al., 2014).

At the tissue level, the root hair on fine roots (fine extensions of the epidermal cells) increase the surface area for root-soil contact, increasing the potential for water uptake. Water uptake from the root surface follows two main pathways: the apoplastic and symplasmic pathways (Figure 1. 1). Water can move within the outer cell walls and water-filled intercellular spaces - apoplastic

pathway - or can enter the cell symplasm and moves between adjacent cells through plasmodesmata, narrow symplast connections - symplastic pathway. Once water reaches the endodermis, apoplastic water is forced to enter the cells' symplasm via water-channel proteins - aquaporins - as it encounters the Casparian strip, a single cell layer of which anticlinal walls are impregnated with hydrophobic compounds, such as lignin, suberin and wax. The presence of the Casparian strip and the aquaporins allow for active regulation of root water uptake and loss. The water then enters the water conducting elements in the root vascular bundle, the xylem.

From the root to the canopy: vascular transport system

The vascular system is composed of two main components: the xylem as the main water-conducting pathway, and the phloem, the main photosynthate-conducting tissue (Holbrook and Zwieniecki, 2005; Lambers et al., 2008). The xylem is mainly comprised of dead cells which can be broadly distinguished between vessel elements (found in angiosperms) and tracheids (found across the plant's kingdom), organized axially end-to-end (Figure 1. 1). The cell walls of the shorter and broader vessels are perforated at their end, forming perforation plates through which water movement is facilitated through reduced resistance. Tracheids are much longer and thinner and lack perforation plates, forcing the water to move through smaller connections between connected elements, increasing the axial resistance to water flow. Tension in the xylem water column generated from leaf transpiration drives the ascent of the sap from the roots to the canopy, representing a pathway of several dozen meters in tall trees. However, some downward and lateral movement of water in the xylem occurs. The presence of small pits between xylem elements allows for lateral movement of water within the xylem tissue, providing flexibility in the path taken by the water across the conducting sapwood area. Apart from the conducting vessel elements and tracheids, the xylem is also composed of fibers (providing structure) and living parenchyma cells,

which may also facilitate lateral movement of both water and solutes in and out of conducting elements. In climates with distinctly different seasons, the production of secondary xylem in trees generally follows a seasonal pattern, resulting from the influence of water availability and temperature on cell production and expansion (Holbrook and Zwieniecki, 2005). Xylem produced during the favorable or growing season tends to display less dense and wider vessels - early wood - while xylem produced later or outside of the growing season has typically denser and narrower vessels - latewood. These differences in xylem properties affect water transport in terms of flow rate and resistance to the rupture of the water column (cavitation). Depending on the species and environmental conditions, the structural and visual distinction between early- and latewood can be minimal (diffuse-porous species) or clear (ring-porous species). As the tree grows, the past year's xylem vessels may become non-conducting resulting in the formation of heartwood.

Along with the xylem, the phloem constitutes the other component of the vascular system and is comprised of two types of living cells: sieve elements and companion cells, in addition to parenchyma cells and fibers. While the transport of water in the xylem is tension-driven, photosynthate transport in the phloem is driven by an osmotically generated pressure gradient between source and sink compartments (Münch, 1930). Recent re-examination of the Münch hypothesis suggests that the phloem and xylem do not operate independently from each other. Water exchanges may occur along the entire length of the phloem pathway, as suggested by the presence of aquaporins (Almeida-Rodriguez and Hacke, 2012; Stanfield et al., 2017), modifying the pressure gradient from source to sink and maintaining phloem transport in tall trees (Stanfield et al., 2019). Phloem and xylem may thus be intimately connected in terms of water flows and exchanges, allowing for a dynamic control of water and sugar transport within trees.

Transpiration from the leaves

As water reaches the leaves it is drawn out by the highly negative water potential of the atmosphere. Water vapor fills the substomatal cavities and intercellular air spaces and evaporates from the mesophyll cells' surface following the water potential gradient between the leaves' air space and the atmosphere (Figure 1. 1). The water molecules exit the leaves through cuticular and stomatal transpiration. The stomatal aperture can vary in size following changes in the two guard cells framing it triggered by hormonal, electrical and hydraulic signals. This allows for relatively quick (in the order of minutes) changes in stomatal conductance. Stomatal conductance is a key element in the trade-off between maximizing photosynthesis and carbon allocation and minimizing water loss through transpiration (Holbrook and Zwieniecki, 2005). Stomatal transpiration is controlled in response to an ensemble of environmental factors, defining the iso-anisohydric spectrum of species-specific stomatal strategies. Soil water potential, nutrient availability, atmospheric irradiance, temperature and vapor pressure deficit (*i.e.* air "dryness") all participate in controlling the stomatal closure to limit transpiration, at the expense of decreased photosynthetic activity. The distribution of stomates on the leaf surface, along with leaf shape and orientation in the canopy can contribute to avoiding excessive transpiration losses and increasing water-use efficiency (carbon gain per water lost). Altogether, changes in stomatal conductance and thus transpiration rate due to environmental and internal factors will translate to changes in the leaf water potential and have direct impacts on sap flow rate measured along the water pathway in trees.

Measuring tree water uptake using sap flow sensors

So how can we monitor and quantify the water flow within trees? The advent of gas exchange systems allowed for the measurement of transpiration rates directly from individual leaves; however it rapidly becomes highly labor-intensive and operationally complex when moving

beyond small plants to larger and taller trees while accounting for complexity in leaf physiology resulting from variations in leaf age, illumination and boundary layer conditions (Niinemets, 2007; Shirke, 2001). Similarly, weighing lysimeters and chamber-based measurements of whole-plant transpiration are inadequate for large trees and the latter may directly alter the microclimate experienced by the tree (Goulden and Field, 1994). The idea to use tracers to monitor water flow directly within the conducting portion of a trees' stem has been developed over a century ago using dyes (Arndt, 1929; Dixon, 1914; James and Baker, 1933; Kramer, 1940), as well as radio- and stable isotopes (Calder et al., 1986; Waring and Roberts, 1979). In order to assess water flow *in vivo*, the use of heat as a tracer has first been proposed to determine sap flow in the 1930's (Dixon, 1936; Huber and Schmidt, 1937): by measuring the time it took for heat to travel a known distance within the stem with the sap, sap flow rate can be calculated. Marshall (1958) provided the theoretical basis for the development of heat-pulse based sap flow sensors.

Diversity of sap flow methods

From then on, several heat-based sap flow sensors were developed (Fernández et al., 2017). The stem, branch or root is heated electrically, and the heat balance is solved for heat travelling with the moving sap stream to calculate the mass flow of sap. Two main distinctions can be made in the diverse array of sap flow sensors in the application of heat: continuous and heat-pulse methods. Continuous application of heat to the stem allows for the determination of sap flow rate (g hr^{-1}) - stem heat balance (Sakuratani, 1981; Vieweg and Ziegler, 1960) and trunk heat balance (Čermák et al., 2004, 1973) methods - or sap flux density (cm^3 cm^{-2} hr^{-1}) - thermal dissipation (Granier, 1985) and heat field deformation methods (Nadezhdina et al., 1998). Detailed description of the methods and operating principles are available in Smith and Allen (1996) as well as the previously cited references. Heat-pulse methods rely on the intermittent application of a heat pulse and

measured temperature differences at specific locations to determine heat pulse velocity (Marshall, 1958) which is then converted to sap flux density. Currently, four main heat-pulse methods are available: the compensation heat-pulse CHP and associated methods (Green, 1998; Swanson and Whitfield, 1981; Testi and Villalobos, 2009), the Tmax method (Cohen et al., 1981), the Sapflow+ method (Vandegehuchte and Steppe, 2012a) and the heat ratio method HRM (Burgess et al., 2001). Briefly, one (Tmax), two (CHPM, HRM) or three (Sapflow+) temperature probes are inserted to equal depth in the conductive sapwood at specific locations around a heater probe.

The heat ratio method HRM

Compared to the CHPM which calculates the heat pulse velocity using the time to thermal equilibration of the temperature probes after release of the heat pulse, the heat ratio method measures the ratio of the increase in temperature approximately 60 to 100 s after the release of a heat pulse of the two equidistant temperature probes to calculate the heat pulse velocity V_h (cm hr^{-1}):

$$V_h = \frac{k}{x} \times \ln({}^{v_d}/_{v_u}) \times 3600$$

Where k is the thermal diffusivity of fresh sapwood (assigned a value of 2.5 10^{-3} cm^2 s^{-1} (Marshall, 1958) before further resolution once sapwood properties have been measured), x is the distance between the heater and either temperature probes ($x = 0.6\ cm$), and v_d and v_u are the increases in temperatures of the downstream and upstream temperature probes respectively (Figure 1. 2). Heat pulse velocity is calculated for two thermistors; Outer and Inner; located 12.5 and 27.5 mm respectively from the base of the temperature probes, allowing for two discrete readings along sapwood depth or varying depths of bark and phloem (Figure 1. 2).

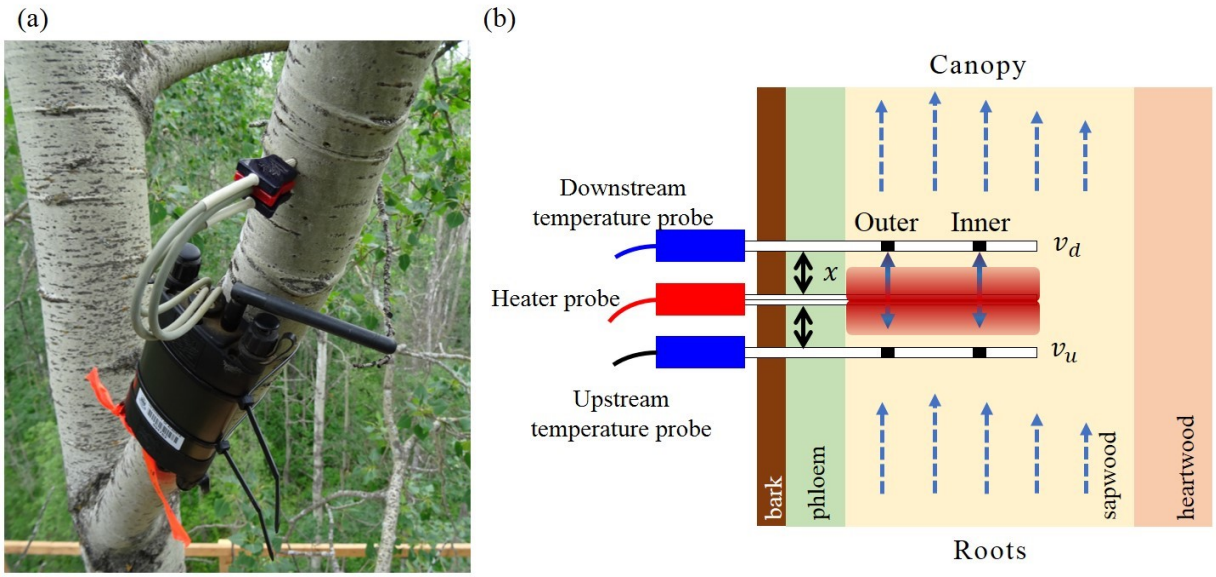

*Figure 1. 2. Heat ratio method principle and sensor (ICT International). Panel a shows an HRM sensor installed on a branch in the canopy of a large mature trembling aspen (*Populus tremuloides *Michx.) tree (see Chapter 4). Panel b shows the equidistant (distance* x*) insertion of the two temperature probes around the heater probe in the conductive sapwood. The increase in temperature following the release of a heat pulse (red shading) from the heater probe is measured at the Outer and Inner thermistor locations on the downstream (*v_d*) and upstream (*v_u*) temperature probes allowing for calculation of the heat pulse velocity indicative of the sap flux (dotted blue lines) density. For ease of reading, the cambium is not represented in panel b.*

The insertion of probes in the xylem tissue causes substantial mechanical damage, leading to a wounding response of the tree, forming tyloses (Barrett et al., 1995). This reaction affects the measurement of heat pulse velocity and can be linearly corrected for according to Burgess et al. (2001) for small wound sizes. Excessive wounding resulting from long-term installation of the sensors may require a reinstallation as to avoid underestimating sap flow. Additionally, correct spacing and parallel installation are crucial to proper and accurate calculation of sap flux density

for the heat ratio method. Incorrect spacing can be determined *posteriori* when sap flow is null to correct the measurements of heat pulse velocity.

After correction for wounding and potential probe misalignment, sap flux density J_s (cm^3 cm^2 hr^{-1}) can be determined from the heat pulse velocity V_h (Burgess et al., 2001):

$$J_s = \frac{V_h \times \rho_w \times (c_w + m_c \times c_s)}{\rho_{water} c_s}$$

Where ρ_w and ρ_{water} are the basic density of wood and water respectively, c_w and c_s are the specific heat capacity of the wood matrix (1200 J kg^{-1} $°C^{-1}$) and sap (equivalent to water 4182 J kg^{-1} $°C^{-1}$) at 20°C respectively and m_c is the water content of sapwood, all of which can be determined from processing sapwood samples.

Volumetric sap flow (Q, cm^3 hr^{-1}) can be derived as the product of sap flux density and the cross-sectional area of conducting sapwood (SA, cm^2):

$$Q = J_s \times SA$$

Conducting sapwood area can be determined by observing natural or artificial (staining) color changes marking the sapwood-heartwood boundary. Sap flux density can be hypothesized to remain constant across the sapwood depth, decrease linearly to reach zero at the heartwood boundary, or follow a distinct radial profile which can be determined when sap flux density is estimated along multiple sapwood depths. Further processing of the obtained data can be necessary, specifically the correct determination of baseline or zero flow, to ensure the accuracy of the sensor-derived measurements of sap flow.

Using sap flow sensors to inform tree water fluxes from the individual to the stand and landscape-level

Studies using sap flow sensors have recently started to steadily increase in number since 1985, nearing 1200 (searching for the terms "stem", "tree" and "sap flow" in Scopus (www.scopus.com) and Web of Science (apps.webofknowledge.com) in November 2019). The relative simplicity of the sensor design and methods, their affordability (Davis et al., 2012) and easy deployment in the field made sap flow sensors the most widely used approach to estimate tree-level water fluxes (Poyatos et al., 2016).

Using sap flow sensors to investigate the environmental drivers on tree water uptake at the stand scale

Studies focused on elucidating the environmental drivers of forest transpiration have become critical for understanding the complex network of interactions between forest ecosystem dynamics, forest management and the hydrological cycle as ongoing climate and global changes alter the distribution of global water resources (Bernacchi and VanLoocke, 2015; Bonan, 2008; Ellison et al., 2017; Sperry and Love, 2015; Zhang et al., 2016). Sap flow sensors are widely used tools as they provide direct and long-term estimates of tree-level water fluxes with little limitations to their deployment (Granier et al., 1996). Their use in ecophysiological studies have helped to shed light on the interactive role of climate and edaphic conditions on transpiration rate across ecosystems and tree species (Børja et al., 2016; Eller et al., 2015; Hassler et al., 2018; Link et al., 2014; Nadezhdina et al., 2015; Pappas et al., 2018; Tie et al., 2017; Zeppel et al., 2008). The ability of different tree species to maintain high transpiration rates through drought stress at the risk of hydraulic failure, or conversely risk carbon starvation but maintain hydraulic integrity (gradient

from iso- to anisohydric stomatal behavior) contributes to determining different tree species' distribution and productivity along hydrological gradients (McDowell et al., 2008). In heavily managed forest ecosystems (plantations, reclaimed landscapes), management decisions can alleviate drought stress through density management (Bottero et al., 2017; D'Amato et al., 2013), adaptive planting (Axelsson et al., 2019; Park et al., 2018) and modifications of soil properties (Barbour et al., 2007; Jung et al., 2014) for example. The combination of growth, survival and water uptake measurements using sap flow sensors in the short and long-term can help assessing the impacts of water-related management decisions in ensuring the establishment, survival and productivity of forest ecosystems under current and future climate (Chmura et al., 2011; Keenan, 2015).

Measuring sap flow in large versus *small young trees*

Surprisingly, the effect of tree size on the measurement of sap flux using the current design of sap flow sensors, especially those measuring sap flux density (including the HRM) has not been thoroughly investigated (but see Olbrich 1991, Vertessy et al. 1997, James et al. 2002), although it may have a large impact on the validity and accuracy of stand-level measurements of tree water uptake derived from individual tree measurements. At the stand level, the biomass, microenvironment, climate and structure of many forests is affected by the presence and abundance of large diameter trees (Lutz et al., 2018; Slik et al., 2013). Recent studies have highlighted a size and height-dependent mortality risk during drought (Bennett et al., 2015; Nepstad et al., 2007; Stovall et al., 2019), resulting from the interaction between high water demand, increased vulnerability to cavitation and carbon starvation during drought of large trees (Koch et al., 2004; McDowell, 2011; Zhang et al., 2009). Consequently, being able to accurately quantify and monitor water uptake in large trees is crucial to properly estimate the dynamics of

tree water uptake across tree sizes in a forested stand under varying water availability conditions. Per design, sap flow sensors measure the sap flux density over a relatively small region of conductive sapwood (except for the heat balance methods), which is then extrapolated to the entire sapwood cross-section. This extrapolation may not have a large impact on the sap flow estimates obtained on small and young trees due to the relative homogeneity of their sapwood, and the relatively small water volumes measured, as confirmed by the sap flow sensors validation studies performed on small trees. We currently lack data assessing whether it is appropriate and feasible to directly extrapolate sap flow measurements obtained on small young trees to large ones. The extrapolation may not hold as well for large trees, as spatial variability in the distribution of sap flow within the sapwood cross-section of large trees is likely. Differences in micro-climate (wind direction, radiation) and environment (soil water distribution, canopy and root sectorization) as well as past disturbances (fire scars, pests and mechanical damages) affect wood properties (Bär et al., 2019; Gartner, 1995) and thus the sap flow pathway within the stem. The design of commercially available sap flow sensors and the current deployment strategies adopted in the field (*i.e.* the common use of a single sensor per tree) do not allow to capture this variability. Hence, the estimates of whole-tree water uptake obtained with sap flow sensors may be severely biased for large trees, potentially contributing to propagating errors in stand-level estimates of tree transpiration. Properly mapping the spatial and temporal dynamics of sap flow along the SPAC in large and tall trees is however experimentally challenging and labor-intensive, and thus has remained relatively understudied.

Do sap flow sensors provide accurate estimates of large trees' water fluxes?

Several studies have already raised concerns regarding the validation and accuracy of the sap flow sensors (Fuchs et al., 2017; Lu et al., 2004; Vandegehuchte and Steppe, 2013). Considering the

challenges associated with accurately measuring water uptake in large trees and the importance of sap flow sensors in ecophysiology studies, directly assessing their accuracy is paramount for correctly interpreting the data they provide. Calibration studies rely on the direct comparison between sensor-derived and direct gravimetric or volumetric measurements of sap flow rates, using stem segments, the aboveground portion of the plant or whole potted plants. A recent synthesis on the accuracy of sap flow methods showed that across methods, sap flow measurements produced biased estimates of water flow rates even after proper application, but relatively good qualitative accuracy (Flo et al., 2019). As most calibration studies are done on relatively small plants (or stem segments) and under controlled and relatively stable conditions, the authors urged to expand validation studies to more field-realistic settings. Beyond the accuracy of the methods themselves, the data obtained from sap flow sensors requires several data-processing steps, at each of which errors and bias can be introduced from methodological decisions (see Fig.1 in Looker et al. (2016)): the estimation of wood thermal diffusivity and wounding corrections (Looker et al., 2016; Vandegehuchte and Steppe, 2012b; Wiedemann et al., 2016), the adequate determination of a baseline or zero flow (Lu et al., 2004; Rabbel et al., 2016) and the integration of sap flux density over the cross-sectional sapwood area (and its estimation) (Hatton et al., 1990; Looker et al., 2016), with no systematic handling currently available. This is especially important to achieve for large trees, for which calibration studies of the different sap flow methods are few despite their quantitative and qualitative importance in the water dynamics of forests across biomes. It is unknown whether the calibration studies done on small young trees are directly translatable to large trees or not. A proper assessment and incorporation of measurement errors and methodological choices for the different sap flow methods in large trees will greatly improve our

understanding of individual tree-level sap fluxes, help the inter-comparison of sap flow studies and extrapolating to regional and global forest-water dynamics.

Using sap flow sensors to map small-scale spatial and temporal variations in trees' sap flow in large trees?

Despite representing an obstacle when scaling up to whole-tree and larger spatial scales water use (Hernandez-Santana et al., 2015), the high-frequency measurements of sap flow over a relatively small sapwood volume using sap flux density sensors provides a unique opportunity to investigate the short and long-term spatial variability of sap flow within individual large trees. Species-specific and environmentally-driven differences in wood properties contribute in determining the pattern of spatial variability of sap flux density along the radial depth (Cohen et al., 2008; Ford et al., 2004; Gebauer et al., 2008). Circumferential variation in sap flow has also been frequently observed, however the drivers of this pattern remain elusive, due to the interactions among architectural, environmental and stochastic factors (Loustau et al., 1996; Sato et al., 2012; Tsuruta et al., 2010; Zhang et al., 2018). Whereas sapwood is more likely to be homogeneous in small young trees, the combination of radial and circumferential variability in sapwood and thus sap flow leads to the formation of potentially complex spatial and temporal patterns of water flow within large trees (Chiu et al., 2016b; Cohen et al., 2008; Dietrich et al., 2018; Shinohara et al., 2013; Van de Wal et al., 2015). As tree size increases, it is also important to consider that sap flow rates measured at the base of the tree may not be equal to the crown's transpiration rate in the short term, despite the assumption oftentimes made by studies examining the transpiration fluxes of forest stands using sap flow sensors. Temporal differences between the water supply and demand due to tree size and properties of xylem water transport may be relieved by the transient use of water stored in the cells of the surrounding stem tissues to support canopy transpiration (Čermák

et al., 2007; Goldstein et al., 1998; Meinzer et al., 2004). The strategic placement of sap flow sensors across a tree's canopy and along its stem has provided valuable information on the contribution of the stem water storage to transpiration (Betsch et al., 2011; Nadezhdina et al., 2015; Zweifel and Häsler, 2001). However, studies remain relatively few in large trees as access to the upper part of the tree's stem and canopy is challenging operationally, resulting in a poor spatial resolution of sap flow and unclear assumptions about sap flow transport along the stem.

Altogether, our growing understanding of tree physiology, sap flow sensors limitations and advantages offers the opportunity to map spatially and temporally the individual tree-level water fluxes across tree species, sizes and environmental conditions.

Thesis objective and outline

The objective of this thesis is to demonstrate the challenges and opportunities in using sap flow sensors, and more specifically the heat ratio method sap flow sensors, to monitor and quantify tree water uptake at the individual tree level in the mixedwood boreal forest of Alberta, Canada, across three individual research chapters.

In my first research chapter (**Chapter 2**), I focused on the opportunities offered by sap flow sensors to assess the effects of edaphic and climatic factors on sap fluxes in a young mixedwood stand to make inferences on the effect of forest cover on water availability in a forest reclamation landscape. I evaluated and quantified the impact of changes in soil water availability with soil depth and topography on two co-occurring tree species with distinct rooting and physiological characteristics, using trembling aspen (*Populus tremuloides* Michx.) and white spruce (*Picea*

glauca [Moench] Voss.) growing on a 15-year-old forest reclamation site. The objectives for this chapter were to address the following questions:

1. How do rooting space and soil moisture availability affect the rooting depth, leaf area and water uptake and use of aspen and spruce?
2. Does soil capping depth and topography alter water uptake response to seasonal variations in soil water availability and are there differences between the two species?

While this study was done on juvenile small diameter trees, the question was raised on whether sap flow measurements in large trees (aging forest) can be assessed similarly to measurements taken in juvenile trees. In the next two chapters, I assessed the challenges associated with using sap flow sensors in large trees, and the potential opportunities these sensors offer in improving our understanding of water fluxes within large trees.

In a second chapter (**Chapter 3**), I provided a direct comparison of measured sap flow rates between the heat ratio method sap flow sensors and a gravimetric measurement using the cut-tree method on a large trembling aspen tree, to be able to quantify the uncertainty associated with the use of sap flow sensors in large trees. The objectives of the study were to:

3. quantify the extent of the uncertainty in sap flow measurements related to circumferential variability, the application of different sapwood area estimation methods and zero-flow corrections
4. assess the impact of each and the combination of these factors on the relationship with atmospheric vapor pressure deficit and on the estimate of cumulative whole-tree water uptake

In the third chapter (**Chapter 4**), I assessed the spatial partitioning of sap flux density and rate across trunk azimuths and within the crown of a large tree, in addition to estimating the contribution of stem water storage to daily sap flow. To do so, sap flow measurements were taken on the same large trembling aspen tree (**Chapter 3)** before cutting the tree. The objectives of the study were to:

5. assess the spatial distribution of sap flow in the trunk and within the crown
6. evaluate the validity of a standardization factor when comparing sap flux rates between different heights within an individual tree
7. estimate the importance of stem water storage in daily flows, and its relationship with atmospheric vapor pressure deficit

CHAPTER 2: Seasonal patterns of water uptake in *Populus tremuloides* and *Picea glauca* on a boreal reclamation site is species specific and modulated by capping soil depth and slope position

Abstract

Soil water availability is important for tree growth and varies with topographic position and soil depth. We aim to understand how two co-occurring tree species with distinct rooting and physiological characteristics respond to those two variables during two climatically distinct growing seasons. Growing season (May to September) sap and transpiration fluxes were monitored using heat ratio method sap flow sensors on *Populus tremuloides* and *Picea glauca* in 2014 and 2015 growing along a hillslope with two different soil cover depths providing different rooting spaces. Across the two growing seasons, a shallow rooting space was the main factor limiting aspen's leaf area and cumulative sap flux, whereas responses of white spruce were more limited by topographical position. Generally, sap and transpiration fluxes decreased with the season; however, a large precipitation event during the 2015 summer triggered a significant recovery in sap and transpiration fluxes in white spruce, while in aspen this response was more muted. The two species distinct rooting and physiological characteristics produced contrasting water uptake and water use dynamics in response to rooting space, soil water availability and climate, inviting a more detailed exploration of sap flux and its interactions with climatic and edaphic variables.

Introduction

Rooting space characteristics are critical components influencing tree and forest establishment, survival and growth across biomes. Spatially, rooting space (defined as the soil volume accessible to roots) determines the extent and expandability of a root system and controls the pool of root-accessible resources. Tree species across biomes have developed different rooting strategies to cope with rooting space limitations including belowground competition with other individuals and/or species (Brédoire et al., 2016; Schenk and Jackson, 2002), potentially leading to segregation of rooting zones. While rooting space can be limited by inter and intraspecific competition for resources, it can also be spatially limited by physical and chemical barriers (Bakker et al., 2006; Sakai et al., 2007). These barriers can restrict growth (Matthes-Sears and Larson, 1999), reproduction potential (Boland et al., 2000; Schaffer et al., 1999), and modify growth allocation strategies among plant organs (*i.e.* leaves, shoots/trunks, and roots) (Bockstette et al., 2017; Jackson et al., 1996). However, rooting space is not only defined spatially, but also by the rooting substrate's quality, in terms of resource availability, aeration levels and soil biological communities. Quality of the rooting substrate is a decisive factor in determining what can be broadly defined as a site's carrying capacity, *i.e.* the plant community characteristics and success at which soil resource consumption is equal to resource supply for a given climatic condition, soil texture and management program (Xia and Shao, 2009), even when rooting space quantity is limited.

Soil resource availability is driven by several factors regionally and seasonally, including topography, climate, and disturbance regime. Variability of these factors may alleviate restrictive growth conditions imposed by physical limitations in rooting space. Among the soil resources critical for tree growth, water availability is fundamental, and highly dependent on rooting space

characteristics. Soil depth, composition and texture affect water retention and thus available water holding capacity (Huang et al., 2015, 2011). Topographic position is associated with both vertical and lateral water movement, with run-on and run-off processes, thereby altering available soil water content. These factors, together with the temporal and seasonal dynamics of soil water availability, are decisive in biomes such as the boreal forest where the growing season is climatically limited to a very short period (Devito et al., 2012) and growing space can be limited by shallow soils or conditions that limit deep rooting such as low soil temperature (Bonan, 1992; Van Cleve and Yarie, 1986).

Boreal tree species have adapted to these soil conditions by developing different rooting strategies. Trembling aspen (*Populus tremuloides* Michx.) and white spruce (*Picea glauca* (Moench) Voss) are two common boreal forest species in the western Canadian boreal region, which co-occur in the boreal mixedwood forest region on mesic upland sites (Alberta Parks, 2015; Cogbill, 1985; Nlungu-Kweta et al., 2014) and their relationship is often considered facilitative. Mixtures of both species have shown higher aboveground productivity than either pure stands (MacPherson et al., 2001), as well as a larger root system for spruce (Lawrence et al., 2012). The root systems of aspen and spruce have distinct characteristics suggesting potential adaptations to limitations in the quantity and quality of rooting space and could result in an avoidance of belowground competition (Novoplansky, 2009). Trembling aspen has an extensive lateral root system, spanning from several meters to tens of meters (Snedden, 2013) that is supported by deep sinker roots that can, depending on soil conditions, well exceed 200 cm in depth (Blake et al., 1996; Snedden, 2013; Strong and LaRoi, 1983). In contrast white spruce has a shallow root system, often limited to the first 40 cm of soil (Kalliokoski et al., 2008; Strong and LaRoi, 1983). These divergent root system

characteristics could contribute to species-specific responses to reduced soil moisture availability and drought tolerance (Bladon et al., 2006).

Addressing the effects of rooting space and water availability on tree success in natural stands is however challenging. Specifically, the complex suite of interactions and legacies related to soil development and stand history complicate the interpretation of responses. Restoration of the forested ecosystems after open pit (surface) mining offers a unique opportunity to investigate these processes without potentially confounding interactions and legacy effects. Restoration of mixedwood stands in the boreal forest region of Alberta after surface mining requires the reconstruction of an entire soil profile and revegetation (Government of Alberta, 2017). The reclamation sites are often located on landforms that are constructed with soil materials (overburden) deemed unsuitable for plant growth (Lilles et al., 2012), potentially limiting root development. Therefore, appropriate soil covers are constructed to protect the root zone from limiting conditions such as elevated salinity and sodicity from the underlying overburden material (Huang et al., 2015; Jung et al., 2014). The soil cover type and thickness provide the rooting space and resources necessary to sustain forests, especially considering the limitations of the overburden, the reconstructed soil covers, and the climatic conditions. However, since there are tradeoffs between ensuring appropriate rooting space for establishing and maintaining forest and the costs associated with the construction of the soil covers (also referred to hereafter as caps) on the landscape, there is an added incentive to optimize capping thickness for forest regrowth and sustainability.

This study aimed to gain insight in the effects of rooting space and moisture stress linked with a topographical gradient on the aboveground characteristics and water uptake of trembling aspen and white spruce trees on a 15-year-old reclamation site in northern Alberta, Canada. Specifically,

this study sought to answer the following questions: How do rooting space and soil moisture availability affect the rooting depth, leaf area and water uptake and use of aspen and spruce? Does soil capping depth and topography alter water uptake response to seasonal variations in soil water availability and are there differences between the two species? We hypothesized that trembling aspen will be most affected by soil capping depth due to its generally deeper-exploring root system than white spruce, restricting both aspen tree size and water uptake in shallow caps. Furthermore, we hypothesized that white spruce will be more physiologically sensitive to seasonally dry periods during the growing season and in the drier topographical positions due to its rather shallow root system.

Materials and Methods

Research area

The research area – South Bison Hills (SBH) study site – is located north of Fort McMurray, Alberta, within Syncrude Canada Ltd.'s Base Open Pit Mine lease. SBH is a landform that was constructed using saline-sodic clay shale overburden material, excavated during the mine establishment, contoured into a shallow sloped hill (15% slope, ~60 m elevation). The overburden material is highly saline, categorizing this substrate as non-suitable for plant growth (Barbour et al., 2007; Fung and Macyk, 2000; Kessler et al., 2010). In 1999, the overburden structure was capped with salvaged subsoil and topsoil materials which are considered suitable for plant growth; first, a layer of salvaged subsoil that consisted of glacial till material, capped with a layer of topsoil material that consisted of a mixture of salvaged peat and mineral soil. The wilting points for vegetation (-1.5 MPa) on the three materials used on site are: ~20 cm^3_{water} cm^{-3}_{soil} for the peat mineral mixture, ~18 cm^3 cm^{-3} for the glacial till subsoil, and ~20 cm^3 cm^{-3} for the shale

overburden (Huang et al., 2015). In the research area, soil caps were constructed with three different thicknesses: a shallow (35 cm cap composed of 20 cm subsoil and 15 cm topsoil), an intermediate (50 cm depth composed of 30 cm subsoil and 20 cm topsoil), and a thick cap (100 cm cap with 80 cm subsoil and 20 cm topsoil). In 2003, the research area was broadcast fertilized (10-30-15-4 N-P-K-S at a rate of 350 kg fertilizer ha^{-1} (Lanoue, 2003)) and seeded with barley (*Hordeum* spp.) at a density of 250 seeds m^{-2} for erosion control. In 2004 one-year-old trembling aspen (*Populus tremuloides* Michx.) and white spruce (*Picea glauca* (Moench) Voss) seedlings were planted on all capping treatments, each at a density of 800 stems ha^{-1}.

The climate of the north-eastern region of Alberta is categorized as sub-humid, cycling through wet and dry periods over both seasonal and longer term time periods (Devito et al., 2012). Temperature climate normals (1981-2010) range from – 17.4°C in January to +17.1°C in July (Environment Canada weather station – Fort McMurray airport, 56° 39’ N and 111° 13’ W, (Environment Canada, 2013)), reflecting the region’s cold winters and warm summers, with a short growing season (late May to early September). Total annual precipitation averages 418.6 mm, with 287.3 mm falling during the growing season, between May and September (Environment Canada, 2013). Despite having a mean annual precipitation similar to the grassland ecoregion further south, the timing of precipitation and the lower temperatures that reduce evaporation provide more available moisture during the growing season.

Study sites and measurements

We explored the effects of rooting space on water uptake and growth on trees growing in the two more extreme soil capping thicknesses – the shallow 35 cm and thick 100 cm caps. Since the reclamation area was located on a large north-facing hill slope and we expected to see higher soil

water availability in the lower topographic position, and *vice versa*, we selected trees in the upper and lower slope sections (Figure 2. 1). At each slope position, three plots were established, and within these, three trees of both species (trembling aspen and white spruce) were selected. Plots were located 10 to 15 m from each other in the slope direction to ensure independence of tree response but similar edaphic conditions. Tree selection in the plots was done following a biased tree selection process, selecting one dominant tree and two healthy neighboring trees (within a 5 m radius) for each species. In total, 18 aspen trees and 18 spruce trees (9 each for each topographical position) were selected for both the 2014 and 2015 measurement years on the 35 cm cap. On the 100 cm cap, nine trees of each species were selected only on the lower slope position in 2014, and only on the upper slope position in 2015. Comparing the tree selection with mensuration data collected along the whole hillslope revealed that the selection of trees for this study was representative of the average trees growing in the respective treatments and topographical positions (data not shown). Aboveground characteristics of the selected trees – diameter at breast height (DBH), height, and total leaf area (destructively sampled for a subset of the selected trees, see below) – were measured at the end of the growing season for both years. Yearly basal area increments (BAI) were calculated for each felled tree between 2011 and 2015. The selected trees (44 trees each year) were equipped with heat ratio method (HRM) sap flow sensors in both years between May and September recording at 10 minutes intervals. The HRM sap flow technique was chosen due to its ability to detect and quantify low flows more reliably than other techniques (Burgess et al., 2001). Description of the technique is available in Burgess et al. (2001). SFM1 sap flow meters (ICT International Pty Ltd.) were used in this study. Obvious deformities in the stem were avoided when installing the sensors. In 2014, the probes were installed at breast height (1.3 m) (representing approximately 38% of the spruce crown, and under the full

aspen crown) and in 2015 sensors were installed in all species below the crown (20 cm height for white spruce, 1.3 m for aspen). All sensors within each plot (six sensors – one per tree) were daisy chained to each other and connected to an external 12 V deep cycle marine battery with protective case, charged by a 22 W solar panel with BX metal sheathed wire. Since this is a very sensitive system, malfunctions of sensors, solar panels, or batteries did occur and led to some gaps in the continuous data (see sap flow data processing below). Application, set-up and limitations of the system have been described previously (Bleby et al., 2004; Burgess and Bleby, 2006; Dawson et al., 2007; Doronila and Forster, 2015; Forster, 2017; Looker et al., 2016; Pfautsch et al., 2011).

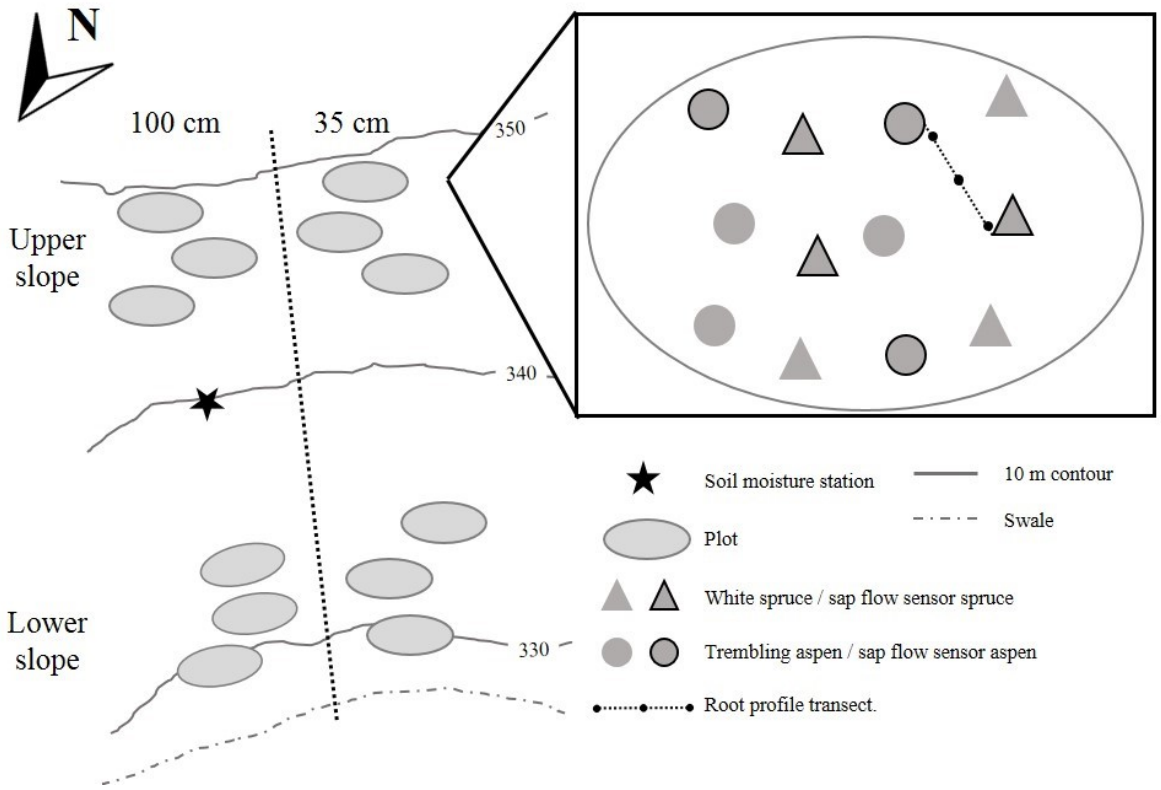

Figure 2. 1. Overview of the study site showing the two capping treatments (35 cm and 100 cm). The soil moisture station (black star) with the TDR (time domain reflectance) sensors measuring soil water content was located mid-slope. Each capping treatment was divided into a lower slope

and an upper slope section. In each section, three tree plots were established. The inset shows an example of the plot layout, with the white spruce and trembling aspen trees selected for the sap flow sensor installation, and the transect used for establishing the root profile.

To assess general vegetation rooting patterns (depths and quantity) as well as both species' maximum rooting depth, soil cores to a depth of 120 cm were collected in October 2015 for each capping thickness. The soil cores were taken along a 2 m long transect between an aspen and a white spruce tree in each plot (Figure 2. 1): one core was taken 15 cm from the base of both the aspen and spruce tree and a third core was taken half-way between the two trees, roughly 1 m equidistance. The 120 cm deep soil cores (diameter 5 cm) were then divided into 10 cm sections to build a detailed root mass profile. Live roots were picked from each 10 cm increment, with no distinction between tree and understory vegetation species. The root mass profile obtained from the soil cores thus included all roots, from all vegetation on site. To determine maximum rooting depth of trembling aspen and white spruce, total genomic DNA was extracted from dried ground root material in each 10 cm section using CTAB extraction protocol using species-specific primers for aspen and spruce previously developed (see Appendix 2.A: Methods). Further refinement on the resolution of fragment length for aspen using FLAP was employed to separate aspen from willow (*Salix* spp.) and balsam poplar (*Populus balsamifera*).

Soil moisture content was continuously monitored using Time-Domain Reflectance (TDR) sensors from O'Kane consultants Inc. for Syncrude Ltd. installed mid-slope on the 100 cm cap at 5 and 20 cm depths (Figure 2. 1). In addition, we monitored soil moisture content between June 9th and September 11th, 2015 in each of the three plots in the 35 cm and 100 cm caps and in the different slope positions at 20 cm depth. Daily precipitation data for 2014 and 2015 were obtained from a weather station installed by Syncrude Ltd. at the top of the slope on the 100 cm cap. Patterns of

precipitation and temperature fluctuations between 2014 and 2015 led to strikingly different seasonal dynamics of soil moisture content in the upper 20 cm of the soil profile (Figure 2. 2). Cumulative precipitation during the growing season amounted to 271.8 mm in 2014 and 238.5 mm in 2015, respectively approximately 15 and 50 mm lower than the 1981-2010 normal. To further explore precipitation as a driver of sap flux, both growing seasons were divided into an initial wet period during spring and early summer, followed by a dry-down period and finally a dry period using piecewise segmented regression to identify the change-points. Throughout both growing seasons, soil moisture content at 5 and 20 cm did not go below the vegetation wilting point of peat mineral mix of 22% (Ojekanmi and Chang, 2014, Figure 2. 2). In 2015, however, a prominent precipitation event (five days with a total of 57 mm of precipitation) during the otherwise dry period led to a significant recharge of the upper soil layers.

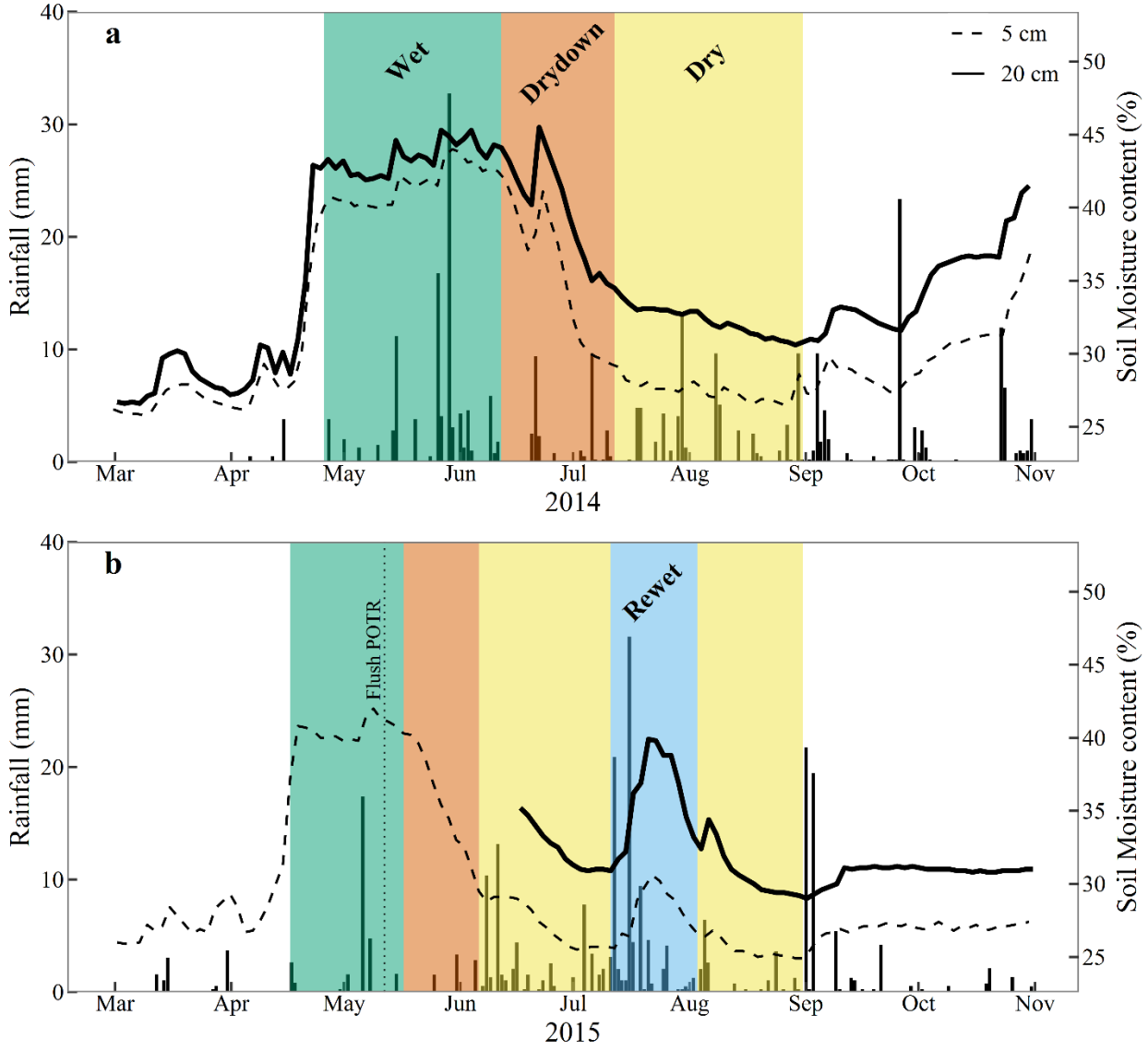

Figure 2. 2. Soil moisture content (%, black line) measured at 5 cm (dotted line) and 20 cm (solid line) in the soil profile in 2014 (panel a) and 2015 (panel b), combined with daily total precipitation (black bars). The different periods: wet, dry-down, dry and rewet are indicated by the green, orange, yellow and blue colors respectively. Data from the 20 cm depth prior to mid-June 2015 was unavailable. The date at which trembling aspen flushed in 2015 is indicated in a vertical dotted line with the label "Flush POTR".

Sap flux data processing

In September 2015, two monitored aspen and one spruce tree were selected in each plot (total of 18 aspen trees and 9 spruce trees). These trees were cut and detailed measurements of bark thickness, sapwood and heartwood thickness, estimates of sapwood dry weight, sapwood volume and wound diameter from the sensors were made according to Burgess et al. (2001) and ICT International guidelines (Burgess and Downey, 2018). Thermal diffusivity properties of the sapwood were calculated following Marshall (1958) and Burgess et al. (2001). Raw heat velocities were corrected for wood thermal diffusivity and wounding diameter using individual measurements for the felled trees and their average for the trees left standing. For the following analyses and for each sensor, the thermistor depth with the larger magnitude of velocity – i.e. the most "active" depth – was chosen to avoid redundancy (both thermistors depths were highly correlated, $R^2 > 0.9$) and less functioning sapwood depths (Link et al., 2014). Raw heat pulse velocity was converted to sap flux density for each 10 minutes interval (J_p, g m^{-2} $_{sapwood}$ h^{-1}) using the software Sap Flow Tool (v1.4.1. ICT International Pty Ltd., Armidale, NSW, Australia). Sapwood area for the un-cut trees was estimated using the existing linear correlation between measured sapwood area and DBH on the cut trees (for spruce: $sapwood\ area = 14.26 \times DBH - 68.66$; for aspen: $sapwood\ area = 11.93 \times DBH - 53.44$, with DBH in cm and $R^2 > 0.9$ for both species). To reduce variability, the sap flux density data was aggregated into hourly intervals. Inspection of the sap flux density data showed significant gaps of individual sensors in both 2014 and 2015. The following data-filling procedure was applied to the 2014 and 2015 datasets independently. A multivariate imputation via chained equation procedure, implemented in the *mice* package in R (van Buuren and Groothuis-Oudshoorn, 2011) was used, assuming the data were missing at random. The algorithm imputes an incomplete sap flux density data series within a tree plot by generating synthetic values following predictive mean matching given the sap flux density

data series of the other trees in the tree plot. An offset based on the average baseline sap flux density during periods when sap flow was likely zero was implemented. Zero sap flow was assumed after leaf fall for aspen in 2014 (29th September 2014 – 15th October 2014) and before leaf flush in 2015 (26th April 2015 – 1st May 2015). Zero sap flow for white spruce was assumed at night (22:00:00 to 04:00:00) during the fall (29th September 2014 – 15th October 2014, 1st September 2015 – 10th September 2015). Daily sap flux (Q, L d^{-1}) was then calculated, as well as cumulative sap flux (Q^c, L) between June 1st and August 31st of both years. Daily transpiration flux (T, L m^{-2} $_{\text{transpiring leaf area}}$ d^{-1}) and cumulative transpiration flux (T^c, L m^{-2} $_{\text{transpiring leaf area}}$) were calculated using the measurements of transpiring leaf area above the sap flow sensor from the cut trees and their estimates based on the DBH of the uncut trees. When taking into account needle shape and stomata distribution, transpiring leaf area of a white spruce is approximately 3.08 times the projected leaf area (Sellin, 2000).

To assess the differences in sap flow dynamics over time, we used normalized sap fluxes to compare temporal dynamics between sensors with different absolute magnitudes. We normalized the time series of daily sap (Q^n, d^{-1}) and transpiration (T^n, d^{-1}) fluxes by their respective maximum value (99.5th percentile daily integral to avoid normalizing by an outlier) (Link et al., 2014). All terms related to sap fluxes and transpiration fluxes are defined following nomenclature recommendations from Lemeur et al. (2008).

Statistical analyses

All data analyses were done using the R statistical software v3.5.1. (R Development Core Team, 2019). For all models, transformations were done to meet the normality assumptions and variance was allowed to change along a variable to meet the homogeneity of variance assumption when

necessary. Each model was re-evaluated after transformations. Initial models contained variables interactions when appropriate. Following a model selection procedure using AIC (Aikaike Information Criterion), the interactions were removed when not significant. Pairwise Tukey post-hoc tests were done to assess the differences between variables levels using the *emmeans* package (Lenth, 2018). When standard errors are presented, the abbreviation "se" is used. All linear mixed effects models were done using the *nlme* package (Pinheiro et al., 2018). The summary statistics of each model are presented in Appendix 2.B: Summary statistics.

Proportional root mass was calculated as the proportion represented by the root mass in one 10 cm increment of a soil core over the whole soil core. To decrease heteroscedasticity in the model, the proportional root mass data was split into two datasets: 0-50 cm and 60-120 cm, and analyzed for differences between depths, capping treatments and slope positions using beta-regression from the *betareg* package (Cribari-Neto and Zeileis, 2010). Tree characteristics were analyzed for each species separately using linear mixed effects model with the plot as a random effect. Slope position and year effects were analyzed only for the trees growing on the 35 cm cap. Capping treatment effects were analyzed separately only for trees on the lower slope in 2014 and only for trees on the upper slope in 2015. Diameter at breast height, transpiring leaf area, height and sapwood area were analyzed following this procedure. Kruskal-Wallis non-parametric tests were used on the study's TDR data to assess differences in seasonal average of soil moisture content between slope positions and capping treatments.

Cumulative sap and transpiration fluxes between June 1st and August 31st of each year were analyzed using mixed effects linear models following the same procedure as for the tree characteristics models. Additionally, species and year differences on the 35 cm cap on cumulative sap and transpiration fluxes were tested.

To evaluate the impact of the slope position and capping treatment on the daily sap flux dynamics during a growing season, the analysis was separated between the different moisture-defined periods. Average daily sap and transpiration fluxes were analyzed for each species separately using linear mixed effects model following the same procedure as for the tree characteristics models. The rate of daily sap flux decline during the growing season was analyzed using generalized additive models (gam) with the *mgcv* package (Wood, 2017) for each species and year separately to evaluate the impact of slope position and capping treatment. Normalized daily sap flux data was used for this analysis to eliminate the differences in absolute magnitudes between trees. The initial model was written as follows:

$$gam(Sap\ flow \sim Variable + s(Date, by = Variable, k = k) + s(Tree, bs = "re")$$
$$+ s(Date, Tree, bs = "re"), method = "REML")$$

With Variable = {Slope position; Capping treatment}, k = {6,10} to avoid over-fitting, Tree: the individual trees identification and "re" = random effect. The residual maximum likelihood method (REML) was used here instead of the generalized cross-validation (GCV) to avoid under-smoothing and penalize overfitting (Wood, 2011). Following a model selection procedure using the AIC and deviance criterion with a Chi-square test, the models were simplified and the linear effect of Variable or interaction with the Date smooth function was removed, as well as the individual smooth term for Tree when necessary. Final models are presented in Appendix Table 2.B. 5. Confidence intervals (95 %) were calculated and used to determine the dates during which the two Variable levels were significantly different. Finally, the impact of the late summer precipitation event on daily sap flux was assessed for the 2015 growing season using two methods. First, the ratio of average daily sap flux during the two days with peak soil moisture content at 5 and 20 cm depths to the average daily sap flux for the two days immediately before the

precipitation event was calculated for each tree. Linear mixed effects models assessing the impact of slope position, species and capping thickness were run following similar procedure as previous linear mixed effects models. Second, the collective contribution of this precipitation period (cumulative rewetting that happened between July 12th and August 3rd, 2015) to the cumulative sap and transpiration fluxes over the dry period of the growing season was explored further. To do so, a "fake" data set was constructed, which created sap and transpiration fluxes data that were representative of the same rewetting period, but with no precipitation event occurring. For that, daily sap and transpiration fluxes for each tree during that period were replaced with data for the same tree using the daily sap and transpiration fluxes 10 days before (July 1st– July 11th) and 11 days after (August 4th – August 15th) the precipitation event. Cumulative sap and transpiration fluxes were calculated for both the real 2015 dataset and the "fake" 2015 dataset between May 17th and August 31st, 2015. The difference ($D_{rewetting}$) and ratio ($R_{rewetting}$) between the two were calculated and analyzed the same way as for the first method for both Q^c and T^c (see Appendix Table 2.B. 6 for model details).

Results

Tree and rooting characteristics in response to capping thickness and slope position

The selected aspen and spruce trees responded differently in their aboveground characteristics to capping thickness and slope position (Table 2. 1). Trembling aspen trees were larger ($p = 0.015$) and had twice the leaf area ($p < 0.01$) when growing on the 100 cm cap than when growing on the 35 cm cap, but only at the lower slope position. Aspen did not show a response to slope position on the 35 cm cap in the measured aboveground variables. In contrast, white spruce trees had a smaller DBH on the 100 cm cap than on the 35 cm cap ($p = 0.016$) and 23% less leaf area ($p =$

0.016) at the lower slope position, however there were no differences between capping thicknesses in the upper slope position (Table 2. 1). Spruce responded to slope position on the 35 cm cap, where trees at the lower slope position had a higher DBH ($p = 0.019$) and a 37% greater leaf area ($p = 0.029$, Table 2. 1) than trees at the upper slope position.

Trembling aspen's sapwood area was positively correlated with leaf area (marginal $R^2 > 0.85$ for all models, slope = $3.4\ 10^{-4}$). Sapwood area was larger on the 100 cm cap than on the 35 cm cap at the upper slope only ($p = 0.041$, Table 2. 1). Aspen trees on the upper slope position on the 35 cm cap had a marginally larger sapwood area than trees growing at the lower slope position ($p = 0.094$, Table 2. 1). Contrastingly, sapwood area of white spruce was positively correlated with transpiring leaf area in 2015 only at the upper slope position across capping thicknesses (slope = $1.1\ 10^{-4}$) and marginally so across slope positions on the 35 cm cap (slope = $0.5\ 10^{-4}$). The absence of a relationship between sapwood area and transpiring leaf area in white spruce in 2014 may be due to installing the sensors at breast height thus only capturing a fraction of the crown (approximately 38% of the crown). Capping thickness and slope position did not affect sapwood area in spruce (Table 2. 1).

*Table 2. 1. Estimated marginal means (standard error) for trembling aspen (*P. tremuloides*) and white spruce (*P. glauca*) trees equipped with the sap flow sensors for the following characteristics: diameter at breast height (DBH, cm), transpiring leaf area (equivalent to projected leaf area for trembling aspen, 3.08×projected leaf area for white spruce, m^2), height (m), sapwood area (cm^2) and maximum rooting depth (cm). Results for sapwood area on the 35 cm cap for white spruce represent the 2015 data only, as sensors were located at breast height in 2014 (see methods). Statistical models were run separately on the 35 cm cap to evaluate the impact of slope position, and results are represented with the letters {a,b}, on the lower slope in 2014 and upper slope in 2015 to evaluate the impact of the capping thickness, using letters from the two sets {x,y} and {α, β}. Different letters represent a statistically significant difference ($p < 0.05$), and a + or - sign represents a marginally significant difference ($p < 0.1$). NA: not available.*

	35 cm cap		**Lower slope**		**Upper slope**	
	Lower slope	**Upper slope**	**35 cm cap**	**100 cm cap**	**35 cm cap**	**100 cm cap**
P. tremuloides						
DBH [cm]	7.64 (0.35) **a**	6.89 (0.32) **a**	7.16 (0.48) **y**	8.98 (0.43) **x**	7.28 (0.57) **α**	8.66 (0.57) **α^+**
Transpiring leaf area (m^2)	8.37 (1.23) **a**	7.22 (1.10) **a**	6.49 (1.56) **y**	13.92 (1.37) **x**	8.76 (1.63) **α**	11.62 (2.17) **α**
Height [m]	8.51 (0.28) **a**	8.01 (0.29) **a**	8.75 (0.35) **x**	9.28 (0.33) **x**	7.86 (0.40) **α**	8.97 (0.40) **α^+**
Sapwood area [cm^2]	42.85 (1.69) **a**	37.53 (1.75) **b**	47.68 (2.19) **x**	42.11 (2.04) **x**	48.19 (3.43) **β**	57.10 (3.43) **α**
Maximum rooting depth [cm]	93.3 (8.82)	103.3 (3.33)	NA	100.0 (10.0)	NA	105.0 (5.0)

P. glauca						
DBH [cm]	9.71 (0.34) **a**	7.76 (0.37) **b**	9.2 (0.31) **x**	8.01 (0.31) **y**	7.81 (0.60) **α**	8.44 (0.60) **α**
Transpiring leaf area (m^2)	83.94 (4.61) **a**	61.30 (4.99) **b**	78.94 (3.85) **x**	64.07 (3.85) **y**	61.91 (8.59) **α**	71.91 (8.59) **α**
Height [m]	6.58 (0.26) **a**	5.66 (0.28) **a**$^{-}$	6.58 (0.28) **x**	6.53 (0.28) **x**	5.47 (0.37) **α**	5.89 (0.37) **α**
Sapwood area [cm^2]	107.2 (7.0) **a**	84.6 (7.0) **a**	105.36 (10.58) **x**	115.14 (10.58) **x**	81.34 (3.31) **α**	82.94 (3.31) **α**
Maximum rooting depth [cm]	93.3 (3.3)	93.3 (3.3)	NA	93.3 (8.8)	NA	100.0 (5.8)

Yearly basal area increments declined from 2011 to 2015 across the site for both species. The decline was particularly pronounced in 2014 and 2015. Trembling aspen's BAI was marginally higher ($p < 0.1$) on the 100 cm cap than on the 35 cm cap on the upper slope, and similar across years between the upper and lower slope positions on the 35 cm cap. Similarly to aspen, BAI of white spruce was marginally higher throughout the years on the 100 cm cap compared to the 35 cm cap on the upper slope position (Appendix Figure 2.C. 1 and Figure 2.C. 2, Table 2.B. 7). White spruce in the upper slope position had consistently smaller BAI from 2013 to 2015 compared to the lower slope position ($p < 0.05$).

Both trembling aspen and white spruce roots were found at or below the 100 cm depth in both capping treatments and therefore penetrated well into the overburden layer, indicating no differences between the capping treatments or the species in occupying the rooting space (Table 2. 1). Total root mass (not separated by species) showed no differences between the capping treatments and slope positions (results not shown). However, differences in proportional root mass distribution between capping thicknesses were visible particularly at the upper slope position (Figure 2. 3). In the upper 20 cm soil layer, proportional root mass was significantly higher on the 35 cm cap compared to the 100 cm cap while in the 50-70 cm soil layers, the opposite was found ($p < 0.05$). While this response was evident in the upper slope position, the root mass distribution was much more uniform at the lower slope positions for both caps (Figure 2. 3).

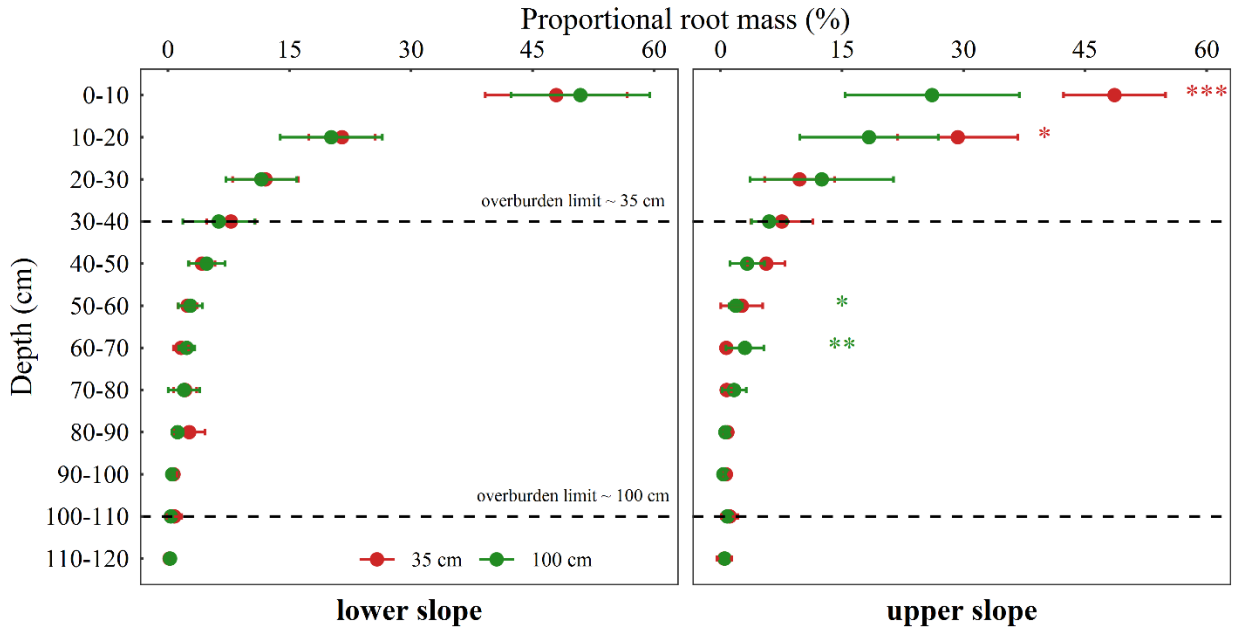

*Figure 2. 3. Proportional root mass distribution in 10 cm increment layers in the soil profile between 0 and 120 cm, expressed as a percentage of total root mass, for the lower slope (left panel) and upper slope (right panel), on both caps (red: 35 cm and green: 100 cm). Each point represents the proportional root mass averaged across plots and soil cores, with 95 % confidence intervals. Statistical differences from the beta-regression on the data split into two datasets (0-50 cm and 60-120 cm) are as follows: red labels represent post-hoc comparisons for which the 35 cm cap has a higher proportional root mass, green labels represent post-hoc comparisons for which the 100 cm cap has a higher proportional root mass. See Materials and Methods for more details about the models. Labels: "***": $p < 0.001$, "**": $p < 0.01$, "*": $p < 0.05$.*

Soil moisture and cumulative sap flux in response to capping thickness and slope position

Soil water content at 20 cm depth during the 2015 growing season differed between the two capping treatments and the associated slope positions. The 100 cm cap was marginally wetter than the 35 cm cap at the upper slope position (upper slope; 35cm = 14.5 %, 100cm = 15.3 %, (se = 0.6

%), Kruskal-Wallis non-parametric test $p < 0.06$). On the 35 cm cap, the lower slope position had a significantly higher soil moisture content than the upper slope position (35 cm cap; lower slope = 17.4 % (se = 0.9 %), upper slope = 14.5 % (se = 0.6 %), Kruskal-Wallis non-parametric test $p < 0.001$).

Cumulative sap flux (Q^c) in trembling aspen was on average 0.90 10^3 L (± 0.65 10^3 L) on the 35cm cap, and 1.59 10^3 L (± 0.91 10^3 L) on the 100 cm cap across both growing seasons. Q^c on the 100 cm cap compared to the 35 cm cap was twice as high ($p < 0.05$) on the lower slope position and only marginally higher in the upper slope position (Figure 2. 4, Appendix Table 2.C. 1). No differences between slope positions on the 35 cm cap were found for Q^c for trembling aspen (Figure 2. 4, Appendix Table 2.C. 2). Cumulative transpiration fluxes (T^c) in aspen were similar between capping thicknesses and slope positions in both 2014 and 2015; however T^c was higher in 2015 than in 2014 at the lower slope position but only on the 35 cm cap (Appendix Table 2.C. 1 and Table 2.C. 2).

On the 35 cm cap, cumulative sap flux (Q^c) of white spruce was 2.05 10^3 L (± 0.83 10^3 L) in 2014 and 0.91 10^3 L (± 0.67 10^3 L) in 2015, highlighting a significant drop in Q^c between years ($p < 0.001$). This is despite the 2014 data reflecting only the cumulative sap flux of a partial crown of spruce (measured at breast height and representing on average 38% of total crown area) compared to a full crown measurement (measured at basal height) in 2015. Cumulative sap flux of spruce on the 100 cm cap was on average 1.58 10^3 L (±1.19 10^3 L) across both years. Q^c was not affected by capping thickness at the lower slope; however, at the upper slope Q^c of spruce was marginally higher on the 100 cm cap compared to the 35 cm cap ($p < 0.07$, Figure 2. 4). On the 35 cm cap, Q^c in spruce was significantly lower on the upper slope than on the lower slope for both years ($p < 0.05$); on average 58% lower (Figure 2. 4, Appendix Table 2.C. 2). Cumulative transpiration flux

in spruce was not different between capping thicknesses or slope positions (Appendix Table 2.C. 1). Overall, Q^c of white spruce on the 35 cm cap in 2014 was approximately twice that of trembling aspen ($p < 0.001$), but both were similar in 2015 (Appendix Table 2.C. 2).

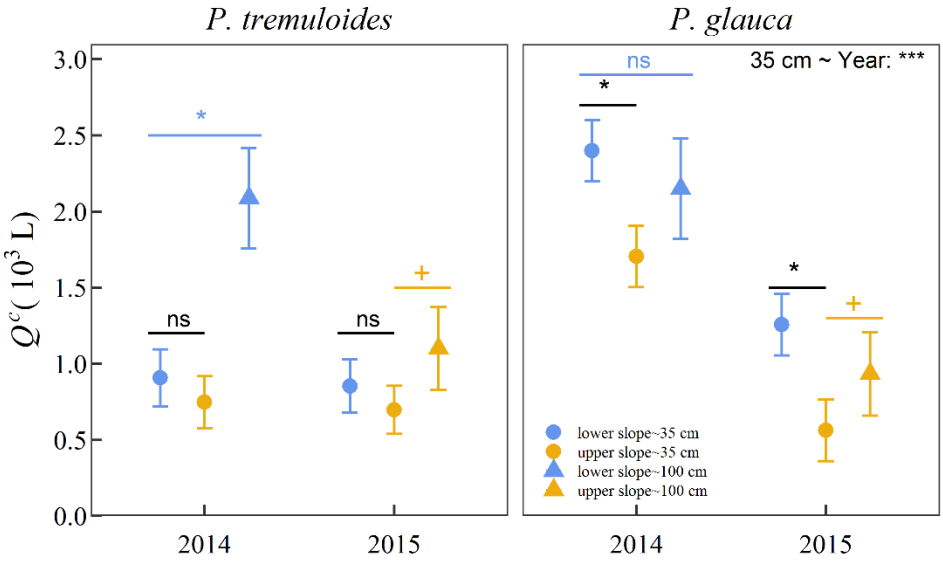

Figure 2. 4. Estimated marginal mean and standard error for individual tree cumulative sap flux (Q^c, 10^3 L) estimated between June 1st and August 31st of each year (2014 and 2015) for P. tremuloides *(left) and* P. glauca *(right) for the 35 cm (circle) and 100 cm (triangle) capping treatments at each slope position (lower slope: blue, upper slope: gold). Outliers were excluded from the statistical analysis. Following the analysis described in Materials and Methods, for each species, the results of three statistical models are presented: the effect of slope position within the 35 cm capping treatment (in black), the effect of capping treatment within the lower slope position in 2014 (in blue) and upper slope position in 2015 (in gold). Results from the statistical analysis are presented here with the following labels, ns: non-significant, "+": $p < 0.1$, "*": $p < 0.05$, "***": $p < 0.001$.*

Seasonal sap flux dynamics

Daily sap Q and transpiration T fluxes in trembling aspen were higher in trees growing on the 100 cm cap than in trees on the 35 cm cap, but this difference was only observed at the upper slope position. During the initial wet spring conditions, Q and T of both species were not different between slope positions on the 35 cm cap (Appendix Table 2.C. 3); however, Q was higher in 2014 compared to 2015 ($p < 0.07$ for white spruce, $p < 0.001$ for aspen).

While daily sap and transpiration fluxes were relatively constant during the wet spring, they continuously declined during the dry-down and dry soil moisture periods in both species. Normalization of the daily fluxes eliminated the time-invariant differences in absolute magnitudes in fluxes between trees. Daily normalized transpiration fluxes (T^n) declined at different rates between the two capping thicknesses, but these differences were not consistent between years and species. By the end of the dry season of each year, T^n of each species were similar between the two soil caps (Appendix Figure 2.C. 3). Daily normalized transpiration fluxes declined at different rates between the two slope positions, indicating a faster decline at the upper slope in both aspen and spruce compared to the lower slope position on the 35 cm cap in 2014 (Figure 2. 5). In 2015, there were small differences in the decline of T^n between slope positions for white spruce, however trembling aspen displayed a similar response to the one observed in 2014 (Figure 2. 5). For both years and species, T^n of trees in the lower slope position was lower than for trees on the upper slope position at the end of the dry season, albeit not significantly.

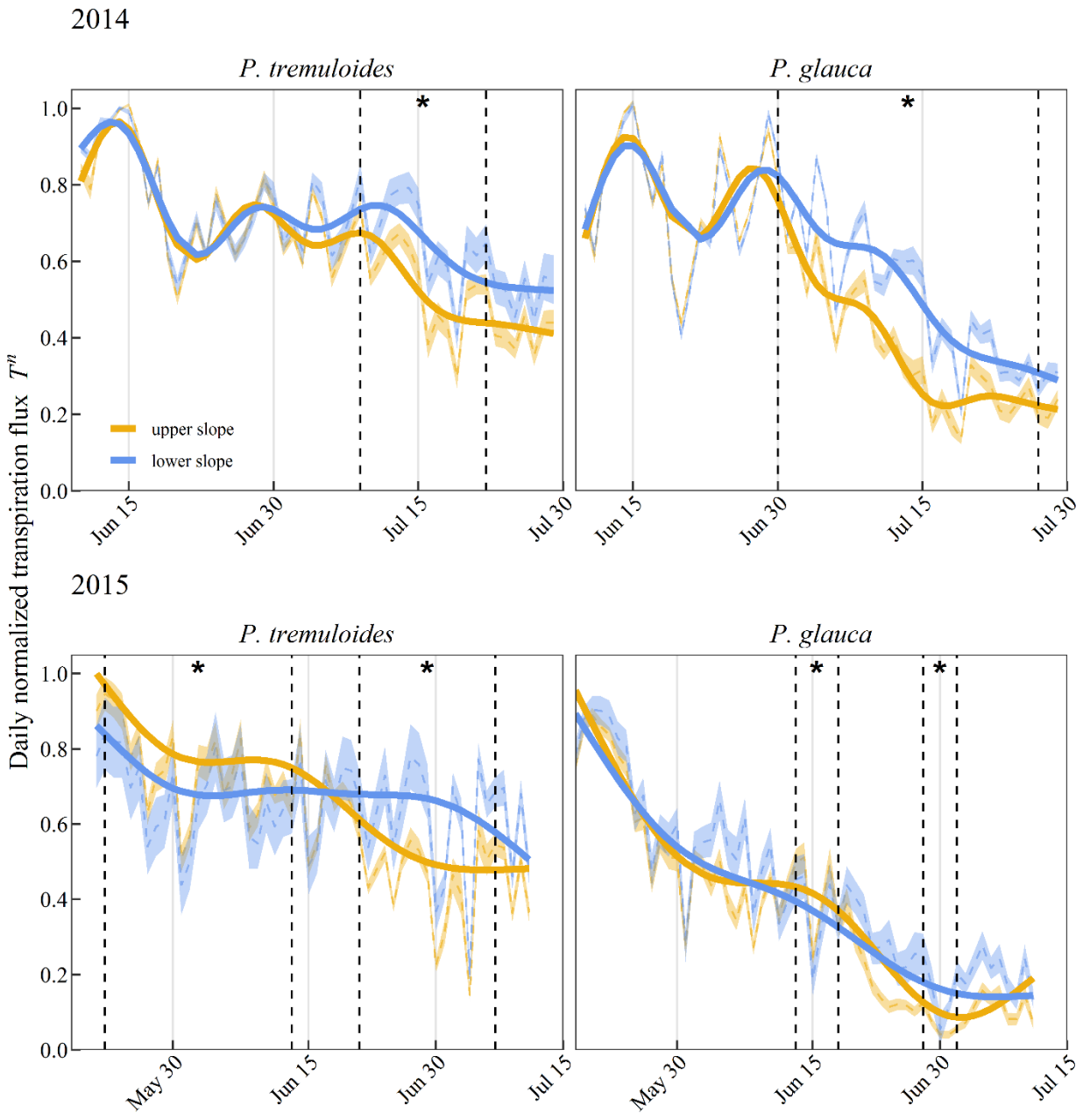

Figure 2. 5. Average normalized daily transpiration flux T^n (dotted line) during the dry-down and dry soil moisture periods and 95 % confidence intervals for each slope position (lower slope: blue, upper slope: gold) on the 35 cm cap for both species (left: P. tremuloides *and right:* P. glauca*) for 2014 (top panels) and 2015 (bottom panels). Results from the generalized additive models assessing the effect of slope for each species and year independently are presented in solid lines*

with the respective slope colors. Time periods with a significant difference between the models fit for each slope position are indicated with vertical dotted black lines and a "" label (p<0.05).*

The five-days precipitation event in 2015 (July 12th to July 16th) led to a significant increase in soil moisture content during the dry period (Figure 2. 2). During peak soil moisture content, daily sap flux (Q) of trembling aspen increased on average by 150 % compared to immediately before the precipitation period on both the 35 and 100 cm caps. On the 35 cm cap, aspen trees in the upper slope position had a larger absolute increase in daily sap flux than the trees growing in the lower slope position ($p < 0.01$, Appendix Figure 2.C. 4). This increase in Q translated into an increase of in Q^c of 50 L on average or 7% (Figure 2. 6) compared to a situation where the dry period had continued. Daily and cumulative transpiration fluxes showed a similar response, as cumulative transpiration increased by 4.5 L m^{-2} $_{\text{transpiring leaf area}}$ (results not shown). Aspen growing on the 100 cm cap marginally benefitted from this rewetting event ($p < 0.1$, upper slope position only). White spruce showed a much more pronounced response to this precipitation event on both caps, as Q increased on average by 350 % compared to the time immediately before the precipitation event. On the 35 cm cap, spruce trees growing in the upper slope position had a larger increase in Q than trees growing in a lower slope position ($p < 0.01$, Appendix Figure 2.C. 4). This rewetting event contributed to an increase in Q^c by on average 170 L compared to a situation where the dry period had continued. This increased uptake was significantly lower for the lower slope position, representing an increase in water uptake of 22% compared to 45% for the upper slope position (Figure 2. 6). Daily and cumulative transpiration fluxes showed a similar response, and cumulative transpiration increased by 1.7 (lower slope) to 2.4 (upper slope) L m^{-2} $_{\text{transpiring leaf area}}$ (results not shown). Spruce growing on the 100 cm cap showed a smaller response to this precipitation event than when growing on the 35 cm cap ($p < 0.05$, upper slope position only).

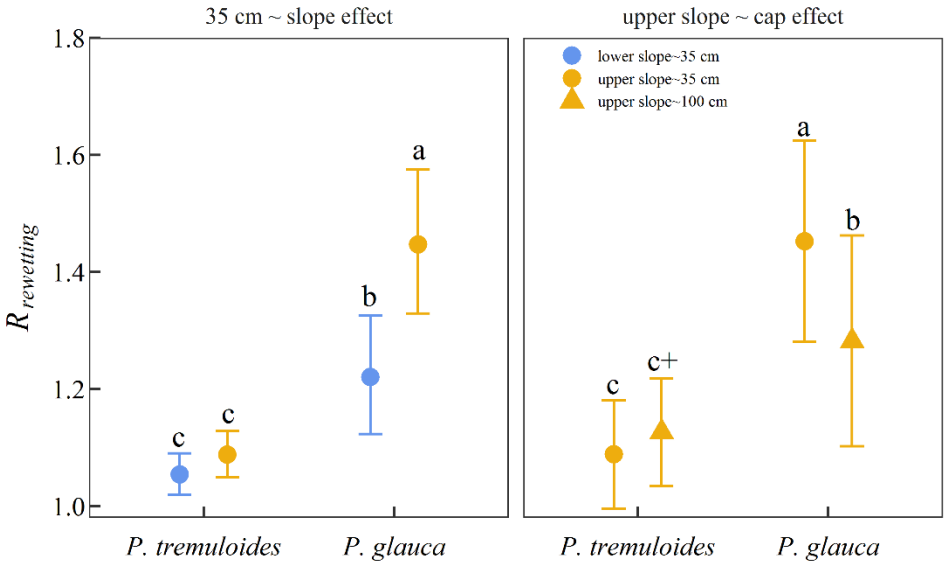

Figure 2. 6. Estimated marginal mean and 95 % confidence interval of the ratio of the rewetting event contribution to the whole tree Q^c during the dry-down and dry periods of the 2015 growing season (6^{th} of June 2015 to 31^{st} of August) to the hypothetical Q^c during the dry-down and dry periods of 2015 with no rewetting event ($R_{rewetting}$,see the methods section for description of the calculations). Results are presented for each species, slope position (lower slope: blue, upper slope: gold) and capping thickness (only for the upper slope, 35 cm cap: circles,100 cm cap: triangles) for both species P. tremuloides *and* P. glauca*. Significance ($p < 0.05$) is indicated by different letters for both models, marginal significance ($p < 0.1$) is indicated by a "+" sign.*

Discussion

Water use and growth of trembling aspen was limited by a reduction of rooting space (*i.e.* cover soil capping thickness) on this restoration site, while spruce was more sensitive to the topographical position along the hillslope. This confirms our hypothesis that based on the root system architecture, growth of trembling aspen would be most affected by soil capping depth,

while white spruce would be more sensitive to the topographical position. Aspen trees had as much as twice the leaf area and cumulative sap flux on the thicker cap (100 cm), attaining levels similar to natural sites values (Hogg et al., 2000), compared to trees growing on the thinner cap (35 cm); however, transpiration per unit leaf area was similar. This suggests that, beyond soil water availability, other factors such as nutrient supply may have limited aboveground growth and leaf area development in our study in aspen on the 35 cm capping treatment. A cover soil cap of 35 cm led to a greater proportion of roots found in the upper layers and limited the vertical extension of root systems into the overburden material. Commonly, aspen roots extend vertically well below 100 cm (Strong and LaRoi, 1983) and preferentially proliferate in resource-rich soil areas (Bauhus and Messier, 1999) while avoiding competitors roots (Messier et al., 2009; Mundell et al., 2007). Although aspen roots were found beyond the first 35 cm layer in the overburden layer, its high salinity and electrical conductivity is known to restrict root growth (Lazorko and Van Rees, 2012). Therefore, the resources available for trees at 100 cm depth in the overburden soil profile on the 35 cm cap could have been limited compared to the same depths on the 100 cm cap. This could have resulted in the reduced growth observed over the last four years (2011-2015) (see BAI results) on the thinner cap compared to the thicker cap.

Despite differences in Q^c between the two capping thicknesses for aspen, cumulative transpiration flux (*i.e.* Q^c per unit of leaf area; T^c) was similar, regardless of tree size. Thus, differences in water uptake in trembling aspen across the site appear to be regulated by leaf area rather than by differences in physiological responses to climatic drivers. Indeed, leaf transpiration in aspen (and by extension sap flux) have been shown to be closely coupled with climatic conditions (Bladon et al., 2006; Blanken, 1997; Hogg and Hurdle, 1997). When climatic conditions are relatively similar across sampled trees, such as in this study, the development and extent of leaf area thus becomes

crucial in determining the bulk of the growing season's water uptake capacity regardless of capping treatment (see also Tie et al., 2017 for leaf area control on water uptake). Spring conditions (*e.g.* water availability and air temperature) rather than internal root signaling have been shown to drive the early development of the bulk of leaf area in aspen (DeByle and Winokur, 1985; Delbart et al., 2008; Huang et al., 2010; Pollard, 1970). This has an impact on aspen's ability and potential to respond to climatic variability later in the growing season. The development of a large leaf area during a wet early growing season is beneficial in terms of increased photosynthetic yield and ultimately growth and reserve status; however, this holds true only if climatic conditions stay favorable. If water limiting conditions occur later in the season, an adjustment of the transpiration fluxes for this large leaf area may become necessary. Such an adjustment in aspen was notable when comparing trees between 2014 and 2015 located on the lower slope position on the 35 cm cap where, after leaf area differences were considered, T^c was lower in 2015 than in 2014. This potentially reflects a higher physiological sensitivity to drought of aspen trees growing in more favorable and wet conditions (*i.e.* lower slope position) compared to the more drought-prone trees at the upper slope position, which may have developed greater drought-resistance and avoidance strategies (see Kelln et al., 2008). This is further supported by the higher daily normalized transpiration fluxes early in the dry season of aspen trees growing on the upper slope position in the 35 cm cap compared to those growing in the lower slope position. Ultimately, when down regulation of the transpiration fluxes at the leaf level reaches the physiological limits of aspen, leaf area adjustment during the growing season (*i.e.* leaf abscission) may be required to prevent major drought damage or mortality. The environmental controls of leaf area expansion and coincidental xylem formation in aspen during spring conditions are therefore important periods in determining

(among other factors) the short term (within a growing season) and long-term resilience of aspen to climatic variability and ongoing climate change.

Beyond our initial hypotheses, we expected to find potentially some differences in aboveground growth and water uptake and use in aspen between slope positions particularly for the 35 cm cap. However, we detected no differences in aspen's growth, Q^c and T^c between the slope positions. Lateral root length was not measured in our study; however the ability of aspen to produce long lateral surface roots often spanning dozens of meters in length (DeByle and Winokur, 1985) likely resulted in the formation of asymmetrical root systems leading downslope (Snedden, 2013). These long feeder roots may have enabled aspen trees at upper slope positions to locate, access, and utilize moisture-rich areas further downslope.

The more shallow-rooted white spruce strongly responded to topographical position on the 35 cm cap. Spruce trees on the upper slope position were smaller in size and had less leaf area than trees growing on the lower slope position. This response might be driven by increased water stress, which may have been enough to generally reduce spruce growth over the years as reflected in the reduced BAI (also see Grossnickle, 2000; Wiley et al., 2018). The sap flux measurements partly corroborated the results of the aboveground characteristics of spruce. Drier soil moisture conditions on the upper slope on the shallow cap contributed to a reduction of cumulative sap flux by 30% and by close to 60% during the dry year of 2015 when compared to trees at a lower slope position. While tree size differences partially contributed to this difference, daily transpiration fluxes were also lower on the upper slope, most probably caused by lower water availability, which limited daily transpiration flux under high evaporative demand. Similar observations have been made in spruce and other conifers, showing a reduction in water uptake in periods of low soil water availability (Ježík et al., 2015; Nadezhdina et al., 2007; Schuster et al., 2016). Correspondingly,

the drier 2015 growing season had also a large impact on water use of white spruce at both slope positions on the shallow cap: Q^c dropped between 50% (lower slope) and 70% (upper slope) compared to the previous year. This drop is most likely an underestimation, as in 2014 the sap flow sensors were installed at breast height (*i.e.* missing about 62% of the total leaf area of the crown). This excluded the water demand of the portion of the crown that was below the sensor, which represents a significant fraction of the total tree water uptake (Herzog et al., 1998).

Early stomatal closure could have contributed to the observed accelerated decline of sap flux in spruce in response to slope positions and climate (2014 *versus* 2015) on the 35 cm cap, ultimately lowering Q^c and T^c. Soil water deficit and sustained high vapor pressure deficit conditions during the growing season have been shown to lead to early stomatal closure in spruce (Grossnickle, 2000; Leo et al., 2014; Zweifel et al., 2002). Furthermore, Střelcová et al., (2013) demonstrated that as soil moisture gradually decreases, the dependency of transpiration in spruce on evaporative demands of atmosphere decreased, leading to significant reduction of transpiration fluxes in spruce under soil drought. Further, it can be speculated that fine root mortality during the drier soil conditions of the surface layer might have played a role in the additional sap flux decline of spruce. It has been shown that soil moisture stress can lead to fine root mortality (Brunner et al., 2015; Gaul et al., 2008), which can result in a negative feedback loop of decreased in root hydraulic conductivity and associated tree hydraulic decline (Cuneo et al., 2016). All these factors could have translated into reduced carbon acquisition and radial growth for spruce trees supported by the decreased BAI under water-stressed conditions.

Seasonal sap flux dynamics and final cumulative water uptake of both species were affected by seasonal climatic variability, particularly during the dry period of the growing season. As climatic variability is thought to increase with climate change (IPCC, 2014), large but stochastic

precipitation events may become more vital for trees and their water needs. A species' adaptation to these changing conditions would be important, as these events would not only provide short-term relieve from drought stress but could also be important for longer-term soil moisture recharge. A large rewetting event in the late dry period of 2015 was a unique opportunity to investigate the trees responses and their ability to take advantage of the temporarily improved conditions. White spruce greatly benefitted from the rewetting period, as the large increase in its daily sap and transpiration fluxes in response to the precipitation event contributed to an increase of T^c and Q^c of 33 % compared to if it had continued to be dry. This increase was particularly pronounced on the upper slope position of the 35 cm cap, where this recovery represented an increase of approximately 45 % of the cumulative water uptake and use, compared to an increase of 7% for aspen. Most likely, the relatively shallow root system of white spruce contributed to the rapid uptake of rainwater from the shallow soil layers. Rapid increase of transpiration fluxes after re-watering during a drought has been reported previously for spruce species (Roberts and Dumbroff, 1986), and is consistent with the low drought-resistance of the spruce trees (Blake and Li, 2003). In a drier future with changed precipitation patterns, boreal forest trees might rely heavily on those large precipitation events for relieving drought stress (Børja et al., 2016). Interestingly, while aspen appears to be less adapted to these sporadic precipitation events, it might allow for greater soil moisture recharge at the stand level, due to reduced crown interception and limited water uptake response (*i.e.* less leaf area) compared to white spruce, which has more leaf area intercepting precipitation and uses more of the available soil water (Elliott et al., 1998; Herzog et al., 1998).

Trembling aspen and white spruce are two major components in the northern continental boreal forest region of Canada that showed specific responses to soil water availability driven by rooting space and topography. Their distinct rooting characteristics and physiological differences led to

contrasting behaviors in terms of aboveground growth, leaf area development and water uptake and use on the reclaimed site. In light of a drier, but more variable climate, the differing responses of aspen and spruce to seasonal variability and stochastic precipitation events will have profound effects on water cycling and how it associated with forest composition and cover at the stand and landscape level.

CHAPTER 3: Quantification of uncertainties introduced by data-processing procedures of sap flow measurements using the cut-tree method on a large mature tree

Abstract

Sap flow sensors are crucial instruments to understand whole-tree water use. The lack of direct calibration of the available methods on large trees and the application of several data-processing procedures may jeopardize our understanding of water uptake dynamics by increasing the uncertainties around sensor-based estimates. We directly compared the heat ratio method (HRM) sap flow measurements to water uptake measured gravimetrically using the cut-tree method on a large mature aspen tree to quantify those uncertainties for ten consecutive days. The influence of the azimuthal position of the sensors and the application of different data-processing procedures on the accuracy of the sap flow sensors' estimates was assessed using different metrics. Overall, the sap flow measurements showed high temporal precision with the gravimetric data. Azimuthal and radial variability of measured sap flux density showed the most substantial effect on the accuracy of the sensors' estimates of whole tree sap flow. The zero-flow corrections applied altered the accuracy and linearity of the sensors' measurements at the hourly scale, while the sapwood area method used had a lesser impact. Across the ensemble of available data-processing procedures, the cumulative whole-tree water uptake estimates for five consecutive days from the sensor diverged from the gravimetric measurements by less than 1 % to more than 50 % depending on the sensors azimuthal position and data corrections applied. This study illustrates some of the

uncertainties associated with the methodological approaches chosen when using sap flow sensors to estimate water uptake in tall and large diameter trees.

List of abbreviations

Abbreviation	Units	Description
AD	-	average of the two thermistor depths from the SFM1 HRM probes, the Outer and Inner thermistors
MD	-	thermistor depth with the maximum magnitude - *i.e.* largest range of sap flux density measurements from the SFM1 HRM probes, between the Outer and Inner thermistors
SS	-	study-specific zero-flow correction
PD	-	Pre-dawn zero-flow correction
PD_d	-	Daily pre-dawn zero-flow correction
LR	-	Linear regression zero-flow correction
DLR	-	Double linear regression zero-flow correction
SA_{true}	cm^2	true sapwood area measured on tree disks
SA_{tc}	cm^2	sapwood area derived from a unique sapwood length for each of the cardinal directions
$SA_{tc\text{-}avg}$	cm^2	sapwood area derived from the average of the sapwood lengths from the four cardinal directions
$SA_{tc\text{-}opp}$	cm^2	sapwood area derived from the average of the sapwood lengths from two opposite cardinal directions
$SA_{tc\text{-}per}$	cm^2	sapwood area derived from the average of the sapwood lengths from two perpendicular cardinal directions
R	-	radial profile of sap flux density
J_s	g cm^{-2} hr^{-1}	sap flux density at each cardinal orientation *i*
Q_i *or* Q	L hr^{-1}	whole-tree hourly sap flux rate calculated from the sensor placed at each cardinal orientation *i*
$Q_{quarter}$	L hr^{-1}	whole-tree hourly sap flux rate calculated as the sum of the four cardinal sap flux rates
Q_{scale}	L hr^{-1}	gravimetrically-measured whole-tree hourly sap flux rate
Q^d	L d^{-1}	whole-tree daily sap flux rate calculated from the sensor placed at each cardinal orientation
$Q^d{}_{scale}$	L d^{-1}	gravimetrically-measured whole-tree daily sap flux rate
Q^c	L	whole-tree cumulative water uptake calculated from the sensor placed at each cardinal orientation
$Q^c{}_{scale}$	L	gravimetrically-measured whole-tree cumulative water uptake
VPD	kPa	Atmospheric vapor pressure deficit

Introduction

Heat-based sap flow methods have become a principal means to non-destructively provide whole-tree water use estimates across spatiotemporal scales (Hassler et al., 2018), while also improving our understanding of the impact(s) of a changing climate (Berdanier and Clark, 2018; Zhang et al., 2016) and forest management practices (Doody et al., 2015) on forested landscapes. Several sap flow methods are available to measure tree-water use (Fernández et al., 2017) using heat as a tracer for sap flow. Calculating whole-tree sap flux rates from temperature measurements requires several steps of data-processing (Looker et al., 2016; Peters et al., 2018). Proper estimation of the sapwood thermal diffusivity as well as corrections for probe misalignment and wounding need to be considered (Burgess et al., 2001; Burgess and Downey, 2018; Marshall, 1958). Zero-flow determination is an additional crucial step, for which a range of empirical, systematic (Granier, 1987; Lu et al., 2004), and physically-based (Burgess and Downey, 2018; Oishi et al., 2008) methods are available. Additionally, strong radial and circumferential variations (Van de Wal et al., 2015) are often ignored, potentially leading to over- or under-estimating whole-tree water use when extrapolating a single sensor measurement across the entire stem. A global assessment of the impact of the combination of those data-processing steps on sap flow studies is currently lacking (but see Looker et al., 2016; Peters et al., 2018; Rabbel et al., 2016; Van de Wal et al., 2015 among others, addressing individual data-processing approaches), challenging the interpretation, comparison, and integration of individual tree-based studies when used in large-scale ecohydrology models.

A general quantification of the uncertainties generated by both the sap flow sensor method itself and the combination of methodological decisions and data-processing procedures on large mature trees is lacking, but crucial (Flo et al., 2019), particularly when attempting to derive landscape-

scale processes (*e.g.* ecosystem water and carbon fluxes, catchment hydrological and vegetation responses to climate and land-use changes; Bonan, 2008; Schlesinger and Jasechko, 2014). Calibration studies addressing the accuracy of the sap flow measurements in woody plants have been previously conducted (see the Supplementary Material in Flo et al., (2019) for a list of studies and calibration materials), however, many of them were mostly focused on smaller trees (less than 10 cm in diameter), shrubs, or branch segments, which are unlikely to provide reliable or appropriate estimates of water-use in larger diameter trees. To date, only a few studies have directly assessed the accuracy of sap flow sensors in estimating the water uptake of large mature trees (Olbrich, 1991; Roberts, 1977; Vertessy et al., 1997). However, the height (> 10 m), diameter (> 20 cm) and weight of mature forest trees presents experimental and logistical challenges for obtaining a direct measurement of water uptake to compare with the sap flow sensors' estimates, and thus, these studies are very limited in scope. The anatomical, morphological, and physiological variability in the stem of large mature trees can result in potentially strong diverging patterns between and within-trees in sap flux densities (Cohen et al., 2008; Shinohara et al., 2013; Van de Wal et al., 2015). The choice of the method in correcting for zero-flows and extrapolating to whole-tree sap flux rates may increase the error in sensor-based estimates of water use of an individual tree. Ultimately, this can jeopardize the interpretation of climate-response analyses and stand-level water uptake estimates for large and mature trees across temporal and spatial scales.

In this study, we aimed to: (1) quantify the extent of uncertainty in sap flow measurements related to circumferential variability, the application of different sapwood area estimation methods and zero-flow corrections; and (2) assess the impact of each and the combination of these factors on the relationship with climate variables and estimates of cumulative whole-tree water uptake. We used heat ratio method (HRM) sap flow heat-pulse sensors (Burgess et al., 2001) which have

shown relatively good performance in accuracy when compared to other sap flow methods (Flo et al., 2019). Furthermore, we used the cut-tree technique to directly measure trunk water uptake gravimetrically by immersing the stem of a large tree (20 m tall, 35 cm in diameter) in water (Roberts, 1977). Using this technique, we can directly compare the HRM sap flux estimates to the gravimetrically-measured water uptake, and then quantitatively assess the uncertainty and error associated with several data-processing methods applied to the sap flow data.

Materials and Methods

Study site and weather

The study was carried out in Thorhild County (54°17'11.6" N, 112°46'08.6" W), approximately 120 km northeast of Edmonton, Alberta, Canada. The site is located within the dry mixedwood natural sub-region of the boreal region, composed of a mixture of trembling aspen (*Populus tremuloides* Michx.) and white spruce (*Picea glauca* (Moench) Voss), surrounded by agricultural lands. The selected trees for the study were part of a 60 - 70-year-old trembling aspen dominated stand (~ 600 stems per hectare). The stand is located on a relatively flat site with a well-drained orthic gray luvisol that is easily accessible by machinery to access the trees' crown. This region has a mean temperature of -13.4˚C in January and +16.6 ˚C in July and annual precipitation of 478.7 mm (1981 – 2010 climate normal, Athabasca station, 54˚82'00" N, 113˚54'00" W)(Alberta Climate Information Service (ACIS), 2018). Hourly weather data (relative humidity (%), air temperature (°C)) was retrieved from the Alberta Climate Information Service (Alberta Climate Information Service (ACIS), 2018) for the Abee weather station (54°14'16"N 113°01'40"W), located 16.6 km from the research site. For all sources of weather data, vapor pressure deficit

(VPD, kPa) was calculated. The whole study was carried out between July 15th, 2017 and August 28th, 2017.

Sap flow measurements

A mature (60-year-old) healthy trembling aspen (deciduous broadleaved species with diffuse-porous wood) was selected as the focus tree for this study, on a slightly elevated area of the study site. The focus tree was a 20 m tall co-dominant tree in the stand, had a diameter of 28.8 cm at breast height (1.3 m) and a relatively symmetrical crown (~ 6-7 m in diameter, starting at 11 m above the ground). The focus tree had no apparent deformities in the stem or indications of fungal infection or decay (which was confirmed later after cutting). In addition to the focus tree, three co-dominant trembling aspen trees were also selected as controls for the entire period of the experiment. These trees were within the vicinity (10 - 15 m) of the focus tree and had similar tree and site characteristics. More information on the tree characteristics and sensor locations are provided in Appendix Table 3.A. 1.

The focus tree was equipped with four HRM sap flow sensors installed at the four cardinal directions (north, east, south, and west) at a trunk height of 2.5 m. The sensors were not installed at the commonly used 1.3 m trunk height as the cutting procedure removed the lowest 2 m of trunk of the focus tree (see Appendix Figure 3.A. 1). The three control trees were each equipped with one HRM sap flow sensor located at 1.3 m on the north-facing aspect. The difference in height between the sensors on the focus and control trees was assumed negligible for the purpose of the study. Sensors were installed on July 17th and 18th, 2017, and recorded sap flux density at 10 minutes intervals between July 18th and August 22nd, 2017.

The HRM sap flow technique was chosen due to its ability to detect and quantify low flows more reliably than other techniques (Burgess et al., 2001). We used commercially available HRM sap flow sensors (SFM1, ICT International Pty Ltd., Armidale, Australia). The sensors consist of a three individual needles (length: 35 mm; diameter: 1.3 mm): a heater needle delivering a 20 J heat pulse for 2.5 seconds every 10 minutes, a downstream and upstream needles with two thermocouples - thermistors - spaced 17.5 mm apart and positioned 12.5 (Outer thermistor) and 27.5 (Inner thermistor) mm from the needle base. The needles are each installed 0.5 cm apart. Power to all sap flow sensors was supplied by external 12 V deep cycle marine batteries, and their charge was maintained with solar panels. Application, set-up, and limitations of the SFM1 HRM sap flow sensors have been described previously (Bleby et al., 2004; Burgess and Downey, 2018; Forster, 2017).

Cut-tree procedure

The study set-up and cutting procedure are shown in Appendix Figure 3.A. 1 and Figure 3.A. 2, described hereafter. Prior to cutting the focus tree, a wooden structure was built to support the tree. The wooden structure had two platforms (4.5 m × 4.5 m) with enforced beams placed at 4.5 m and 9.0 m height above ground, and an additional enforced support beam at 2.0 m above ground. Additional support of the tower was provided by securing it to neighboring (non-study) trees and using soil anchors. To secure the suspended position of the cut tree and to allow it to rest on the enforced support beams, friction blocks were used. These friction blocks were made of 5 × 10 × 20 cm blocks of hardwood wood (oak), where each block contained 20-30 wood screws (7.6 cm long) inserted with their tips protruding 2-5 mm from the block. Several of these blocks were arranged around the circumference of the trunk, each resting on the three respective support beams once tightly strapped to the stem using ratchet straps. Once cut, the ring of friction blocks ensured

that the tree remained suspended and supported by the cross beams. The screw tips did not affect the xylem tissue and impacted only the bark and potentially some of the outer portions of the phloem.

Since the HRM sap flow sensors estimates of water uptake of the focus tree were to be compared directly with a the cut-tree method (Roberts, 1977), the focus tree needed to be cut at its base and inserted into a bucket of water. To avoid cavitation of the sapwood during cutting, the focus tree needed to be pre-cut underwater. A flexible temporary watertight container was used to allow for a pre-cut underwater. This temporary container was made from heavy-duty rubber material (pond liner) that was wrapped, secured, and sealed around the trunk (height of 1.0 m). The outer rim of the temporary container was then attached to the support structure. An initial girdling cut was made underwater and inside the water-filled temporary container using a chainsaw. This cut was around the circumference of the stem and about 15 cm deep to ensure all sapwood was included in this cut. The center part of the heartwood was left intact to support the tree initially. After the initial girdling cut, two additional cuts were performed cross-sectionally; one full cut directly below the temporary container and a second full cut at ground level; fully removing the portion of the trunk located underneath the temporary container. Now supported by the wooden structure, a large poly-ethylene bucket (600 L) sitting on a large commercial scale 1,000 kg capacity floor scale (FSP 3x3’ - Anyload, Fairfield, NJ, USA) was placed under the cut trunk. To monitor and record water uptake as a negative weight changes (200 g precision), a weight indicator connected to a storage unit (480Plus weight indicator and Go-Between Data Storage unit, Rice Lake Weighing Systems, Rice Lake, WI, USA) was used. Weights were recorded every sixty seconds. After the scale and bucket were placed under the tree, the bucket was filled with water. A final full cut of the trunk was made underwater, approximately 10 cm above where the initial girdling cut was made,

providing a clean-cut surface and the ability to remove the temporary container (*i.e.* pond liner). The newly exposed cut end of the tree was now submerged (~30 cm) under water in the large bucket. Throughout the entire study period, the cut end of the tree was continuously submerged to avoid cavitation. To reduce the blockage of xylem vessels (through wounding, accumulation of phloem exudates, or from impurities in the water), a sharp broad-bladed planer was used daily (at dawn) for the entirety of the study to shave the xylem on the cut end. Water levels within the bucket were checked daily and were topped up when needed. Additionally, a fresh chainsaw cut of the exposed end was made 5 and 10 days following the initial cut; to minimize surface blockage of xylem vessels in the sapwood. Evaporation from the container was prevented by covering the top of the bucket with a black plastic sheet sealing it around the trunk of the tree. Inputs from precipitation were excluded by covering the lowest platform and sides of the structure with tarps that shielded the bucket from all precipitation.

Transpiration rates were measured in the crowns using the LI-6400XT portable photosynthesis system (LiCor, Inc., Lincoln, NE, USA) on three shade leaves (lower branches in the canopy) and three sun leaves (top branches of the canopy) accessed using an articulated boom lift. Measurements were taken 4 and 8 days after the cut-tree was submerged in the bucket between 10:00 and 14:00 on the focus tree and a control tree during which the cuvette settings were 400 ppm CO_2; 60 % incoming relative humidity; and ambient leaf temperature and light levels. Leaf water potential was measured on three upper canopy leaves using a Scholander pressure bomb (Scholander et al., 1965) (model 600, PMS Instrument Company, Albany, OR, USA) to assess the water status of the crown. One measurement was made at noon eight days after the cut, and another measurement 14 days after the cut, before dawn (06:00 – 07:00).

Sap flow data baseline corrections

The raw heat velocities from the sap flow sensors were initially corrected for the wounding coefficient (Burgess et al., 2001; Marshall, 1958) using the software Sap Flow Tool (v1.4.1. ICT International Pty Ltd., Armidale, NSW, Australia). Wound diameter was visually quantified for all sensor locations from the sapwood cross-section (focus tree) or tree cores (control trees) and ranged between 0.25 and 0.30 cm. The estimation of the sapwood thermal diffusivity is required in the calculations of sap flux density. The thermal diffusivity of fresh sapwood was calculated for each sensor location on the focus tree. Fresh sapwood samples from each sensor location were taken directly after the removal of the sap flow sensors at the end of the experiment to determine fresh weight, volume (using Archimedes' principle) and oven-dried weight (72 h at 70°C). Specific heat of the dry wood matrix and sap were assumed constant, and equal to 1.2 10^3 J kg^{-1} $°C^{-1}$ and 4.19 10^3 J kg^{-1} $°C^{-1}$ respectively. We obtained thermal diffusivity values ranging from 2.25 10^{-3} to 2.29 10^{-3} cm^2 s^{-1}. We used the average thermal diffusivity measured at 1.3 m high on the focus tree at the four cardinal directions for application to the sap flow sensor's data of the control trees. Before further processing, the 10-minutes sap flux densities were averaged into 30 minutes intervals to reduce variance.

Thermistor data usage, zero-flow determination and sapwood area calculations

Three data-processing steps are necessary to convert sap flux density measurements to whole-tree sap flux rates. We evaluated the different options available based on published methods and most commonly applied approaches for the radial integration (Burgess and Downey, 2018; Link et al., 2014), the zero-flow determination approaches (Burgess and Downey, 2018; Granier, 1987; Lu et al., 2004; Oishi et al., 2016, 2008), and the sapwood area calculations (Looker et al., 2016). These three variables were evaluated to assess their relative contribution to the accuracy of the estimates

of whole tree sap flow obtained with the HRM sap flow sensors compared to gravimetrically-measured water uptake at the hourly timescale and in terms of cumulative water uptake.

Radial integration: the HRM sensor is equipped with two thermistors (an outer, the shallowest measuring point, and inner) to measure the sap flux density along a fixed depth of sapwood. Before correcting for zero-flow and extrapolating to the entire sapwood area, two measures can be used that are derived from the two thermistors:

- Maximum magnitude depth (MD): The thermistor depth (Inner or Outer) with the maximum magnitude – *i.e.* the most "active" depth for which the range of sap flux density is the largest (Link et al., 2014) – is chosen and kept constant across the length of the sapwood radius. Both thermistor depths are highly correlated – $R^2 > 0.9$ on average (data not shown), thus no information on the hourly dynamics of sap flux density is lost when using only one of the thermistor depths. For the focus tree, this approach resulted in the use of the Inner thermistor for all four azimuths.
- Mean depths (AD): the inner and outer sap flux density measurements are averaged (Burgess and Downey, 2018)

Zero-flow determination: In theory, the HRM sensors should not require correcting for a zero-flow baseline. However, in practice, a small misalignment of the probes from improper installation or differential pressure exerted on the probes due to differential sapwood properties often lead to an offset in the zero in sap flux density measurements (Burgess and Downey, 2018). Determining a baseline sap flux density relative to zero flow conditions is a way to correct for that offset seen in practice when using the HRM sensors in the field. Several approaches are available to determine the zero-flow baseline in the literature from other types of sap flow sensors. Those approaches

were individually tested to assess their impact on the precision of the sap flux estimates from the sap flow sensors (Rabbel et al., 2016). The first two, pre-dawn and study-specific approaches are commonly used in the literature for determining zero-flow (Burgess and Downey, 2018; Oishi et al., 2016, 2008). The regression methods are less commonly used but consider any temporal drift in the zero-flow measured by the sap flow sensors over time (Granier, 1987; Lu et al., 2004).

- Pre-dawn correction (PD): commonly applied, this technique identifies the lowest daily sap flux density representing zero flow when environmental conditions are propitious for negligible water loss to the atmosphere and recharge of water above sensor height is negligible. We identified the lowest daily sap flux density for each sensor during the periods when solar radiation was less than 5 W m^{-2} (nighttime), and the average minimum two hour VPD (vapor pressure deficit) was less than 0.05 kPa (Oishi et al., 2008) between July 19th and August 22nd, 2017. We thus obtained the average lowest hourly sap flux density during the night of 18 individual days during this period. Two calculations were then made. First, these individual lowest measurements of sap flux density were averaged to yield a unique value of pre-dawn sap flux density (PD). Second, a linear interpolation based on these individual average lowest measurements of sap flux density was performed, returning a complete daily series of lowest sap flux density measurements (PD_d). Each sensor's dataset was corrected for either PD or PD_d.
- Study-specific environmental and experimental conditions (SS): when possible, zero-flow is determined following a cut made just below the sap flow sensors, effectively severing all flows (Burgess and Downey, 2018). In our study, sap flow towards the end of the experiment (days 10 to 12 after the initial cut) was near zero at night based on the direct gravimetric measurements, mimicking a cut directly under the sensor. We selected the

nighttime (22:00 to 04:00) of the last two days (August 21st and August 22nd) as the reference for zero-flow for each sensor. Zero sap flux density was then defined as the average sap flux density measured for each sensor during that time interval.

- Linear regression (LR): to overcome the potential issues of drifts in the data due to long-term installation of the sensors, and issues of nocturnal flow measurement, a linear regression of the lowest daily sap flux density identified over the whole length of the installation by a 10-day moving window is performed. The predicted lowest daily sap flux density from the linear regression is then used as daily zero-flow (Granier, 1987; Lu et al., 2004).
- Double linear regression (DLR): This technique further refines the one above, by eliminating the data points above the regression line and performing a second regression on the restricted dataset (Lu et al., 2004).

For all techniques, once zero-flow was estimated, the entire sap flux density dataset was corrected for the estimated zero sap flux density, either using a unique average value (PD and SS) or on a per-day basis (PD_d, LR and DLR) by subtracting the hourly sap flux density measurements with the calculated zero-flow baseline.

Sapwood area measurements: The conversion of corrected sap flux density J_s to whole-tree sap flux (Q, L hr^{-1}) is a step where an introduction of bias is likely (Looker et al., 2016). Sap flux density is either assumed constant across the sapwood depth and multiplied by the measured sapwood area to obtain Q or allowed to exhibit a radial pattern along with the sapwood depth. For the former option, the method used to determine sapwood depth and by extension sapwood area will modify the calculated estimates of sap flux rates. We assess the impact of the commonly used approximations of sapwood area and depth, as well as the use of a radial profile of sap flux density

on the calculated estimates of sap flux rates. At each sensor location, tree disks were obtained to measure sapwood area and depth. For each disk the conductive sapwood was stained using a 0.0413 % bromocresol green solution (Kutscha and Sachs, 1968). The samples were then scanned, and the total stained area or sapwood depth measured using scanning software ImageJ® (Schneider et al., 2012). Sapwood area was estimated as follows (for the three locations across the trunk below the canopy):

- True sapwood area SA_{true}: total sapwood area was measured for the disks sampled at each tree height.
- One sapwood depth $SA_{tc;i}$: using the tree disk, sapwood (Sw_i, mm) and heartwood depths (Hw_i, mm) to pith was measured at each sap flow sensor cardinal position at each height. Assuming a perfect annulus shape, the total sapwood area was calculated when measured from each cardinal direction ($SA_{tc;i}$).

$$SA_{tc;i} = \pi \times \left({Hw_i}^2 - (Hw_i - Sw_i)^2\right)$$

- Four sapwood depths averaged $SA_{tc;avg}$: the measured sapwood and heartwood depths were averaged across cardinal positions. Assuming a perfect annulus, the total sapwood area was then calculated.

$$SA_{tc;avg} = {\pi}/{4} \times \left({Hw_{avg}}^2 - \left(Hw_{avg} - Sw_{avg}\right)^2\right)$$

- Two sapwood depths averaged: the measured sapwood and heartwood depths from opposite ($SA_{tc;opp}$, N - S, E - W) and side-by-side cardinal positions ($SA_{tc;per}$, N - E, S - W, S - E, N - W) were averaged across cardinal positions and total sapwood area was then calculated assuming a perfect annulus.

Sap flux Q was calculated by multiplying the measured sap flux density from each cardinal direction by one of the four sapwood area estimates. In order to provide a first look at incorporating a more realistic description of the radial distribution of sap flux density along the sapwood length, sap flux was also calculated using a radial profile of sap flux density, specific to the diffuse-porous quality of the wood of trembling aspen (Berdanier et al., 2016).

Spatial variability between cardinal orientations and the use of single sap-flow sensors

Costs often limit the number of commercial sap flow sensors that can be installed in sap flux studies that could quantify the within-tree variability in sap flux rates (particularly on large trees) rather than only the between-tree variability. This might be very important for large trees where distinct microclimatic exposures, wood properties, or idiosyncrasies between cardinal aspects in the trunk may lead to different sap flux rates based on the position of the sap flow sensor. Extrapolating the measured sap flux rates on one cardinal aspect of the tree to the entire sapwood area, to the whole tree may lead to gross estimation errors of whole-tree sap flux rates and cumulative water volumes. To assess whether using multiple sensors would lead to more accurate estimates of whole-tree sap flux rates, we compared the use of single sensors with the use of four sensors placed at each cardinal direction (i.e., north, south, east, and west), summed up to obtain whole-tree estimates with the scale data. For the purpose of these comparisons, we first corrected the sap flux density using the most commonly applied approaches, hence AD for radial integration method, PD for the zero-flow determination, and the best sapwood area measurement - SA_{true}. The calculations were as followed, $for\ i\ in\ \{N, S, E, W\}$:

- The use of single sensor extrapolated to the whole-tree: the sap flux density measured at each cardinal direction is extrapolated to the entire sapwood area SA_{true} to yield estimates of the whole-tree sap flux rates

$$Q_i = J_{s;\,i} \times SA_{true}$$

- The use of four sensors: the sap flux density measured at each cardinal direction is extrapolated to the sapwood area immediately surrounding the sensor location $SA_{true;i}$ (representing about a quarter of the total sapwood area SA_{true}) to obtain sap flux rates. The four cardinal sap flux rates are then summed up to obtain an estimate of whole tree sap flux rates.

$$Q_{quarter;\,i} = J_{s;\,i} \times SA_{true;i};\; Q_{quarter} = \sum_i Q_{quarter;\,i}$$

Statistical analysis

All measurements of sap flux were aggregated into hourly intervals. We report sap flux density J_s (g cm^2 hr^{-1}) and sap flux Q (L hr^{-1}) measured from the sap flow sensors, and gravimetric water flux Q_{scale} (L hr^{-1}) measured from the scale. Daily sap flux (Q^d, L d^{-1}) was calculated, as well as cumulative sap flux (Q^c, L) for both the sap flow sensors and the scale. We limit our analyses to the first five days after the cut (August 12th - 16th, 2017) representing conditions most similar to before the cut.

Physiology measurements: Linear models were fitted on each of the canopy leaf transpiration rate and water potential measurements to test for the interaction between tree (focus *versus* control) and leaf type (shade *versus* sun) or measurement time (leaf water potential only, pre-dawn *versus* midday).

Spatial variability and temporal correlation*:* We visually compared the single-sensor and four-sensors whole tree sap flux rates Q_i and $Q_{quarter}$ against the gravimetric water uptake from the scale at the hourly timescale and in terms of cumulative water uptake. We assessed the temporal discrepancies between sensor-derived sap flux rates and the gravimetric scale data first by calculating the difference between the sap flux rates from both data sources rates during the daytime and nighttime (07:00 – 20:00), and across the seven days after the cut. Secondly, we fitted a linear model with a time series component between the hourly sensor-derived and scale sap flux rates using the function *tslm* from the *forecast* package in R (Hyndman et al., 2019). All of the following data analyses and statistical tests were done on the single-sensor derived sap flux rates, discarding $Q_{quarter}$.

Zero-flow corrections and sapwood area estimation methods: Linear mixed-effects models were used to test for the effect of radial integration method on the difference in the zero-flow correction estimates between PD and SS and on the slope of the relationship between $J_{s,min}$ and time (Date) for PD_d. Additionally, a linear mixed-effects model was fitted on the slope between $J_{s,min}$ and time (Date) defining LR and DLR to assess for differences between radial integration method and zero-flow method. Paired t-tests were used to assess whether the difference between the tree-core methods of sapwood area measurements (SA_{tc}, $SA_{tc\text{-}avg}$, $SA_{tc\text{-}opp}$, $SA_{tc\text{-}per}$, $SA_{tc\text{-}quarter}$) and SA_{true} was significantly different from zero across trunk locations on the focus-tree.

Calibration performance metrics*:* Calibration performance was assessed using four dimensionless metrics assessing the performance of the data-processing procedures and cardinal orientation installation when comparing to the reference gravimetric scale data (Flo et al., 2019) over the first five days after the cut (August 12th - 16th, 2017). All data points less or equal to zero were filtered out for the calculation of these metrics. The following metrics were calculated per day after the

cut: the natural logarithm ratio ("Ln ratio") between the measured (*i.e.* sap flow sensor data) and reference scale water uptake as a measure of accuracy; the slope of the relationship between the measured and reference sap flux to represent proportional bias ("Slope"), as well as the slope of the ln-ln relationship to characterize linearity ("Slope (ln-ln)"), and the Z Pearson's correlation coefficient ("Z-correlation") to describe precision. Linear models were used to assess the differences in these calibration metrics between different zero-flow corrections and different sapwood area estimations for each cardinal direction separately. Three of the four calibration performance metrics declined progressively after the cut across cardinal orientations, even more so at night (data not shown). We chose to restrict our analyses to the first five days after the cut during the daytime (07:00-20:00) to assess the performance of the data-processing procedures for these calibration performance metrics. In that period, the four calibration metrics were relatively stable, and sap flux was most similar to before the cut and to the control trees (Figure 3. 1a, Figure 3. 2).

Differences in cumulative water uptake estimates*:* The absolute difference in cumulative water uptake over the first five days after the cut (August 12th - 16th, 2017) between sensor-derived and scale water uptake measurements was calculated and linear models assessing the effect of cardinal orientation and the three data-processing procedures applied.

Impact of the spatial variability and data-processing procedures on the relationship with atmospheric vapor pressure deficit: We used all days before the cut with no precipitation and the first day after the cut (*i.e.* 27 days). The data from the subsequent days (August 13th - 22nd, 2017) was not included, as the water flux through the cut-tree likely got disconnected from the atmosphere. We assessed the relationship between sap flux and atmospheric VPD (kPa) at the hourly timescales using a modified logistic equation (equation (1)):

$$Q\ (L\ hr^{-1}) = \frac{Asymptote}{1 + e^{-steep \times (x - midpoint)}} + Constant \qquad (1)$$

Differences in cumulative water uptake estimates: The absolute difference in cumulative water uptake over the first five days after the cut (August 12th - 16th, 2017) between sensor-derived and scale water uptake measurements was calculated and linear models assessing the effect of cardinal orientation and the three data-processing procedures applied.

Impact of the spatial variability and data-processing procedures on the relationship with climate: We used all days before the cut with no precipitation and the first day after the cut (*i.e.* 27 days). The data from the subsequent days (August 13th - 22nd, 2017) was not included, as the water flux through the cut-tree likely got disconnected from its climatic drivers. We assessed the relationship between sap flux and atmospheric VPD (kPa) at the hourly timescales using a modified logistic equation (equation (1)):

$$Q\ (L\ hr^{-1}) = \frac{Asymptote}{1 + e^{-steep \times (x - midpoint)}} + Constant \qquad (2)$$

The equation parameters (Asymptote, Constant, Mid-point and Steep) were individually estimated for each combination of cardinal orientation, radial integration, zero-flow correction and sapwood area estimation. The effects of cardinal orientations and the three data-processing procedures were assessed using individual linear models on the asymptote, mid-point and steep parameters. The squared correlation between the fitted and observed values are reported as r^2 values. The same equation at the hourly timescale was used on the gravimetric scale data for the first two days after the cut to avoid introducing artificial bias resulting from the decline in sap flow induced by the cut-tree method by including days 3 to 10 after the cut.

All statistical analysis were performed using the R statistical software v3.5.1. (R Development Core Team, 2019). All the analyses were performed using linear models or linear mixed-effects models with the package *nlme* (Pinheiro et al., 2018). Normality and homoscedasticity assumptions were checked for all models, and corrections applied when necessary. Models specifics and summary statistics (degrees of freedom, sample size, test statistic, coefficient of determination) are also provided in the Appendix 3.B: Summary statistics. Estimated marginal means and 95 % confidence intervals were calculated using the package *emmeans* (Lenth, 2018) to summarize the effects of the fixed factors ($\alpha = 0.05$). The coefficient of determination r^2 is reported for linear models and the marginal and conditional r^2 for mixed effects models.

Results

Sap flow response to the cutting

Immediately after the cut and for the next 48 h, sap flux density (J_s) was similar to measurements taken before the cut and to those measured in the three control trees (Figure 3. 1a Sap flux density then declined in the focus tree over the next eight days compared to the three control trees, which all maintained higher J_s. Interestingly the crown of our focus tree showed no sign of hydraulic damage for the duration of the study (*i.e.* wilting or color changes; Figure 3. 1b and c). Transpiration rate of the focus tree after the cut was about 20 -30 % of the transpiration rate of the control trees (Figure 3. 1d). Shoot water potential at pre-dawn was slightly higher (less negative) than the control, indicating ample water supply over the ten days after the cut, this response became more apparent during midday when shoot water potentials were somewhat lower in the focus tree, but dropped by more than 10 kPa in the control trees (Figure 3. 1d).

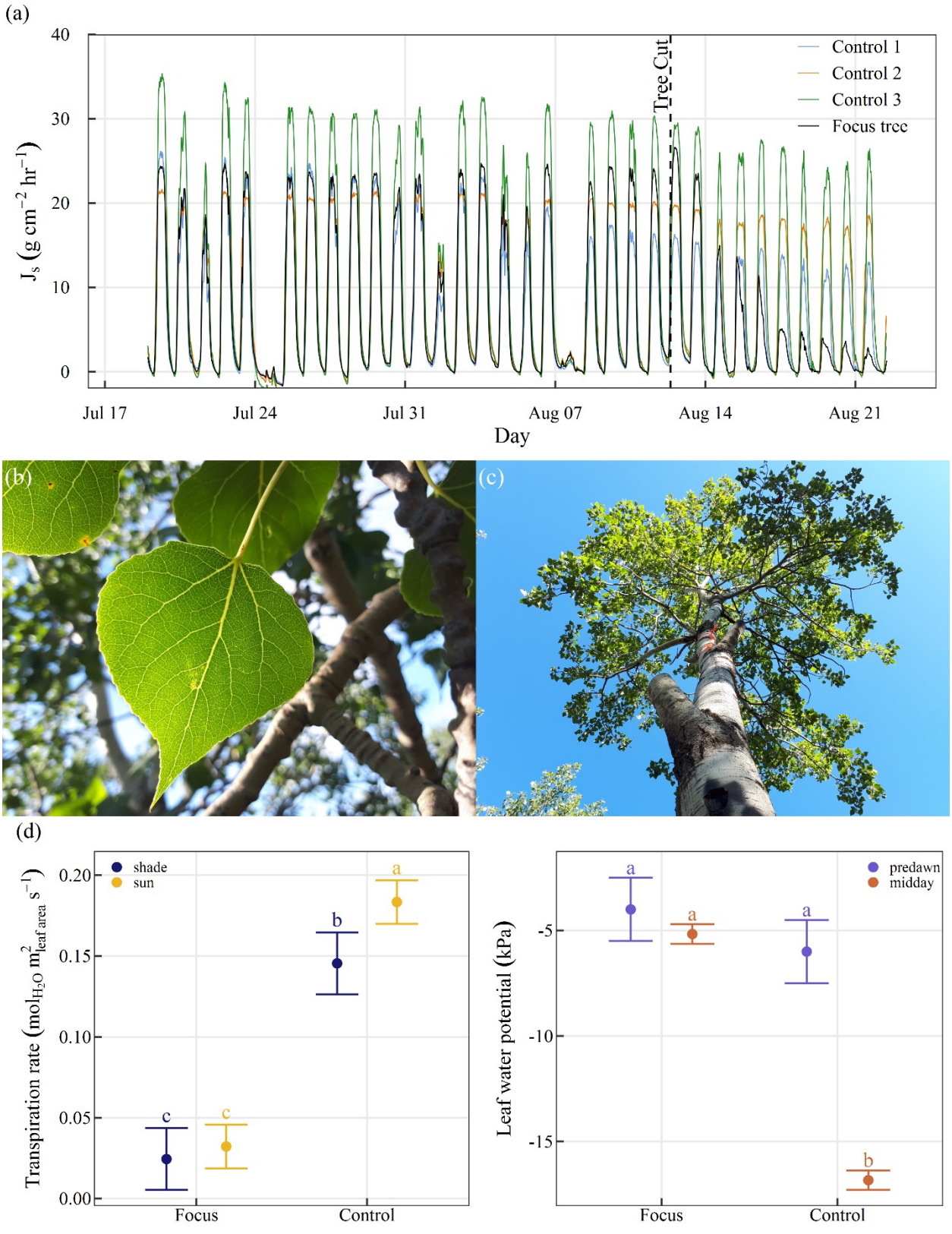
(a)
40
30
20
10
0
J_s (g cm^{-2} hr^{-1})
Tree_Cut
Control 1
Control 2
Control 3
Focus tree
Jul 17
Jul 24
Jul 31
Aug 07
Aug 14
Aug 21
Day
(b)
(c)
(d)
shade
sun
Transpiration rate (mol$_{H_2O}$ m$^2_{leaf\ area}$ s^{-1})
0.20
0.15
0.10
0.05
0.00
a
b
c
c
Focus
Control
predawn
midday
Leaf water potential (kPa)
-5
-10
-15
a
a
a
b
Focus
Control

Figure 3. 1. Impact of the cut on the focus tree sap flux density and canopy health. Panel a shows the sap flux density J_s (g cm^2 hr^{-1}, corrected using the PD zero-flow correction) at 30 minutes time intervals calculated on the north-facing sensor of the focus tree and three control trees between July 19th and August 22nd, 2017. The day the focus tree was cut is indicated by a vertical black dotted line with the label "Tree Cut" on August 12th, 2017. Panel b shows a single leaf from mid-canopy on August 17th (5 days after the cut). Panel c shows a view of the canopy on August 26th (14 days after cut, four days after the end of the study and after the sap flow sensors were uninstalled from the focus tree (the lower branches were removed to ease the collection of the canopy leaf area). Panel d shows the leaf physiology described by transpiration rate (measured at midday on sun and shade leaves on days 4 and 8 after the cut), and leaf water potential (measured on sun leaves at midday on day 4 and predawn on day 8 after the cut) measured on the focus and control trees. Error bars represent 95 % confidence intervals, and letters indicate statistical significance.

Spatial variability in sap flow sensor location between cardinal aspects

Using standard data-processing procedures (AD, PD, and SA_{tc}), the agreement of the sap flux with the gravimetrically measured Q_{scale} was variable and heavily depended on the cardinal position of the sensor on the trunk (Figure 3. 2a). Summing up the sap fluxes calculated at each cardinal orientation into $Q_{quarter}$ did not improve or worsen the fit with the gravimetric data (Figure 3. 2b). The difference between the scale and sensor sap flux rates was lowest during high flow periods (i.e. the first four days after the cut and during the day). The higher discrepancies between the scale and the sensors sap flux rates particularly at night might have been due to the relatively low precision of the scale (0.2 L hr^{-1}). However, the temporal correlation of Q_i and $Q_{quarter}$ with Q_{scale} was high, with no time lag between the two (data not shown, $R^2 = 0.99$). Cumulative water uptake

over the five days after the cut was 191.2 L from the scale data. Using those standard data-processing procedures (AD, PD, and SA_{tc}), the cumulative water uptake estimates using single sensors ranged between 124.1 L (south-facing sensor) to 209.7 L (north-facing sensor). Using the sum of the cardinal fluxes yielded an estimate of 178.9 L.

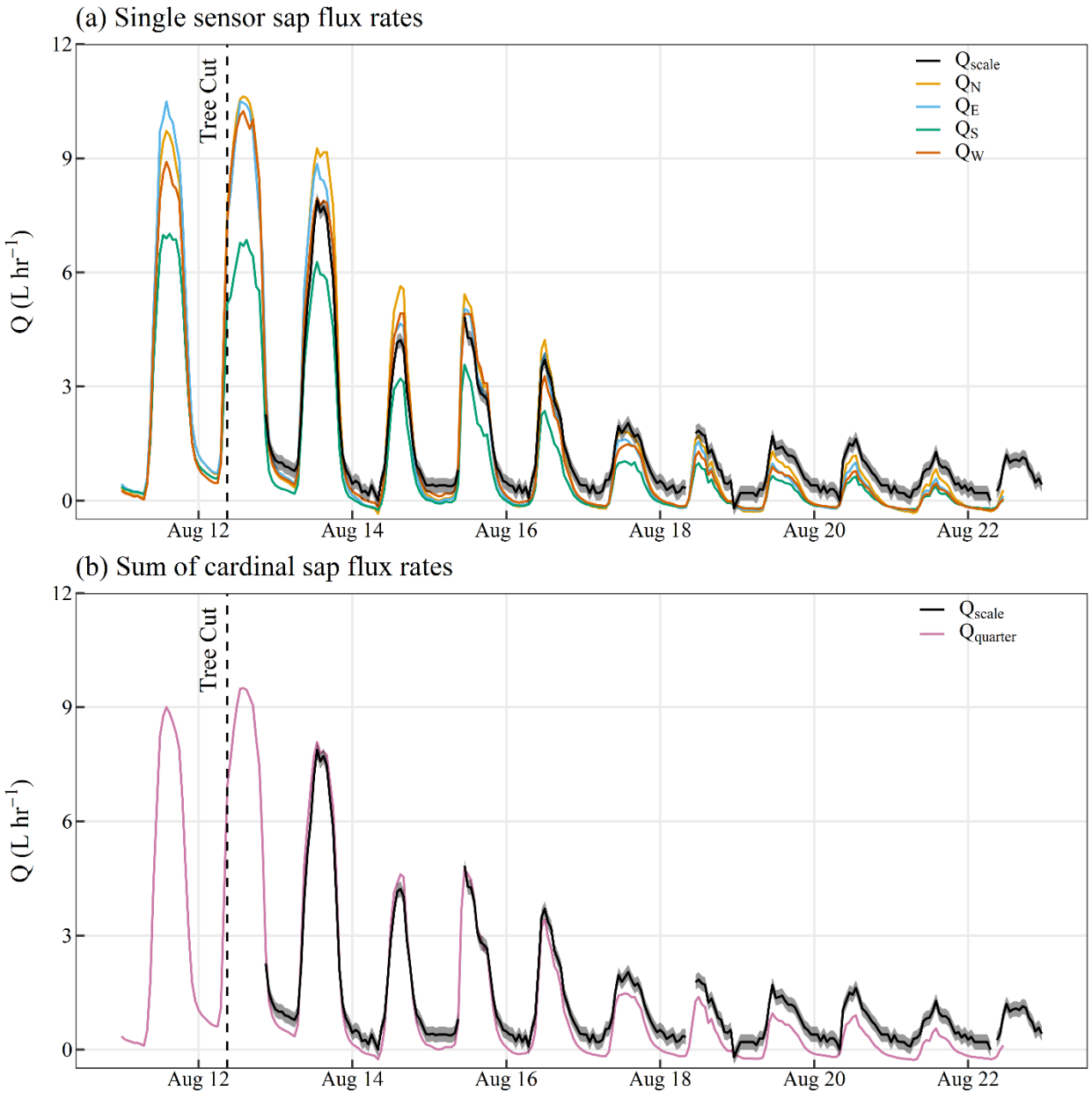

Figure 3. 2 Comparison between the individual sensor-measured and scale hourly sap flux rates. The scale sap flux rate is shown in black, with its 0.2 L hr^{-1} precision as grey shaded area. Panel a shows single sensor sap flux rates Q_i for each cardinal orientation i. Panel b shows the sap flux rates calculated as the sum of the cardinal fluxes, $Q_{quarter}$. All sensor-derived sap flux rates were calculated using the AD radial integration, PD zero-flow determination and SA_{tc} for the sapwood area calculation, with n = 1.

Zero-flow determination approaches and sapwood area calculations

The zero-flow $J_{s,min}$ strongly depended on the correction method and varied between cardinal orientations and thermistor used (Appendix Figure 3.C. 1a). Under the PD correction, $J_{s,min}$ was higher than under the SS correction (mean difference: 0.420 g cm^2 hr^{-1}), more so with AD than with MD (difference estimate: AD = 0.544 g cm^2 hr^{-1}; MD = 0.296 g cm^2 hr^{-1}) (Appendix Table 3.B. 1). Under the PD_d correction $J_{s,min}$ significantly declined over 30 days, marginally more so with AD than MD (slope estimate: AD = -0.047 [-0.055; -0.039]; MD = -0.037 [-0.045; -0.029]), however, most of the variation was explained by the sensor cardinal placement. The slope in the defining regression of the LR and DLR corrections was overall not significantly different from 0 but largely varied between cardinal orientations and radial integration method used.

None of the tree-core derived estimates of sapwood area were significantly different from SA_{true} (Appendix Table 3.B. 2). Using $SA_{tc\text{-}quarter}$ or $SA_{tc\text{-}avg}$ yielded the lowest deviation from the SA_{true}, followed by $SA_{tc;\text{-}per}$, then $SA_{tc\text{-}opp}$. Using SA_{tc} resulted in a large variation across trunk heights and cardinal direction, with up to 60 cm^2 difference with SA_{true} (Appendix Figure 3.C. 1b).

Impact of the corrections methods on the accuracy of the sap flux rates

Hourly estimates

The cardinal placement of the sensor and data-processing procedures applied to the data set significantly influenced the calibration performance metrics (Figure 3. 3). Accuracy and linearity were closest to the reference for the north, and west orientations; however, proportional bias was lowest for the east and south orientations. Precision was highest for the north orientation. The use of the MD radial integration method showed a larger proportional bias but better accuracy than AD, with similar linearity and precision. Regarding the zero-flow corrections, the linear regression

methods LR and DLR showed the highest accuracy and linearity, followed by the SS correction. The use of a radial profile decreased accuracy but improved the proportional bias compared to the other sapwood area estimation methods. None of the data-processing procedures showed any significant differences in precision. The integration of the four cardinal measurements of sap flux rates into $Q_{quarter}$ improved proportional bias for the AD radial integration method (0.99 [0.97 ; 1.01]) and slightly increased the precision but did not lead to an overall improvement of the accuracy and linearity (Appendix Figure 3.C. 2).

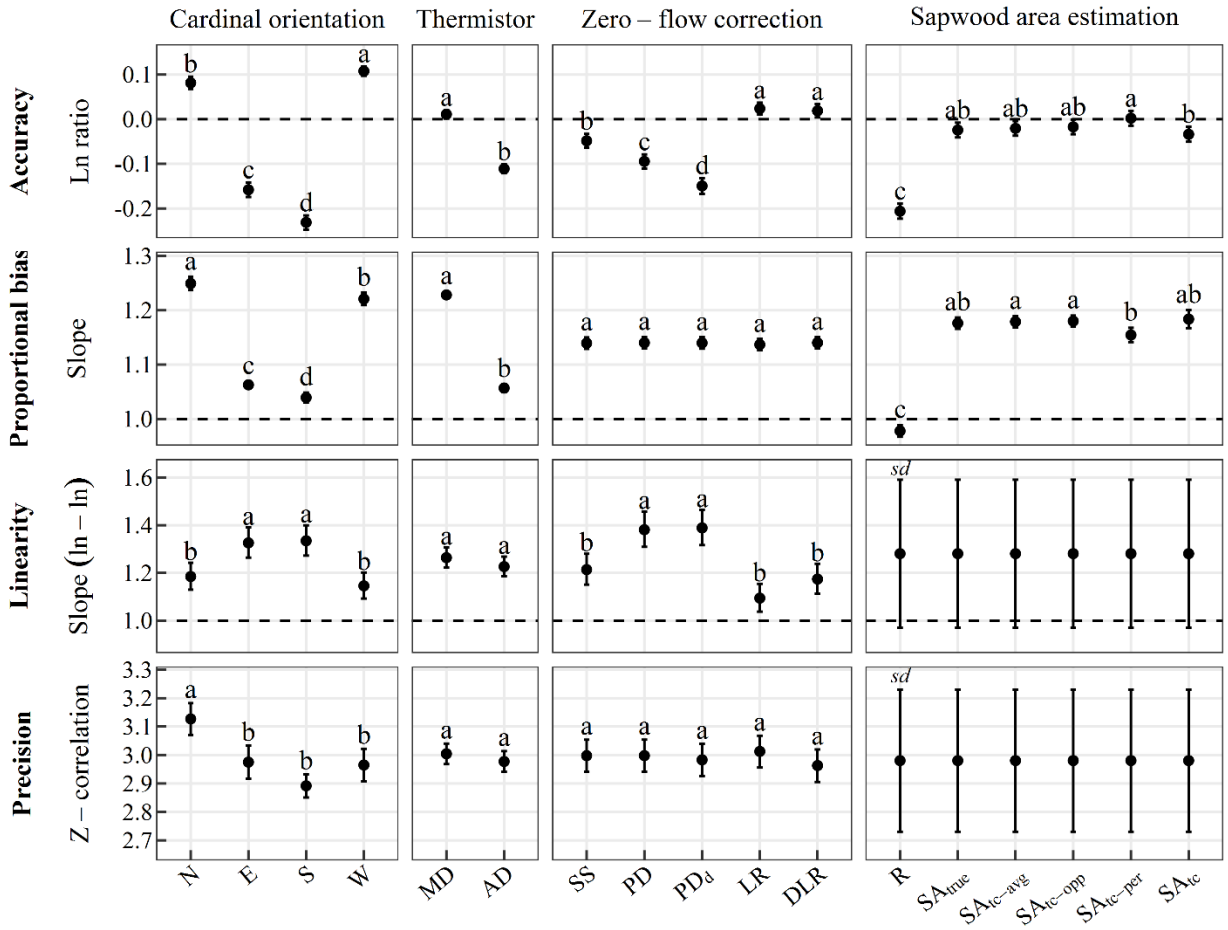

Figure 3. 3. Summary of the calibration performance metrics for the azimuthal sensor placement and the different methods applied in the three data-processing procedures (radial integration,

zero-flow correction, and sapwood area estimation). The metrics were estimated during the daytime (07:00 to 20:00) the first four days after the cut. Means and 95 % confidence intervals are shown. Different letters indicate significant differences across data correction procedures (Appendix Table 3.B. 3). Note that for the slope (ln-ln) and the Z-correlation for the sapwood area estimation variable, the values were identical across the different methods; hence the figure shows mean and standard deviation ("sd" label). Horizontal dotted lines indicate reference value, for a perfect calibration value for each metric. The intersection between the confidence interval and the reference line indicates that the metric is not significantly different from the reference. Data distribution of the calibration performance metrics across the azimuthal sensor placement and the three data-processing procedures is shown in Appendix Figure 3.B. 1.

Cumulative estimates

Over the five days after the cut, the hourly discrepancies between the gravimetric scale and the single-sensor sap flux rates cumulated to differences that ranged from less than 1 L to near 125 L in the final cumulative water uptake tally, with a significant interaction between sensor placement and data-processing procedures (Figure 3. 4a). Using MD significantly decreased the deviation from the gravimetric cumulative water uptake compared to AD when a sensor was positioned on the south (and marginally on the east) side of the trunk, but the deviation increased for the north and west positions. The SS, PD and PD_d zero-flow corrections produced a deviation of 25 L or less on average from the gravimetric cumulative water volume (Figure 3. 4b). The use of R, SA_{tc} and $SA_{tc\text{-}per}$ sapwood area estimation methods produced larger differences with the gravimetric cumulative water volume (Figure 3. 4b) Integrating the four aspects into a single whole-tree cumulative sap flux resulted in a smaller deviation from the gravimetric measurements, ranging

between 10 to 30 L on average, with no differences between radial integration, zero-flow and sapwood area estimation approaches (Appendix Figure 3.C. 2).

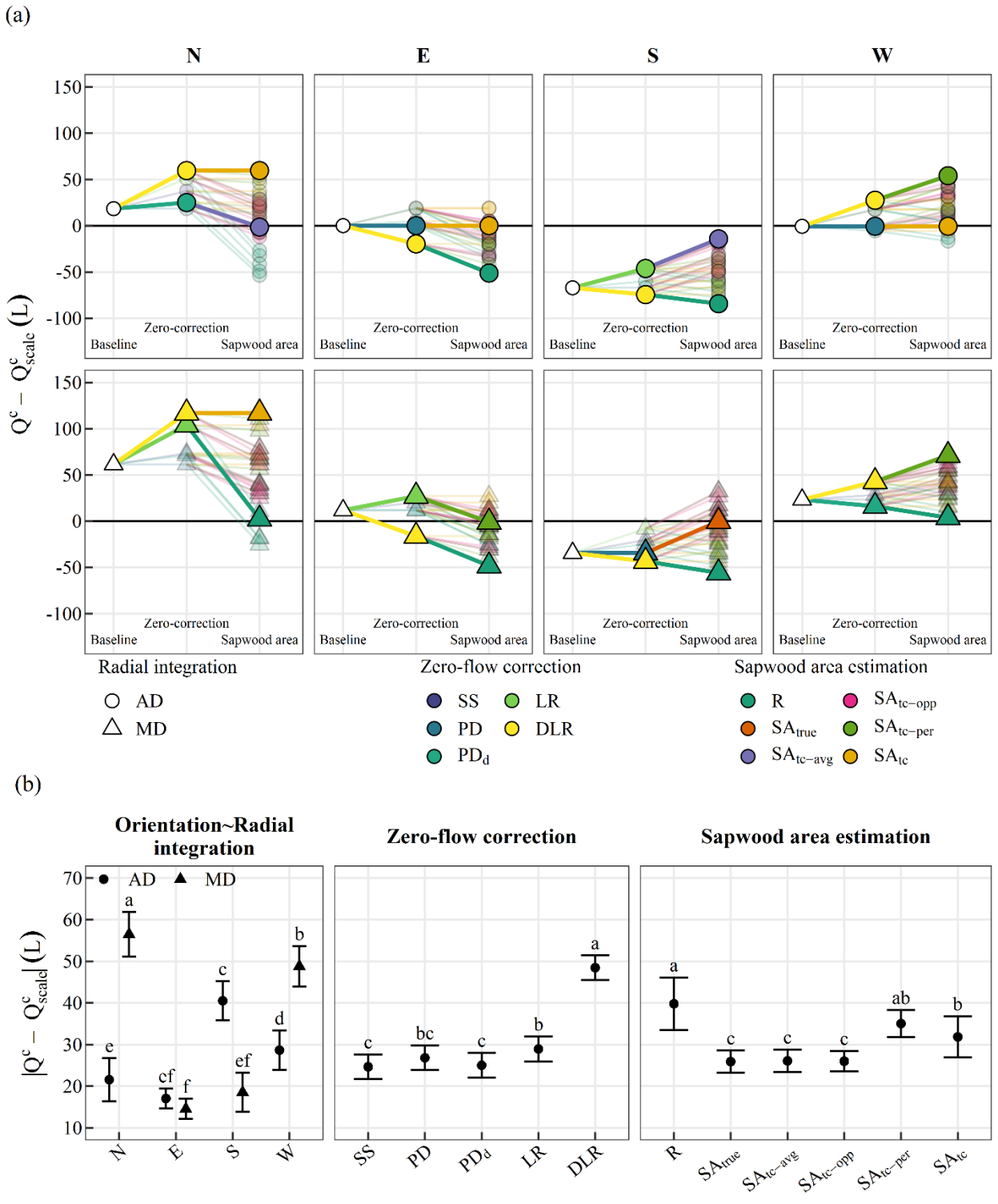

Figure 3. 4. Difference between sensor (Q^c) and gravimetric (Q^c_{scale}) estimates of cumulative water uptake over the five days after the cut for cardinal placement of the sap flow sensor and the three

data-processing procedures. Panel a presents all data-processing combinations, highlighting the best (closest to zero) and worst (farthest from zero). Baseline: PD and SA_{tc}. We show how the use of different zero-flow corrections alter the cumulative water uptake estimate from the Baseline ("Zero-correction"), followed by the use of different sapwood area calculation methods ("Sapwood area"). Panel b shows the mean and 95 % confidence interval in the estimate of the absolute difference between the sensor and gravimetric cumulative water uptake for the interaction between the cardinal placement of the sensor and radial integration approach, zero-flow correction and sapwood area estimation methods. Letters indicate statistical differences.

Nighttime cumulative water uptake represented 20 % and 10 % of the total daily volume from the gravimetric and sensor measurements respectively (*i.e.* 53.1 L and 26.6 L respectively, results not shown). The sensor estimates were slightly higher before the tree was cut (13 % of total cumulative sap flux).

Consequences of correlating sap flux rates with climatic drivers

All data-processing procedures showed a very good fit with hourly VPD, with little difference between the best and worst fits in terms of r^2 (Figure 3. 5). No differences in the strength of the fit were found among the different sapwood area estimates, as they only differed by a multiplicative factor. The gravimetric data showed a lower asymptote, higher mid-point and higher steepness estimates than most of the data-processing procedure combinations (Figure 3. 5 and Table 3. 1). The cardinal orientation and radial integration explained most of the variation in the parameters of the logistic relationship between hourly sap flux and VPD (Table 3. 1, Appendix Table 3.B. 4). The asymptote and mid-point were significantly higher when MD while the opposite was true for the steepness parameter. All zero-flow determination approaches yielded very similar parameter

estimates; however, the LR and DLR had a lower mid-point and steepness parameters than the other corrections. Only the use of the radial profile differed from the other sapwood area estimation methods, with a lower asymptote (Table 3. 1, Appendix Table 3.B. 4)

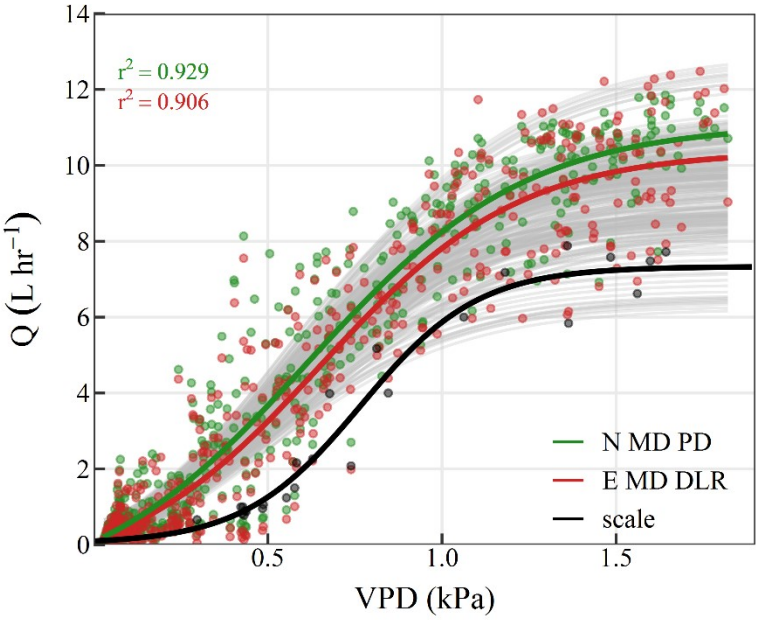

Figure 3. 5. Hourly measured (points) and modelled logistic relationship (line) between hourly sap flux rates (hourly) and atmospheric VPD (kPa) for each combination of the sensor cardinal placement and data-processing procedures (light grey) and for the scale gravimetric flux (black). The individual relationships with the best (green) and worst (red) fit (r^2) are shown, and the combination explicit in the legend (cardinal orientation ~ radial integration ~ zero-flow correction) for each panel. The sapwood area estimation is not explicit as it did not have an impact on the fit.

Table 3. 1. Mean and 95% confidence intervals of the parameters of the logistic relationship between hourly gravimetric (scale) and sensor-based sap flux rates and VPD (Asymptote, mid-point and steepness; rows). The means and 95 % confidence intervals obtained from the models assessing the effects of the sensor placement and the three data-processing procedures are shown for each parameter (columns). Letters indicate significant differences between methods for each data-processing procedure. As all zero-flow determination approaches yielded very similar estimates, they are summarized in a unique value. The same is applied for all the sapwood area estimation methods (SA_{true}, $SA_{tc\text{-}avg}$, $SA_{tc\text{-}per}$, $SA_{tc\text{-}opp}$ and SA_{tc} summarized in S_{all}) but R. Mean and standard deviation (sd) are presented for the mid-point and steepness for the sapwood area estimation as the values were identical.

		Sensor								
	Scale	**Orientation**				**Radial integration**		**Zero-flow approach**	**Sapwood area estimation**	
		N	**E**	**S**	**W**	**AD**	**MD**	**All**	**R**	**SA_{all}**
Asymptote	7.31	11.25 [10.85;11.64] **ab**	10.98 [10.79;11.17] **b**	9.39 [9.1;9.68] **c**	11.24 [11.06;11.41] **a**	10.21 [10.05;10.38] **b**	11.21 [11.02;11.41] **a**	10.69 [10.47;10.91]	9.22 [9.04;9.42] **b**	10.98 [10.71;11.25] **a**
Mid-point	0.77	0.57 [0.56;0.58] **c**	0.61 [0.6;0.62] **a**	0.6 [0.6;0.6] **b**	0.56 [0.53;0.59] **c**	0.52 [0.5; 0.53] **b**	0.63 [0.63;0.64] **a**	0.59 [0.58;0.59]	0.58 [sd: 0.05]	
Steep	5.95	3.38 [3.37;3.4] **c**	3.77 [3.76;3.78] **b**	3.84 [3.83;3.86] **a**	3.38 [3.35;3.41] **c**	3.8 [3.79;3.81] **a**	3.38 [3.37;3.39] **b**	3.59 [3.58;3.61]	3.59 [sd: 0.3]	

A summary of the results comparing the sap flow sensor data and the gravimetric scale data using the different categories of descriptors is presented in Table 3. 2. Cardinal orientation and radial integration often had the most considerable effect on the descriptors, while the zero-flow corrections and sapwood area estimation methods had a subtler effect. For each data-processing procedure, no best method clearly appeared across all descriptors, except for the SS zero-flow correction and the north orientation which seemed to perform slightly better on the majority of descriptors than other approaches.

Table 3. 2. Summary of the best cardinal orientation, radial integration method, zero-flow correction and sapwood area estimation for the three following categories: calibration performance metrics (Flo et al., 2019) (accuracy, proportional bias, linearity, and precision), correlation with VPD (kPa, hourly) and cumulative water uptake. For the first and third categories, the sap flow sensor data is compared to the gravimetric scale data. For the relationship with VPD, the factor levels for which the parameters were closest to the gravimetric parameters of the logistic relationship between sap flux and VPD are shown. When no significant differences were found between methods, "NA" is displayed.

	Calibration performance metrics				**VPD relationship**	**Cumulative water uptake**
	Accuracy	**Proportional bias**	**Linearity**	**Precision**	**Closest to gravimetric parameters**	
Orientation	N	S	N; W	N	S	W
Radial integration	MD	AD	*NA*	*NA*	AD	*NA*
Zero-flow correction	SS; DLR	*NA*	SS; LR; DLR	*NA*	*NA*	SS; PD; PD_d;
Sapwood area estimation	All but R	R	*NA*	*NA*	R	SA_{true}, $SA_{tc\text{-}avg}$; $SA_{tc\text{-}opp}$

Discussion

We quantified the uncertainties introduced by the placement of sap flow sensors (cardinal directions) and the application of different data-processing approaches (radial integration method used, zero-flow correction, and sapwood area estimation methods) on sap flow estimates for large diameter trees. These estimates were compared to gravitational measurements using the cut-tree method. The temporal precision of sensor-derived fluxes with the gravimetrically-measured water uptake was high when estimated across the different cardinal orientations and data-processing approaches for the HRM sensors. Almost all data-processing procedures showed a positive proportional bias, unlike previous studies reporting negative proportional bias (Flo et al., 2019; Fuchs et al., 2017). The limited range of sap flux densities in our study likely precluded the commonly reported saturation effect of the HRM responsible for the previous studies' results. Altogether, the choice of azimuthal placement of the sensor and the choice of data-processing approach resulted in a broad range of cumulative water uptake estimates over a short period of five days.

Most sap flow measurement errors are related to azimuthal and radial variability of sap flux density

Despite the visual symmetry of the focus tree and its sapwood area, the cardinal placement of the sensors and the radial integration method used had a significant impact on the sensor-derived sap flux rates. These two factors had the largest effect on the sensor's accuracy, proportional bias, and precision. A relatively small number of studies have considered azimuthal variations in sap fluxes, finding them related to structural anatomy and wood properties (López-Bernal et al., 2010), microclimatic conditions (Zhang et al., 2018), and seasonal variation (Chiu et al., 2016b). No

systematic pattern across and within species and studies have appeared so far (Sato et al., 2012; Van de Wal et al., 2015). In this study, the north-facing sensor seemed to perform slightly better than all other orientations across the performance descriptors in comparison with the gravimetric measurements, which we speculate may due to the lower influence of natural temperature gradients on the sensor measurements of sap flux density (Vandegehuchte et al., 2015, not the scope of the study). Integrating sap flux measurements among the four cardinal positions instead of using single-position measurements did not generally improve the calibration performance metrics results but significantly decreased the deviation in the estimate of whole-tree cumulative water uptake in the first five days before the cut. The inclusion of the azimuthal aspect in any future sap flow experiment should be carefully considered (Tseng et al., 2017), especially for large trees with a higher probability of azimuthal variability in sap fluxes and when a limited number of sap flow sensors is available (Komatsu et al., 2017). An initial pilot study assessing whether there is a basis for strong environmentally-driven circumferential variability in sap flow in individual trees in a stand would help improve the decision-making process in the sensor allocation, to integrate or ignore this within-tree circumferential variability in water uptake.

Radial patterns of sap flux density within the sapwood have an equally significant impact on whole tree sap flux estimation. Sap flux density measurements from the two thermistors of the HRM sensors are highly correlated but display a different range of sap flux density measurements following their positioning at different sapwood depths. Arguments have been made to use the thermistor depth with the maximum magnitude of measurements to focus on the "most functioning" xylem depth, especially when relating to environmental variables such as VPD (Link et al., 2014). However, this can potentially overestimate sap flux rates when extrapolating to whole-tree estimates. Using MD increased the proportional bias in hourly sap flux and the

deviation from the gravimetric measurements of cumulative water uptake for the north and west aspects only, highlighting an interactive effect between azimuthal and radial variability of sap flux density (Lu et al., 2004; Zhang et al., 2018). Most of our results are inconclusive regarding the use of MD or AD for our study tree. Integrating multiple point measurements over a species-specific radial profile of sap flux density could significantly improve the performance of the sap flow sensors (Hernandez-Santana et al., 2015). The coarse application of a diffuse-porous radial profile (Berdanier et al., 2016) to our dataset showed overall mixed results. Proportional bias was reduced, but accuracy decreased substantially, and the absolute difference with gravimetric cumulative water volume was the highest across sapwood area estimation methods. A proper calibration of the radial profile equation for this species and other large-diameter trees using multi-sensor needles across the sapwood depth would likely improve our results (Forster, 2017; Hatton et al., 1990; Wullschleger and King, 2000) but is often not feasible when using costly commercially available sap flow sensors. In the absence of information regarding the radial profile of sap flux density, extrapolating constant sap flux density across SA_{true} or $SA_{tc\text{-}avg}$ and $SA_{tc\text{-}opp}$ showed the best results.

Differences in sap flux estimation caused by zero-flow corrections

The five different zero-flow corrections tested in the study were in the range of 0-2 g cm^2 s^{-1}, similar to what has been reported previously (Rabbel et al., 2016). The environmentally-defined pre-dawn zero flow corrections (PD and PD_d) showed the lowest scores in accuracy and linearity, unexpectedly, considering this type of correction has been highlighted as the most likely to yield the best zero-flow estimation (Oishi et al., 2008; Peters et al., 2018; Rabbel et al., 2016). Significant nocturnal sap flux (representing 20% of total daily cumulative sap flux in this large aspen tree) or the influence of stem water storage dynamics may have contributed to this result in our focus tree (Peters et al., 2018). When the application of the well-performing SS correction is

not available, the linear regression techniques performed best in terms of accuracy and linearity, although the use of the DLR led to the highest absolute difference in cumulative water uptake. It has been hypothesized that zero-flow conditions may develop over time, and the use of more static methods such as PD and SS could lead to increasing discrepancies (Rabbel et al., 2016), hence the use of the regression techniques. It is, however, possible that over an extended time period linear regression methods may not fare as well, as changes in phenology, wood thermal properties, and climatic conditions may trigger non-linear changes in minimum sap flux densities (Peters et al., 2018; Rabbel et al., 2016; Vergeynst et al., 2014). The zero-flow determination, though not as crucial for the heat pulse velocity sap flow sensors as for other sensor families, remains a data-processing step for which there is little consensus as to which to use. To our knowledge, no study has yet been able address the issue of potential evolution of the zero-flow baseline during an entire experiment while accurately and directly measuring instances of null flow.

Implications for correlating sap flux with climatic variables and for stand-level transpiration estimates

All sensor cardinal positions and data-processing approaches showed very high correlation ($R^2 > 0.9$) with atmospheric VPD, showing a high consistency regardless of the position and correction method chosen, unlike what has been found in other studies (Peters et al., 2018; Rabbel et al., 2016). Sensor position and the variability in sap flux estimates with sapwood depth significantly affected the parameters defining the hourly relationship with VPD, showing a significant departure from the gravimetric data. All sensor cardinal orientations and data-processing methods largely overestimated the asymptote, *i.e.* maximum water use rate at high VPD, and underestimated the mid-point and steepness parameters compared to the relationship based on gravimetric measurements. Although the dataset used to derive the latter was restricted to only two days, this

result highlights that the modeled dynamics between VPD and sensor-based sap flux rates may not be fully representative of large tree's behaviors. Deriving estimates of canopy conductance and water usage in response to climatic variables based on sap flux measurements is a common approach, but as highlighted here, decisions such as the placement of the sap flow sensors or the choice of data-processing approach may lead to significant discrepancies that impact the interpretation of responses to changes in VPD. Those seemingly small differences at the individual tree scale accumulate significantly when upscaled spatially and temporally. Over only five days, we saw total cumulative water uptake misestimated between 1 to more than 50 %. This uncertainty will most likely increase when considering an entire growing season, and when upscaling water use from a single tree to a stand- or landscape-level (Čermák et al., 2004; Peters et al., 2018). Deliverables from sap flux studies (*e.g.* their relationships with climatic and environmental variables and their extrapolation of cumulative water volumes transpired by forests) play a significant role in current vegetation models and forest and land management decisions. Considering the critical questions these models address (forest productivity and mortality, species distribution, hydrological cycling, and climate change impacts) it becomes necessary to assess in more detail and across sap flow sensor families how different methodological steps impact our current and future understanding and interpretation of water flow in trees and their extrapolation to various spatial and temporal scales (Ward, 2016).

Conclusion

This cut-tree study of sap flux measurements on a large mature tree using the HRM sap flow sensors highlighted that uncertainties arise from several methodological steps from sensor installation to the calculation of hourly sap fluxes. Although the cut-tree method provides a unique way to directly obtain gravimetric measurement of water uptake at a fine temporal scale for large

trees (Olbrich, 1991; Roberts, 1977; Smith, 1992; Vertessy et al., 1997), these studies are complex to set up and present disadvantages and limitations. The separation of the crown and stem from the root system and the total immersion of the stem surface in water have contributed to the steady decline of sap flux density we observed in our study (beyond the scope of this paper). Conducting parallel experiments, using the weighing lysimeter and cut-tree methods may contribute to filling in the gaps in our interpretation of the observed decline in sap flux rate signals seen in this study, strengthening the conclusions drawn on the appropriate data-processing procedures to reduce uncertainties in sap flux rates in large trees. Nonetheless, we showed that for this large mature aspen tree, placing the sap flow sensors on the north-facing side of the tree, using either the LR or SS zero-flow correction and using tree disks or a minimum of two opposing tree-cores to estimate sapwood area were the best choices for increased accuracy with the gravimetric data. This study highlights the need for systematic and explicit handling of uncertainties in sap flow studies. Further comprehensive testing of the impact of sensor placement and the choice of data-processing methods on sap flux estimates is required to obtain a comprehensive handbook guiding the best available practices for using different families of sap flow sensors in trees of varying diameter and wood properties. It will eventually improve our understanding of tree water use at different spatial and temporal scales.

CHAPTER 4: Insights into the spatial and functional partitioning of sap flow in a large diffuse-porous tree

Abstract

Sap flow sensors recently became crucial tools to help better quantify water uptake dynamics in tress that can be extrapolated to larger scales. Estimating canopy transpiration using sap flow sensors is operationally efficient but can fail to incorporate spatial variability of sap flow, especially in large mature trees. Using a collection of heat ratio method sap flow sensors, we assessed the different aspects of sap flow partitioning on a 20 m tall, 60 years old trembling aspen (*Populus tremuloides* Michx.) over a month in summer 2017 and compared against gravimetric measurements of water uptake by cutting the tree under water. The distribution of sap flow across the four cardinal directions and along trunk height was uneven, with higher sap flux density in the north orientation at the low and upper trunk positions and in the east at the mid-trunk position. Furthermore, sap flux rate in the lowest crown branches was lower than expected from the leaf area associated with and represented a declining percentage of the whole-tree sap flow as daily vapor pressure deficit (VPD) increased. In addition to spatial partitioning, a significant difference in daily sap flow between trunk heights (up to 50 L per day) suggests important exchanges of water supporting water demand of other woody tissues in a trunk. Once considered, stem water storage represented on average 15 % of total daily flows, with marked variability among trunk azimuths and VPD. Overall, this study highlights the complexity of spatial and functional distribution of sap flow in trees, providing a basis for further exploration of spatial and temporal dynamics of water transport particularly within large trees.

List of abbreviations

Abbreviation	Units	Description
χ^2_{DU}		Dykes and Unwin's chi square statistic
$J_{s,i}$	g cm^{-2} hr^{-1}	sap flux density J_s at each azimuth i
Q *and* Q_q	L hr^{-1}	Hourly sap flux rate across the sapwood area and across a quarter of the total sapwood area (from each azimuth, $\sum Q_q = Q$)
Q^d *and* Q^d_q	L d^{-1}	Daily sap flux rate across the sapwood area and across a quarter of the total sapwood area (from each azimuth)
Q^c	L	Whole-tree cumulative water uptake
$Q^c_{th,q}$	L	Theoretical cumulative water uptake over a quarter sapwood area, assuming uniform distribution of sap flow across the quarter sapwood area ($Q^c_{th,q} = \frac{1}{4} * Q^c$)
Q^d_{excess}	L d^{-1}	"Excess" daily sap flux rate, measured as the daily difference in measured sap flux rates between a lower and an upper trunk position across the sapwood area.
$Q_{storage}$ *and* $Q_{storage;q}$	L hr^{-1}	Hourly sap flux rate related to the use of internal stem water storage across the sapwood area and across a quarter of the sapwood area (each of the azimuths)
VPD	kPa	Atmospheric vapor pressure deficit
TDW		Total daily water correction factor

Introduction

Water uptake, transport and transpiration of trees are important components of the global hydrologic cycle and forest ecosystem functioning. The relatively recent development of sensors allowing a continuous measurement of sap flow *in vivo* has led the way to better quantify and understand the dynamics of water uptake from an individual tree to the landscape and regional scales (Link et al., 2014). Common methods of sap flow measurements involve the use of a single or a couple point-based sap flow measurements taken at the base of individual trees to estimate the whole-tree water dynamics and transpiration volumes over a range of temporal and spatial scales. There are, however, several factors to consider when utilizing and interpreting these sap flux measurements, particularly for large trees where spatial variability within an individual's trunk (**Chapter 3**, Flo et al. 2019). Refining our knowledge of the spatial and functional distribution of sap flow within individual trees will ultimately help us improve our understanding of the complex responses of trees, forests and landscapes to changes in water availability.

Spatial variability of sap flow in large trees originates from a combination of internal and external factors. Internal factors most likely relate to sapwood properties and xylem vessels arrangement (e.g. ring- *versus* diffuse-porous species) that impact the distribution of sap flow across the sapwood area due to differences in the distribution and area of conductive sapwood (Gebauer et al., 2008; Umebayashi et al., 2008). Diverging xylem vessels properties and parenchyma organization (Barij et al., 2011; Morris et al., 2018) and potential crown and root sectorization of sap flow (López-Bernal et al., 2010) across the sapwood area may also lead to significant azimuthal variability in the distribution of sap flow across the trunk. Externally, varying microclimate and microenvironments across the sapwood area will further interact with these factors and lead to an uneven distribution of sap flow across azimuths (Cabibel et al., 1997; Van de Wal et al., 2015).

Most studies that have shown substantial azimuthal variability focused on measurements at the base of the tree. Considering the tall heights of trees in most forested landscapes, we need to understand whether the variability measured at the base of the tree is conserved and representative throughout the entire tree height (Loustau et al., 1996), as it can significantly affect the extrapolation to larger scales.

Beyond its spatial distribution, the sap flow measured at the base of the tree may be functionally partitioned at relatively small timescales between different streams such as transpiration, storage and exchanges with other woody tissues. Substantial volumes of internally stored water, divided between symplastic (Pfautsch et al., 2015) and apoplastic stem water storage (Hölttä et al., 2009), can significantly support daily transpiration demands (Scholz et al., 2007; Waring and Running, 1978; Yu et al., 2019) and contribute to mitigating drought effects (Betsch et al., 2011). The importance of the use of stored water to temporarily meet transpiration demands depends on tree size (Goldstein et al., 1998; Meinzer et al., 2004; Phillips et al., 2003), wood anatomy (Oliva Carrasco et al., 2015) and environmental conditions (Beedlow et al., 2017; Loustau et al., 1996). Considering the spatially variable distribution of sap flow across the sapwood area, it is likely that stem water storage is also unevenly distributed across azimuths and with tree height.

However, some caution must be taken when interpreting stem water storage dynamics from studies using sap flow sensors placed in large mature trees (Burgess and Dawson, 2008; Phillips et al., 2009). Commonly, a daily conservation of mass is assumed when comparing sap flow measurements between two locations along the height of a tree, assuming that net daily sapwood water content is constant and thus daily sap flows measured along the trunk height are equal. In practice, a correction factor has been commonly applied in most studies to meet the assumption that total daily crown transpiration is equal to daily sap volumes measured at the base of a tree

(Čermák et al., 2007; Goldstein et al., 1998; James et al., 2003; Kocher et al., 2013; Meinzer et al., 2004; Oliva Carrasco et al., 2015; Phillips et al., 2003; F. G. Scholz et al., 2008). Interestingly this correction factor has never been validated or experimentally tested for large trees against veritable measurements of sap flow (such as gravimetric or full crown transpiration measurements), most likely because of the experimental and technical challenges involved with working with large trees. Using a recent study showing the high accuracy of heat ratio method sap flow sensors against gravimetric measurements (**Chapter 3**), there was an opportunity to investigate the validity of this correction factor.

The objective of this study was to provide some insights into the use of sap flow sensors to investigate the spatial and functional partitioning of sap flow in a large mature boreal forest tree. We equipped a 20 m tall, 60 year old mature trembling aspen (*Populus tremuloides* Michx.) with several heat ratio method (HRM) sap flow sensors (Burgess et al., 2001) in various positions along the trunk and in the crown in the summer 2017. Using these sensors, we sought to: 1) assess the spatial distribution of sap flow in the trunk and within the crown, 2) evaluate the validity of a correction factor when comparing sap flux rates between different heights within an individual tree, and 3) estimate the importance of stem water storage in daily flows, and its relationship with atmospheric vapor pressure deficit conditions. Ultimately, improving our understanding of the spatial and functional distribution of sap flow in large trees will further our understanding of the water uptake dynamics of forested landscapes at large spatial and temporal timescales.

Materials and Methods

Study site and weather

The study was carried out on the same study site described in **Chapter 3**. Briefly, the study site was located in a mixed trembling aspen (*Populus tremuloides* Michx.) and white spruce (*Picea glauca* (Moench) Voss) stand part of the dry mixed-wood boreal ecoregion. Mean temperature in this region is -13.4˚C in January and +16.6 ˚C in July and has an annual precipitation of 478.7 mm (1981 – 2010 climate normal, Athabasca station, 54˚82'00" N, 113˚54'00" W) (Alberta Climate Information Service (ACIS), 2018). Hourly and daily vapor pressure deficit (VPD, kPa) for the duration of the study was calculated from hourly weather data retrieved from the Abee weather station located 16.6 km from the research site (Alberta Climate Information Service (ACIS), 2018). Those data were validated with data collected from a weather station that had been installed on the research site for a portion of the study (starting August 1st 2017, Appendix Table 4.A. 1). For a more complete data set we therefore used the data from the Abee weather station. The whole study was carried out between July 18th, 2017 and August 12th, 2017.

Sap flow measurements

The study was carried out on the same focus mature aspen tree and three control trees as described in **Chapter 3**. The focal tree was cut to confirming the sap flow sensors measurements against a gravimetric measurement (**Chapter 3**). To estimate sap flow at different positions within the tree, the focal tree was equipped with total of 19 heat ratio method (HRM) sap flow sensors (SFM1, ICT International Pty Ltd.) placed along the trunk, on three accessible main branches in the lower crown, and on the large branch supporting the upper crown (Figure 4. 1). Twelve sensors were installed at three heights along the trunk in the four azimuths (north, east, south and west) to represent the potential variability in sap flow distribution across the sapwood area. Sensors were installed at 2.3 m (hereafter referred to as "low trunk"), at 5 m (hereafter "mid trunk"), and at 10 m trunk height, just below the start of the crown (hereafter "upper trunk"). Six sap flow sensors

were installed on the three lowest branches of the crown (located at 10.9, 11.5 and 12.5 m high, oriented south-west, east and south respectively), and another sensor on the main large branch just above the lowest three branches (lower crown) supporting the rest of the crown, and named hereafter “upper crown” (see Appendix Table 4.A. 2 for a description of the anatomical characteristics of each sensor location).

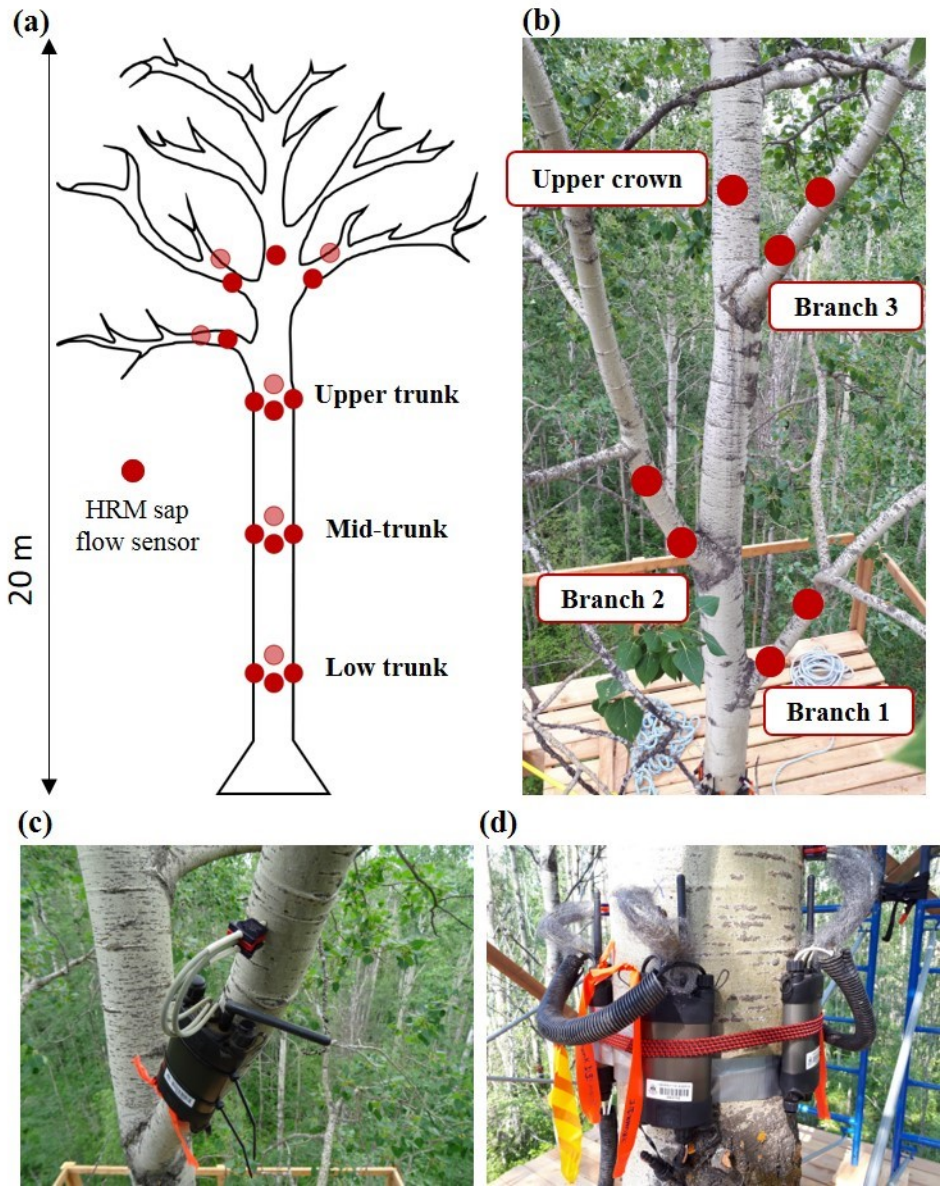

Figure 4. 1. Schematic and pictures of the placement of the HRM sap flow sensors (red circles) on the focus trembling aspen tree. Panel a: schematic of the placement of the 19 HRM sap flow sensors along the trunk and in the crown of the focal tree. Panels b and c: Detailed pictures of the lower part of the crown highlighting the placement of the HRM sap flow sensors on the three low crown branches (branch 1, 2 and 3; panel c shows one sap flow sensor placed on branch 3) and

on the upper crown (just above the three low crown branches). Panel d: placement of the sap flow sensors at the four azimuths on the trunk below the crown - here the mid-trunk position is shown.

An additional twelve sensors were installed on three control trees (four sensors across the north, east, south and west azimuths per tree) chosen within a 20 m radius of the focal tree at 1.3 m. The sensors were installed on July 17th and 18th, 2017, and sap flux density was recorded at 10 minutes intervals. All sap flow sensors were connected to external 12 V deep cycle marine batteries and charged by 12 W solar panels. The use, set-up, and potential limitations of these HRM sensors have been described previously (Bleby et al., 2004; Burgess and Downey, 2018; Forster, 2017).

Before further processing, the raw heat velocities from the sap flow sensors were corrected for wounding coefficient and sapwood thermal diffusivity (Burgess et al., 2001; Marshall, 1958) using the software Sap Flow Tool (v1.4.1. ICT International Pty Ltd., Armidale, NSW, Australia). To reduce variance, the 10-minutes sap flux densities were averaged into 60 minutes intervals. Small data gaps that occurred during monitoring were filled using a multivariate imputation via chained equation procedure, implemented in the *mice* package in R (van Buuren and Groothuis-Oudshoorn, 2011), assuming the data were missing at random. The data was separated into trunk and crown sensors positions and the procedure applied to each position independently. Following **Chapter 3**, the sap flux density of the most "active" sapwood depth (between the two thermistor depths for each sensor) was corrected for zero-flow using a study-specific correction (*i.e.* average sap flux density measured for each sap flow sensor at nighttime on August 21st and August 22nd, 2017 at the final days of the study). Sap flux density was extrapolated to sap flux (Q, L hr^{-1}) at each sensor location using measured sapwood area from tree disks taken from the focal tree after the study was terminated. For all trunk locations, the sapwood area used for estimating sap flow was represented by a quarter of total sapwood area and centered around the sensor insertion point, measured from

tree disks collected at each sensor position for the focal tree. Sap flux reported for each azimuth (Q_q) thus represents a quarter of the whole tree sap flux (Q or Q_{total}). For the branches (two sensors) and the mid-crown position (one sensor), sap flux was based on to the total sapwood area for each position and sap flux in the branches was averaged between the two sensors installed.

Azimuthal partitioning of sap flow in the trunk

Hourly sap flux density and rate were compared among the four azimuths at each of the three trunk locations independently during the day (11:00 h - 18:00 h) and night (22:00 h - 05:00 h). Those two time periods had relatively stable hourly measurements and were chosen to avoid the transitioning periods of the day (early morning and evening) during which the variability between time measurements obscured the variability between azimuths. A theoretical average hourly sap flux density and rate was calculated as the average of the four azimuthal sap flux densities and as the quarter of whole-tree Q_{total} (equal to the sum of the four azimuthal hourly sap fluxes) to represent a theoretically even distribution of sap flow across the four azimuths. The Dykes and Unwin's chi square statistic (Dykes and Unwin, 2001) χ^2_{DU} (equation (1)) was calculated to assess how the azimuthal variable Var_i (sap flux density $J_{s,i}$ and sap flux rates Q_i) deviated from the expected theoretical average Var_{th}:

$$\chi^2_{DU} = \frac{Var_i - Var_{th}}{\sqrt{Var_{th}}} \qquad (1)$$

Negative values represent less than expected rates and positive values represent greater than expected rates. Daily sap flux (Q_q^d, L d^{-1}) and cumulative water uptake (Q_q^c, L) were calculated for each of the azimuths and trunk locations and compared to their theoretical average equivalent ($Q^d_{th;\,q}$ and $Q^c_{th;\,q}$).

The effects of azimuth on the hourly relationship between sap flux rate and VPD was assessed for each of the trunk locations independently using a Weibull growth curve model for the 24 days of the study. Hourly sap flux rates from each location were normalized in respect to their maximum value, thus removing the effect of differences in sap flow magnitude on the relationship with VPD. The average hysteresis between normalized sap flux rates $Q_{n;\,q}$ and VPD was drawn at each of the trunk locations independently for the four azimuths.

Longitudinal partitioning of sap flows along the height of the tree

Whole-tree sap flow correction: When comparing sap flow rates measured at the different heights along a trunk and within the crown, an assumption of conservation of mass is being made. This assumption is based on the assertion that tree trunks (most specifically sapwood) have a zero daily net water content change and that daily sap flow measured at lower positions on a tree must be equal to the daily sap flow measured at a position higher up or in the crown. As a result, sap flow studies in trees are commonly corrected for this by first transforming the hourly sap flux from higher positions into fractions of their summed daily total flows. These fractional sap flow rates are then multiplied by the daily sap flow total from the lower position (Čermák et al., 2007; Goldstein et al., 1998; James et al., 2003; Kocher et al., 2013; Meinzer et al., 2004; Oliva Carrasco et al., 2015; Phillips et al., 2003; F. G. Scholz et al., 2008). Although commonly used, this correction ("TDW (total daily water) correction" hereafter) excludes the possibility of flow exchanges between and within sapwood and phloem, bark or other woody tissues that could lead to significant differences in flow along the height of the tree.

In this study, the low and mid trunk positions, as well as the sum of the crown fluxes were corrected using the TDW correction with the upper trunk position as reference (most likely to represent the

true volume of water transpired by the crown due to its position). We report here both the uncorrected (Q) and corrected (Q_c) hourly sap fluxes when comparing sap fluxes between different positions along the focal tree. To explore this comparison, the cumulative daily difference between the corrected and uncorrected sap flux rates (Q^d_{excess}) was calculated for the following tree sections: between the low and upper trunk position, between the mid and upper trunk position, and between the sum of the crown fluxes (lower branches and mid crown) and the upper trunk positions. Its relative importance compared to the total daily sap flows of the upper trunk position (taken as reference see above) was calculated as a percentage. Both the difference and the percentage variables were then modelled against mean daily VPD to assess whether atmospheric conditions affected Q^d_{excess} for the different tree sections.

Sap flow partitioning in the crown: The partitioning of sap flux in the crown was assessed by focusing on both sap flux density and sap flux measurements. Hourly sap flux density was averaged across the three lowest crown branches and compared to the sap flux density in the upper crown and upper trunk (averaged across the four azimuths). To assess the relative allocation of total sap flow to the three lower branches, the percentage of daily total tree flows $Q^d_{upper\ trunk}$ represented by each of the three lowest branches was calculated, for both the uncorrected and corrected datasets (see above). We assessed the relationship between the crown fluxes and atmospheric VPD for both the hourly sap flux rates and contribution of these branches to daily trunk flow. For the hourly sap flux rates, the uncorrected and corrected datasets were normalized. Hourly sap flux rates from each location (upper trunk, each of the three branches and upper crown) were normalized in respect to their maximum value, thus removing the effect of differences in sap flow magnitude in response to differences in VPD. An asymptotic regression and a Weibull growth curve were used to model the hourly relationship of normalized sap flux rates Q_n with VPD for the

uncorrected and corrected datasets. The effects of the sensor position within the crown (between the three lowest branches and the upper crown) was assessed on each of the model parameters.

Stem water storage along the trunk: We calculated the daily withdrawal from and recharge of the stem water storage compartment along the trunk of the focal tree. We assessed the stem water storage dynamics at two spatial scales: for each of the azimuths over the entire length of the trunk (*i.e.* between the low and upper trunk positions), and at the whole-trunk scale (*i.e.* across the entire sapwood area, adding up the measurements from the four azimuths) between the low-to-mid, the mid-to-upper and low-to-upper trunk sections. For both scales, the hourly sap flux rates from the lower trunk positions were subtracted from the hourly sap flux rates of the upper trunk positions. We made these calculations for two water storage scenarios:

- **Daily overnight refilling:** in this scenario, the stem store is completely refilled overnight (Čermák et al., 2007), such that the sap flux rate dataset is corrected so that the daily total tree flows are equal across trunk locations. This is equivalent to the data correction described in the methods (TDW correction factor) but named hereafter for the analysis of water storage dynamics as "overnight refilling" assumption. Considering the relatively low daily VPD values during the study period, we believe that this scenario is reasonable as it is likely no extreme stem water deficit occurred and thus the stem water reservoirs could have been completely refilled overnight.
- **Longer-lasting stem water deficit:** under this alternate scenario, a deficit in the stem water storage was allowed to occur over a period of more than a day, a scenario suggested by other studies (Beedlow et al., 2017; Kocher et al., 2013; Phillips et al., 2003; Waring and Running, 1978). Instead of assuming that total daily flows are equal across trunk locations, we assume here that the total tree cumulative water volume at the end of the 24-

day study period is equal across trunk locations - as the focal tree was cut under water without cavitation and immersed in a bucket of water at the end of the 24 days for another 12 days during which no water deficit incurred (see **Chapter 3**). In this case, hourly sap flux at each azimuths and trunk location was transformed into a fraction of their summed cumulative water uptake. These fractional sap flow rates were then multiplied by the total cumulative water uptake from the upper trunk location, chosen as reference. Therefore, the calculated daily flows in and out of the stem water storage did not necessarily match.

For both scenarios, a positive difference between trunk locations indicates inflow to stem water storage - "recharge" - while a negative difference indicates an outflow from stem water storage - "withdrawal". Generalized additive models were used to describe the temporal dynamics of the recharge and withdrawal over a day for each of the azimuths over the entire length of the trunk and for each trunk section at the whole-tree scale. The percentage of daily total flows represented by recharge (comparing to the total daily lower trunk positions flows) and by withdrawal (compared to the total daily upper trunk positions flows) of the stem water storage was calculated under both scenarios. At the whole tree scale, the total daily flows, recharge and withdrawal were related to mean daily VPD for each trunk section using an exponential regression. Cumulative volumes of recharge and withdrawal were calculated over the 24 days of the study and compared to Q^c.

Statistical analyses

All statistical analysis were performed using the R statistical software v3.6.1. (R Development Core Team, 2019). The effects of azimuth, trunk location and other factorial variables were assessed using linear models and generalized least squares to allow for unequal variances and

corrections for normality when necessary. Estimated marginal means and trends were calculated using the package *emmeans* (Lenth, 2018) to summarize the effects of the fixed factors, using 95 % confidence intervals (using $\alpha = 0.05$). Nonlinear models using generalized least squares from the *nlme* package (Pinheiro et al., 2018) were used to assess the relationships between sap flux rates and atmospheric VPD at the hourly and daily timescales, allowing for unequal variances across factor levels when necessary. Each model is described in the Appendix 4.B: Summary statistics.

Results

Azimuthal partitioning of the trunk sap flow

Sap flux density was not uniformly distributed across the azimuths at each trunk location during both day and night periods (Figure 4. 2a). The χ^2_{DU} statistic indicates a significant deviation from the theoretical sap flux density (calculated as the average of the four azimuthal sap flux densities). Those differences in sap flux densities extended to differences in sap flux rates (Figure 4. 2b), with overall a similar pattern among azimuths at each trunk location. The sap flux density of the three control trees showed a different azimuthal pattern than the focal tree during the day. Sap flux density was higher than expected at the west azimuth for the control 1, at the north azimuth for the control tree 3 and the azimuthal partitioning was not as pronounced for the tree control 2 (Appendix Figure 4.B. 1).

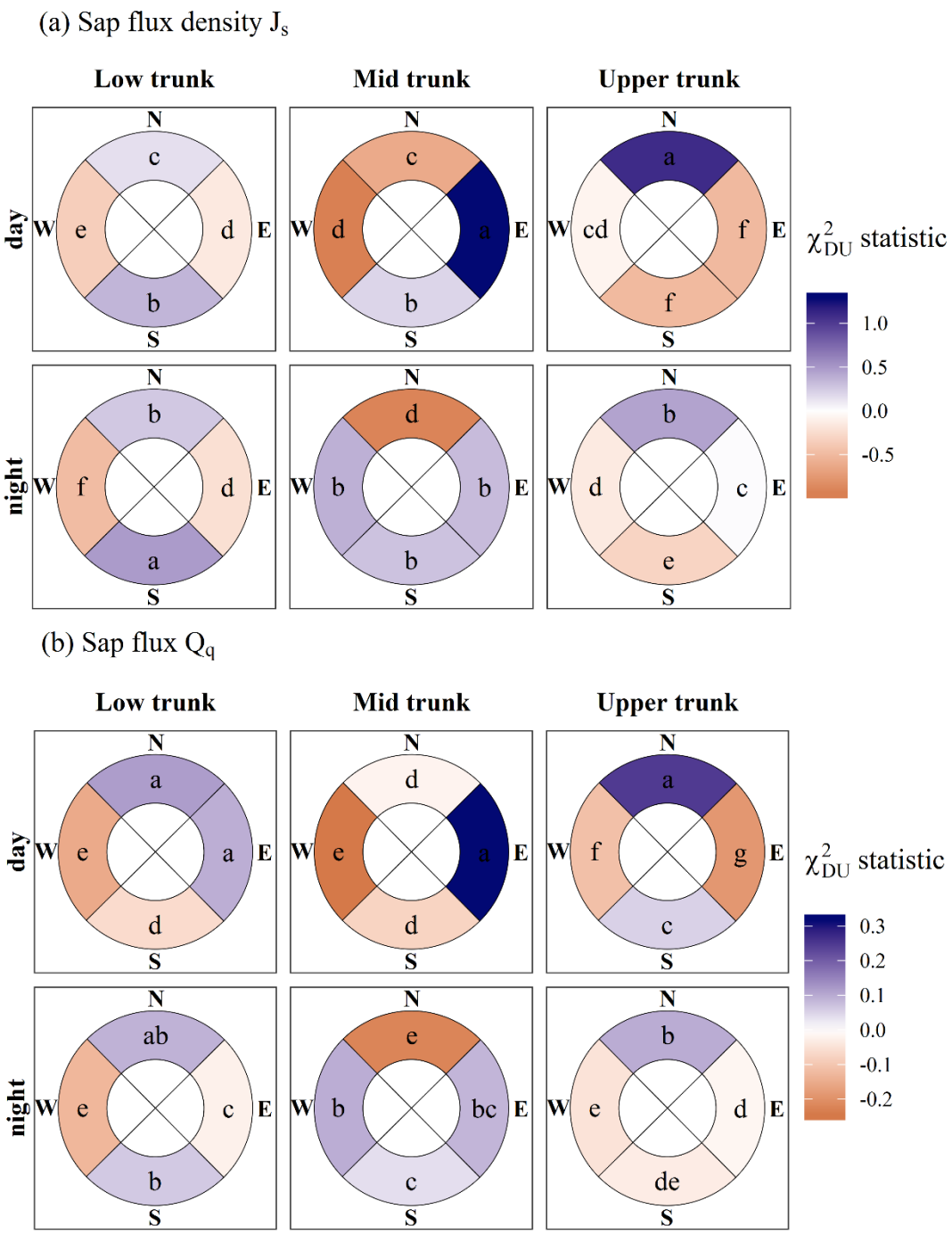

Figure 4. 2. Differences across azimuths between measured and theoretical sap flux density (panel a) and sap flux (panel b) using the Dykes and Unwin χ^2_{DU} statistic for the three trunk locations independently during the day (11:00 h -18:00 h) and night (22:00 h -05:00 h). The colored gradient varies from deep blue (positive values) to deep red (negative values). Letters indicate

statistical significance ($p < 0.05$) for each trunk locations separately, between azimuths and daytime.

The daily difference between the measured azimuthal sap flux rates and the theoretical reached up to 7.5 L d^{-1} for the focal tree, and 12 L d^{-1} for the control trees (Appendix Figure 4.B. 2). These differences cumulated to a difference ranging between 20 and 115 L in Q_q^c for the focal tree during the 24 days of the study (Table 4. 1), representing between 5 and 25% of the whole-tree cumulative water uptake. Similar results were found for the three control trees (results not shown).

Table 4. 1. Difference with theoretical average quarter cumulative water uptake $Q_{th;\,q}^c$ (L) for each of the four azimuths at the three trunk positions of the focal tree and total tree water uptake Q^c for the 24 days of the study. The data was not corrected for the TDW correction.

Focal tree	**Difference from $Q_{th;\,q}^c$** [L]				**Q^c** [L]
	North	**East**	**South**	**West**	
Low trunk	64.4	38.3	-24.6	-78.0	568.9
Mid-trunk	-25.1	116.5	-20.9	-70.6	438.6
Upper trunk	91.2	-65.8	23.5	-48.9	382.6

The differences in hourly sap flux rates among azimuths led to varying degrees of differences in the relationship between the normalized hourly sap flux rates and atmospheric VPD during the day at each of the trunk positions (Appendix Figure 4.B. 3). Normalized sap flux at the west orientation quickly increased to its maximum value with increasing VPD at the mid trunk position. At the upper trunk position however, the rate of increase of $Q_{n;\,q}$ with VPD was higher for the east and south orientations. No differences in the rate of response to VPD were found for the sap flux rates measured in the low trunk position. The hysteresis between $Q_{n;\,q}$ and VPD was similar among azimuths, but significantly increased from the low to the upper trunk position (Appendix Figure 4.B. 3).

Excess sap flow excluded from the TDW correction

When not corrected for TDW, hourly sap flux rates Q at the low and mid trunk positions were higher (more so for the low trunk position) during the period of study than when corrected for TDW (*i.e.* Q_c), while the opposite was true for the crown (Figure 4. 3a). The absolute daily "excess" sap flow Q_{excess}^{d} reached up to 15, 20 and 40 L d^{-1} for the mid trunk, crown and low trunk positions respectively, and was positively correlated to daily VPD. As daily VPD increased, Q_{excess}^{d} increased at a faster rate at the low trunk position compared to the mid trunk and crown positions (Figure 4. 3b). The proportion of Q_{excess}^{d} as part of the daily sap flow also increased as VPD increased (Figure 4. 3c), with the crown showing a greater increase than the trunk positions. Overall, the excess sap flow between the entire crown and the base of the tree ranged between less than 5 L d^{-1} to more than 50 L d^{-1} depending on VPD.

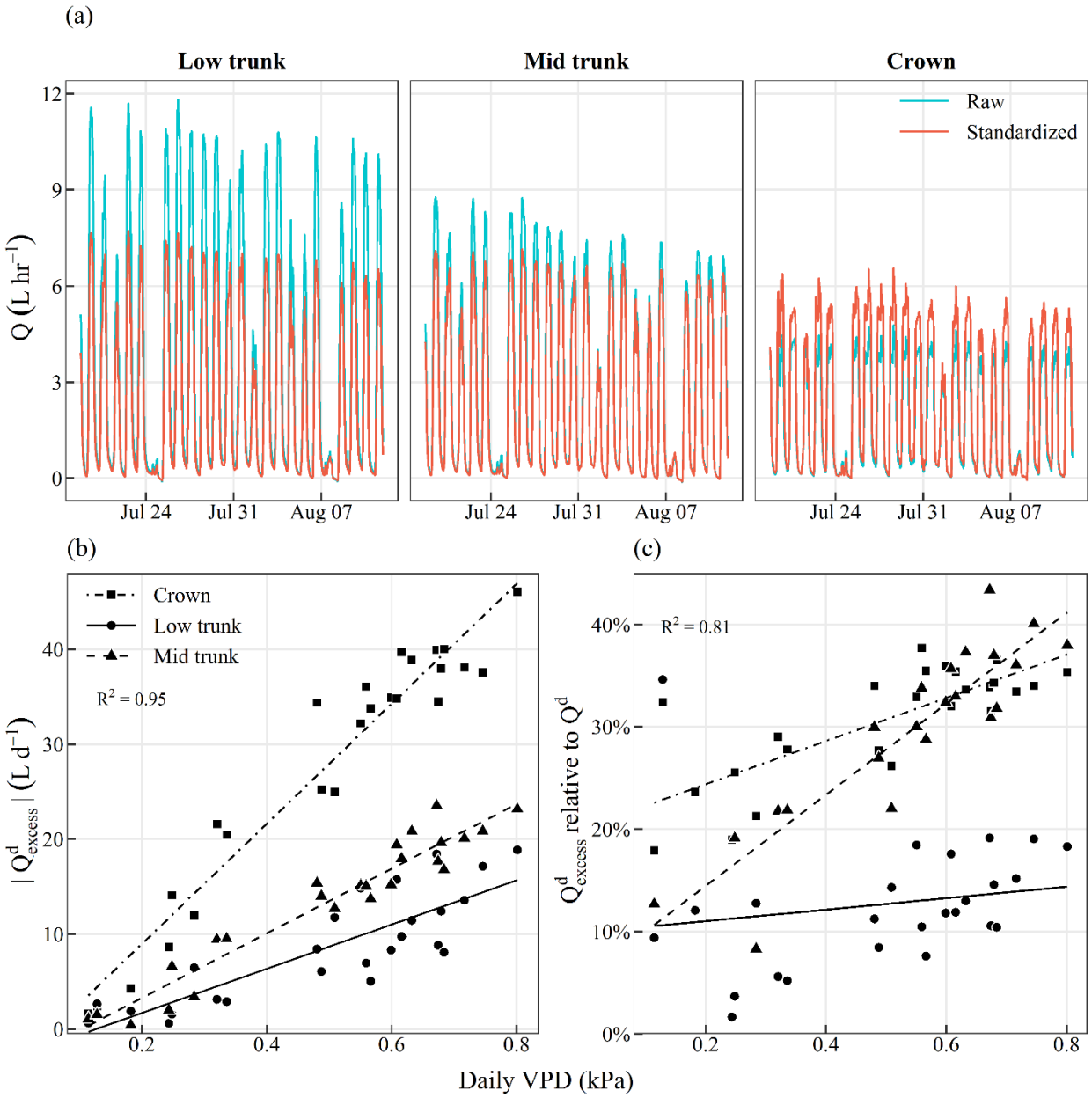

Figure 4. 3. Excess daily sap flow Q^d_{excess} for the low and mid trunk positions and the entire crown (sum of the three lowest branches and the upper crown, see methods). Panel a: uncorrected and corrected hourly sap flow Q (L hr^{-1}). The corrected hourly sap flow is corrected for the TDW correction factor, using the upper trunk position as a reference (see Materials and Methods). Panels b and c: absolute excess daily sap flow Q^d_{excess} expressed as a volume (panel b, L d^{-1}) and as a percentage of uncorrected Q^d (panel c) in relation with daily VPD (kPa) for the crown

(squares, dot-dash line), the low trunk (circles, solid line) and mid trunk (triangles, dotted line) positions. The modeled relationships between Q^d_{excess} and VPD for each trunk position are shown along with the coefficient of determination R^2 of the models.

Partitioning of the sap flow between the lower branches and the rest of the crown

Sap flux density (J_s) of the lower crown branches represented slightly more than one third of the J_s in the upper trunk (0.34 [0.33; 0.35]), while J_s of the upper crown was on average slightly higher than that of the upper trunk (1.19 [1.16; 1.22]) (Figure 4. 4a). No time lag was observed in the onset of sap flux over the course of a day between the upper trunk, the lower branches and the upper crown locations (results not shown). When extrapolating to sap flux rates, the three lower crown branches represented on average less than 3 % of $Q^d_{\text{upper trunk}}$ (Figure 4. 4b and c) while supporting between 8 and 12% of the total crown leaf area. The upper crown (supporting 72 % of the total crown leaf area) represented between 70 - 90 % of $Q^d_{\text{upper trunk}}$ for the uncorrected dataset, and more than 95% for the corrected dataset. Over the duration of the experiment, the relative branch daily sap flux (relative to the upper trunk total sap flux) showed varying relationships with daily VPD depending on the application of the TDW correction (Figure 4. 4c). The uncorrected data showed a significant decline in the relative branch daily sap flux with increasing VPD for all three branches but was less pronounced for branch 1. When applying the TDW correction, only branch 2 showed a similar decrease, while branch 1 showed a slight increase and no relationship was found for branch 3. Following this result, the relative daily sap flux of the upper crown showed a significant decline with increasing VPD for the uncorrected dataset dropping from 90 % to less than 70 % of $Q^d_{\text{upper trunk}}$, while no relationship was found for the corrected dataset (Figure 4. 4c).

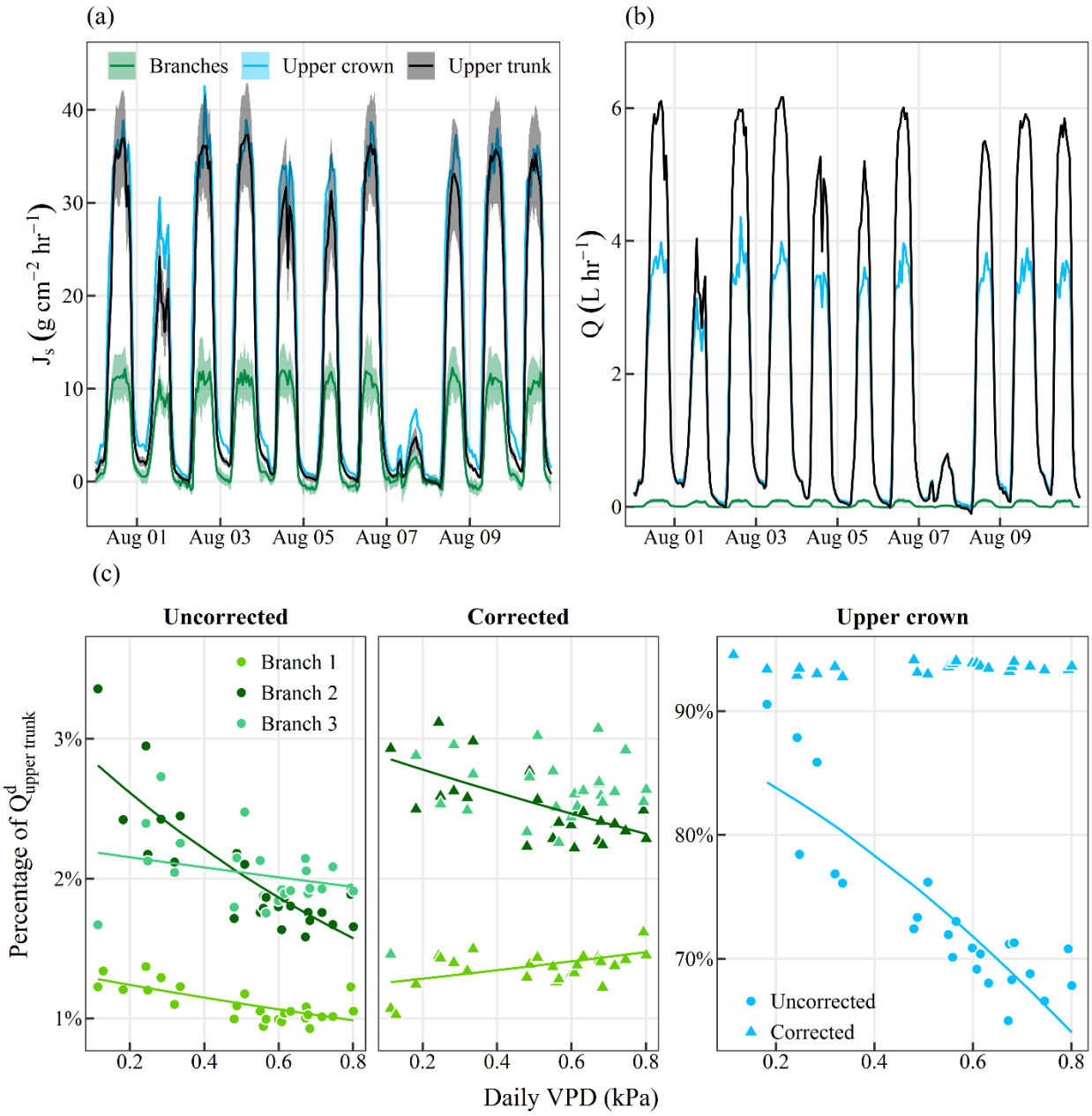

Figure 4. 4. Comparison between the lower branches, upper crown and upper trunk hourly and daily sap flux density and rates. Panels a and b: mean (and standard deviation) hourly sap flux density (J_s, g cm^{-2} hr^{-1}) and uncorrected sap flux rates (Q, L hr^{-1}, panel b) between August 1st, 2017 and August 10th, 2017. Panel c: Branches and upper crown percentage of daily upper trunk flow ($Q^d_{upper\ trunk}$) and VPD (kPa) for the uncorrected (circles) and corrected (triangles) datasets. The

regression lines from the beta-regression models applied to each dataset are shown when significant ($p < 0.05$).

The Weibull growth curve models between normalized hourly sap flux and atmospheric VPD yielded similar parameter estimates between branches and the upper crown, except for branch 2 showing a slightly elevated increase rate. The upper trunk showed elevated asymptote and drop, and decreased rate parameters. No major differences in the Weibull growth curve models were notable between the uncorrected and corrected datasets (Appendix Figure 4.B. 4). Similarly, the correction of the data lead to a slight reduction in the mean hysteresis area but no differences between crown locations.

Functional and spatial partitioning of trunk sap fluxes and dynamics between water storage and transpiration

Daily dynamics

The significant difference in sap flux rate between two trunk positions suggests that stem water storage is a part of the daily sap flow dynamics. Across the entire trunk height (*i.e.* between the low and upper trunk positions), the use of stored water was significant, but was spatially variable among the four azimuths under both refilling scenarios (*i.e.* the daily overnight refilling - Figure 4. 5, and the longer-lasting stem water deficit - Appendix Figure 4.B. 5). For all azimuths, water was withdrawn from the stem reservoir early in the morning (starting at 06:00 h), withdrawal reached its maximum between 09:00 and 10:00 h. Later, the east facing part of the trunk switched over to water storage, reaching its maximum near 14:00 h. On average, the north and south orientations displayed mostly pattern of water withdrawal during the day (Figure 4. 5a). At the whole-tree scale, withdrawal from storage occurred in the morning, reaching just below -1 L hr^{-1}

on average around 09:00 h. The switch to recharge occurred near noon, reaching a maximum of 0.5 L hr^{-1} around 14:00 h (Figure 4. 5b). The whole-tree pattern of recharge-withdrawal of stored water was similar in the low-to-mid and mid-to-upper trunk sections (Figure 4. 5c). The mid-to-upper trunk section showed an earlier switch from withdrawal to recharge (between 11:00 and 12:00 h) than the low-to-mid section (12:00 h) and a late afternoon period of withdrawal between 18:00 and 20:00 h under the overnight refilling assumption. The diurnal patterns were similar under the longer-lasting stem water deficit scenario (Appendix Figure 4.B. 5).

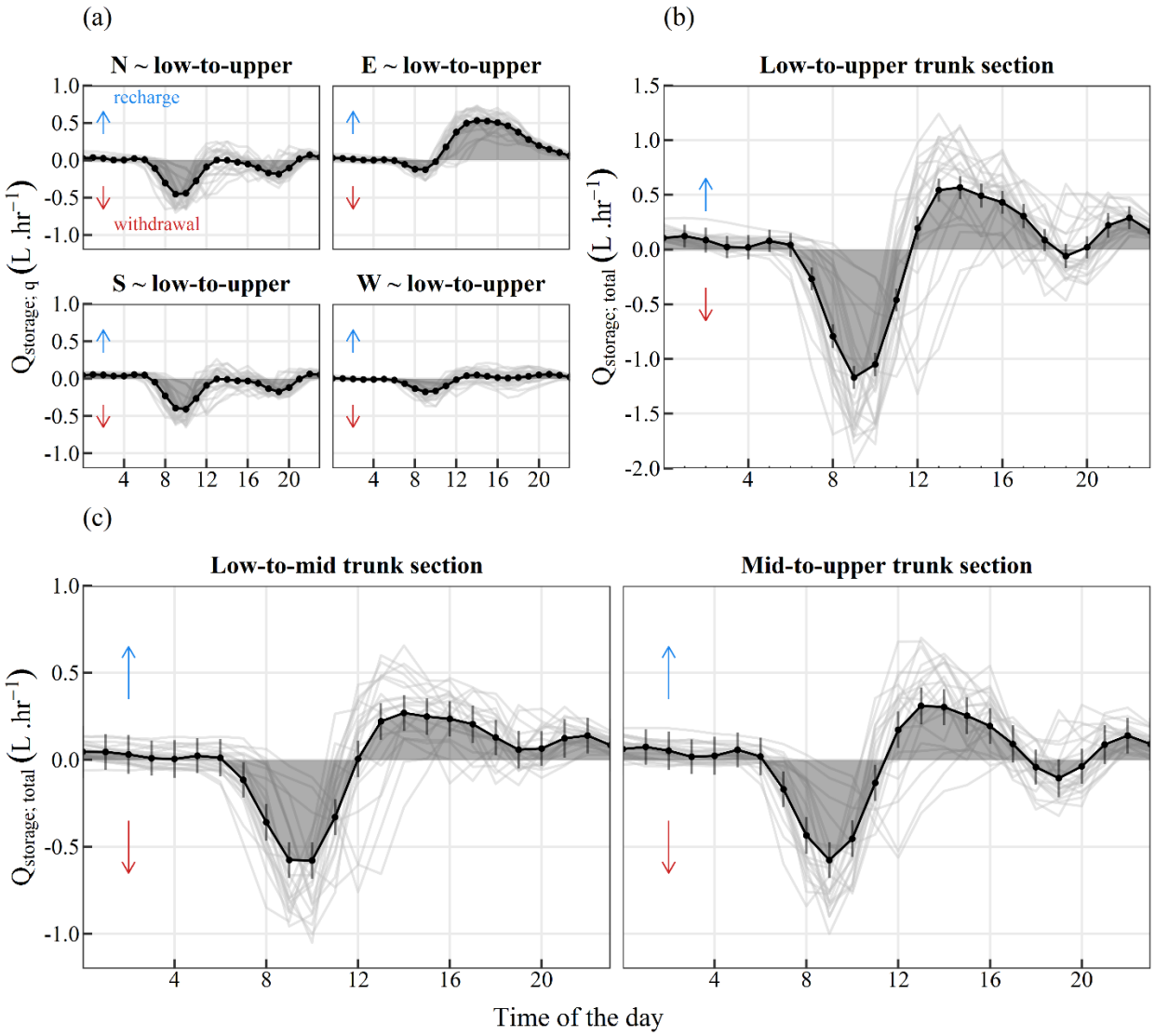

Figure 4. 5. Diurnal recharge and withdrawal $Q_{storage}$ *(L* hr^{-1}*) from the stem reservoir under the overnight refilling scenario (see methods for more detail) between azimuths across the entire trunk height (*$Q_{storage;\ q}$*, low-to-upper trunk section, panel a) or between trunk sections across the entire sapwood area (*$Q_{storage;\ total}$*, panels b and c). For all panels, the results from the generalized additive models fit to assess differences between azimuths (panel a) or trunk sections (panels b and c) are shown as a solid black line, and with pointwise 95% confidence intervals (error bars). The time course of stem reservoir usage for each of the 24 days of the experiment are shown in faded grey*

lines for each of the plots. Negative values indicated water withdrawal between the two trunk height locations, and positive values indicate refilling.

The average amount of stored stem water used per day varied from 0.8 L d^{-1} to 9.3 L d^{-1} between recharge and withdrawal across the four azimuths, ranging between under 10 % to almost 50 % of total daily sap flux (Table 4. 2). The north and south orientations showed larger withdrawal than recharge, while the opposite was true for the east orientation. The west orientation showed relatively balanced volumes of daily recharge and withdrawal. Similar trends were observed under the assumption of long-lasting stem water deficit.

Table 4. 2. Daily use of stored stem water expressed as a percentage relative to total daily sap flux (relative contribution, %) and as an absolute volume (L) split into recharge and withdrawal under the assumption of overnight refilling or long-lasting stem water deficit for each of the azimuths and the whole-tree estimates. Estimated means and 95 % confidence intervals (between brackets) are shown, along with letters indicating statistical difference for each of the assumptions independently.

	Overnight refilling		**Longer-lasting stem water deficit**	
	Recharge	**Withdrawal**	**Recharge**	**Withdrawal**
Relative contribution [%]				
North	5.8 [4.2; 7.7] **d**	26.6 [23.0; 30.4] **b**	8.4 [5.4; 11.4] **d**	28.8 [23.5; 34.1] **b**
East	50.4 [47.3; 53.7] **a**	5.7 [4.7; 6.8] **d**	49.4 [43.5; 55.3] **a**	8.0 [5.1; 10.9] **d**
South	9.1 [7.0; 11.5] **c**	27.0 [23.2; 31.0] **b**	11.7 [8.1; 15.2] **cd**	29.1 [23.8; 34.4] **b**
West	10.6 [6.9; 15.3] **c**	12.4 [8.6; 16.8] **c**	10.7 [7.1; 14.4] **cd**	14.2 [10.2; 18.1] **c**
Whole-tree	13.6 [13.2; 14.1]		14.5 [11.4; 17.6]	16.3 [13.0; 19.5]
Absolute volume [L d^{-1}]				
North	1.10 [0.66; 1.53]	5.24 [4.89; 5.59]	1.28 [0.75; 1.95]	5.40 [4.61; 6.25]

East	**de** 9.29 [8.71; 9.86]	**b** 0.84 [0.39; 1.28]	**cd** 8.56 [7.08; 10.19]	**b** 0.85 [0.55; 1.20]
South	**a** 1.43 [1.06; 1.81]	**e** 4.56 [4.26; 4.86]	**a** 1.59 [0.99; 2.34]	**d** 4.67 [3.94; 5.47]
West	**de** 1.36 [0.71; 2.01]	**c** 1.74 [1.24; 2.24]	**cd** 1.29 [0.73; 2.00]	**b** 1.83 [1.39; 2.34]
Whole-tree	**de** 8.78 [8.30; 9.25]	**d**	**cd** 9.98 [7.327; 12.64]	**c** 9.72 [8.38; 11.06]

Over the 24 days of the study, the total volume of water allocated to the withdrawal from the stem water storage ranged between 20 to 125 L depending on the azimuth, while the cumulative recharge of the storage ranged between 25 to almost 200 L following the daily differences reported above. At the whole-tree scale, stem water storage usage reached 200 L in withdrawal and recharge over 24 days, an approximate 14 % of the cumulative 1443 L.

Relationship with VPD at the tree level

Daily water use was positively related to mean daily VPD for all azimuths and trunk locations (Appendix Figure 4.B. 6a) under both refilling scenarios. At the whole-tree scale, the absolute daily difference in total daily sap flux rate between the two refilling scenarios reached up to 6 L d^{-1} for both the low and mid-trunk positions. As mean daily VPD increased, the daily difference moved from higher daily sap flux rate under the overnight refilling scenario to higher daily sap flux rates under the longer-lasting stem water deficit scenario (Appendix Figure 4.B. 6b).

Usage of stored water also responded to increases in VPD. Daily recharge and withdrawal volumes increased with increasing daily VPD under the overnight refilling scenario for all trunk sections (Figure 4. 6a), however it translated to a slight decrease of its representative percentage of total daily flows (only for the whole-tree and low-to-mid trunk section, at a rate of a drop in 2 % for a unit increase in daily VPD, Figure 4. 6b). Under the longer-lasting stem water deficit scenario, the

withdrawal volume decreased at a rate of 4 L d^{-1} per unit of VPD, while recharge increased from less than 2 L d^{-1} to more than 8 L d^{-1} as daily VPD increased (whole-tree and mid-to-upper trunk section only, Figure 4. 6a). The percentage of total daily flows represented by withdrawal decreased exponentially, dropping from more than 15 % to less than 5 % for all trunk sections. Recharge, however, showed a linear increase with VPD from less than 5 % to slightly above 10 % for the whole-tree and mid-to-upper trunk sections (Figure 4. 6b).

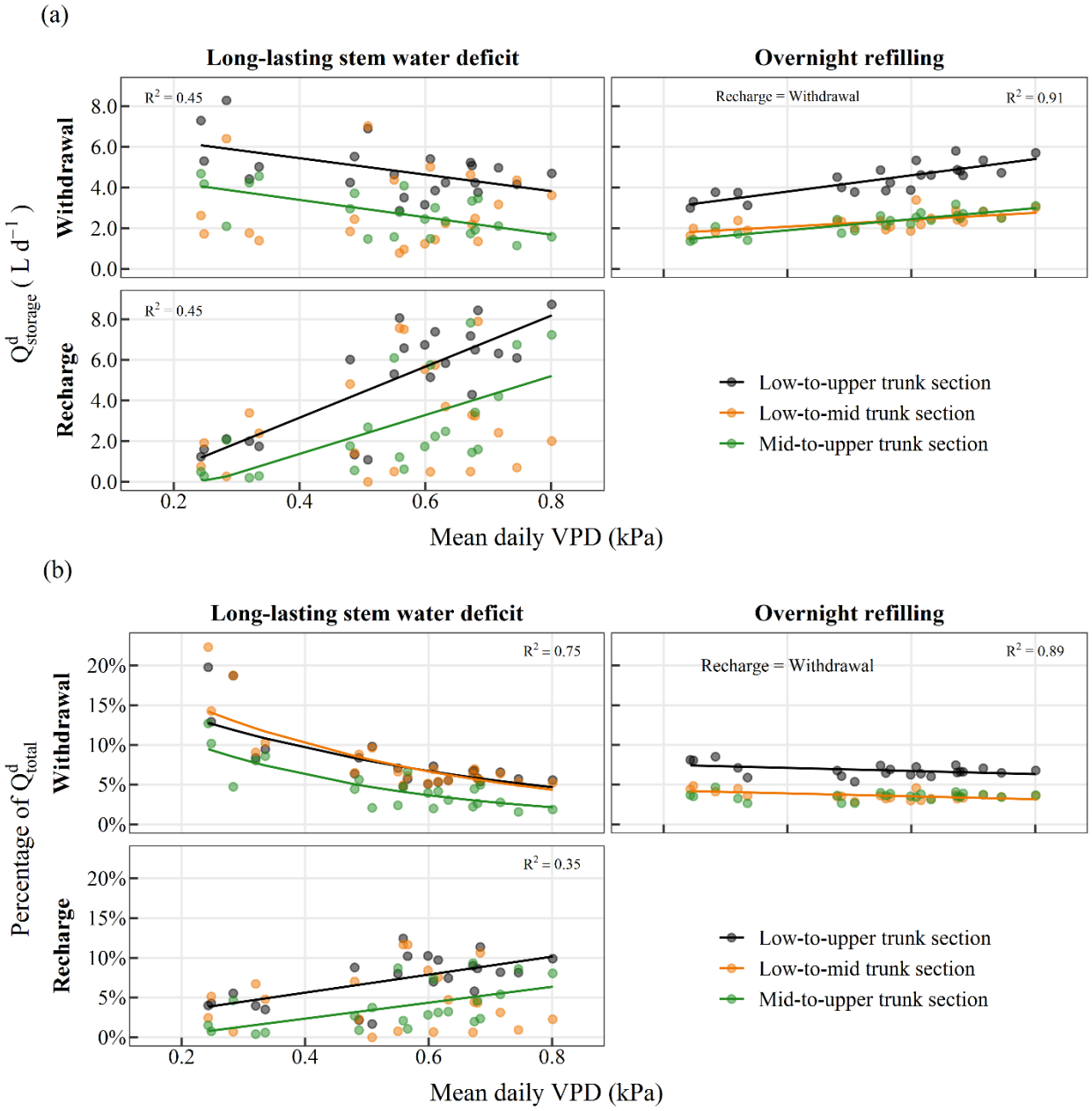

Figure 4. 6. Daily withdrawal and recharge of the stem water storage at each of the trunk sections expressed as a volume (panel a) and a percentage of the total daily flows (panel b) relative to mean daily VPD (kPa) under both refilling assumptions. Significant relationship ($p < 0.05$) with VPD are shown, and the coefficient of determination of the models (R^2) displayed. Per definition, recharge = withdrawal for the overnight refilling assumption.

Discussion

The measurements in this study provide evidence for significant spatial and functional partitioning of sap fluxes within a large diffuse porous tree. Spatial partitioning of sap flux was evident within the crown, along the trunk, and among trunk azimuths. In addition, our results call into question the rationale of using of a correction factor (TDW correction) when comparing sap flux rates among different trunk heights. This research highlights that the differences in sap flux rates between trunk heights might play physiologically important roles, such as the contribution of stem water storage to the daily sap flux.

Azimuthal variation in sap flux density and sap flux rate

Despite the relative symmetry of the focal tree trunk and crown, we observed significant differences in the magnitude of sap flux density and rates among azimuths and the differences changed with trunk height. Differences were more pronounced during daytime compared to the night. Azimuthal variability in sap flow in mature trees has been commonly observed (Loustau et al., 1998; Molina et al., 2016; Sato et al., 2012; Zhang et al., 2018), however, its drivers remain unclear, and may be species-specific and vary genetically and phenotypically. The azimuthal patterns in sap flux density we observed at the low trunk position differed between the focal tree and the three control trees, suggesting that a combination of drivers may be involved in these patterns. Differences in physical, structural and/or hydraulic properties of the conducting sapwood may be the primary drivers for the azimuthal partitioning of sap flow (Barij et al., 2011; Tateishi et al., 2008), which could be further amplified by differences in microclimatic conditions in response to azimuth, particularly during the day (Cabibel et al., 1997; Shinohara et al., 2013; Van de Wal et al., 2015). A sectorization of sap flux based on crown architecture (López-Bernal et al.,

2010; Lu et al., 2000) or root distribution could also drive the azimuthal patterns observed at the base of the tree. However, the inconsistent azimuthal pattern along the trunk suggests that either the impact of crown sectorization was insignificant driver or it interacted with other factors such as wood properties and was therefore not identifiable. The upper trunk position displayed a higher variability in sap flux density and rate among azimuths than the low trunk position, contrary to what Loustau et al. (1998) found in maritime pine. Although the sample size of our study is small, we were able to confirm the dynamics and magnitude of hourly sap flux rates obtained with sap flow sensors with direct gravimetric measurement of hourly water uptake in the focal tree (**Chapter 3**). The results of this study identifies some of the remaining gaps and lack of understanding of the drivers behind vertical and cross-sectional variability in sap flow along the trunk of large trees, such as differences in anatomical traits (Longuetaud et al., 2017; Tyree and Zimmermann, 2002) and their relationship with atmospheric and edaphic conditions (Kim et al., 2014), especially when attempting to extrapolate individual measurements of sap flow to larger scales (Chiu et al., 2016b; Kume et al., 2012; Tsuruta et al., 2010).

Lower crown represents minor fraction of total tree water uptake

The sap flux density and rates of the three lowest branches of the crown did not reflect the leaf area they supported, as daily transpiration rates (*i.e.* sap flux rate per unit of leaf area) were less than a third of the rest of the crown (results not shown). Within-crown variability in leaf traits and microclimatic conditions alter leaf physiology (Bauerle and Bowden, 2011; Niinemets, 2007), vertically structuring the distribution of sap flux in the crown (Herzog et al., 1998; Hinckley and Ritchie, 1970). The three lowest branches sampled in this study represented a minor fraction of the whole-tree water uptake, decreasing with daily VPD. The range of daily VPD experienced in our study was limited, and it may be possible that under higher VPD levels and under drought,

water use efficiency of these lowest branches may improve when conditions are too severe for the upper crown (as shown in defoliation studies, see Quentin et al. (2011), Stephens et al. (2018)). Our study does not allow for further elucidation of the role of these lowest branches under non-limiting and limiting conditions, and thus invites further consideration of partitioning of sap flux dynamics within a mature crown under variable environmental conditions and how it may relate to carbon assimilation. Furthermore, the application of the TDW correction factor significantly modified the modelled relationship between the percentage of daily upper trunk sap flow allocated to the crown and atmospheric VPD. The TDW correction factor masked a general decreasing trend in the proportion of upper trunk sap flow allocated to the crown with increasing VPD. The strong differences seen here in the relationships between the sap flow allocation to the crown with or without the TDW correction factor would potentially be propagated when extrapolating to larger spatial and temporal scales, one of the main goals of sap flow studies. Consequently, there is a need for further investigation and caution around the use of the TDW correction factor when using sap flow sensors at different positions along the trunk and crown of mature trees (see also below).

Large volumes of sap flow found "in excess" along the height of the tree

It has become a common practice to correct the measured sap flux rates when assessing the whole-tree sap flux rates between two positions along the height of the tree, assuming conservation of the water mass from the base to the crown over 24 h (named here the TDW correction) (see methods for a list of references using this correction). The underlying reasons for the use of this correction factor are (or at least appear) not clear. This correction allows to effectively assess the dynamics of stem water storage use along the trunk assuming no net changes in the sapwood daily water content. However, it effectively removes the possibility to detect potentially physiological relevant patterns in sap flux rates between trunk heights. In our tree these differences reached 50 L per day

between the base of the tree and the entire crown in this study, as daily uncorrected sap flux rate declined steadily along the trunk height towards the crown. Overestimation of sap flux at the lower trunk position due to a misestimation of sapwood area could result in these differences, however gravimetric measurements done on the focal tree after August 12th, 2017 invalidate this hypothesis as gravimetric flux rate was similar in magnitude to the sap flow rates measured by the HRM sensors (see **Chapter 3**). The daily "excess" sap volume increased with increasing VPD; thus, it is more likely to be physiologically significant. Corticular photosynthesis, refixating woody tissue CO_2 (Foote and Schaedle, 1978; Pfanz et al., 2002; Tarvainen et al., 2018), may constitute one of the sinks for the excess sap flow, however its quantification and relationship with sap flow in mature trees remains relatively understudied (but see Bloemen et al. 2016). Exchanges of water between the xylem and phloem may be another potential driver of the observed excess sap flow. Xylem and phloem are hydraulically connected, and advances in understanding phloem flow consider the importance of radial water flows for the phloem transport pathway and NSC translocation (Daudet et al., 2002; Hesse et al., 2019; Nikinmaa et al., 2014; Stanfield et al., 2019; Windt et al., 2006). Further studies with high-resolution spatial and temporal measurements of xylem sap flow in mature trees could focus on the fate of xylem sap flow and its connections with other tissues when travelling from the base of the tree to the crown to further elucidate the importance and role of the excess sap flow and the relevance of the TDW correction.

Uneven stem water storage between azimuths and relationship with VPD

We observed substantial use of stem water storage to support daily sap flux rates in this large tree. The stored water is *a priori* constituted mainly of the elastic symplastic reservoir from which water can be transiently drawn out to buffer short-term diurnal water stress and maximize carbon assimilation (Betsch et al., 2011; Pfautsch et al., 2015), especially for diffuse-porous deciduous

species (Oliva Carrasco et al., 2015) such as aspen. Regardless of the refilling scenario used, total tree water storage recharge and withdrawal represented on average 15 % of the total daily sap flux rates, ranging between 2 L d^{-1} to 10 L d^{-1}, well within previous reports for broadleaved mature trees (Kocher et al., 2013; Oliva Carrasco et al., 2015; Phillips et al., 2003; F. C. Scholz et al., 2008). The stem water storage dynamics varied notably among azimuths, which has rarely been reported (but see Nadezhdina et al. 2015). Recharge was significantly larger in the east aspect, close to 50 % of the total daily east sap flux, while withdrawal was mainly in the north and south aspects. Lateral exchanges of stored stem water (Tyree and Zimmermann, 2002) combined with a differential distribution of wood properties related to the elastic water storage reservoir (Jupa et al., 2016; Morris et al., 2016; Oliva Carrasco et al., 2015; Pratt and Jacobsen, 2017) between azimuths could explain this pattern. Diverging exposures to microclimatic conditions and solar radiation between the azimuths in the crown (Burgess and Dawson, 2008) may further limit or accentuate the azimuthal variation in use of the elastic water reservoir (Zweifel and Häsler, 2001). Our study design does not allow for further exploration of this pattern; however, it provides the basis on which to build an understanding of the potentially inequal use of the elastic water storage in the stem between azimuths.

Outside of azimuthal differences in the use of the elastic water reservoir, the daily relationship in recharge and withdrawal with VPD depended on the refilling scenarios we considered, and the positions along the trunk. Under the overnight refilling scenario, the daily volume withdrawn from storage (and by extension daily recharged) increased with increasing VPD. Increased evaporative demand early in the day should lead to an increased transpiration demand, increasing the volume of water withdrawn from storage provided that the stem water storage is not depleted (Kocher et al., 2013). Later in the day, this increased VPD may lead to stomatal closure, reducing the

transpiration demand. This reduced transpiration may not immediately translate to a synchronous decrease in sap flux rates in the trunk if xylem tensions persist (Perämäki et al., 2005), increasing the recharge and relieving the remaining xylem tensions. The decrease of the absolute volume of sap withdrawn from storage under the alternate refilling scenario suggests that even over the limited range of daily VPD experienced by our focal tree, the refilling of the elastic stem water storage was incomplete and happened over several days, decreasing the amount of water available for withdrawal. Incomplete overnight refilling following several days with high VPD could contribute to an increasing water deficit, limiting withdrawal and thus decreasing the relative fraction of daily sap flux available for withdrawal from storage. It is important to note however that the difference in total daily flows between the two refilling scenarios remained relatively small in our study, under 7 L d^{-1}. This suggests that under the atmospheric conditions experienced during our study, the development of a longer-lasting stem water deficit was limited. Nonetheless, the mechanisms governing the use of the elastic stem water storage in large trees remain unclear, and the limited range of daily VPD values experienced by the aspen tree in our study limits the interpretation of our results. Expanding this study to a wider range of daily VPD testing the limits of the elastic stem water storage and further exploring the mechanisms governing its use is a promising research avenue to better understand tree hydraulic functioning and the role of elastic stem water storage under non-limiting and limiting climatic conditions.

Overall, this study highlights the complexity of the partitioning of sap flux within a large tree, both spatially (among azimuths within the trunk, trunk positions, and between branches in the crown) and functionally (the large volumes of "excess" sap flow and dynamic use of the elastic stem water storage). The interpretation of the observed results was somewhat limited as our study was restricted by focusing on a single large trembling aspen, and temporally, by being able to explore

a reduced range of climatic conditions that were experienced during the study. Nonetheless, this study is based on measurements that were validated gravimetrically (**Chapter 3**) and provides a fundamental basis for further exploration of the spatial and temporal xylem sap flow dynamics in large trees, eventually leading to improved modelling of forest water use at multiple spatial and temporal scales.

CHAPTER 5: General conclusions and perspectives

The focus of this PhD thesis was to explore some of the limits, challenges and opportunities associated with the use of heat ratio method sap flow sensors to monitor and quantify tree water fluxes. In this concluding chapter, I briefly summarize the findings of each research chapter, review their combined contributions and suggest future research directions using sap flow sensors.

Using sap flow sensors to estimate transpiration rate at the stand level

In **Chapter 2**, I examined the impact of rooting space and soil water availability on the leaf area development, rooting characteristics and water uptake dynamics of 15-year-old trembling aspen and white spruce planted in a forest reclamation landscape using sap flow sensors. The smaller size of the sampled trees, together with the focus on differences between treatment and temporal dynamics rather than absolute water uptake values provided confidence in the results, despite the uncertainties and knowledge gaps still remaining in the use of sap flow sensors as seen in **Chapters 3** and **4**. In this first chapter, we observed a species-specific response of leaf area development and its connection with water uptake to rooting space and topographical position. As a deeper-rooted species (Bauhus and Messier, 1999; Strong and LaRoi, 1983), trembling aspen was most limited by shallow rooting space (thin cover soil), while topographical position (upper vs. lower slope) had a much stronger impact on white spruce. During the 2014 and 2015 growing seasons, sap flow decreased with soil moisture declines. Interestingly, white spruce was able to respond positively to a stochastic precipitation event during the dry period, showing a significantly larger rebound of sap flux rate compared to aspen. The combination of morphological measurements and use of sap flow sensors highlighted that physiological and morphological differences between the two species were the main drivers to responses to rooting space availability and the variability in atmospheric

and edaphic conditions. It is important to note however that these results were obtained during two years of study only. Setting up a study on a longer term and achieving a more explicit mapping of the soil water resource across the site would have helped to further explain the observed patterns of sap flux rates during the growing season.

Spatial variability in sap flux density and data-processing methods impact the accuracy of the HRM sap flow sensors on large trees

In **Chapter 3**, I examined the influence of the azimuthal position of the HRM sap flow sensor and the application of different data-processing procedures on the accuracy of sensor estimates of whole-tree water uptake compared to gravimetric measurements on a large mature tree. The cutting procedure is operationally challenging, labor-intensive and represents highly artificial conditions. The removal of the entire belowground section of the tree contributed to a strong modification of the physiology of the tree, as transpiration and thus sap flow steadily declined after the cut, further restricting the amount of available data most closely resembling natural field conditions. Nonetheless, this method is among the few techniques which can provide an accurate estimation of the precision of sap flow sensors when installed in large trees. The results of the study showed that by far, the azimuthal positioning of a sap flow sensor had the largest impact on the whole tree sap flow estimate, along with the radial variability of sap flux density across the sapwood depth. In contrast, the methods used to determine the baseline or zero-flow and to calculate sapwood area had a much lesser impact on the hourly sap flow rate. The cumulative whole-tree water uptake obtained across azimuthal position and data-processing procedures applied diverged from “true” (gravimetric) water uptake by less than 2% to more than 50%, showing remarkable variability. However, little consensus arose across the diverse metrics used in this study to assess the sensors’ accuracy to be able to extract the best available method for each of the data-processing procedures

regardless of azimuthal positioning of the sap flow sensors. Nonetheless, this study follows the steps of recent studies in ascertaining the accuracy of sap flow sensors (Flo et al., 2019; Forster et al., 2019; Forster, 2017; Fuchs et al., 2017) and lays the foundation for improved methodology to explicitly and systematically handle uncertainties across current and future sap flow studies.

Refining our understanding of the spatial and functional partitioning of sap flow in large trees

Chapter 4 aimed to investigate how the data provided by an extensive deployment of sap flow sensors across a large tree can offer insights in the spatial and functional partitioning of sap flow. Following **Chapter 3**'s results, sap flux density and sap flow were heterogeneously distributed across azimuths, but also along the trunk height and within the canopy. This research highlighted that lateral movements of water along the trunk height were significant and measured differences in sap flow were likely the result of interactions among anatomical traits and microclimatic and edaphic conditions (Barij et al., 2011; López-Bernal et al., 2010; Molina et al., 2016; Van de Wal et al., 2015; Zhang et al., 2018). In addition to spatial partitioning, we observed a significant difference in daily sap flow along the height of the trunk, between 10 and 50 L per day, linearly increasing with atmospheric evaporative demand. Although **Chapter 3** highlighted the uncertainty associated with sap flow sensor measurements, we are confident in the difference estimates between trunk heights reported here, suggesting that between 5 and 40 % of the sap flux rate measured at the base of the tree does not reach the top of the tree to support daily transpiration, and may instead be exchanged with surrounding tissues such as parenchyma and phloem, supporting corticular photosynthesis and/or phloem flow (Hesse et al., 2019; Stanfield et al., 2019; Tarvainen et al., 2018). Once this « excess » sap flow has been taken into account, data in **Chapter 4** shows that water used in stem water storage represented on average 15 % of the total daily sap flows with distinct differences in the contribution among azimuths, supporting early transpiration

rate and refilling depleted reservoirs and relieving xylem tensions in the afternoon and night (Kocher et al., 2013; Oliva Carrasco et al., 2015; Perämäki et al., 2005; Tyree and Zimmermann, 2002).

Altogether, the three data chapters highlight that heat pulse sap flow sensors are a crucial tool for improving our understanding of the spatial and temporal dynamics of trees' water relations, however they may not be the most reliable and accurate tool when a precise quantification of whole-tree water uptake sought. This may be particularly true when used with large trees, which may display a strong spatial partitioning of sap flow across their sapwood area or along the length of the trunk as shown in **Chapter 4**. Continuous work on validating and improving the current sap flow methods is vital for proper use and data interpretation. Overcome the sensors' limitation in their measurement range across tree species and sizes (Forster et al., 2019; Testi and Villalobos, 2009) is essential for future use of sap flow sensors across the world's forests. Providing explicit frameworks for data processing (Oishi et al., 2016; Rabbel et al., 2016) and for handling uncertainties in existing sap flow datasets are necessary for the interpretation and comparison of sap flow datasets across studies (Poyatos et al., 2016). Beyond resolving their current methodological limitations, the use of sap flow sensors might greatly advance our understanding of how water flows in tree stems. Water flow from the roots, along the stem to the canopy appears not to be a straight-forward unidirectional and homogeneous flow, isolated from its surroundings. Combining sap flow sensors with other methods (dendrometers, imagery, etc.) might allow us to map and quantify the temporal and spatial relationships between sap flow, stem water storage and water exchanges with neighboring tissues (Brodersen et al., 2016; Cochard et al., 2015; Fromm et al., 2001; Longuetaud et al., 2016; Mares et al., 2016; Mencuccini et al., 2017; Nagata et al., 2016;

Nolf et al., 2015). This will enable us to expand on the findings of this dissertation and explore questions in tree ecophysiology such as:

- Does the spatial distribution of sap flux within the stem or canopy change following a disturbance (such as mechanical damage to the stem or canopy) to maintain the water demands and productivity of the canopy?
- What is the significance of the exchange of water between the xylem and the phloem across tree sizes? What role do internal (wood properties) and external (microclimatic and edaphic conditions) factors play in the water exchanges dynamics?
- How does tree size affect the volume and availability of the elastic water pool supporting total daily transpiration across a climatic gradient?
- Can recovery and mortality patterns observed in the field be explained by differential depletion in the elastic and capillary (capacitive effect of cavitation) water pools?

While this PhD work was mainly focused on the aboveground water flows, it invites considering the temporal and spatial distribution of sap flow in the belowground root system, and consider these following questions:

- Is there redundancy within the root system of small to large trees in root water uptake? In other words, is root water uptake plastic to accommodate for the removal of a substantial part of the root system?
- Is root water uptake homogeneously distributed in space and time, and how does it interact with edaphic conditions?
- What is the role for hydraulic redistribution in supporting aboveground sap flow and transpiration in large trees?

Overall, obtaining a detailed understanding of trees' water relations across tree sizes will improve the extrapolations made from individual tree-level water fluxes to stand and landscape-level (Aranda et al., 2012; Chiu et al., 2016a) as well as improve the models linking vegetation water uptake measured with sap flow sensors and hydrological fluxes in the soil and atmosphere (Asbjornsen et al., 2011; Rabbel et al., 2018) to better understand how current and future forested landscapes will respond to global changes in climate and water availability.

REFERENCES

Alberta Climate Information Service (ACIS), 2018. Interpolated weather data since 1961 for Alberta townships [WWW Document]. URL https://agriculture.alberta.ca/acis/alberta-weather-data-viewer.jsp (accessed 9.10.17).

Alberta Parks, 2015. Natural Regions and Subregions of Alberta. A Framework for Alberta's Parks. Alberta Tourism, Parks and Recreation., Edmonton, Alberta.

Allen, C.D., Breshears, D.D., 1998. Drought-induced shift of a forest-woodland ecotone: Rapid landscape response to climate variation. Proc. Natl. Acad. Sci. 95, 14839–14842. doi:10.1073/pnas.95.25.14839

Allen, C.D., Breshears, D.D., McDowell, N.G., 2015. On underestimation of global vulnerability to tree mortality and forest die-off from hotter drought in the Anthropocene. Ecosphere 6, 1–55. doi:10.1890/ES15-00203.1

Almeida-Rodriguez, A.M., Hacke, U.G., 2012. Cellular localization of aquaporin mRNA in hybrid poplar stems. Am. J. Bot. 99, 1249–1254. doi:10.3732/ajb.1200088

Anderegg, W.R.L., Plavcová, L., Anderegg, L.D.L., Hacke, U.G., Berry, J.A., Field, C.B., 2013. Drought's legacy: multiyear hydraulic deterioration underlies widespread aspen forest die-off and portends increased future risk. Glob. Chang. Biol. 19, 1188–1196. doi:10.1111/gcb.12100

Andréassian, V., 2004. Waters and forests: from historical controversy to scientific debate. J. Hydrol. 291, 1–27. doi:10.1016/J.JHYDROL.2003.12.015

Aranda, I., Forner, A., Cuesta, B., Valladares, F., 2012. Species-specific water use by forest tree species: From the tree to the stand. Agric. Water Manag. 114, 67–77. doi:10.1016/J.AGWAT.2012.06.024

Arndt, C.H., 1929. The Movement of Sap in *Coffea arabica* L. Am. J. Bot. 16, 179. doi:10.2307/2435746

Asbjornsen, H., Goldsmith, G.R., Alvarado-Barrientos, M.S., Rebel, K., Van Osch, F.P., Rietkerk, M., Chen, J., Gotsch, S., Tobon, C., Geissert, D.R., Gomez-Tagle, A., Vache, K., Dawson, T.E., 2011. Ecohydrological advances and applications in plant-water relations research: a review. J. Plant Ecol. 4, 3–22. doi:10.1093/jpe/rtr005

Axelsson, E.P., Grady, K.C., Lardizabal, M.L.T., Nair, I.B.S., Rinus, D., Ilstedt, U., 2019. A pre-adaptive approach for tropical forest restoration during climate change using naturally occurring genetic variation in response to water limitation. Restor. Ecol. 1–10. doi:10.1111/rec.13030

Bakker, M.R., Augusto, L., Achat, D.L., 2006. Fine root distribution of trees and understory in mature stands of maritime pine (*Pinus pinaster*) on dry and humid sites. Plant Soil 286, 37–51. doi:10.1007/s11104-006-9024-4

REFERENCES

Bär, A., Hamacher, M., Ganthaler, A., Losso, A., Mayr, S., 2019. Electrical resistivity tomography: patterns in *Betula pendula*, *Fagus sylvatica*, *Picea abies* and *Pinus sylvestris*. Tree Physiol. 39, 1262–1271. doi:10.1093/treephys/tpz052

Barbour, S.L., Chanasyk, D., Hendry, J., Leskiw, L., Macyk, T., Mendoza, C., Naeth, A., Nichol, C., O'Kane, M., Purdy, B., Qualizza, C., Quideau, S., Welham, C., 2007. Soil Capping Research in the Athabasca Oil Sands Region, vol. 1, Technology Synthesis. Syncrude Canada Ltd.

Barij, N., Čermák, J., Stokes, A., 2011. Azimuthal variations in xylem structure and water relations in cork oak (*Quercus suber*). IAWA J. 32, 25–40. doi:https://doi.org/10.1163/22941932-90000040

Barrett, D.J., Hatton, T.J., Ash, J.E., Ball, M.C., 1995. Evaluation of the heat pulse velocity technique for measurement of sap flow in rainforest and eucalypt forest species of south-eastern Australia. Plant, Cell Environ. 18, 463–469. doi:10.1111/j.1365-3040.1995.tb00381.x

Bathke, G.R., Cassel, D.K., Hargrove, W.L., Porter, P.M., 1992. Modification of soil physical properties and root growth response. Soil Sci. 154, 316–329.

Bauerle, W.L., Bowden, J.D., 2011. Separating foliar physiology from morphology reveals the relative roles of vertically structured transpiration factors within red maple crowns and limitations of larger scale models. J. Exp. Bot. 62, 4295–307. doi:10.1093/jxb/err156

Bauhus, J., Messier, C., 1999. Soil exploitation strategies of fine roots in different tree species of the southern boreal forest of eastern Canada. Can. J. For. Res. 29, 260–273. doi:10.1139/x98-206

Beck, P.S.A., Juday, G.P., Alix, C., Barber, V.A., Winslow, S.E., Sousa, E.E., Heiser, P., Herriges, J.D., Goetz, S.J., 2011. Changes in forest productivity across Alaska consistent with biome shift. Ecol. Lett. 14, 373–379. doi:10.1111/j.1461-0248.2011.01598.x

Beedlow, P.A., Waschmann, R.S., Lee, E.H., Tingey, D.T., 2017. Seasonal patterns of bole water content in old growth Douglas-fir (*Pseudotsuga menziesii* (Mirb.) Franco). Agric. For. Meteorol. 242, 109–119. doi:10.1016/J.AGRFORMET.2017.04.017

Bennett, A.C., McDowell, N.G., Allen, C.D., Anderson-Teixeira, K.J., 2015. Larger trees suffer most during drought in forests worldwide. Nat. Plants 1, 1–5. doi:10.1038/nplants.2015.139

Berdanier, A.B., Clark, J.S., 2018. Tree water balance drives temperate forest responses to drought. Ecology 99, 2506–2514. doi:10.1002/ecy.2499

Berdanier, A.B., Miniat, C.F., Clark, J.S., 2016. Predictive models for radial sap flux variation in coniferous, diffuse-porous and ring-porous temperate trees. Tree Physiol. 36, 932–941. doi:10.1093/treephys/tpw027

Bernacchi, C.J., VanLoocke, A., 2015. Terrestrial ecosystems in a changing environment: a dominant role for water. Annu. Rev. Plant Biol. 66, 599–622. doi:10.1146/annurev-arplant-043014-114834

REFERENCES

Bertrand, G., Masini, J., Goldscheider, N., Meeks, J., Lavastre, V., Celle-Jeanton, H., Gobat, J.-M., Hunkeler, D., 2014. Determination of spatiotemporal variability of tree water uptake using stable isotopes ($\delta^{18}O$, $\delta^{2}H$) in an alluvial system supplied by a high-altitude watershed, Pfyn forest, Switzerland. Ecohydrology 7, 319–333. doi:10.1002/eco.1347

Betsch, P., Bonal, D., Breda, N., Montpied, P., Peiffer, M., Tuzet, A., Granier, A., 2011. Drought effects on water relations in beech: The contribution of exchangeable water reservoirs. Agric. For. Meteorol. 151, 531–543. doi:10.1016/J.AGRFORMET.2010.12.008

Bladon, K.D., Silins, U., Landhäusser, S.M., Lieffers, V.J., 2006. Differential transpiration by three boreal tree species in response to increased evaporative demand after variable retention harvesting. Agric. For. Meteorol. 138, 104–119. doi:10.1016/J.AGRFORMET.2006.03.015

Blake, T.J., Li, J., 2003. Hydraulic adjustment in jack pine and black spruce seedlings under controlled cycles of dehydration and rehydration. Physiol. Plant. 117, 532–539. doi:10.1034/j.1399-3054.2003.00059.x

Blake, T.J., Sperry, J.S., Tschaplinski, T.J., Wang, S.S., 1996. Water relations, in: Stettler, R.F., Bradshaw, H.D.J., Heilman, P.E., Hinckley, T.M. (Eds.), Biology of *Populus* and Its Implications for Management and Conservation. NRC Research Press, National Research Council of Canada, Ottawa, ON, pp. 401–422.

Blanken, P.D., 1997. Evaporation within and above a boreal aspen forest. PhD thesis. University of British Columbia.

Bleby, T.M., Burgess, S.S.O., Adams, M.A., 2004. A validation, comparison and error analysis of two heat-pulse methods for measuring sap flow in *Eucalyptus marginata* saplings. Funct. Plant Biol. 31, 645. doi:10.1071/FP04013

Bloemen, J., Vergeynst, L.L., Overlaet-Michiels, L., Steppe, K., 2016. How important is woody tissue photosynthesis in poplar during drought stress? Trees 30, 63–72. doi:10.1007/s00468-014-1132-9

Bockstette, S.W., Pinno, B.D., Dyck, M.F., Landhäusser, S.M., 2017. Root competition, not soil compaction, restricts access to soil resources for aspen on a reclaimed mine soil. Botany 95, 685–695. doi:10.1139/cjb-2016-0301

Boland, A.M., Jerie, P.H., Mitchell, P.D., Goodwin, I., Connor, D.J., 2000. Long-term effects of restricted root volume and regulated deficit irrigation on peach: II. Productivity and water use. J. Am. Soc. Hortic. Sci. 125, 143–148.

Bolte, A., Ammer, C., Löf, M., Madsen, P., Nabuurs, G.-J., Schall, P., Spathelf, P., Rock, J., 2009. Adaptive forest management in central Europe: Climate change impacts, strategies and integrative concept. Scand. J. For. Res. 24, 473–482. doi:10.1080/02827580903418224

Bonan, G.B., 2008. Forests and Climate Change: Forcings, Feedbacks, and the Climate Benefits of Forests. Science (80-.). 320, 1444–1449. doi:10.1126/SCIENCE.1155121

Bonan, G.B., 1992. Soil temperature as an ecological factor in boreal forests, in: Shugart, H.H., Leemans, R., Bonan, G.B. (Eds.), A Systems Analysis of the Global Boreal Forest.

Cambridge University Press, Cambridge, pp. 126–143. doi:10.1017/CBO9780511565489.005

Børja, I., Světlík, J., Nadezhdin, V., Čermák, J., Rosner, S., Nadezhdina, N., 2016. Sap flux – a real time assessment of health status in Norway spruce. Scand. J. For. Res. 31, 450–457. doi:10.1080/02827581.2015.1130851

Bottero, A., D'Amato, A.W., Palik, B.J., Bradford, J.B., Fraver, S., Battaglia, M.A., Asherin, L.A., 2017. Density-dependent vulnerability of forest ecosystems to drought. J. Appl. Ecol. 54, 1605–1614. doi:10.1111/1365-2664.12847

Brédoire, F., Nikitich, P., Barsukov, P.A., Derrien, D., Litvinov, A., Rieckh, H., Rusalimova, O., Zeller, B., Bakker, M.R., 2016. Distributions of fine root length and mass with soil depth in natural ecosystems of southwestern Siberia. Plant Soil 400, 315–335. doi:10.1007/s11104-015-2717-9

Brodersen, C.R., Rico, C., Guenni, O., Pittermann, J., 2016. Embolism spread in the primary xylem of *Polystichum munitum* : implications for water transport during seasonal drought. Plant. Cell Environ. 39, 338–346. doi:10.1111/pce.12618

Brunner, I., Herzog, C., Dawes, M.A., Arend, M., Sperisen, C., 2015. How tree roots respond to drought. Front. Plant Sci. 6, 547. doi:10.3389/fpls.2015.00547

Buma, B., Barrett, T.M., 2015. Spatial and topographic trends in forest expansion and biomass change, from regional to local scales. Glob. Chang. Biol. 21, 3445–3454. doi:10.1111/gcb.12915

Burgess, S.S.O., Adams, M.A., Turner, N.C., Beverly, C.R., Ong, C.K., Khan, A.A.H., Bleby, T.M., 2001. An improved heat pulse method to measure low and reverse rates of sap flow in woody plants. Tree Physiol. 21, 589–598. doi:10.1093/treephys/21.9.589

Burgess, S.S.O., Bleby, T.M., 2006. Redistribution of soil water by lateral roots mediated by stem tissues. J. Exp. Bot. Bot. 57, 3283–91. doi:10.1093/jxb/erl085

Burgess, S.S.O., Dawson, T.E., 2008. Using branch and basal trunk sap flow measurements to estimate whole-plant water capacitance: a caution. Plant Soil 305, 5–13. doi:10.1007/s11104-007-9378-2

Burgess, S.S.O., Downey, A., 2018. SFM1 Sap Flow Meter Manual. ICT International Pty Ltd. Armidale, NSW, Australia.

Cabibel, B., Isbérie, C., Horoyan, J., 1997. Flux de sève et alimentation hydrique de cerisiers irrigués ou non en localisation. Agronomie 17, 97–112. doi:10.1051/agro:19970203

Calder, I.., Narayanswamy, M.., Srinivasalu, N.., Darling, W.., Lardner, A.., 1986. Investigation into the use of deuterium as a tracer for measuring transpiration from eucalypts. J. Hydrol. 84, 345–351. doi:10.1016/0022-1694(86)90132-0

Calder, I.R., 1998. Water use by forests, limits and controls. Tree Physiol. 18, 625–631. doi:10.1093/treephys/18.8-9.625

Campbell, N.A., Williamson, B., Heyden, R.J., 2006. Biology: exploring life. Pearson Prentice Hall.

Casper, B.B., Jackson, R.B., 1997. Plant competition underground. Annu. Rev. Ecol. Syst. 28, 545–570. doi:10.1146/annurev.ecolsys.28.1.545

Čermák, J., Deml, M., Penka, M., 1973. A new method of sap flow rate determination in trees. Biol. Plant. 15, 171–178. doi:10.1007/BF02922390

Čermák, J., Kučera, J., Bauerle, W.L., Phillips, N., Hinckley, T.M., 2007. Tree water storage and its diurnal dynamics related to sap flow and changes in stem volume in old-growth Douglas-fir trees. Tree Physiol. 27, 181–198. doi:10.1093/treephys/27.2.181

Čermák, J., Kučera, J., Nadezhdina, N., 2004. Sap flow measurements with some thermodynamic methods, flow integration within trees and scaling up from sample trees to entire forest stands. Trees 18, 529–546. doi:10.1007/s00468-004-0339-6

Chiu, C.-W., Komatsu, H., Katayama, A., Otsuki, K., 2016a. Scaling-up from tree to stand transpiration for a warm-temperate multi-specific broadleaved forest with a wide variation in stem diameter. J. For. Res. 21, 161–169. doi:10.1007/s10310-016-0532-7

Chiu, C.-W., Kume, T., Komatsu, H., Tseng, H., Wey, T.-H., Otsuki, K., 2016b. Seasonal changes of azimuthal, radial, and tree-to-tree variations in sap flux affect stand transpiration estimates in a *Cryptomeria japonica* forest, central Taiwan. J. For. Res. 21, 151–160. doi:10.1007/s10310-016-0525-6

Chmura, D.J., Anderson, P.D., Howe, G.T., Harrington, C.A., Halofsky, J.E., Peterson, D.L., Shaw, D.C., St.Clair, B.J., 2011. Forest responses to climate change in the northwestern United States: Ecophysiological foundations for adaptive management. For. Ecol. Manage. 261, 1121–1142. doi:10.1016/J.FORECO.2010.12.040

Cochard, H., Delzon, S., Badel, E., 2015. X-ray microtomography (micro-CT): a reference technology for high-resolution quantification of xylem embolism in trees. Plant. Cell Environ. 38, 201–206. doi:10.1111/pce.12391

Cogbill, C. V., 1985. Dynamics of the boreal forests of the Laurentian Highlands, Canada. Can. J. For. Res. 15, 252–261. doi:10.1139/x85-043

Cohen, Y., Cohen, S., Cantuarias-Aviles, T., Schiller, G., 2008. Variations in the radial gradient of sap velocity in trunks of forest and fruit trees. Plant Soil 305, 49–59. doi:10.1007/s11104-007-9351-0

Cohen, Y., Fuchs, M., Green, G.C., 1981. Improvement of the heat pulse method for determining sap flow in trees. Plant, Cell Environ. 4, 391–397. doi:10.1111/j.1365-3040.1981.tb02117.x

Cribari-Neto, F., Zeileis, A., 2010. Beta Regression in *R*. J. Stat. Softw. 34, 1–24. doi:10.18637/jss.v034.i02

Cuneo, I.F., Knipfer, T., Brodersen, C.R., McElrone, A.J., 2016. Mechanical Failure of Fine Root Cortical Cells Initiates Plant Hydraulic Decline during Drought. Plant Physiol. 172, 1669–

1678. doi:10.1104/pp.16.00923

D'Amato, A.W., Bradford, J.B., Fraver, S., Palik, B.J., 2013. Effects of thinning on drought vulnerability and climate response in north temperate forest ecosystems. Ecol. Appl. 23, 1735–1742. doi:10.1890/13-0677.1

Daudet, F.A., Lacointe, A., Gaudillère, J.P., Cruiziat, P., 2002. Generalized Münch Coupling between Sugar and Water Fluxes for Modelling Carbon Allocation as Affected by Water Status. J. Theor. Biol. 214, 481–498. doi:10.1006/JTBI.2001.2473

Davis, T.W., Kuo, C.-M., Liang, X., Yu, P.-S., Davis, T.W., Kuo, C.-M., Liang, X., Yu, P.-S., 2012. Sap Flow Sensors: Construction, Quality Control and Comparison. Sensors 12, 954–971. doi:10.3390/s120100954

Dawson, T.E., Burgess, S.S.O., Tu, K.P., Oliveira, R.S., Santiago, L.S., Fisher, J.B., Simonin, K.A., Ambrose, A.R., 2007. Nighttime transpiration in woody plants from contrasting ecosystems. Tree Physiol. 27, 561–75. doi:10.1093/TREEPHYS/27.4.561

DeByle, N. V., Winokur, R.P., 1985. Aspen: Ecology and management in the western United States, USDA Forest Service General Technical Report RM-119. Rocky Mountain Forest and Range Experiment Station, Fort Collins, Colo. 283 p. doi:10.2737/RM-GTR-119

Delbart, N., Picard, G., Le Toan, T., Kergoat, L., Quegan, S., Woodward, I., Dye, D., Fedotova, V., 2008. Spring phenology in boreal Eurasia over a nearly century time scale. Glob. Chang. Biol. 14, 603–614. doi:10.1111/j.1365-2486.2007.01505.x

Devito, K., Mendoza, C., Qualizza, C., 2012. Conceptualizing water movement in the Boreal Plains. Implications for watershed reconstruction. Synthesis report prepared for the Canadian Oil Sands Network for Research and Development, Environmental and Reclamation Research Group.

Dietrich, L., Hoch, G., Kahmen, A., Körner, C., 2018. Losing half the conductive area hardly impacts the water status of mature trees. Sci. Rep. 8, 15006. doi:10.1038/s41598-018-33465-0

Dixon, F., 1914. Transpiration and the Ascent of Sap in Plants. Mcmillan and Co. Ltd, London.

Dixon, H.H., Joly, J., 1895. On the ascent of sap. Philos. Trans. R. Soc. London. 186, 563–576. doi:10.1098/rstb.1895.0012

Dixon, K.W., 1936. The convection of heat and materials in the stem of a tree. Proc. R. Dublin Soc. 21, 477–488.

Doerr, S.H., Shakesby, R.A., Walsh, R.P.D., 2000. Soil water repellency: its causes, characteristics and hydro-geomorphological significance. Earth-Science Rev. 51, 33–65. doi:10.1016/S0012-8252(00)00011-8

Doody, T.M., Colloff, M.J., Davies, M., Koul, V., Benyon, R.G., Nagler, P.L., 2015. Quantifying water requirements of riparian river red gum (*Eucalyptus camaldulensis*) in the Murray-Darling Basin, Australia - implications for the management of environmental flows.

Ecohydrology 8, 1471–1487. doi:10.1002/eco.1598

Doronila, A.I., Forster, M.A., 2015. Performance measurement via sap flow monitoring of three *Eucalyptus* species for mine site and dryland salinity phytoremediation. Int. J. Phytoremediation 17, 101–108. doi:10.1080/15226514.2013.850466

Dykes, J.A., Unwin, D.J., 2001. Maps of the Census: A Rough Guide, in: Case Studies of Visualization in the Social Sciences: Technical Report. pp. 29–54.

Eller, C.B., Burgess, S.S.O., Oliveira, R.S., 2015. Environmental controls in the water use patterns of a tropical cloud forest tree species, *Drimys brasiliensis* (Winteraceae). Tree Physiol. 35, 387–399. doi:10.1093/treephys/tpv001

Elliott, J.A., Toth, B.M., Granger, R.J., Pomeroy, J.W., 1998. Soil moisture storage in mature and replanted sub-humid boreal forest stands. Can. J. Soil Sci. 78, 17–27. doi:10.4141/S97-021

Ellison, D., Morris, C.E., Locatelli, B., Sheil, D., Cohen, J., Murdiyarso, D., Gutierrez, V., van Noordwijk, M., Creed, I.F., Pokorny, J., Gaveau, D., Spracklen, D. V., Bargués Tobella, A., Ilstedt, U., Teuling, A.J., Gebreyohannis Gebrehiwot, S., Sands, D.C., Muys, B., Verbist, B., Springgay, E., Sugandi, Y., Sullivan, C.A., 2017. Trees, forests and water: Cool insights for a hot world. Glob. Environ. Chang. 43, 51–61. doi:10.1016/J.GLOENVCHA.2017.01.002

Environment Canada, 2013. Canadian Climate Normals 1981-2010 Station Data - Climate - Environment and Climate Change Canada - Environment and Climate Change Canada [WWW Document]. URL http://climate.weather.gc.ca/climate_normals/results_1981_2010_e.html?stnID=2519&dispBack=0&month1=1&month2=9 (accessed 7.10.18).

FAO, 2018. The State of the World's Forests 2018 - Forest pathways to sustainable development. Rome.

Fernández, E., Čermák, J., Cohen, Y., Ferreira, I., Nadezhdina, N., Testi, L., Steppe, K., 2017. Methods to estimate sap flow, in: ISHS Working Group on Sap Flow. pp. 1–9.

Flo, V., Martinez-Vilalta, J., Steppe, K., Schuldt, B., Poyatos, R., 2019. A synthesis of bias and uncertainty in sap flow methods. Agric. For. Meteorol. 271, 362–374. doi:10.1016/J.AGRFORMET.2019.03.012

Foote, K.C., Schaedle, M., 1978. The Contribution of Aspen Bark Photosynthesis to the Energy Balance of the Stem. For. Sci. 24, 569–573. doi:10.1093/forestscience/24.4.569

Ford, C.R., Goranson, C.E., Mitchell, R.J., Will, R.E., Teskey, R.O., 2004. Diurnal and seasonal variability in the radial distribution of sap flow: predicting total stem flow in *Pinus taeda* trees. Tree Physiol. 24, 951–960. doi:10.1093/treephys/24.9.951

Forster, M., Forster, A., M., 2019. The Dual Method Approach (DMA) Resolves Measurement Range Limitations of Heat Pulse Velocity Sap Flow Sensors. Forests 10, 46. doi:10.3390/f10010046

Forster, M.A., 2017. How reliable are heat pulse velocity methods for estimating tree

transpiration? Forests 8, 350. doi:10.3390/f8090350

Fromm, J.H., Sautter, I., Matthies, D., Kremer, J., Schumacher, P., Ganter, C., 2001. Xylem Water Content and Wood Density in Spruce and Oak Trees Detected by High-Resolution Computed Tomography. Plant Physiol. 127, 416–425. doi:10.1104/PP.010194

Fuchs, S., Leuschner, C., Link, R., Coners, H., Schuldt, B., 2017. Calibration and comparison of thermal dissipation, heat ratio and heat field deformation sap flow probes for diffuse-porous trees. Agric. For. Meteorol. 244–245, 151–161. doi:10.1016/J.AGRFORMET.2017.04.003

Fung, M.Y.P., Macyk, T.M., 2000. Reclamation of Oil Sands Mining Areas, in: Barnhisel, R.I., Darmody, R.G., Daniels, W.L. (Eds.), Reclamation of Drastically Disturbed Lands, ASA, CSSA and SSSA. American Society of Agronomy, Crop Science Society of America, Soil Science Society of America, Madison, Wisconsin, pp. 755–774. doi:10.2134/agronmonogr41.c30

Gartner, B.L., 1995. Patterns of Xylem Variation within a Tree and Their Hydraulic and Mechanical Consequences, in: Gartner, B.L. (Ed.), Plant Stems. Academic Press, pp. 125–149. doi:10.1016/B978-012276460-8/50008-4

Gaul, D., Hertel, D., Borken, W., Matzner, E., Leuschner, C., 2008. Effects of experimental drought on the fine root system of mature Norway spruce. For. Ecol. Manage. 256, 1151–1159. doi:10.1016/J.FORECO.2008.06.016

Gebauer, T., Horna, V., Leuschner, C., 2008. Variability in radial sap flux density patterns and sapwood area among seven co-occurring temperate broad-leaved tree species. Tree Physiol. 28, 1821–1830. doi:10.1093/treephys/28.12.1821

Goldstein, G., Andrade, J.L., Meinzer, F.C., Holbrook, N.M., Cavelier, J., Jackson, P., Celis, A., 1998. Stem water storage and diurnal patterns of water use in tropical forest canopy trees. Plant, Cell Environ. 21, 397–406. doi:10.1046/j.1365-3040.1998.00273.x

Gonçalves, J.L., Alvares, C.A., Rocha, J.H., Brandani, C.B., Hakamada, R., 2017. Eucalypt plantation management in regions with water stress. South. For. a J. For. Sci. 79, 169–183. doi:10.2989/20702620.2016.1255415

Goulden, M.L., Field, C.B., 1994. Three Methods for Monitoring the Gas Exchange of Individual tree Canopies: Ventilated-Chamber, Sap-Flow and Penman-Monteith Measurements on Evergreen Oaks. Funct. Ecol. 8, 125. doi:10.2307/2390121

Government of Alberta, 2017. Environmental protection and enhancement act. Revised Statutes of Alberta 2000 Chapter E-12 [WWW Document]. URL http://www.qp.alberta.ca/documents/acts/e12.pdf (accessed 4.20.18).

Granier, A., 1987. Evaluation of transpiration in a Douglas-fir stand by means of sap flow measurements. Tree Physiol. 3, 309–320. doi:10.1093/treephys/3.4.309

Granier, A., 1985. Une nouvelle méthode pour la mesure du flux de sève brute dans le tronc des arbres. Ann. des Sci. For. 42, 193–200. doi:10.1051/forest:19850204

Granier, A., Biron, P., Bréda, N., Pontailler, J.-Y., Saugier, B., 1996. Transpiration of trees and forest stands: short and long-term monitoring using sapflow methods. Glob. Chang. Biol. 2, 265–274. doi:10.1111/j.1365-2486.1996.tb00078.x

Green, S.R., 1998. Measurements of sap flow by the heat-pulse method. An Instruction Manual for the HPV system.

Grossnickle, S.C., 2000. Ecophysiology of Northern Spruce Species : the Performance of Planted Seedlings. NRC Research Press, Ottawa, Ontario, Canada. 409 pp.

Hanes, C.C., Wang, X., Jain, P., Parisien, M.-A., Little, J.M., Flannigan, M.D., 2019. Fire-regime changes in Canada over the last half century. Can. J. For. Res. 49, 256–269. doi:10.1139/cjfr-2018-0293

Hassler, S.K., Weiler, M., Blume, T., 2018. Tree-, stand- and site-specific controls on landscape-scale patterns of transpiration. Hydrol. Earth Syst. Sci. 22, 13–30. doi:10.5194/hess-22-13-2018

Hatton, T.J., Catchpole, E.A., Vertessy, R.A., 1990. Integration of sapflow velocity to estimate plant water use. Tree Physiol. 6, 201–209. doi:10.1093/treephys/6.2.201

Hernandez-Santana, V., Hernandez-Hernandez, A., Vadeboncoeur, M.A., Asbjornsen, H., 2015. Scaling from single-point sap velocity measurements to stand transpiration in a multispecies deciduous forest: uncertainty sources, stand structure effect, and future scenarios. Can. J. For. Res. 45, 1489–1497. doi:10.1139/cjfr-2015-0009

Herzog, K., Thum, R., Kronfus, G., Heldstab, H.-J., Hasler, R., 1998. Patterns and mechanisms of transpiration in a large subalpine Norway spruce (*Picea abies* (L.) Karst.). Ecol. Res. 13, 105–116. doi:10.1046/j.1440-1703.1998.00250.x

Hesse, B.D., Goisser, M., Hartmann, H., Grams, T.E.E., 2019. Repeated summer drought delays sugar export from the leaf and impairs phloem transport in mature beech. Tree Physiol. 39, 192–200. doi:10.1093/treephys/tpy122

Hinckley, T.M., Ritchie, G.A., 1970. Notes: Within-crown patterns of transpiration, water stress, and stomatal activity in Abies amabilis. For. Sci. 16, 490–492.

Hogg, E.H., Hurdle, P.A., 1997. Sap flow in trembling aspen: implications for stomatal responses to vapor pressure deficit. Tree Physiol. 17, 501–509. doi:10.1093/treephys/17.8-9.501

Hogg, E.H., Saugier, B., Pontailler, J.-Y., Black, T.A., Chen, W., Hurdle, P.A., Wu, A., 2000. Responses of trembling aspen and hazelnut to vapor pressure deficit in a boreal deciduous forest. Tree Physiol. 20, 725–734. doi:10.1093/treephys/20.11.725

Holbrook, N.M., Zwieniecki, M.A., 2005. Vascular transport in plants. Elsevier Academic Press.

Holmgren, M., Lin, C.-Y., Murillo, J.E., Nieuwenhuis, A., Penninkhof, J., Sanders, N., van Bart, T., van Veen, H., Vasander, H., Vollebregt, M.E., Limpens, J., 2015. Positive shrub-tree interactions facilitate woody encroachment in boreal peatlands. J. Ecol. 103, 58–66. doi:10.1111/1365-2745.12331

Hölttä, T., Cochard, H., Nikinmaa, E., Mencuccini, M., 2009. Capacitive effect of cavitation in xylem conduits: results from a dynamic model. Plant. Cell Environ. 32, 10–21. doi:10.1111/j.1365-3040.2008.01894.x

Huang, J., Tardif, J.C., Bergeron, Y., Denneler, B., Berninger, F., Girardin, M.P., 2010. Radial growth response of four dominant boreal tree species to climate along a latitudinal gradient in the eastern Canadian boreal forest. Glob. Chang. Biol. 16, 711–731. doi:10.1111/j.1365-2486.2009.01990.x

Huang, M., Barbour, S.L., Carey, S.K., 2015. The impact of reclamation cover depth on the performance of reclaimed shale overburden at an oil sands mine in Northern Alberta, Canada. Hydrol. Process. 29, 2840–2854. doi:10.1002/hyp.10229

Huang, M., Lee Barbour, S., Elshorbagy, A., Zettl, J., Cheng Si, B., 2011. Water availability and forest growth in coarse-textured soils. Can. J. Soil Sci. 91, 199–210. doi:10.4141/cjss10012

Huber, B., Schmidt, E., 1937. Eine Kompensationsmethode zur thermoelektrischen Messung langsamer Saftströme. Ber. Dtsch. Bot. Ges. 55, 514–529. doi:10.1111/J.1438-8677.1937.TB01282.X

Hyndman, R., Athanasopoulos, G., Bergmeir, C., Caceres, G., Chhay, L., O'Hara-Wild, M., Petropoulos, F., Razbash, S., Wang, E., Yasmeen, F., 2019. _forecast: Forecasting functions for time series and linear models_.

IPCC, 2014. Climate Change 2014: Synthesis Report. Contribution of Working Groups I, II and III to the Fifth Assessment Report of the Intergovernmental Panel on Climate Change, [Core Writing Team, R.K. Pachauri and L.A. Meyer (eds.)]. IPCC, Geneva, Switzerland.

Jackson, R.B., Canadell, J., Ehleringer, J.R., Mooney, H.A., Sala, O.E., Schulze, E.D., 1996. A global analysis of root distributions for terrestrial biomes. Oecologia 108, 389–411. doi:10.1007/BF00333714

James, S.A., Clearwater, M.J., Meinzer, F.C., Goldstein, G., 2002. Heat dissipation sensors of variable length for the measurement of sap flow in trees with deep sapwood. Tree Physiol. 22, 277–283. doi:10.1093/treephys/22.4.277

James, S.A., Meinzer, F.C., Goldstein, G., Woodruff, D., Jones, T., Restom, T., Mejia, M., Clearwater, M., Campanello, P., 2003. Axial and radial water transport and internal water storage in tropical forest canopy trees. Oecologia 134, 37–45. doi:10.1007/s00442-002-1080-8

James, W.O., Baker, H., 1933. Sap pressure and the movement of sap. New Phytol. 32, 317–355. doi:10.1111/j.1469-8137.1933.tb07018.x

Ježík, M., Blaženec, M., Letts, M.G., Ditmarová, Ľ., Sitková, Z., Střelcová, K., 2015. Assessing seasonal drought stress response in Norway spruce (*Picea abies* (L.) Karst.) by monitoring stem circumference and sap flow. Ecohydrology 8, 378–386. doi:10.1002/eco.1536

Jung, K., Duan, M., House, J., Chang, S.X., 2014. Textural interfaces affected the distribution of roots, water, and nutrients in some reconstructed forest soils in the Athabasca oil sands region.

Ecol. Eng. 64, 240–249. doi:10.1016/j.ecoleng.2013.12.037

Jupa, R., Plavcová, L., Gloser, V., Jansen, S., 2016. Linking xylem water storage with anatomical parameters in five temperate tree species. Tree Physiol. 36, 756–769. doi:10.1093/treephys/tpw020

Kalliokoski, T., Nygren, P., Sievänen, R., 2008. Coarse root architecture of three boreal tree species growing in mixed stands. Silva Fenn. 42. doi:10.14214/sf.252

Keenan, R.J., 2015. Climate change impacts and adaptation in forest management: a review. Ann. For. Sci. 72, 145–167. doi:10.1007/s13595-014-0446-5

Kelln, C., Barbour, S.L., Qualizza, C., 2008. Controls on the spatial distribution of soil moisture and solute transport in a sloping reclamation cover. Can. Geotech. J. 45, 351–366. doi:10.1139/T07-099

Kessler, S., Barbour, S.L., van Rees, K.C.J., Dobchuk, B.S., 2010. Salinization of soil over saline-sodic overburden from the oil sands in Alberta. Can. J. Soil Sci. 90, 637–647. doi:10.4141/cjss10019

Kim, H.K., Park, J., Hwang, I., 2014. Investigating water transport through the xylem network in vascular plants. J. Exp. Bot. 65, 1895–1904. doi:doi:10.1093/jxb/eru075

Koch, G.W., Sillett, S.C., Jennings, G.M., Davis, S.D., 2004. The limits to tree height. Nature 428, 851–854. doi:10.1038/nature02417

Kocher, P., Horna, V., Leuschner, C., 2013. Stem water storage in five coexisting temperate broad-leaved tree species: significance, temporal dynamics and dependence on tree functional traits. Tree Physiol. 33, 817–832. doi:10.1093/treephys/tpt055

Komatsu, H., Kume, T., Shinohara, Y., 2017. Optimal sap flux sensor allocation for stand transpiration estimates: a non-dimensional analysis. Ann. For. Sci. 74, 38. doi:10.1007/s13595-017-0638-x

Kramer, P.J., 1940. Sap pressure and exudation. Am. J. Bot. 27, 929–931. doi:10.1002/j.1537-2197.1940.tb13956.x

Kume, T., Otsuki, K., Du, S., Yamanaka, N., Wang, Y.-L., Liu, G.-B., 2012. Spatial variation in sap flow velocity in semiarid region trees: its impact on stand-scale transpiration estimates. Hydrol. Process. 26, 1161–1168. doi:10.1002/hyp.8205

Kutscha, N.P., Sachs, I.B., 1968. Color tests for differentiating heartwood and sapwood in certain softwood tree species, U.S. Forestry Products Laboratory Report No. 2246. Madison, WI, USA. Madison, Wisconsin.

Lambers, H., Chapin, F.S., Pons, T.L., 2008. Plant Physiological Ecology. Springer New York, New York, NY. doi:10.1007/978-0-387-78341-3

Lanoue, A.V.L., 2003. Phosphorus content and accumulation of carbon and nitrogen in boreal forest soils. M.Sc. Thesis. University of Alberta, Edmonton, AB.

Lawrence, D.J., Luckai, N., Meyer, W.L., Shahi, C., Fazekas, A.J., Kesanakurti, P., Newmaster, S., 2012. Distribution of white spruce lateral fine roots as affected by the presence of trembling aspen: root mapping using simple sequence repeat DNA profiling. Can. J. For. Res. 42, 1566–1576. doi:10.1139/x2012-082

Lazorko, H., Van Rees, K.C.J., 2012. Root distributions of planted boreal mixedwood species on reclaimed saline–sodic overburden. Water, Air, Soil Pollut. 223, 215–231. doi:10.1007/s11270-011-0852-3

Lee, J.-E., Frankenberg, C., van der Tol, C., Berry, J.A., Guanter, L., Boyce, C.K., Fisher, J.B., Morrow, E., Worden, J.R., Asefi, S., Badgley, G., Saatchi, S., 2013. Forest productivity and water stress in Amazonia: observations from GOSAT chlorophyll fluorescence. Proc. R. Soc. B Biol. Sci. 280, 20130171. doi:10.1098/rspb.2013.0171

Lemeur, R., Fernández, J.E., Steppe, K., 2008. Symbols, SI units and physical quantities within the scope of sap flow studies, in: Fernández, E., Diaz-Espejo, A. (Eds.), Acta Horticulturae. International Society for Horticultural Science (ISHS), Leuven, Belgium, pp. 21–32.

Lenth, R. V., 2018. emmeans: Estimated Marginal Means, aka Least-Squares Means. R package version 1.2.3. https://CRAN.R-project.org/package=emmeans.

Leo, M., Oberhuber, W., Schuster, R., Grams, T.E.E., Matyssek, R., Wieser, G., 2014. Evaluating the effect of plant water availability on inner alpine coniferous trees based on sap flow measurements. Eur. J. For. Res. 133, 691–698. doi:10.1007/s10342-013-0697-y

Li, H., Si, B., Li, M., 2018. Rooting depth controls potential groundwater recharge on hillslopes. J. Hydrol. 564, 164–174. doi:10.1016/J.JHYDROL.2018.07.002

Li, Y., Zhao, M., Mildrexler, D.J., Motesharrei, S., Mu, Q., Kalnay, E., Zhao, F., Li, S., Wang, K., 2016. Potential and Actual impacts of deforestation and afforestation on land surface temperature. J. Geophys. Res. Atmos. 121, 14,372-14,386. doi:10.1002/2016JD024969

Lilles, E.B., Purdy, B.G., Macdonald, S.E., Chang, S.X., 2012. Growth of aspen and white spruce on naturally saline sites in northern Alberta: Implications for development of boreal forest vegetation on reclaimed saline soils. Can. J. Soil Sci. 92, 213–227. doi:10.4141/cjss2010-032

Link, P., Simonin, K., Maness, H., Oshun, J., Dawson, T., Fung, I., 2014. Species differences in the seasonality of evergreen tree transpiration in a Mediterranean climate: Analysis of multiyear, half-hourly sap flow observations. Water Resour. Res. 50, 1869–1894. doi:10.1002/2013WR014023

Liu, Y., 2011. A numerical study on hydrological impacts of forest restoration in the southern United States. Ecohydrology 4, 299–314. doi:10.1002/eco.178

Liu, Y., Stanturf, J., Lu, H., 2008. Modeling the Potential of the Northern China Forest Shelterbelt in Improving Hydroclimate Conditions. JAWRA J. Am. Water Resour. Assoc. 44, 1176–1192. doi:10.1111/j.1752-1688.2008.00240.x

Longuetaud, F., Mothe, F., Fournier, M., Dlouha, J., Santenoise, P., Deleuze, C., 2016. Within-stem maps of wood density and water content for characterization of species: a case study on

three hardwood and two softwood species. Ann. For. Sci. 73, 601–614. doi:10.1007/s13595-016-0555-4

Longuetaud, F., Mothe, F., Santenoise, P., Diop, N., Dlouha, J., Fournier, M., Deleuze, C., 2017. Patterns of within-stem variations in wood specific gravity and water content for five temperate tree species. Ann. For. Sci. 74, 64. doi:10.1007/s13595-017-0657-7

Looker, N., Martin, J., Jencso, K., Hu, J., 2016. Contribution of sapwood traits to uncertainty in conifer sap flow as estimated with the heat-ratio method. Agric. For. Meteorol. 223, 60–71. doi:10.1016/J.AGRFORMET.2016.03.014

López-Bernal, Á., Alcántara, E., Testi, L., Villalobos, F.J., 2010. Spatial sap flow and xylem anatomical characteristics in olive trees under different irrigation regimes. Tree Physiol. 30, 1536–1544. doi:10.1093/treephys/tpq095

Loustau, D., Berbigier, P., Roumagnac, P., Arruda-Pacheco, C., David, J.S., Ferreira, M.I., Pereira, J.S., Tavares, R., 1996. Transpiration of a 64-year-old maritime pine stand in Portugal. Oecologia 107, 33–42. doi:10.1007/BF00582232

Loustau, D., Domec, J.-C., Bosc, A., 1998. Interpreting the variations in xylem sap flux density within the trunk of maritime pine (*Pinus pinaster* Ait.): application of a model for calculating water flows at tree and stand levels. Ann. des Sci. For. 55, 29–46. doi:10.1051/forest:19980103

Lu, P., Muller, W.J., Chacko, E.K., 2000. Spatial variations in xylem sap flux density in the trunk of orchard-grown, mature mango trees under changing soil water conditions. Tree Physiol. 20, 683–692. doi:10.1093/treephys/20.10.683

Lu, P., Urban, L., Zhao, P., 2004. Granier's Thermal Dissipation Probre (TDP) method for measuring sap flow in trees : theory and practice. Acta Bot. Sin. 46, 631–646.

Lutz, J.A., Furniss, T.J., Johnson, D.J., Davies, S.J., Allen, D., Alonso, A., Anderson-Teixeira, K.J., Andrade, A., Baltzer, J., Becker, K.M.L., Blomdahl, E.M., Bourg, N.A., Bunyavejchewin, S., Burslem, D.F.R.P., Cansler, C.A., Cao, K., Cao, M., Cárdenas, D., Chang, L.-W., Chao, K.-J., Chao, W.-C., Chiang, J.-M., Chu, C., Chuyong, G.B., Clay, K., Condit, R., Cordell, S., Dattaraja, H.S., Duque, A., Ewango, C.E.N., Fischer, G.A., Fletcher, C., Freund, J.A., Giardina, C., Germain, S.J., Gilbert, G.S., Hao, Z., Hart, T., Hau, B.C.H., He, F., Hector, A., Howe, R.W., Hsieh, C.-F., Hu, Y.-H., Hubbell, S.P., Inman-Narahari, F.M., Itoh, A., Janík, D., Kassim, A.R., Kenfack, D., Korte, L., Král, K., Larson, A.J., Li, Y., Lin, Y., Liu, S., Lum, S., Ma, K., Makana, J.-R., Malhi, Y., McMahon, S.M., McShea, W.J., Memiaghe, H.R., Mi, X., Morecroft, M., Musili, P.M., Myers, J.A., Novotny, V., de Oliveira, A., Ong, P., Orwig, D.A., Ostertag, R., Parker, G.G., Patankar, R., Phillips, R.P., Reynolds, G., Sack, L., Song, G.-Z.M., Su, S.-H., Sukumar, R., Sun, I.-F., Suresh, H.S., Swanson, M.E., Tan, S., Thomas, D.W., Thompson, J., Uriarte, M., Valencia, R., Vicentini, A., Vrška, T., Wang, X., Weiblen, G.D., Wolf, A., Wu, S.-H., Xu, H., Yamakura, T., Yap, S., Zimmerman, J.K., 2018. Global importance of large-diameter trees. Glob. Ecol. Biogeogr. 27, 849–864. doi:10.1111/geb.12747

Macdonald, S.E., Landhäusser, S.M., Skousen, J., Franklin, J., Frouz, J., Hall, S., Jacobs, D.F.,

Quideau, S., 2015. Forest restoration following surface mining disturbance: challenges and solutions. New For. 46, 703–732. doi:10.1007/s11056-015-9506-4

MacPherson, D.M., Lieffers, V.J., Blenis, P. V., 2001. Productivity of aspen stands with and without a spruce understory in Alberta's boreal mixedwood forests. For. Chron. 77, 351–356. doi:10.5558/tfc77351-2

Mares, R., Barnard, H.R., Mao, D., Revil, A., Singha, K., 2016. Examining diel patterns of soil and xylem moisture using electrical resistivity imaging. J. Hydrol. 536, 327–338. doi:10.1016/J.JHYDROL.2016.03.003

Marshall, D.C., 1958. Measurement of sap flow in conifers by heat transport. Plant Physiol. 33, 385–396. doi:10.1104/PP.33.6.385

Martínez-Vilalta, J., Lloret, F., 2016. Drought-induced vegetation shifts in terrestrial ecosystems: The key role of regeneration dynamics. Glob. Planet. Change 144, 94–108. doi:10.1016/J.GLOPLACHA.2016.07.009

Matthes-Sears, U., Larson, D.W., 1999. Limitations to seedling growth and survival by the quantity and quality of rooting space: implications for the establishment of *Thuja occidentalis* on cliff faces. Int. J. Plant Sci. 160, 122–128. doi:10.1086/314105

McDowell, N., Pockman, W.T., Allen, C.D., Breshears, D.D., Cobb, N., Kolb, T., Plaut, J., Sperry, J., West, A., Williams, D.G., Yepez, E.A., 2008. Mechanisms of plant survival and mortality during drought: why do some plants survive while others succumb to drought? New Phytol. 178, 719–739. doi:10.1111/j.1469-8137.2008.02436.x

McDowell, N.G., 2011. Mechanisms linking drought, hydraulics, carbon metabolism, and vegetation mortality. Plant Physiol. 155, 1051–9. doi:10.1104/pp.110.170704

McElrone, A.J., Choat, B., Gambetta, G.A., Brodersen, C.R., 2013. Water Uptake and Transport in Vascular Plants. Nat. Educ. Knowl. 4, 6.

Meinzer, F.C., Clearwater, M.J., Goldstein, G., 2001. Water transport in trees: current perspectives, new insights and some controversies. Environ. Exp. Bot. 45, 239–262. doi:10.1016/S0098-8472(01)00074-0

Meinzer, F.C., James, S.A., Goldstein, G., 2004. Dynamics of transpiration, sap flow and use of stored water in tropical forest canopy trees. Tree Physiol. 24, 901–909. doi:10.1093/treephys/24.8.901

Mencuccini, M., Salmon, Y., Mitchell, P., H?ltt?, T., Choat, B., Meir, P., O'Grady, A., Tissue, D., Zweifel, R., Sevanto, S., Pfautsch, S., 2017. An empirical method that separates irreversible stem radial growth from bark water content changes in trees: theory and case studies. Plant. Cell Environ. 40, 290–303. doi:10.1111/pce.12863

Messier, C., Coll, L., Poitras-Larivière, A., Bélanger, N., Brisson, J., 2009. Resource and non-resource root competition effects of grasses on early- versus late-successional trees. J. Ecol. 97, 548–554. doi:10.1111/j.1365-2745.2009.01500.x

Molina, A.J., Aranda, X., Carta, G., Llorens, P., Romero, R., Savé, R., Biel, C., 2016. Effect of irrigation on sap flux density variability and water use estimate in cherry (*Prunus avium*) for timber production: Azimuthal profile, radial profile and sapwood estimation. Agric. Water Manag. 164, 118–126. doi:10.1016/J.AGWAT.2015.08.019

Morris, H., Gillingham, M.A.F., Plavcová, L., Gleason, S.M., Olson, M.E., Coomes, D.A., Fichtler, E., Klepsch, M.M., Martínez-Cabrera, H.I., McGlinn, D.J., Wheeler, E.A., Zheng, J., Ziemińska, K., Jansen, S., 2018. Vessel diameter is related to amount and spatial arrangement of axial parenchyma in woody angiosperms. Plant. Cell Environ. 41, 245–260. doi:10.1111/pce.13091

Morris, H., Plavcová, L., Cvecko, P., Fichtler, E., Gillingham, M.A.F., Martínez-Cabrera, H.I., McGlinn, D.J., Wheeler, E., Zheng, J., Ziemińska, K., Jansen, S., 2016. A global analysis of parenchyma tissue fractions in secondary xylem of seed plants. New Phytol. 209, 1553–1565. doi:10.1111/nph.13737

Münch, E., 1930. Stoffbewegungen in der Pflanze.

Mundell, T.L., Landhäusser, S.M., Lieffers, V.J., 2007. Effects of *Corylus cornuta* stem density on root suckering and rooting depth of *Populus tremuloides*. Can. J. Bot. 85, 1041–1045. doi:10.1139/B07-089

Nadezhdina, N., Cermak, J., Downey, A., Nadezhdin, V., Peramaki, M., David, J.S., Pinto, C.A., David, T.S., 2015. Sap flow index as an indicator of water storage use. J. Hydrol. Hydromechanics 63, 124–133. doi:https://doi.org/10.1515/johh-2015-0013

Nadezhdina, N., Cermák, J., Meiresonne, L., Ceulemans, R., 2007. Transpiration of Scots pine in Flanders growing on soil with irregular substratum. For. Ecol. Manage. 243, 1–9. doi:10.1016/J.FORECO.2007.01.089

Nadezhdina, N., Čermák, J., Nadezhdin, V., 1998. Heat field deformation method for sap flow measurements, in: Nadezhdina, N., Čermak, J. (Eds.), Proceedings of the "4th International Workshop on Measuring Sap Flow in Intact Plants." Publishing House of Mendel University, Brno (Czech Republic), pp. 72–92.

Nagata, A., Kose, K., Terada, Y., 2016. Development of an outdoor MRI system for measuring flow in a living tree. J. Magn. Reson. 265, 129–138. doi:10.1016/J.JMR.2016.02.004

Nepstad, D.C., de Carvalho, C.R., Davidson, E.A., Jipp, P.H., Lefebvre, P.A., Negreiros, G.H., da Silva, E.D., Stone, T.A., Trumbore, S.E., Vieira, S., 1994. The role of deep roots in the hydrological and carbon cycles of Amazonian forests and pastures. Nature 372, 666–669. doi:10.1038/372666a0

Nepstad, D.C., Tohver, I.M., Ray, D., Moutinho, P., Cardinot, G., 2007. Mortality of large trees and lianas following experimental drought in an Amazon forest. Ecology 88, 2259–2269. doi:10.1890/06-1046.1

Niinemets, Ü., 2007. Photosynthesis and resource distribution through plant canopies. Plant. Cell Environ. 30, 1052–1071. doi:10.1111/j.1365-3040.2007.01683.x

Nikinmaa, E., Sievänen, R., Hölttä, T., 2014. Dynamics of leaf gas exchange, xylem and phloem transport, water potential and carbohydrate concentration in a realistic 3-D model tree crown. Ann. Bot. 114, 653–666. doi:10.1093/aob/mcu068

Nlungu-Kweta, P., Leduc, A., Bergeron, Y., 2014. Conifer recruitment in trembling aspen (*Populus tremuloides* Michx.) stands along an east-west gradient in the boreal mixedwoods of Canada. Forests 5, 2905–2928. doi:10.3390/f5112905

Nolf, M., Beikircher, B., Rosner, S., Nolf, A., Mayr, S., 2015. Xylem cavitation resistance can be estimated based on time-dependent rate of acoustic emissions. New Phytol. 208, 625–632. doi:10.1111/nph.13476

Norby, R.J., Delucia, E.H., Gielen, B., Calfapietra, C., Giardina, C.P., King, J.S., Ledford, J., McCarthy, H.R., Moore, D.J.P., Ceulemans, R., De Angelis, P., Finzi, A.C., Karnosky, D.F., Kubiske, M.E., Lukac, M., Pregitzer, K.S., Scarascia-Mugnozza, G.E., Schlesinger, W.H., Oren, R., 2005. Forest response to elevated CO_2 is conserved across a broad range of productivity. Proc. Natl. Acad. Sci. U. S. A. 102, 18052–6. doi:10.1073/pnas.0509478102

Notaro, M., Liu, Z., 2008. Statistical and dynamical assessment of vegetation feedbacks on climate over the boreal forest. Clim. Dyn. 31, 691–712. doi:10.1007/s00382-008-0368-8

Novoplansky, A., 2009. Picking battles wisely: plant behaviour under competition. Plant. Cell Environ. 32, 726–741. doi:10.1111/j.1365-3040.2009.01979.x

Oishi, A.C., Hawthorne, D.A., Oren, R., 2016. Baseliner: An open-source, interactive tool for processing sap flux data from thermal dissipation probes. SoftwareX 5, 139–143. doi:10.1016/J.SOFTX.2016.07.003

Oishi, A.C., Oren, R., Stoy, P.C., 2008. Estimating components of forest evapotranspiration: A footprint approach for scaling sap flux measurements. Agric. For. Meteorol. 148, 1719–1732. doi:10.1016/J.AGRFORMET.2008.06.013

Ojekanmi, A.A., Chang, S.X., 2014. Soil quality assessment for peat–mineral mix cover soil used in oil sands reclamation. J. Environ. Qual. 43, 1566. doi:10.2134/jeq2014.02.0061

Olbrich, B.W., 1991. The verification of the heat pulse velocity technique for estimating sap flow in *Eucalyptus grandis*. Can. J. For. Res. 21, 836–841. doi:10.1139/x91-117

Oliva Carrasco, L., Bucci, S.J., Di Francescantonio, D., Lezcano, O.A., Campanello, P.I., Scholz, F.G., Rodriguez, S., Madanes, N., Cristiano, P.M., Hao, G.-Y., Holbrook, N.M., Goldstein, G., 2015. Water storage dynamics in the main stem of subtropical tree species differing in wood density, growth rate and life history traits. Tree Physiol. 35, 354–365. doi:10.1093/treephys/tpu087

Pappas, C., Matheny, A.M., Baltzer, J.L., Barr, A.G., Black, T.A., Bohrer, G., Detto, M., Maillet, J., Roy, A., Sonnentag, O., Stephens, J., 2018. Boreal tree hydrodynamics: asynchronous, diverging, yet complementary. Tree Physiol. 38, 953–964. doi:10.1093/treephys/tpy043

Park, A., Talbot, C., Smith, R., 2018. Trees for tomorrow: an evaluation framework to assess potential candidates for assisted migration to Manitoba's forests. Clim. Change 148, 591–

606. doi:10.1007/s10584-018-2201-7

Peng, C., Ma, Z., Lei, X., Zhu, Q., Chen, H., Wang, W., Liu, S., Li, W., Fang, X., Zhou, X., 2011. A drought-induced pervasive increase in tree mortality across Canada's boreal forests. Nat. Clim. Chang. 1, 467–471. doi:10.1038/nclimate1293

Perämäki, M., Vesala, T., Nikinmaa, E., 2005. Modeling the dynamics of pressure propagation and diameter variation in tree sapwood. Tree Physiol. 25, 1091–1099. doi:10.1093/treephys/25.9.1091

Peters, R.L., Fonti, P., Frank, D.C., Poyatos, R., Pappas, C., Kahmen, A., Carraro, V., Prendin, A.L., Schneider, L., Baltzer, J.L., Baron-Gafford, G.A., Dietrich, L., Heinrich, I., Minor, R.L., Sonnentag, O., Matheny, A.M., Wightman, M.G., Steppe, K., 2018. Quantification of uncertainties in conifer sap flow measured with the thermal dissipation method. New Phytol. 219, 1283–1299. doi:10.1111/nph.15241

Pfanz, H., Aschan, G., Langenfeld-Heyser, R., Wittmann, C., Loose, M., 2002. Ecology and ecophysiology of tree stems: corticular and wood photosynthesis. Naturwissenschaften 89, 147–162. doi:10.1007/s00114-002-0309-z

Pfautsch, S., Hölttä, T., Mencuccini, M., 2015. Hydraulic functioning of tree stems—fusing ray anatomy, radial transfer and capacitance. Tree Physiol. 35, 706–722. doi:10.1093/treephys/tpv058

Pfautsch, S., Keitel, C., Turnbull, T.L., Braimbridge, M.J., Wright, T.E., Simpson, R.R., O'Brien, J.A., Adams, M.A., 2011. Diurnal patterns of water use in *Eucalyptus victrix* indicate pronounced desiccation-rehydration cycles despite unlimited water supply. Tree Physiol. 31, 1041–1051. doi:10.1093/treephys/tpr082

Phillips, N.G., Ryan, M.G., Bond, B.J., McDowell, N.G., Hinckley, T.M., Cermak, J., 2003. Reliance on stored water increases with tree size in three species in the Pacific Northwest. Tree Physiol. 23, 237–245. doi:10.1093/treephys/23.4.237

Phillips, N.G., Scholz, F.G., Bucci, S.J., Goldstein, G., Meinzer, F.C., 2009. Using branch and basal trunk sap flow measurements to estimate whole-plant water capacitance: comment on Burgess and Dawson (2008). Plant Soil 315, 315–324. doi:10.1007/s11104-008-9741-y

Pinheiro, J., Bates, D., DebRoy, S., Sarkar, D., R Core Team, 2018. _nlme: Linear and nonlinear mixed effects models_. R package version 3.1-137, <URL: https://CRAN.R-project.org/package=nlme>.

Pollard, D.F.W., 1970. Leaf area development on different shoot types in a young aspen stand and its effect upon production. Can. J. Bot. 48, 1801–1804. doi:10.1139/b70-264

Poyatos, R., Granda, V., Molowny-Horas, R., Mencuccini, M., Steppe, K., Martínez-Vilalta, J., 2016. SAPFLUXNET: towards a global database of sap flow measurements. Tree Physiol. 36, 1449–1455. doi:10.1093/treephys/tpw110

Pratt, R.B., Jacobsen, A.L., 2017. Conflicting demands on angiosperm xylem: Tradeoffs among storage, transport and biomechanics. Plant. Cell Environ. 40, 897–913.

doi:10.1111/pce.12862

Prevedello, J.A., Winck, G.R., Weber, M.M., Nichols, E., Sinervo, B., 2019. Impacts of forestation and deforestation on local temperature across the globe. PLoS One 14, e0213368. doi:10.1371/journal.pone.0213368

Prieto, I., Armas, C., Pugnaire, F.I., 2012. Water release through plant roots: new insights into its consequences at the plant and ecosystem level. New Phytol. 193, 830–41. doi:10.1111/j.1469-8137.2011.04039.x

Quentin, A.G., O'Grady, A.P., Beadle, C.L., Worledge, D., Pinkard, E.A., 2011. Responses of transpiration and canopy conductance to partial defoliation of *Eucalyptus globulus* trees. Agric. For. Meteorol. 151, 356–364. doi:10.1016/J.AGRFORMET.2010.11.008

R Development Core Team, 2019. R: A Language and Environment for Statistical Computing.

Rabbel, I., Bogena, H., Neuwirth, B., Diekkrüger, B., Rabbel, I., Bogena, H., Neuwirth, B., Diekkrüger, B., 2018. Using Sap Flow Data to Parameterize the Feddes Water Stress Model for Norway Spruce. Water 10, 279. doi:10.3390/w10030279

Rabbel, I., Diekkrüger, B., Voigt, H., Neuwirth, B., Rabbel, I., Diekkrüger, B., Voigt, H., Neuwirth, B., 2016. Comparing ΔTmax Determination Approaches for Granier-Based Sapflow Estimations. Sensors 16, 2042. doi:10.3390/s16122042

Rita, A., Camarero, J.J., Nolè, A., Borghetti, M., Brunetti, M., Pergola, N., Serio, C., Vicente-Serrano, S.M., Tramutoli, V., Ripullone, F., 2019. The impact of drought spells on forests depends on site conditions: The case of 2017 summer heat wave in southern Europe. Glob. Chang. Biol. gcb.14825. doi:10.1111/gcb.14825

Roberts, D.R., Dumbroff, E.B., 1986. Relationships among drought resistance, transpiration rates, and abscisic acid levels in three northern conifers. Tree Physiol. 1, 161–167. doi:10.1093/treephys/1.2.161

Roberts, J., 1977. The Use of Tree-cutting Techniques in the Study of the Water Relations of Mature *Pinus sylvestris* L. J. Exp. Bot. 28, 751–767. doi:10.1093/jxb/28.3.751

Rosan, T.M., Aragão, L.E.O.C., Oliveras, I., Phillips, O.L., Malhi, Y., Gloor, E., Wagner, F.H., 2019. Extensive 21st-Century Woody Encroachment in South America's Savanna. Geophys. Res. Lett. 46, 6594–6603. doi:10.1029/2019GL082327

Sakai, Y., Takahashi, M., Tanaka, N., 2007. Root biomass and distribution of a *Picea—Abies* stand and a *Larix—Betula* stand in pumiceous Entisols in Japan. J. For. Res. 12, 120–125. doi:10.1007/s10310-006-0270-3

Sakuratani, T., 1981. A heat balance method for measuring water flux in the stem of intact plants. J. Agric. Meteorol. 37, 9–17. doi:10.2480/agrmet.37.9

Salas, J.D., Govindaraju, R.S., Anderson, M., Arabi, M., Francés, F., Suarez, W., Lavado-Casimiro, W.S., Green, T.R., 2014. Introduction to Hydrology, in: Modern Water Resources Engineering. Humana Press, Totowa, NJ, pp. 1–126. doi:10.1007/978-1-62703-595-8_1

Sato, T., Oda, T., Igarashi, Y., Suzuki, M., Uchiyama, Y., 2012. Circumferential sap flow variation in the trunks of Japanese cedar and cypress trees growing on a steep slope. Hydrol. Res. Lett. 6, 104–108. doi:10.3178/hrl.6.104

Schaffer, B., Whiley, A.W., Searle, C., 1999. Atmospheric CO_2 enrichment, root restriction, photosynthesis, and dry-matter partitioning in subtropical and tropical fruit crops. Hortic. Sci. 34, 1033–1037.

Schenk, H.J., Jackson, R.B., 2002. The global biogeography of roots. Ecol. Monogr. 72, 311–328. doi:10.1890/0012-9615(2002)072[0311:TGBOR]2.0.CO;2

Schlesinger, W.H., Jasechko, S., 2014. Transpiration in the global water cycle. Agric. For. Meteorol. 189–190, 115–117. doi:10.1016/j.agrformet.2014.01.011

Schneider, C.A., Rasband, W.S., Eliceiri, K.W., 2012. NIH Image to ImageJ: 25 years of image analysis. Nat. Methods 9, 671–675. doi:10.1038/nmeth.2089

Scholander, P.F., Bradstreet, E.D., Hemmingsen, E.A., Hammel, H.T., 1965. Sap pressure in vascular plants, negative hydrostatic pressure can be measured in plants. Science 148, 339–346. doi:10.1126/science.148.3668.33

Scholz, F.C., Bucci, S.J., Goldstein, G., Meinzer, F.C., Franco, A.C., Miralles-Wilhelm, F., 2008. Temporal dynamics of stem expansion and contraction in savanna trees: withdrawal and recharge of stored water. Tree Physiol. 28, 469–480. doi:10.1093/treephys/28.3.469

Scholz, F.G., Bucci, S.J., Goldstein, G., Meinzer, F.C., Franco, A.C., Miralles-Wilhelm, F., 2007. Biophysical properties and functional significance of stem water storage tissues in Neotropical savanna trees. Plant. Cell Environ. 30, 236–248. doi:10.1111/j.1365-3040.2006.01623.x

Scholz, F.G., Bucci, S.J., Goldstein, G., Moreira, M.Z., Meinzer, F.C., Domec, J.-C., Villalobos-Vega, R., Franco, A.C., Miralles-Wilhelm, F., 2008. Biophysical and life-history determinants of hydraulic lift in Neotropical savanna trees. Funct. Ecol. 22, 773–786. doi:10.1111/j.1365-2435.2008.01452.x

Schuster, R., Oberhuber, W., Gruber, A., Wieser, G., 2016. Soil drought decreases water-use of pine and spruce but not of larch in a dry inner alpine valley. Austrian J. For. Sci. 133, 1–17.

Sellin, A., 2000. Estimating the needle area from geometric measurements: application of different calculation methods to Norway spruce. Trees 14, 215–222. doi:10.1007/PL00009765

Shinohara, Y., Tsuruta, K., Ogura, A., Noto, F., Komatsu, H., Otsuki, K., Maruyama, T., 2013. Azimuthal and radial variations in sap flux density and effects on stand-scale transpiration estimates in a Japanese cedar forest. Tree Physiol. 33, 550–558. doi:10.1093/treephys/tpt029

Shirke, P.A., 2001. Leaf Photosynthesis, Dark Respiration and Fluorescence as Influenced by Leaf Age in an Evergreen Tree, *Prosopis Juliflora*. Photosynthetica 39, 305–311. doi:10.1023/A:1013761410734

Slik, J.W.F., Paoli, G., McGuire, K., Amaral, I., Barroso, J., Bastian, M., Blanc, L., Bongers, F.,

Boundja, P., Clark, C., Collins, M., Dauby, G., Ding, Y., Doucet, J.-L., Eler, E., Ferreira, L., Forshed, O., Fredriksson, G., Gillet, J.-F., Harris, D., Leal, M., Laumonier, Y., Malhi, Y., Mansor, A., Martin, E., Miyamoto, K., Araujo-Murakami, A., Nagamasu, H., Nilus, R., Nurtjahya, E., Oliveira, Á., Onrizal, O., Parada-Gutierrez, A., Permana, A., Poorter, L., Poulsen, J., Ramirez-Angulo, H., Reitsma, J., Rovero, F., Rozak, A., Sheil, D., Silva-Espejo, J., Silveira, M., Spironelo, W., ter Steege, H., Stevart, T., Navarro-Aguilar, G.E., Sunderland, T., Suzuki, E., Tang, J., Theilade, I., van der Heijden, G., van Valkenburg, J., Van Do, T., Vilanova, E., Vos, V., Wich, S., Wöll, H., Yoneda, T., Zang, R., Zhang, M.-G., Zweifel, N., 2013. Large trees drive forest aboveground biomass variation in moist lowland forests across the tropics. Glob. Ecol. Biogeogr. 22, 1261–1271. doi:10.1111/geb.12092

Smith, D.M., Allen, S.J., 1996. Measurement of sap flow in plant stems. J. Exp. Bot. 47, 1833–1844. doi:10.1093/jxb/47.12.1833

Smith, R.E., 1992. The heat pulse velocity technique for determining water uptake of *Populus deltoides*. South African J. Bot. 58, 100–104. doi:10.1016/S0254-6299(16)30879-1

Snedden, J.E., 2013. The root distribution, architecture, transpiration and root sapflow dynamics of mature trembling aspen (*Populus tremuloides*) growing along a hillslope. M. Sc. Thesis. University of Alberta.

Sperry, J.S., Love, D.M., 2015. What plant hydraulics can tell us about responses to climate-change droughts. New Phytol. 207, 14–27. doi:10.1111/nph.13354

Stanfield, R.C., Hacke, U.G., Laur, J., 2017. Are phloem sieve tubes leaky conduits supported by numerous aquaporins? Am. J. Bot. 104, 719–732. doi:10.3732/ajb.1600422

Stanfield, R.C., Schulte, P.J., Randolph, K.E., Hacke, U.G., 2019. Computational models evaluating the impact of sieve plates and radial water exchange on phloem pressure gradients. Plant. Cell Environ. 42, 466–479. doi:10.1111/pce.13414

Stanturf, J.A., Palik, B.J., Dumroese, K., 2014. Contemporary forest restoration: A review emphasizing function. For. Ecol. Manage. 331, 292–323. doi:10.1016/J.FORECO.2014.07.029

Stephens, J.J., Black, T.A., Jassal, R.S., Nesic, Z., Grant, N.J., Barr, A.G., Helgason, W.D., Richardson, A.D., Johnson, M.S., Christen, A., 2018. Effects of forest tent caterpillar defoliation on carbon and water fluxes in a boreal aspen stand. Agric. For. Meteorol. 253–254, 176–189. doi:10.1016/J.AGRFORMET.2018.01.035

Stovall, A.E.L., Shugart, H., Yang, X., 2019. Tree height explains mortality risk during an intense drought. Nat. Commun. 10, 4385. doi:10.1038/s41467-019-12380-6

Střelcová, K., Kurjak, D., Leštianska, A., Kovalčíková, D., Ditmarová, Ľ., Škvarenina, J., Ahmed, Y., 2013. Differences in transpiration of Norway spruce drought stressed trees and trees well supplied with water. Biologia (Bratisl). 68, 1118–1122. doi:10.2478/s11756-013-0257-4

Strong, W.L., LaRoi, G.H., 1983. Root-system morphology of common boreal forest trees in Alberta, Canada. Can. J. For. Res. 13, 1164–1173. doi:10.1139/x83-155

Sun, G., Liu, Y., 2013. Forest Influences on Climate and Water Resources at the Landscape to Regional Scale, in: Landscape Ecology for Sustainable Environment and Culture. Springer Netherlands, Dordrecht, pp. 309–334. doi:10.1007/978-94-007-6530-6_15

Swanson, R.H., Whitfield, D.W.A., 1981. A Numerical Analysis of Heat Pulse Velocity Theory and Practice. J. Exp. Bot. 32, 221–239. doi:10.1093/jxb/32.1.221

Taberlet, P., Gielly, L., Pautou, G., Bouvet, J., 1991. Universal primers for amplification of three non-coding regions of chloroplast DNA. Plant Mol. Biol. 17, 1105–1109. doi:10.1007/BF00037152

Tarvainen, L., Wallin, G., Lim, H., Linder, S., Oren, R., Ottosson Löfvenius, M., Räntfors, M., Tor-ngern, P., Marshall, J., 2018. Photosynthetic refixation varies along the stem and reduces CO_2 efflux in mature boreal *Pinus sylvestris* trees. Tree Physiol. 38, 558–569. doi:10.1093/treephys/tpx130

Tateishi, M., Kumagai, T., Utsumi, Y., Umebayashi, T., Shiiba, Y., Inoue, K., Kaji, K., Cho, K., Otsuki, K., 2008. Spatial variations in xylem sap flux density in evergreen oak trees with radial-porous wood: comparisons with anatomical observations. Trees 22, 23–30. doi:10.1007/s00468-007-0165-8

Testi, L., Villalobos, F.J., 2009. New approach for measuring low sap velocities in trees. Agric. For. Meteorol. 149, 730–734. doi:10.1016/J.AGRFORMET.2008.10.015

Tie, Q., Hu, H., Tian, F., Guan, H., Lin, H., 2017. Environmental and physiological controls on sap flow in a subhumid mountainous catchment in North China. Agric. For. Meteorol. 240–241, 46–57. doi:10.1016/J.AGRFORMET.2017.03.018

Tseng, H., Chiu, C.-W., Laplace, S., Kume, T., 2017. Can we assume insignificant temporal changes in spatial variations of sap flux for year-round individual tree transpiration estimates? A case study on *Cryptomeria japonica* in central Taiwan. Trees 31, 1239–1251. doi:10.1007/s00468-017-1542-6

Tsuruta, K., Kume, T., Komatsu, H., Higashi, N., Umebayashi, T., Kumagai, T., Otsuki, K., 2010. Azimuthal variations of sap flux density within Japanese cypress xylem trunks and their effects on tree transpiration estimates. J. For. Res. 15, 398–403. doi:10.1007/s10310-010-0202-0

Tyree, M.T., Zimmermann, M.H., 2002. Xylem Structure and the Ascent of Sap, Springer Series in Wood Science. Springer Berlin Heidelberg, Berlin, Heidelberg. doi:10.1007/978-3-662-04931-0

Umebayashi, T., Utsumi, Y., Koga, S., Inoue, S., Fujikawa, S., Arakawa, K., Matsumura, J., Oda, K., 2008. Conducting Pathways in North Temperate Deciduous Broadleaved Trees. IAWA J. 29, 247–263.

van Buuren, S., Groothuis-Oudshoorn, K., 2011. mice : Multivariate Imputation by Chained Equations in R. J. Stat. Softw. 45, 1–67. doi:10.18637/jss.v045.i03

Van Cleve, K., Yarie, J., 1986. Interaction of Temperature, Moisture, and Soil Chemistry in

Controlling Nutrient Cycling and Ecosystem Development in the Taiga of Alaska, in: Forest Ecosystems in the Alaskan Taiga. Springer, New York, NY, pp. 160–189. doi:10.1007/978-1-4612-4902-3_12

Van de Wal, B.A.E., Guyot, A., Lovelock, C.E., Lockington, D.A., Steppe, K., 2015. Influence of temporospatial variation in sap flux density on estimates of whole-tree water use in *Avicennia marina*. Trees 29, 215–222. doi:10.1007/s00468-014-1105-z

Vandegehuchte, M.W., Burgess, S.S.O., Downey, A., Steppe, K., 2015. Influence of stem temperature changes on heat pulse sap flux density measurements. Tree Physiol. 35, 346–53. doi:10.1093/treephys/tpu068

Vandegehuchte, M.W., Steppe, K., 2013. Sap-flux density measurement methods: working principles and applicability. Funct. Plant Biol. 40, 213. doi:10.1071/FP12233

Vandegehuchte, M.W., Steppe, K., 2012a. Sapflow+: a four-needle heat-pulse sap flow sensor enabling nonempirical sap flux density and water content measurements. New Phytol. 196, 306–317. doi:10.1111/j.1469-8137.2012.04237.x

Vandegehuchte, M.W., Steppe, K., 2012b. Improving sap flux density measurements by correctly determining thermal diffusivity, differentiating between bound and unbound water. Tree Physiol. 32, 930–42. doi:10.1093/treephys/tps034

Vergeynst, L.L., Vandegehuchte, M.W., McGuire, M.A., Teskey, R.O., Steppe, K., 2014. Changes in stem water content influence sap flux density measurements with thermal dissipation probes. Trees 28, 949–955. doi:10.1007/s00468-014-0989-y

Vertessy, R.A., Hatton, T.J., Reece, P., O'Sullivan, S.K., Benyon, R.G., 1997. Estimating stand water use of large mountain ash trees and validation of the sap flow measurement technique. Tree Physiol. 17, 747–756. doi:10.1093/treephys/17.12.747

Vieweg, G.H., Ziegler, H., 1960. Thermoelektrische Registrierung der Geschwindigkeit des Transpirationsstromes. Ber. Dtsch. Bot. Ges. 73, 221–226.

Ward, E.J., 2016. Measuring water fluxes in forests: the need for integrative platforms of analysis. Tree Physiol. 36, 929–931. doi:10.1093/treephys/tpw065

Waring, R.H., Roberts, J.M., 1979. Estimating Water Flux through Stems of Scots Pine with Tritiated Water and Phosphorus-32. J. Exp. Bot. 30, 459–471. doi:10.1093/jxb/30.3.459

Waring, R.H., Running, S.W., 1978. Sapwood water storage: its contribution to transpiration and effect upon water conductance through the stems of old-growth Douglas-fir. Plant, Cell Environ. 1, 131–140. doi:10.1111/j.1365-3040.1978.tb00754.x

Wiedemann, A., Marañón-Jiménez, S., Rebmann, C., Herbst, M., Cuntz, M., 2016. An empirical study of the wound effect on sap flux density measured with thermal dissipation probes. Tree Physiol. 36, 1471–1484. doi:10.1093/treephys/tpw071

Wiley, E., Rogers, B.J., Griesbauer, H.P., Landhäusser, S.M., 2018. Spruce shows greater sensitivity to recent warming than Douglas-fir in central British Columbia. Ecosphere 9, 1–

16. doi:10.1002/ecs2.2221

Windt, C.W., Vergeldt, F.J., De Jager, P.A., Van As, H., 2006. MRI of long-distance water transport: a comparison of the phloem and xylem flow characteristics and dynamics in poplar, castor bean, tomato and tobacco. Plant, Cell Environ. 29, 1715–1729. doi:10.1111/j.1365-3040.2006.01544.x

Wood, S.N., 2017. Generalized additive models : an introduction with R, 2nd ed. Chapman & Hall/CRC, Boca Raton, Florida, USA.

Wood, S.N., 2011. Fast stable restricted maximum likelihood and marginal likelihood estimation of semiparametric generalized linear models. J. R. Stat. Soc. Ser. B Stat. Methodol. 73, 3–36. doi:10.1111/j.1467-9868.2010.00749.x

Wullschleger, S.D., King, A.W., 2000. Radial variation in sap velocity as a function of stem diameter and sapwood thickness in yellow-poplar trees. Tree Physiol. 20, 511–518. doi:10.1093/treephys/20.8.511

Xia, Y.Q., Shao, M.A., 2009. Evaluation of soil water-carrying capacity for vegetation: the concept and the model. Acta Agric. Scand. Sect. B - Plant Soil Sci. 59, 342–348. doi:10.1080/09064710802203537

Yu, T., Feng, Q., Si, J., Pinkard, E.A., 2019. Coordination of stomatal control and stem water storage on plant water use in desert riparian trees. Trees 33, 787–801. doi:10.1007/s00468-019-01816-7

Zeppel, M., Macinnis-Ng, C.M.O., Ford, C.R., Eamus, D., 2008. The response of sap flow to pulses of rain in a temperate Australian woodland. Plant Soil 305, 121–130. doi:10.1007/s11104-007-9349-7

Zhang, Y.-J., Meinzer, F.C., Hao, G.-Y., Scholz, F.G., Bucci, S.J., Takahashi, F.S.C., Villalobos-Vega, R., Giraldo, J.P., Cao, K.-F., Hoffmann, W.A., Goldstein, G., 2009. Size-dependent mortality in a Neotropical savanna tree: the role of height-related adjustments in hydraulic architecture and carbon allocation. Plant. Cell Environ. 32, 1456–1466. doi:10.1111/j.1365-3040.2009.02012.x

Zhang, Y., Peña-Arancibia, J.L., McVicar, T.R., Chiew, F.H.S., Vaze, J., Liu, C., Lu, X., Zheng, H., Wang, Y., Liu, Y.Y., Miralles, D.G., Pan, M., 2016. Multi-decadal trends in global terrestrial evapotranspiration and its components. Sci. Rep. 6, 19124. doi:10.1038/srep19124

Zhang, Z., Zhao, Ping, Zhao, X., Zhou, J., Zhao, Peiqiang, Zeng, X., Hu, Y., Ouyang, L., 2018. The tree height-related spatial variances of tree sap flux density and its scale-up to stand transpiration in a subtropical evergreen broadleaf forest. Ecohydrology 11, e1979. doi:10.1002/eco.1979

Zweifel, R., Bohm, J.P., Hasler, R., 2002. Midday stomatal closure in Norway spruce--reactions in the upper and lower crown. Tree Physiol. 22, 1125–1136. doi:10.1093/treephys/22.15-16.1125

Zweifel, R., Häsler, R., 2001. Dynamics of water storage in mature subalpine Picea abies: temporal

and spatial patterns of change in stem radius. Tree Physiol. 21, 561–569. doi:10.1093/treephys/21.9.561

APPENDIX

Chapter 2

Appendix 2.A: Methods

Protocol of root identification of trembling aspen and white spruce

Total genomic DNA is extracted from dried, ground root materials using CTAB extraction protocol. Using species-specific primers for aspen (*Populus tremuloides*) and white spruce (*Picea glauca*) developed in two previous studies of Genesee root ID 2015 and Aurora root ID 2015, fragments of the DNA at a non-coding chloroplast region were amplified by PCR and visualized by gel electrophoresis. The presence of the bands corresponding to aspen and white spruce signifies their presence in the root material. Since the fragment length of aspen is very close to the other two species found within the same experimental field area, namely willow (*Salix bebbiana*) and balsam poplar (*Populus balsamifera*), further refinement on the resolution of fragment lengths using FAFLP is employed to identify aspen from willow and balsam.

Details

Foilage – DNA reference for roots identification

From each plant species found within the experimental area, 12 foliage samples were collected from different individuals spread over the area. The collection included both the target species, *Populus tremuloides* (aspen) and *Picea glauca* (white spruce), and 16 other community species (*Aster ciliolatus, Bromus inermis*, *Carex* sp., *Circium arvense*, *Epilobium angustifolium*, *Lotus corniculatus*, *Medicago sativa*, *Poa pratensis*, *Populus balsamifera*, *Rubus idaeus*, *Salix* sp., *Salix*

bebbiana, *Solidago canadensis, Sonchus* sp., *Taraxacum officanale* and *Trifolium hybridium*). In the lab, all samples were cleaned with deionized water to remove dust and pollens, and freeze-dried. Dried samples were ground using a ball mill (TissueLyser II, QIAGEN, Hilden Germany). Ground materials were saved in 20-mL glass vials or 2-mL safe-lock micro-centrifuge tubes at room temperature for up to three months or at -20 °C for longer times.

Of each sample about 20 mg of ground tissue was extracted with 2 % CTAB followed by cleaning using the 5% CTAB extraction procedure. Yield and purity were quantified using a Nanodrop 2000 (Thermo Fisher Scientific, Wilmington, DE, USA), DNA concentration measured from 6.06 to 1854.8 ng/µL, 260/230 absorbance ratio of 1.22 to 3.05 and 260/280 absorbance ratio of 1.49 to 2.27. Extracts were stored at -20°C for downstream activities.

The DNA signatures of the two target species were established at a non-coding chloroplast region, the *trn*L intron intergenic spacer. From the genomic DNA material extracted, segment within the region was amplified by polymerase chain reaction (PCR) using species-specific primers. We used a universal forward primer (Primer-C (5'-CGAAATCGGTAGACGCTACG-3') (Taberlet et al., 1991)) and two species-specific reverse primers developed in earlier studies, Trem404 (5'-ACAGATTCGAGTCGGTTGTC-3') for aspen and Glau277 (5'-CACATTCCCACTTTTTAGGTG-3') for white spruce. The PCR was done in volumes totaling 25 µL: 5.5 µL autoclaved deionized water, 2.5 µL of forward primer C at 10 µM, 2.5 µL of reverse primer (Trem404 or Glau277) at 10 µM, 12.5 µL of EconoTaq PLUS 2X Master Mix (Lucigen Corp., Middleton, WI, USA), and 2 µL of 1-10 ng/µL of DNA template. Amplifications were performed using an Eppendorf Mastercycler Pro S gradient thermal cycler (Model 6321; Eppendorf Canada, Mississauga, ON, Canada). Thermal cycler conditions: 94 °C for 5 min, 35 cycles of 94 °C for 60 s, 60 °C for 60 s, 72 °C for 80 s, followed by a final extension of 72 °C for

30 min. PCR products were visualized right away by gel electrophoresis on a 10 cm long x 15 cm wide gel slab, 1.5 % agarose, with SYBR® Safe DNA gel stain, ran in 2-tiers at 100V for 35 min (See Protocol of PCR Amplicon Visualization by Gel Electrophoresis). Amplicon lengths were compared with a 700 base-pair (bp) ladder ran simultaneously on the gel.

PCR ran with reverse primer Trem404 produced amplicons of around 400 bp from aspen, 2 willow species and balsam poplar DNA extracts, but none from other species. PCR ran with reverse primer Glau277 produced amplicons of around 270 bp from white spruce DNA extracts, but none from other species. A more precise measurement of the amplicon lengths was done using fluorescent amplified fragment length polymorphisms (FAFLP). First, PCRs were rerun on the DNA extracts of aspen, 2 willow species and balsam poplar using primer set VIC-C/Trem404, and on the DNA extracts of white spruce using primer set VIC-C/Glau277. The forward primer VIC-C is a 5' fluorescently labelled primer C. After PCR, the products were processed for FAFLP (see Sequencing Protocol for Fluorescent Amplified-Fragment Length Polymorphisms). The fragment lengths measured from aspen, 2 willow species, balsam poplar and white spruce were 398-399, 369-378, 387-388 and 276 bp, respectively.

In order to verify the negative result of the species on the gel, DNA extracts of all species (including aspen, spruce and the other community species) were run through a PCR as described above, but replacing the species-specific reverse primers with a universal reverse primer (Primer-D (5'-GGGGATAGAGGGACTTGAAC-3') (Taberlet et al., 1991)). All species gave bands between 400 to 700 bp.

DNA extracts and PCR products were saved at 2-8 °C for up to three months or at -20 °C for longer times.

Roots

Collected soil cores were saved in a -20°C freezer for eight months. After thawed, roots were picked from the soil core material and washed carefully with tap water to remove soil particles. They were further rinsed with deionized water to remove other soluble compounds. Once cleaned, the roots were lyophilized and ground in a ball mill (TissueLyser II, QIAGEN, Hilden Germany). Ground materials were saved in 20-mL glass vials or 2-mL safe-lock micro-centrifuge tubes at room temperature up to three months, or at -20 °C for longer times.

Genomic DNA of the root tissues were extracted in the same way as on the foliage samples using 2% CTAB followed by cleaning using the 5% CTAB extraction procedure, except that up to 50 mg of ground root material were used for the extractions. DNA yield and quality were 0.01 to 968.96 ng/µL, 260/230 absorbance ratio of -0.53 to 11.2 and 260/280 absorbance ratio -6.36 to 2.07. On all root DNA samples, separate PCRs were performed with the species-specific reverse primers (Trem404 or Glau277) and with the Primer-D reverse primer in the same way as on the foliage samples. Samples that gave the corresponding band on the gel using reverse primer Glau 277 were identified as spruce. Samples that gave the corresponding band on the gel using reverse primer Trem404 were identified as aspen/willow/balsam poplar. These DNA samples were rerun in PCR with the reverse primer Trem404 paired with the fluorescently labelled forward primer VIC-C. The resulting PCR products were then processed through FAFLP and the fragment lengths were determined. Samples that gave fragments of lengths 398-399 bp were identified as aspen. DNA extracts and PCR products were saved at 2-8 °C for up to three months, or at -20 °C for longer times.

Appendix 2.B: Summary statistics

Table 2.B. 1. Summary statistics of the mixed effects linear models testing for the impact of slope position within the 35 cm capping treatment, Year of study (2014 or 2015), Capping treatment within slope position and year on the tree characteristics of trembling aspen Populus tremuloides *and white spruce* Picea glauca *(diameter at breast height DBH, tree height, transpiring leaf area and sapwood area). Random effects were defined per Tree plot. Normality and homoscedasticity were checked, and adjustments were made accordingly (see "Model specifics"). Transformations ("Log(X)") were made on the dataset for normality. Outliers removed when necessary. DF: degrees of freedom; N: sample size;* r^2_m*: marginal coefficient of determination;* r^2_c*: conditional coefficient of determination.*

Species	Random effects	Model	Variable	N	r^2_m	r^2_c	Model specifics
P. tremuloides	Random ~ 1|Tree Plot	35 cm ~Slope x Year	DBH	33	0.09	0.09	Log(X)~Slope+Year
			Height		0.07	0.07	Slope+Year
			Transpiring leaf area		0.12	0.12	Log(X)~Slope+Year
			Sapwood area		0.89	0.89	Year+Transpiring leaf area+Slope
		Down slope 2014 ~Capping treatment	DBH	16	0.35	0.35	Transpiring leaf area+Capping treatment
			Height	17	0.07	0.07	
			Transpiring leaf area	16	0.46	0.46	
			Sapwood area	17	0.92	0.92	
		Upper slope 2015 ~Capping treatment	DBH	18	0.16	0.18	Log(X)
			Height		0.19	0.19	
			Transpiring leaf area		0.06	0.06	

			Sapwood area		0.88	0.90	Transpiring leaf area+Capping treatment
P. glauca	Random ~ 1|Tree Plot	35 cm ~Slope x Year	DBH	33	0.36	0.39	Slope+Year
			Height		0.23	0.31	Slope+Year
			Transpiring leaf area		0.31	0.35	Slope+Year
			Sapwood area	18	0.60	0.62	2015 only; Transpiring leaf area+Slope
		Down slope 2014 ~Capping treatment	DBH	18	0.31	0.31	
			Height		< 0.01	< 0.01	
			Transpiring leaf area		0.31	0.31	
			Sapwood area		< 0.01	0.17	Transpiring leaf area+Capping treatment
		Upper slope 2015 ~Capping treatment	DBH	18	0.04	0.1	
			Height		0.04	0.04	
			Transpiring leaf area		0.04	0.13	
			Sapwood area		0.89	0.89	Transpiring leaf area+Capping treatment

Table 2.B. 2. Summary statistics of the beta-regression models testing for the impact of soil depth, slope position and capping treatment on the proportional root weight distribution in the two depths range: 0-50 cm and 60-120 cm. See "Model specifics" for the specific interactions between variables tested. Random effects were defined per year of sampling and nested Tree plot. DF: degrees of freedom; N: sample size, R^2: coefficient of determination.

Variable	Random effects	Depth range	N	R^2	Model specifics
Proportional root weight	Random ~ 1|Year/Tree Plot	0-50 cm	412	0.56	Betareg(X) ~ Depth x Capping treatment x Slope
		60-120 cm	462	0.24	Betareg(X) ~ Depth* Capping treatment +Slope+Slope:Depth

Table 2.B. 3. Summary statistics of the mixed effects linear models testing for the impact of slope position within the 35 cm capping treatment, Year of study (2014 or 2015) and Capping treatment within slope position and year on the cumulative sap flow Q^c and transpiration T^c of trembling aspen Populus tremuloides *and white spruce* Picea glauca*. Random effects were defined per Tree plot. Normality and homoscedasticity were checked, and adjustments were made accordingly (see "Model specifics"). Variance was allowed to vary along a factor level ("varIdent") and transformations ("Log(X)" or "√X") were made on the dataset for normality. Outliers removed when necessary. DF: degrees of freedom; N: sample size; r^2_m: marginal coefficient of determination; r^2_c: conditional coefficient of determination.*

Variable	Species	Random effects	Model	N	r^2_m	r^2_c	Model specifics
Q^c	*P. tremuloides*	Random ~ 1|Tree Plot	35 cm ~Slope x Year	34	0.01	0.01	√X ~ Slope+Year
	P. glauca		35 cm ~Slope x Year	36	0.43	0.43	√X ~ Slope+Year
	Species differences		35 cm ~Species x Year	70	0.33	0.38	√X
			Down slope 2014 ~Species x Capping treatment	35	0.24	0.34	
			Upper slope 2015 ~ Species x Capping treatment	35	0.08	0.48	Plot+Species
T^c	*P. tremuloides*	Random ~ 1|Tree Plot	35 cm ~Slope x Year	35	0.27	0.27	√X
	P. glauca		35 cm ~Slope x Year	36	0.78	0.81	√X ~ Slope+Year
			35 cm	71	0.76	0.77	Log(X)

	~ Species x Year				varIdent(Year*Species)
Species differences	Down slope 2014 ~ Species x Capping treatment	35	0.29	0.33	Plot+Species
	Upper slope 2015 ~ Species x Capping treatment	34	0.97	0.99	Plot+Species varIdent(~Species)

Table 2.B. 4. Summary statistics of the mixed effects linear models testing for the impact of slope position within the 35 cm capping treatment, Year of study (2014 or 2015) and Capping treatment within slope position and year on the average daily sap flow Q and transpiration T of trembling aspen Populus tremuloides *and white spruce* Picea glauca *during the wet spring. Random effects were defined per Tree plot. Normality and homoscedasticity were checked, and adjustments were made accordingly (see "Model specifics"). Variance was allowed to vary along a factor level ("varIdent") and transformations ("√X") were made on the dataset for normality. Outliers removed when necessary. DF: degrees of freedom; N: sample size; r^2_m: marginal coefficient of determination; r^2_c: conditional coefficient of determination.*

Variable	Species	Random effects	Model	N	r^2_m	r^2_c	Model specifics
Wet spring Q	*P. tremuloides*	Random ~ 1|Tree Plot	35 cm ~Slope x Year	34	0.37	0.40	√X ~ Slope + Year varIdent(~Year)
			Down slope 2014 ~Capping treatment	17	0.13	0.13	
			Upper slope 2015 ~Capping treatment	18	0.40	0.53	varIdent(~Capping treatment)
	P. glauca		35 cm ~Slope x Year	36	0.19	0.29	Slope+Year
			Down slope 2014 ~Capping treatment	18	0.02	0.36	
			Upper slope 2015 ~Capping treatment	17	0.1	0.67	varIdent(~Tree plot)
Wet spring T	*P. tremuloides*	Random ~ 1|Tree Plot	35 cm ~Slope x Year	34	0.85	0.87	√X ~ Slope + Year
			Down slope 2014	17	0.03	0.16	

	~Capping treatment				
	Upper slope 2015 ~Capping treatment	18	0.34	0.45	varIdent(~Capping treatment)
	35 cm ~Slope x Year	36	0.63	0.65	√X ~ Slope + Year varIdent(~Year)
P. glauca	Down slope 2014 ~Capping treatment	18	0.01	0.20	
	Upper slope 2015 ~Capping treatment	17	< 0.01	0.30	

Table 2.B. 5. Final generalized additive models for each species and year testing the effects of slope position and capping treatment. The adjusted R^2 and deviance explained are presented as goodness of fit measures.

Species	**Variable tested**	**Model**	**R^2**	**Deviance explained**
P. glauca				
2014	Slope position	$gam(Sap\ flux \sim Slope + s(Date, by = Slope, k = 10) + s(Date, Tree, bs = "re")$	0.866	87.1%
	Capping treatment	$gam(Sap\ flux \sim Capping\ treatment + s(Date, by = Capping\ treatment, k = 10) + s(Tree, bs = "re") + s(Date, Tree, bs = "re")$	0.818	82.5%
2015	Slope position	$gam(Sap\ flux \sim s(Date, k = 6) + s(Tree, bs = "re") + s(Date, Tree, bs = "re")$	0.847	85.3%
	Capping treatment	$gam(Sap\ flux \sim Capping\ treatment + s(Date, by = Capping\ treatment, k = 6) + s(Tree, bs = "re") + s(Date, Tree, bs = "re")$	0.883	88.7%
P. tremuloides				
2014	Slope position	$gam(Sap\ flux \sim Slope + s(Date, by = Slope, k = 10) + s(Tree, bs = "re") + s(Date, Tree, bs = "re")$	0.806	81.5%
	Capping treatment	$gam(Sap\ flux \sim s(Date, k = 10) + s(Tree, bs = "re") + s(Date, Tree, bs = "re")$	0.758	76.7%
2015	Slope position	$gam(Sap\ flux \sim s(Date, by = Slope, k = 6) + s(Tree, bs = "re") + s(Date, Tree, bs = "re")$	0.615	63.2%
	Capping treatment	$gam(Sap\ flux \sim Capping\ treatment + s(Date, by = Capping\ treatment, k = 6) + s(Tree, bs = "re") + s(Date, Tree, bs = "re")$	0.649	66.2%

Table 2.B. 6. Summary statistics of the mixed effects linear models testing for the impact of slope position within the 35 cm capping treatment and Capping treatment on the upper slope in 2015, between trembling aspen Populus tremuloides *and white spruce* Picea glauca *on the ratio in daily transpiration after and before the rewetting event and on the ratio of the cumulative water uptake Q^c with and without the rewetting event. Random effects were defined per Tree plot. Normality and homoscedasticity were checked, and adjustments were made accordingly (see "Model specifics"). Variance was allowed to vary along a factor level ("varIdent") and transformations ("$X^{-1.1}$" or "Log(X)") were made on the dataset for normality. Outliers removed when necessary. DF: degrees of freedom; N: sample size; r^2_m: marginal coefficient of determination; r^2_c: conditional coefficient of determination.*

Variable	Random effects	Model	N	r^2_m	r^2_c	Model specifics
Ratio transpiration after/before rewetting event	Random ~ 1|Tree Plot	35 cm ~Slope x Species	35	0.86	0.86	$X^{-1.1}$~Slope+Species
		Upper slope 2015 ~ Species x Capping treatment	34	0.70	0.70	Log(X)~Plot+Species
Ratio Q^c with/without rewetting event	Random ~ 1|Tree Plot	35 cm ~Slope x Species	35	0.67	0.68	Log(X) varIdent(~Species)
		Upper slope 2015 ~ Species x Capping treatment	35	0.63	0.65	varIdent(~Species)

Table 2.B. 7. Summary statistics of the mixed effects linear models testing for the impact of slope position within the 35 cm capping treatment and Capping treatment on the upper slope across years (2011 - 2015) for trembling aspen Populus tremuloides *and white spruce* Picea glauca *on their basal area increment BAI. Random effects were defined per Tree plot. Normality and homoscedasticity were checked, and adjustments were made accordingly (see "Model specifics"). Variance was allowed to vary along a factor level ("varIdent") and transformations ("Log(X)") were made on the dataset for normality. Outliers removed when necessary. DF: degrees of freedom; N: sample size;* r^2_m*: marginal coefficient of determination;* r^2_c*: conditional coefficient of determination.*

Variable	Species	Random effects	Model	N	r^2_m	r^2_c	Model specifics
BAI Basal area increment	*P. tremuloides*	Random ~ 1|Tree Plot	35 cm ~Slope x Year	60	0.47	0.47	Slope+Species varIdent(~Year)
			Upper slope ~Capping treatment x Year	60	0.87	0.94	Log(X)~Capping treatment + Year varIdent(~Year)
	P. glauca		35 cm ~Slope x Species	30	0.61	0.87	
			Upper slope ~Capping treatment x Year	25	0.80	0.88	Capping treatment + Year varIdent(~Capping treatment)

Appendix 2.C: Supplementary Results

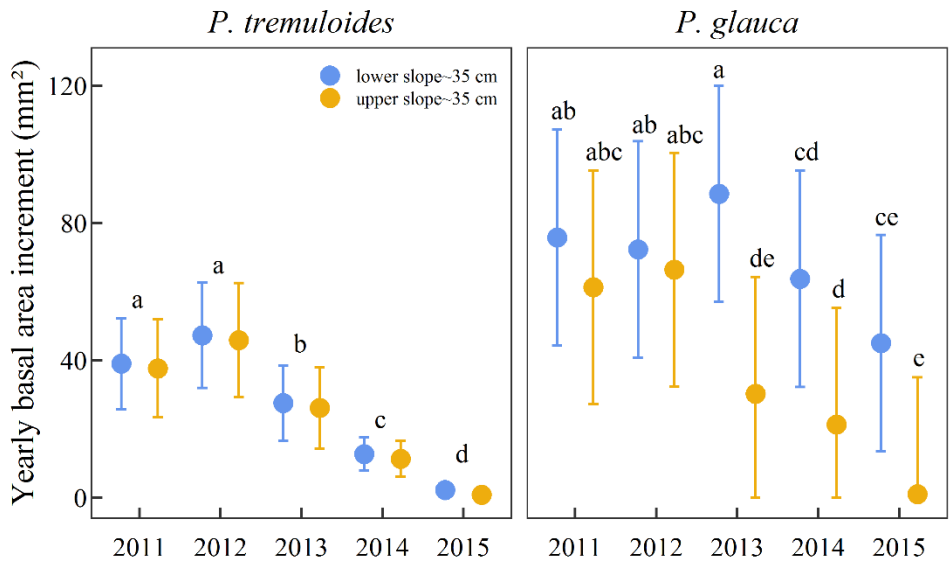

Figure 2.C. 1. Estimated marginal means and 95% confidence interval of yearly tree basal area increment in mm^2 for trembling aspen (left) and white spruce (right) on the 35 cm cap for the lower slope (blue) and upper slope (gold) positions. Letters indicate statistical differences between years (trembling aspen) and between years and slope position (white spruce). Models were run individually for each species.

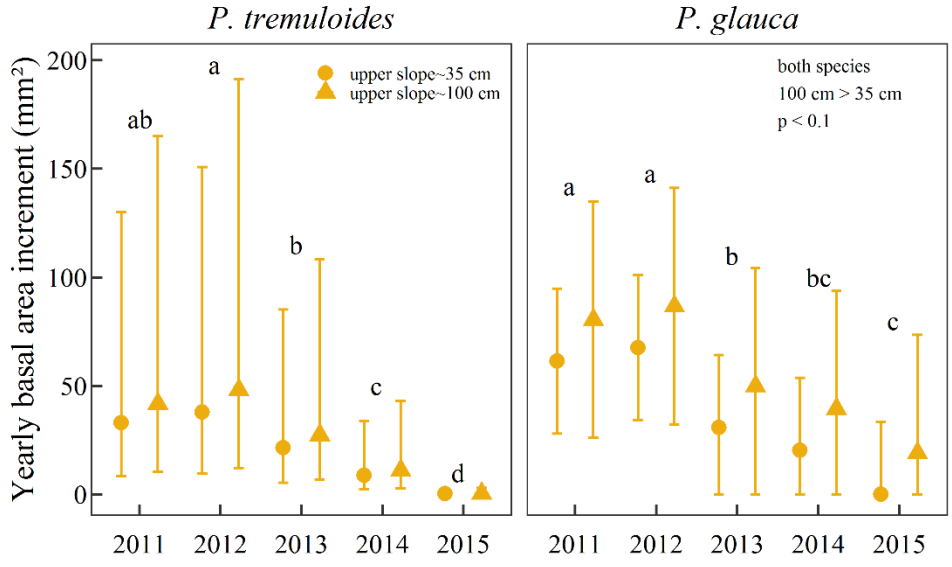

Figure 2.C. 2. Estimated marginal means and 95 % confidence interval of yearly tree basal area increment in mm^2 for trembling aspen (left) and white spruce (right) on upper slope for the 35 cm cap (circles) and 100 cm cap (triangles). Letters indicate statistical differences between years. Capping thickness was marginally significant for both species as indicated on the figure. Models were run individually for each species.

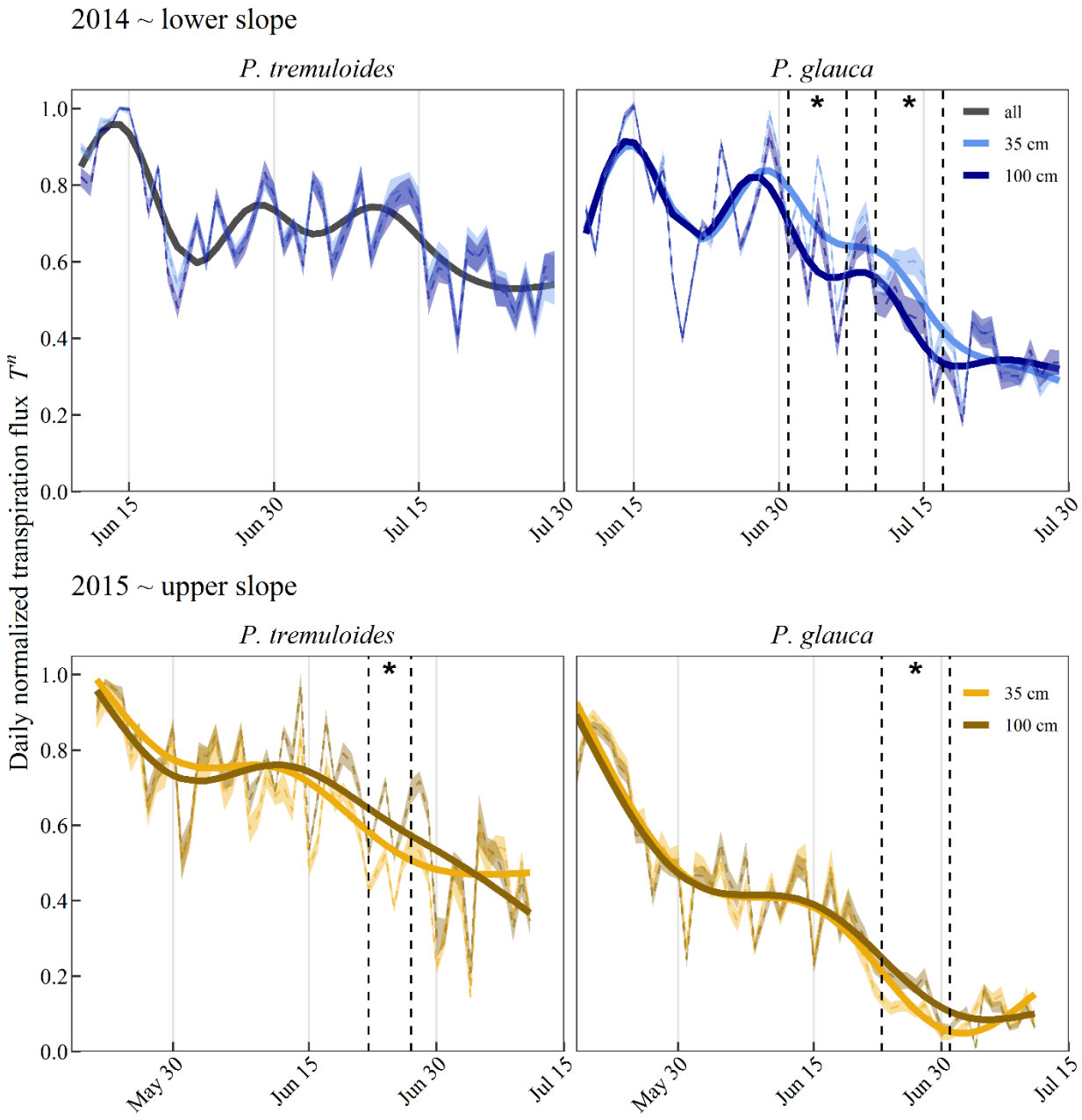

Figure 2.C. 3. Average daily normalized transpiration flux T^n (dotted line) during the dry-down and dry soil moisture periods and 95 % confidence intervals for each cap (blue: 100 cm, gold: 35 cm) in 2014 at the upper slope (top panels) and 2015 at the upper slope (bottom panels) for both species (left: P. tremuloides *and right:* P. glauca*). Results from the generalized additive models assessing the effect of slope for each species and year independently are presented in solid lines*

with the respective slope colors. The grey line for P. tremuloides *in 2014 shows no significant difference between slopes and thus a unique model was fitted.*

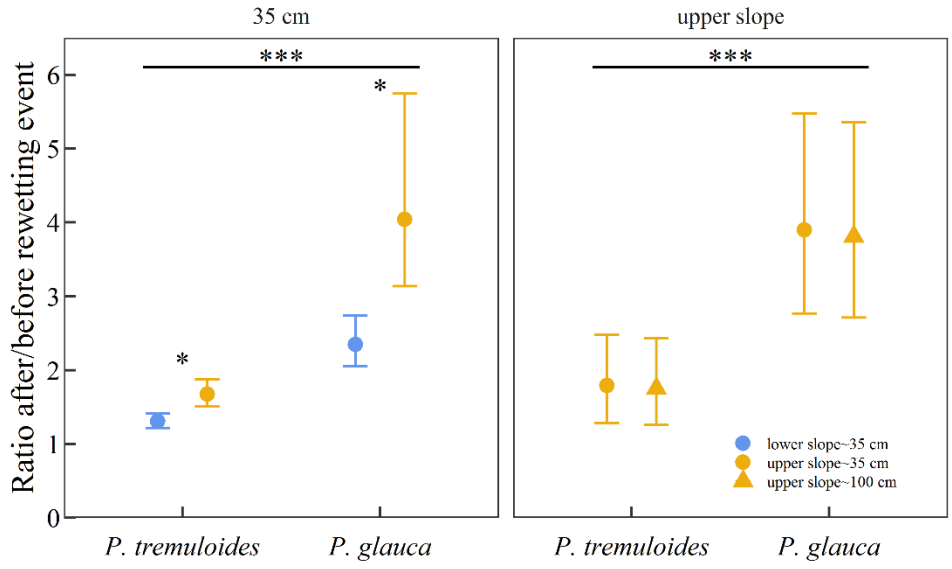

Figure 2.C. 4. Estimated marginal mean and 95 % confidence interval of the ratio of daily normalized transpiration flux of peak soil moisture content (after the two major rain events, 22nd to the 24th of July 2015) to initial low soil moisture content (before the two major rain events, 9th to the 11th of July 2015) for each species, slope position (lower: blue, upper: gold) and capping thickness (only for the upper slope, 35 cm cap: circles, 100 cm cap: triangles) for both species P. tremuloides *and* P. glauca*. Significance was indicated by the following labels: *: $p < 0.05$, ***: $p < 0.001$.*

*Table 2.C. 1. Estimated marginal means (standard error) of whole tree cumulative sap flux Q^c (L) and transpiration flux T^c (L m^{-2} transpiring leaf area) of the two capping thicknesses on the lower slope (2014) and the upper slope (2015) for the trembling aspen (*P. tremuloides*) and white spruce (*P. glauca*) trees. Statistical models were done separately on the two years to evaluate the effects of species and capping thickness on the upper slope in 2014 (letters {x,y}) and the upper slope in 2015 (letters {α,β}). Different letters represent a statistically significant difference ($p < 0.05$), and a + sign represents a marginally significant difference ($p < 0.1$). Please note that the sap flow sensors on white spruce were placed at breast height in 2014, thus encompassing only the upper crown compared to 2015 when they were placed at the base of the tree thus taking the full crown into account.*

	Lower slope ~ 2014				**Upper slope ~ 2015**			
	35 cm cap		**100 cm cap**		**35 cm cap**		**100 cm cap**	
	P. tremuloides	*P. glauca*	*P. tremuloides*	*P. glauca*	*P. tremuloides*	*P. glauca*	*P. tremuloides*	*P. glauca*
$\boldsymbol{Q^c}$ [L]	1098.9 (347.0) **y**	2454.6 (330.0) **x**	2088.2 (330.0) **x**	2149.7 (330.0) **x**	795.3 (271.6) **α**	628.9 (271.6) **α**	1100.3 (271.6) **α^+**	933.8 (274.5) **α^+**
$\boldsymbol{T^c}$ [L m^{-2} transpiring leaf area]	139.3 (11.3) **x**	85.8 (10.9) **y**	142.1 (10.9) **x**	88.6 (10.9) **y**	76.8 (4.6) **α**	10.2 (3.2) **β**	77.6 (4.6) **α**	11.0 (3.3) **β**

Table 2.C. 2. Estimated marginal means (standard error) of whole tree cumulative sap flux Q^c (L) and transpiration flux T^c (L m^{-2} transpiring leaf area) on the 35 cm cap for the trembling aspen (P. tremuloides) and white spruce (P. glauca) trees. Statistical models were done separately on the two years to evaluate the effects of slope position and year for each species separately (letters {a,b}}. Additionally a model to assess the differences between species and years on the 35 cm cap was done (letters {A,B,C}). Different letters represent a statistically significant difference ($p < 0.05$), and a + or - sign represents a marginally significant difference ($p < 0.1$). Please note that the sap flow sensors on white spruce were placed at breast height in 2014, thus encompassing only the upper crown compared to 2015 when they were placed at the base of the tree thus taking the full crown into account.

	35 cm cap			
	2014		**2015**	
	Upper slope	**Lower slope**	**Upper slope**	**Lower slope**
P. tremuloides				
Q^c [L]	746.9 (170.0) **a**	907.1 (187.4) **a**	696.7 (157.9) **a**	851.8 (174.6) **a**
T^c [L m^{-2} transpiring leaf area]	100.2 (11.5) **ab**	129.4 (13.8) **a**	78.2 (10.1) **b**	73.5 (9.8) **b**
P. glauca				
Q^c [L]	1704.3 (201.7) **b**	2398.9 (201.7) **c**	562.0 (201.7) **a**	1256.6 (201.7) **b**
T^c [L m^{-2} transpiring leaf area]	67.2 (11.5) **a**	84.5 (14.4) **a**	9.1 (1.6) **b**	11.4 (2.0) **b**
Species differences	*P. tremuloides*	*P. glauca*	*P. tremuloides*	*P. glauca*
Q^c [L]	834.2 (156.8) **B**	1954.8 (228.8) **A**	772.3 (143.8) **B**	820.3 (148.2) **B**
T^c [L m^{-2} transpiring leaf area]	109.7 (12.0) **A**	75.4 (8.2) **B**	74.2 (5.9) **B**	10.2 (1.3) **C**

*Table 2.C. 3. Estimated marginal means (standard error) for whole tree average daily sap flux Q (L d^{-1}) and transpiration flux T (L d^{-1} m^{-2} $_{transpiring\ leaf\ area}$) during the initial wet spring in 2014 and 2015 for trembling aspen (*P. tremuloides*) and white spruce (*P. glauca*) Statistical models were done on the 35 cm cap to evaluate the impact of slope position and year, and results are represented with the letters {a,b}. Another set of statistical models were done to evaluate the impact of capping thickness on the lower slope (2014) and upper slope (2015) separately, using letters from the two sets {x} and {α}. Different letters represent a statistically significant difference ($p < 0.05$), and a + sign represents a marginally significant difference ($p < 0.1$). Please note that the sap flow sensors on white spruce were placed at breast height in 2014, thus encompassing only the upper crown compared to 2015 when they were placed at the base of the tree thus taking the full crown into account.*

WET SPRING	**35 cm cap**				**Lower slope**		**Upper slope**	
	2014		**2015**					
	Lower slope	**Upper slope**	**Lower slope**	**Upper slope**	**35 cm cap**	**100 cm cap**	**35 cm cap**	**100 cm cap**
P. tremuloides								
Average *Q* [L d^{-1}]	14.8 (3.9) **a**	16.3 (4.1) **a**	1.1 (0.6) **b**	1.6 (0.7) **b**	17.2 (4.1) **x**	26.0 (3.8) **x**	2.1 (0.9) **α**	5.5 (1.7) **α**$^{+}$
Average *T* [L d^{-1} m^{-2} $_{transpiring\ leaf\ area}$]	1.8 (0.2) **a**	1.8 (0.2) **a**	0.1 (0.1) **b**	0.1 (0.1) **b**	2.0 (0.2) **x**	1.9 (0.2) **x**	0.2 (0.1) **α**	0.4 (0.1) **α**$^{+}$
P. glauca								
Average *Q* [L d^{-1}]	38.8 (4.4) **a**	29.0 (4.4) **a**	30.9 (4.4) **b**	21.1 (4.4) **b**	37.8 (5.7) **x**	34.3 (5.7) **x**	22.7 (4.4) **α**	17.7 (4.5) **α**
Average *T*	1.3 (0.1) **a**	1.3 (0.1) **a**	0.3 (0.1) **b**	0.3 (0.1) **b**	1.4 (0.2) **x**	1.3 (0.2) **x**	0.3 (0.1) **α**	0.3 (0.1) **α**

[L d^{-1} m^{-2} transpiring leaf area]

Chapter 3

Appendix 3.A: Study set-up

Table 3.A. 1. Summary of the characteristics (tree height, sensor placement (azimuth and height), diameter, sapwood depth and wood thermodiffusivity) of the focus and control trees used in the study.

Location	**Height** [m]	**DBH** [cm]	**Azimuth**	**Sensor height** [m]	**Diameter at sensor location** [cm]	**Sapwood depth** [cm]	**Wood thermo-diffusivity** [10^{-3} cm^2 s^{-1}]
Focus tree	20.4	28.8	N	2.3	25.6	6.36	2.269
			E		28.9	4.92	2.248
			S		25.6	5.68	2.271
			W		28.9	4.54	2.291
Control tree 1	~ 20.0 (not measured)	30.8	N	1.3	30.8	3.90	2.136
Control tree 2		30.8			30.8	6.04	
Control tree 3		29.9			29.9	7.13	

Figure 3.A. 1. Wooden structure supporting the focus tree after the cut. The focus tree is placed in the white bucket resting on the scale. Taken the 12th of July 2017, in Thorhild County, AB, Canada.

Figure 3.A. 2. Suite of steps taken to cut the focus tree under water and recording the gravimetric water uptake. The tree was cut under water to prevent cavitation of the xylem vessels. Pictures are from July 12th, 2017 in Thorhild County, AB, Canada.

Appendix 3.B: Summary statistics

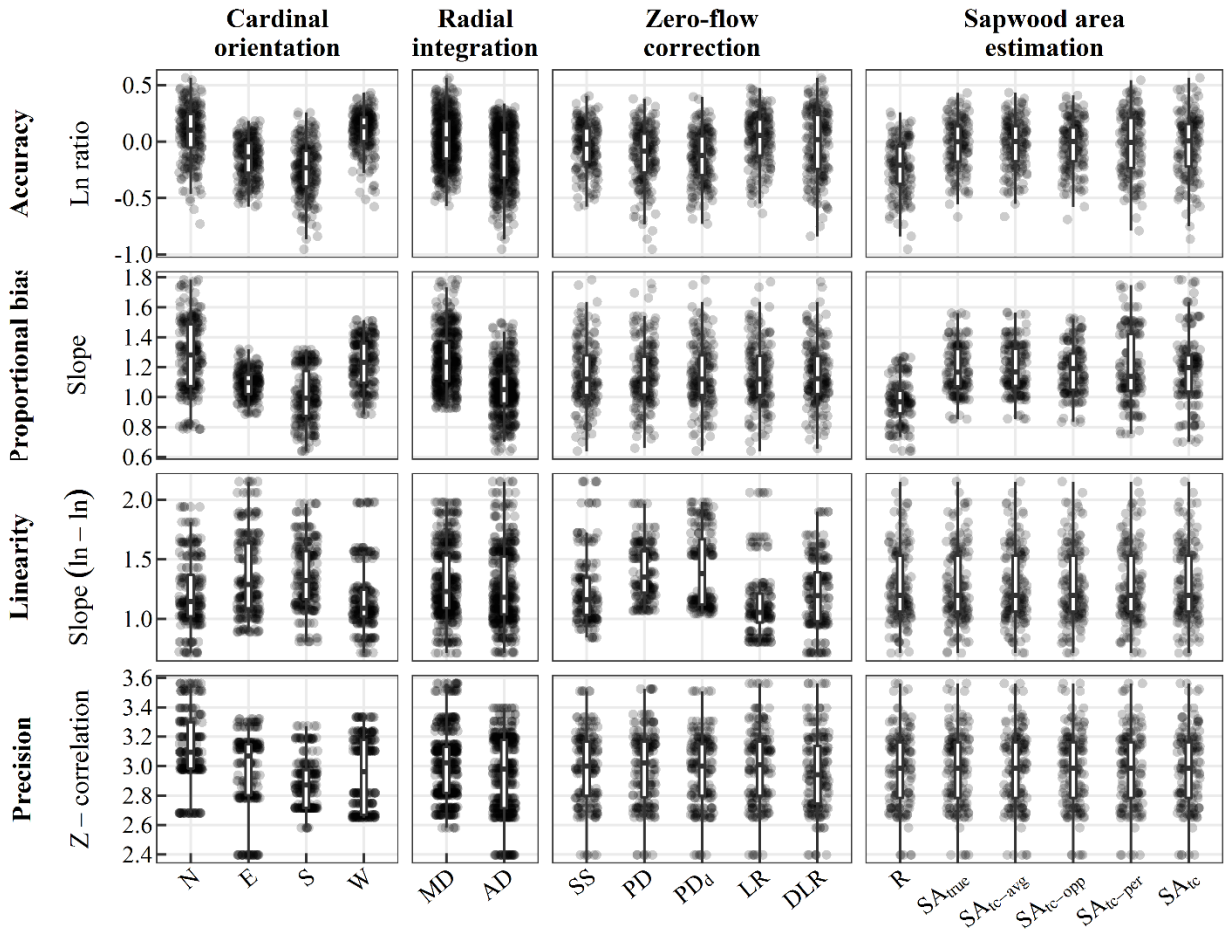

Figure 3.B. 1. Distribution of the four calibration performance metrics (accuracy - ln ratio, proportional bias - slope, linearity - slope (ln-ln) and precision - Z-correlation) across the sensor cardinal orientation and the three data-processing procedures (radial integration, zero-flow correction and sapwood area estimation methods) represented as boxplots. Dots represent the value of each individual calibration metric for each of the four days of analysis.

Table 3.B. 1. Summary statistics of the linear mixed effects models testing for differences in $J_{s,min}$ between zero-flow corrections (PD versus SS), radial integration method and testing for the relationship between the zero-flow correction and date. Normality and homoscedasticity were verified for all models. Random effects are described by the cardinal orientation of the sap flow sensors.CI: confidence interval; DF: degrees of freedom; N: sample size; r^2_m: marginal coefficient of determination; r^2_c: conditional coefficient of determination.

Method	Model	Variable	DF	N	Statistic	p-value	r^2_m	r^2_c	Thermistor	Estimate	95 % CI
PD *vs* SS	ANOVA (difference ~ Radial integration)	**Radial integration**	4	8	9.52	0.022	0.58	0.76	**MD**	0.30	[0.12; 0.48]
									AD	0.54	[0.36; 0.73]
PD_d	ANCOVA ($J_{s,min}$ ~ Date x Radial integration)	**Radial integration: Date (slope)**	273	280	2.97	0.086	0.05	0.94	**MD**	-0.037	[-0.045; -0.029]
									AD	-0.047	[-0.0549; -0.0385]
LR	ANOVA ($slope_{(Js,min\sim Date)}$~ correction + Radial integration)	**Correction**	10	16	0.052	0.82	0.02	0.46	**No differences**	-0.015	[-0.063; 0.032]
DLR										-0.018	[-0.066; 0.029]

Table 3.B. 2. Summary statistics comparing the sapwood area calculations derived from tree-cores to SA_{true}. T-tests were performed on each method individually. The normality assumption was verified. CI: confidence interval; DF: degrees of freedom; N: sample size.

Method	**Estimate**	**95 % CI**	**DF**	**N**	**Statistic**	**p-value**
SA_{tc}	1.09	[-17.0; 19.2]	15	16	0.13	0.9
$SA_{tc;opp}$	1.03	[-9.1; 11.2]	15	16	0.212	0.8
$SA_{tc;per}$	1.27	[-9.8; 12.4]	15	16	0.24	0.8
$SA_{tc;avg}$	1.24	[-5.8; 8.2]	3	4	0.57	0.6
$SA_{tc;quarter}$	1.09	[-6.5; 8.7]	3	4	0.46	0.7

Table 3.B. 3. Summary statistics of the linear models testing for the impact of the cardinal orientation and the three data-processing procedures (radial integration, zero-flow correction and sapwood area estimation) on the four calibration performance metrics described by Flo et al. (2019): accuracy (Ln ratio), proportional bias (slope), linearity (slope (ln-ln)) and precision (Z-correlation). Normality and homoscedasticity were checked, and adjustments were made accordingly (see "Model specifics"). Variance was allowed to vary along a factor level ("varIdent") and transformations ("Log(X)"; "X^2") were made on the dataset for normality. Outliers removed when necessary (the number of data points removed is indicated). CI: confidence interval; DF: degrees of freedom; N: sample size; r^2: coefficient of determination.

Metric		Variable	DF	N	Outlier removed?	Statistic χ^2	p-value	r^2	Model specifics
Accuracy	Ln ratio	General	946	960	No			0.58	$(X+1)^2$
		Orientation	3			830.5	$< 2e^{-16}$		varIdent
		Radial integration	1			185.8	$< 2e^{-16}$		
		Zero-flow	4			144.5	$< 2e^{-16}$		
		Sapwood area	5			230.2	$< 2e^{-16}$		varIdent
Proportional bias	Slope	General	944	958	Yes (n=2)			0.66	Log(X)
		Orientation	3			725.9	$< 2e^{-16}$		varIdent
		Radial integration	1			629.9	$< 2e^{-16}$		varIdent
		Zero-flow	4			0.16	0.997		
		Sapwood area	5			495.2	$< 2e^{-16}$		varIdent
Linearity	Slope (ln-ln)	General	151	160	No			0.24	Log(X)
		Orientation	3			15.9	0.001		

		Radial integration	1			0.79	0.373		
		Zero-flow	4			30.5	$3.92e^{-06}$		
		Sapwood area	5			NA	NA		
Precision	Z-correlation	General	151	160	No			0.14	X^2 varIdent
		Orientation	3			23.3	$3.55e^{-05}$		
		Radial integration	1			0.58	0.445		
		Zero-flow	4			0.89	0.926		
		Sapwood area	5			NA	NA		

Table 3.B. 4. Summary statistics of the linear models testing for the impact of the cardinal orientation and the three data-processing procedures (radial integration method, zero-flow correction and sapwood area estimation) on the four parameters of the logistic relationship between hourly sap flux rates and VPD over the 27 days before the cut (asymptote, mid-point, steepness). Normality and homoscedasticity were checked, and adjustments were made accordingly (see "Model specifics"). Variance was allowed to vary along a factor level ("varIdent") and transformations ("X^2", use of model residuals) were made on the dataset for normality. Outliers removed when necessary (the number of data points removed is indicated). DF: degrees of freedom; N: sample size; r^2: coefficient of determination.

Parameter	Variable	DF	N	Outlier removed?	Statistic χ^2	p-value	r^2_m	Model specifics
Asymptote	General	231	236	Yes (n=4)			0.48	X^2
	Orientation	3			128	$< 2e^{-16}$		varident
	Radial integration	1			76.9	$< 2e^{-16}$		varIdent
	General	222	232	Yes (n=4)			0.41	On residuals of previous model
	Zero-flow	4			1.2	0.87		
	Sapwood area	5			259.5	$< 2e^{-16}$		varIdent
Mid-point	General	31	40	No			0.89	Averaged across sapwood area methods; X^6
	Orientation	3			63.2	$1.24e^{-16}$		varIdent
	Radial integration	1			8548.8	$< 2e^{-16}$		
	Zero-flow	4			56.2	$1.85e^{-11}$		
Steep	General	31	40	No			0.99	Averaged across sapwood area methods
	Orientation	3			2689.4	$< 2e^{-16}$		varIdent

Radial integration	1	4321.2	$< 2e^{-16}$
Zero-flow	4	217.7	$< 2e^{-16}$

Table 3.B. 5. Models statistics of the linear models testing for the impact of cardinal orientation and the three data-processing procedures (radial integration method, zero-flow correction and sapwood area estimation) on the absolute difference in the estimates of cumulative water uptake over 5 days after the cut between the sap flow sensor measurements and the gravimetric scale dataset. Normality and homoscedasticity were checked, and adjustments were made accordingly (see "Model specifics"). Variance was allowed to vary along a factor level ("varIdent"). Outliers removed when necessary (the number of data points removed is indicated). DF: degrees of freedom; N: sample size; r^2: coefficient of determination.

	Variable	**DF**	**N**	**Outlier removed?**	**Statistic χ^2**	**p-value**	***r²***	**Model specifics**
$\lvert Q^c - Q^c_{scale} \rvert$	General	217	234	Yes (n=6)			0.57	
	Orientation:Radial integration	3			177.9	$< 2e^{-16}$		varIdent(form=~1|Orientation)
	Zero-flow	4			222.4	$< 2e^{-16}$		
	Sapwood area	5			47	$5.74e^{-4}$		varIdent

Appendix 3.C: Supplementary Results

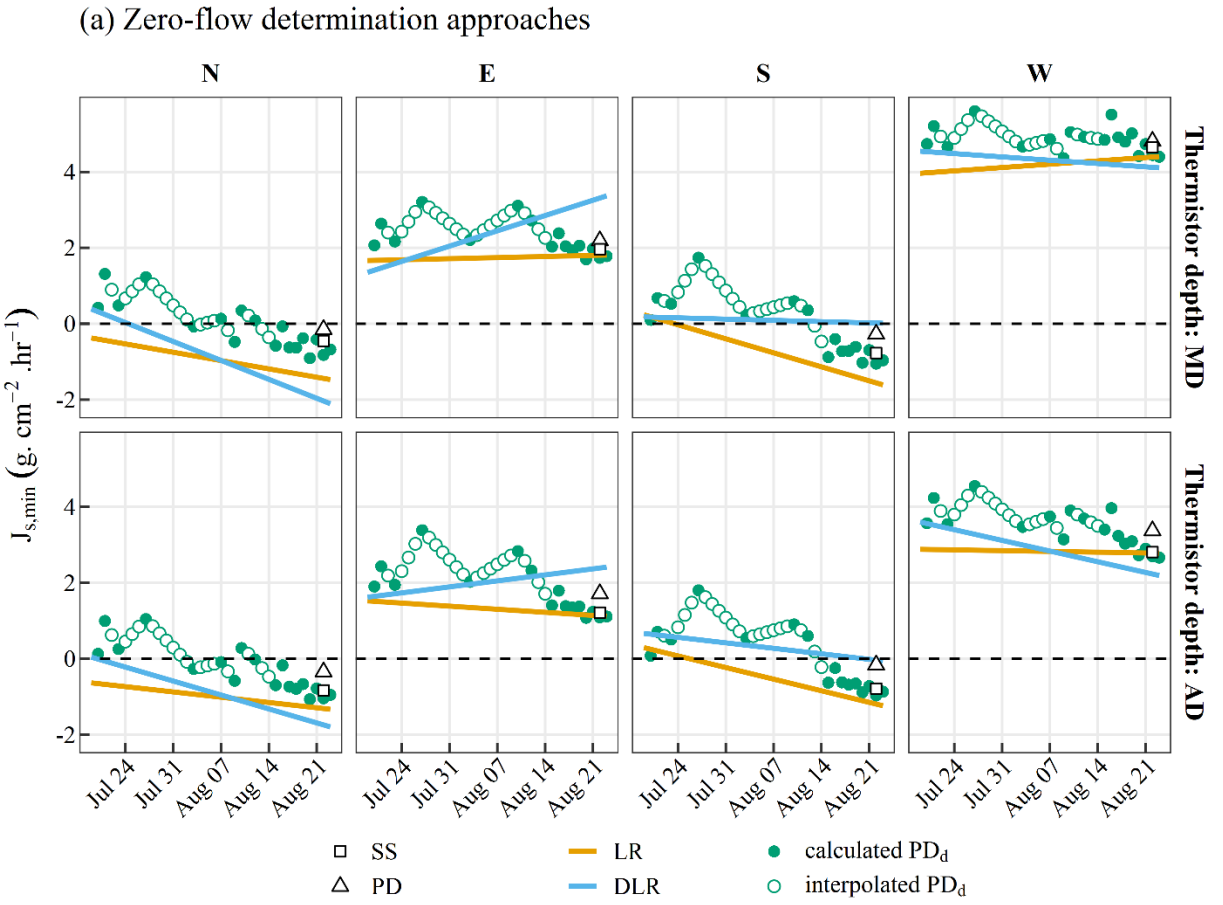

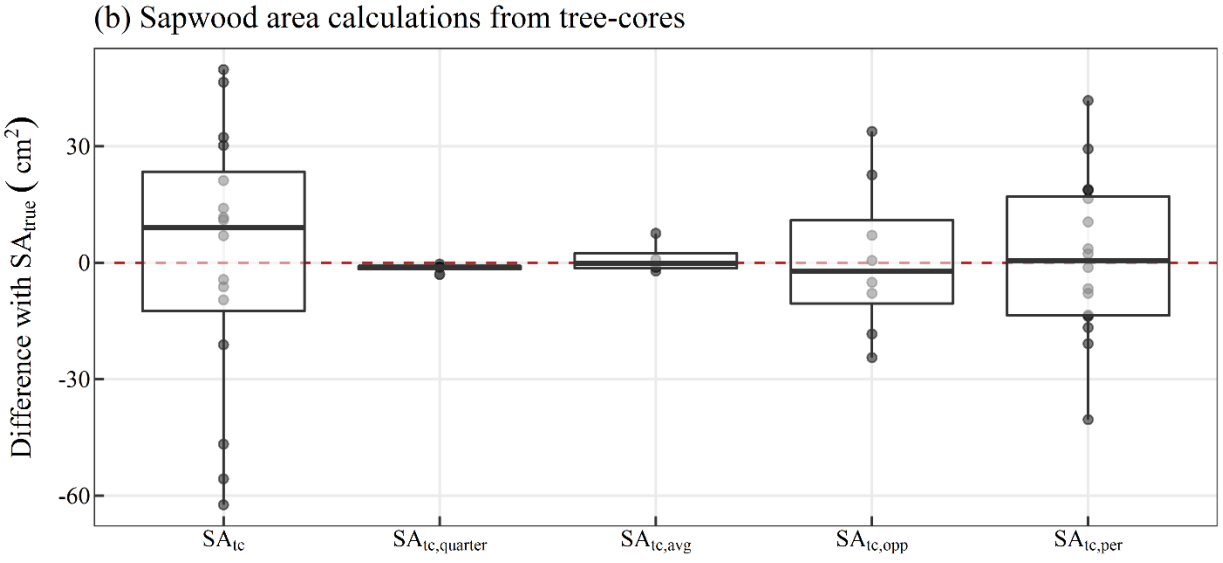

Figure 3.C. 1. Zero-flow determination approaches and sapwood area calculations. Panel a shows the daily minimum sap flux density $J_{s,min}$ (g cm^2 hr^{-1}) for the five zero-flow determination approaches for the four cardinal directions (columns) under the two radial integration method MD and AD (rows). Panel b shows the boxplot of the difference between the true sapwood area SA_{true} and the five sapwood area estimations calculated from tree cores (SA_{tc} n = 12, $SA_{tc;avg}$ n = 4, $SA_{tc;opp}$ and $SA_{tc;per}$ n = 8). Zero is marked by a dotted red line.

(a)

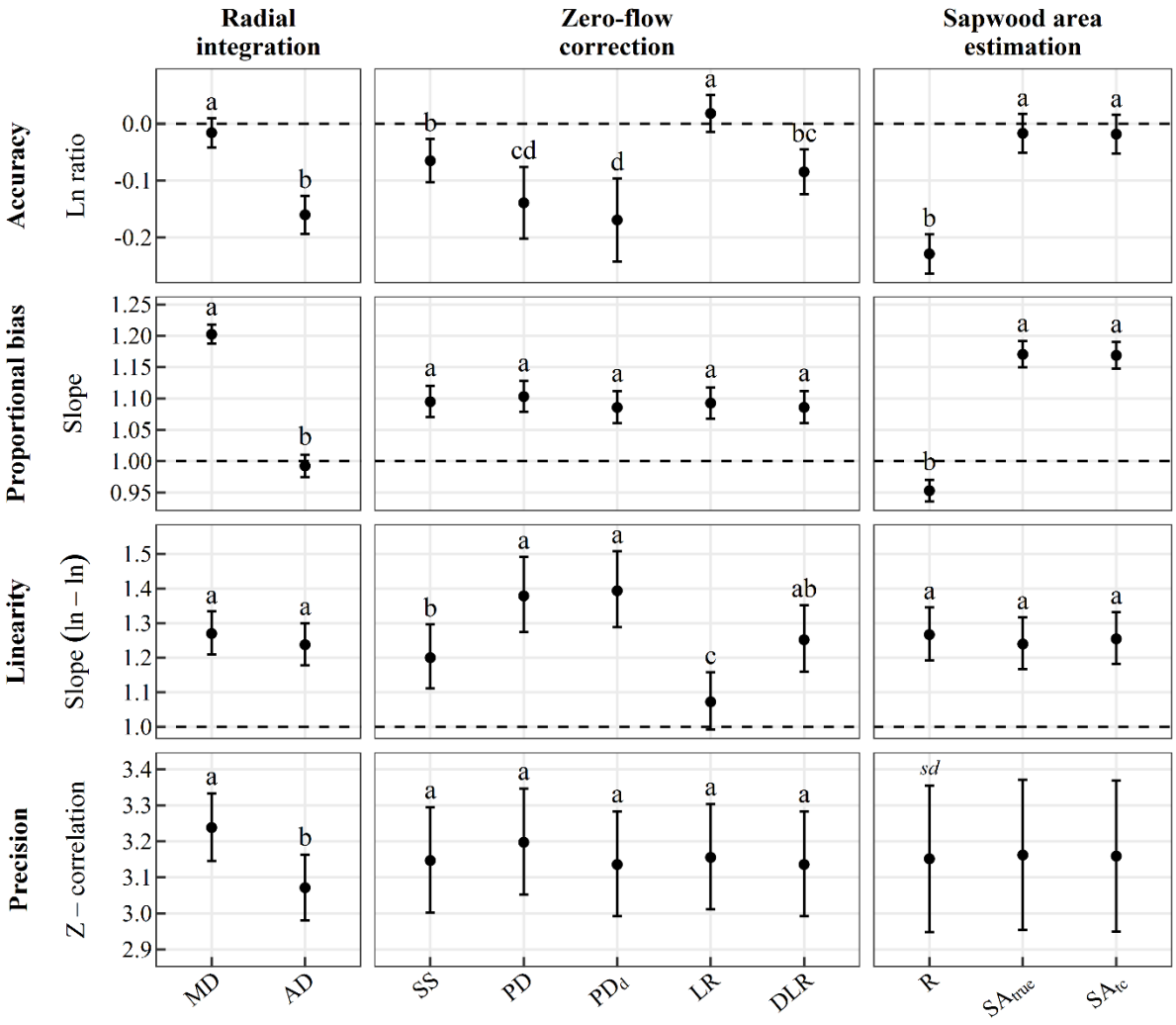
Radial integration
Zero-flow correction
Sapwood area estimation
Accuracy
Ln ratio
Proportional bias
Slope
Linearity
Slope (ln – ln)
Precision
Z – correlation
MD
AD
SS
PD
PDd
LR
DLR
R
SAtrue
SAtc

(b)

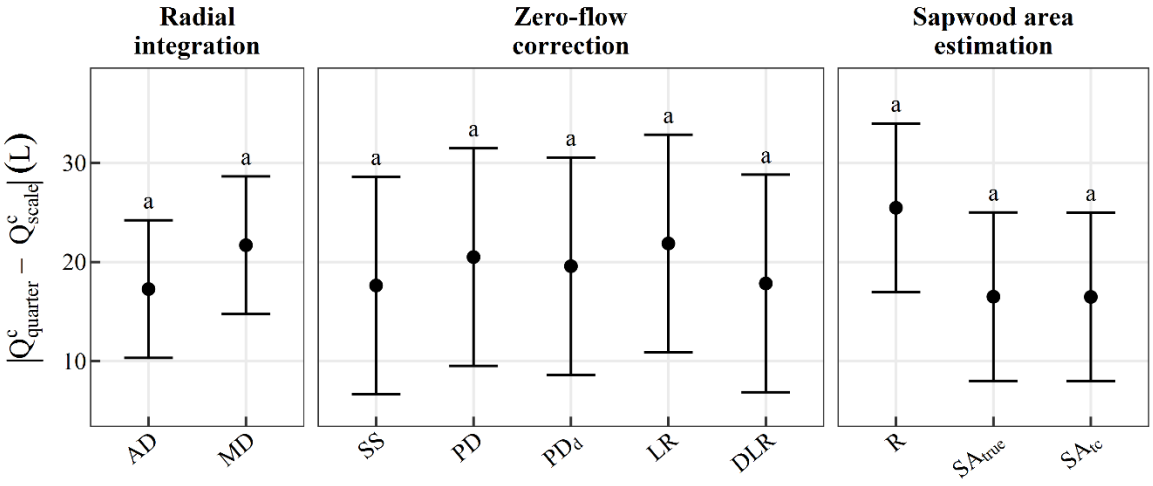
Radial integration
Zero-flow correction
Sapwood area estimation
|Qcquarter – Qcscale| (L)
AD
MD
SS
PD
PDd
LR
DLR
R
SAtrue
SAtc

Figure 3.C. 2. Performance of the integrated sap flux rates $Q_{quarter}$ in terms of the four calibration metrics (panel a; accuracy, proportional bias, linearity and precision) and absolute difference in cumulative water uptake with the gravimetric measurements (panel b) over the first five days after the cut. The effects of the three data-processing procedures are presented. Means and 95 % confidence intervals are shown, with letters to indicate statistical differences. Panel a: the calibration metrics were estimated during the daytime (07:00 h to 20:00 h) the first four days after the cut. Note that for the Z-correlation for the sapwood area estimation variable, the values were near identical across the different methods, hence the figure shows mean and standard deviation ("sd" label). Horizontal dotted lines indicate reference value, for a perfect calibration value for each metric. The intersection between the confidence interval and the reference line indicates that the metric is not significantly different from the reference.

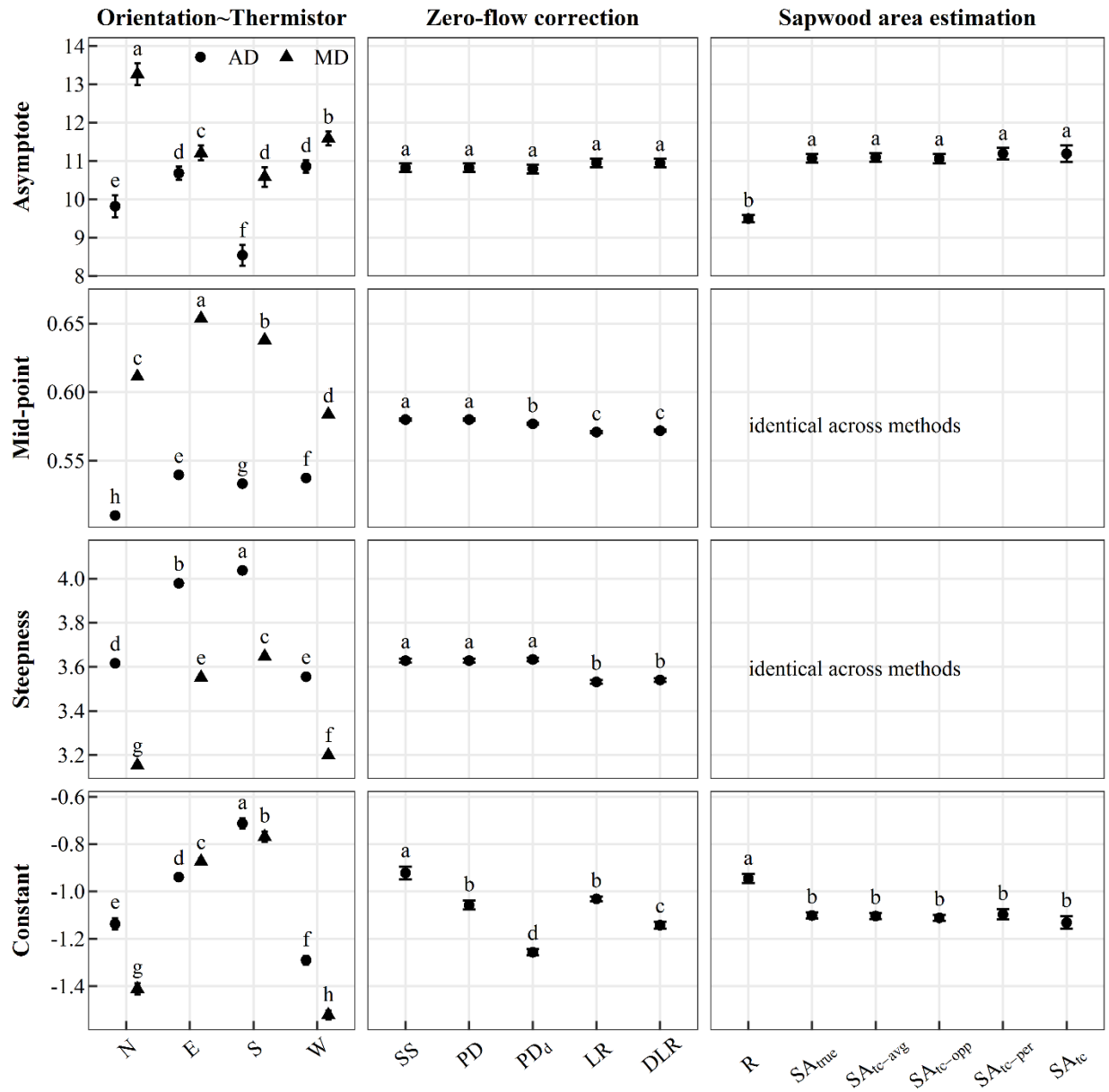

Figure 3.C. 3. Parameters of the logistic relationship between hourly sap flux rates and VPD (Asymptote, mid-point, steepness and constant; rows) for the interaction between cardinal orientation and thermistor depth usage, zero-flow corrections and sapwood area estimation (columns). Letters indicate significant differences within data correction procedures. No results are presented for the mid-point and steepness for the sapwood area estimation as the values were identical.

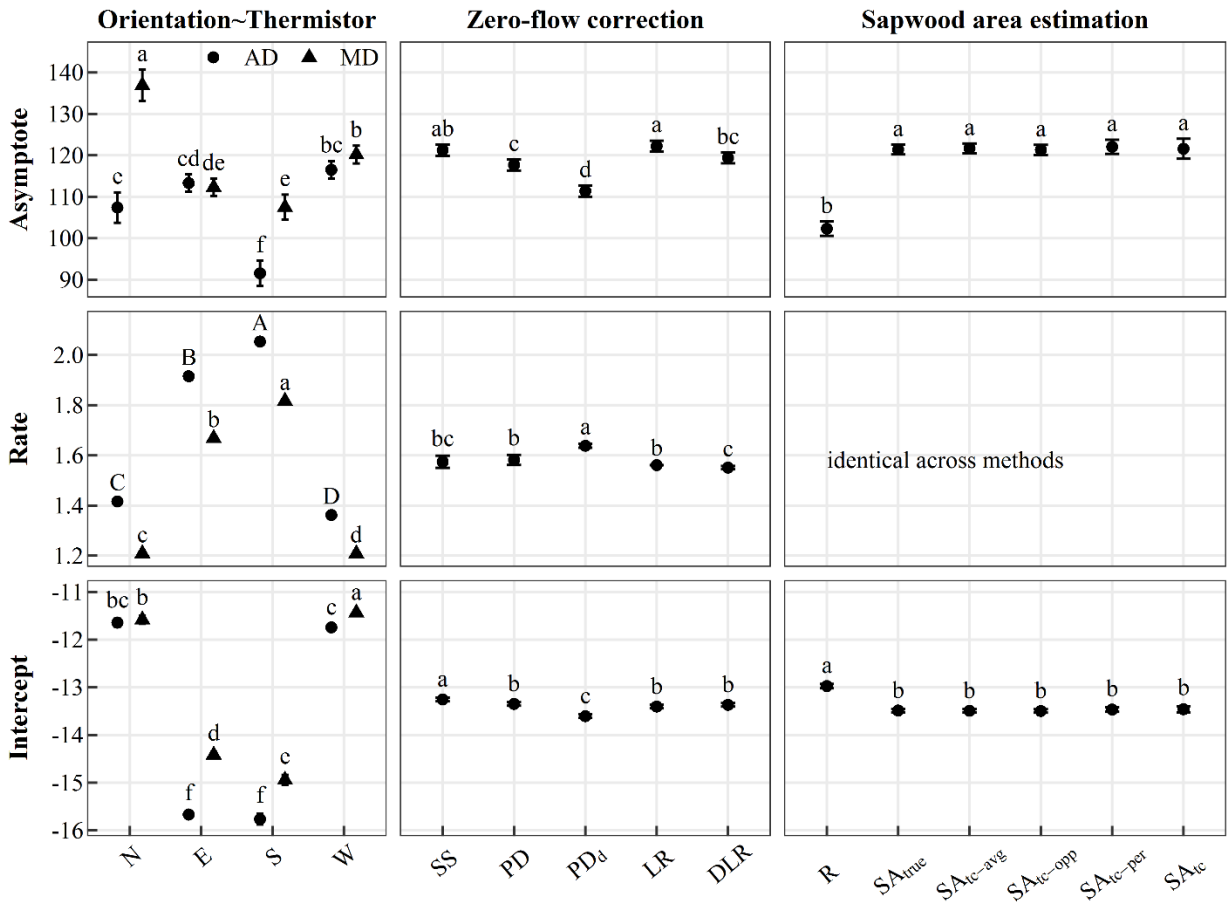

Figure 3.C. 4. Parameters of the asymptotic relationship between daily sap flux rates and VPD (Asymptote, Rate and Intercept; rows) for the interaction between cardinal orientation and thermistor depth usage, zero-flow corrections and sapwood area estimation (columns). Letters indicate significant differences within data correction procedures. Uppercase letters show that the AD thermistor depth had significantly higher parameter than MD for each cardinal orientation. No results are presented for the Log(Rate) parameter for the sapwood area estimation as the values were identical.

Chapter 4

Appendix 4.A: Methods

Table 4.A. 1. Summary of the performance metrics comparing the hourly VPD between the Abee and the focal tree crown weather stations between August 2nd, 2017 and August 22nd, 2017. Two models were run: first, a direct comparison of the two datasets was performed. The accuracy (average of the logarithm of the ratio between the two data sources), proportional bias (slope of the linear relationship between the two data sources), linearity (slope of the linear relationship between the logarithm of two data sources), precision (Z Pearson's correlation coefficient) and NRMSE (normalized root mean square error, %) were calculated. Secondly, a dynamic harmonic regression was performed with the Crown dataset as a response variable and the Abee dataset as the predictor variable, for a Fourier order of 4, with ARIMA (1,1,0). The mean error (ME), root mean squared error (RMSE), mean absolute error (MAE), mean percentage error (MPE), mean absolute percentage error (MAPE) and mean absolute scaled error (MASE) are shown.

Model			**Accuracy**	**Proportional bias**	**Linearity**	**Precision**	**NRMSE**
Direct comparison	Crown~Abee.AGDM		0.146	1 (0.0144)	0.946 (0.0317)	1.88	9.1
		ME	**RMSE**	**MAE**	**MPE**	**MAPE**	**MASE**
Dynamic harmonic regression	Arima(Crown, xreg = fourier(Abee, K = 4), Order=c(1,1,0))	0.00054	0.085	0.059	-5.688	59.619	0.189

Table 4.A. 2. Anatomical and morphological characteristics of the sap flow sensor locations on the large mature aspen tree of the study. Height (m), diameter measured in the N-S and E-W axes (cm), sapwood area measured over a quarter of the total tree disk, centered on each azimuth (cm^2), wood water content (defined as $(M_{wet} - M_{dry})/M_{dry}$), wood density (g cm^{-3}) and wood thermo-diffusivity (10^{-3} cm^2 s^{-1}) measured on fresh sapwood samples at each location and azimuth and total leaf area supported by each location (m^2). All the measurements were made at the end of the full experiment - i.e. *12 days after the tree was cut and immersed in water (see Chapter 3).*

Location	**Azimuth**	**Height** [m]	**Diameter** [cm]	**Sapwood area** [cm^2]	**Wood water content**	**Wood density** [g cm^{-3}]	**Wood thermo-diffusivity** [10^{-3} cm^2 s^{-1}]	**Supported leaf area** [m^2]
Trunk								
Low trunk	**N**	2.3	25.6	101.36	1.16	0.408	2.269	44.13
	E		28.9	88.61	1.20	0.399	2.248	
	S		25.6	76.67	1.15	0.424	2.271	
	W		28.9	81.26	1.12	0.418	2.291	
Mid-trunk	**N**	5.8	23.7	66.97	0.81	0.409	2.542	
	E		24.75	59.88	0.84	0.411	2.512	
	S		23.7	53.19	0.70	0.428	2.650	
	W		24.75	58.77	0.76	0.422	2.589	
Upper trunk	**N**	10.4	18.65	42.19	0.83	0.438	2.506	
	E		18.5	37.85	0.93	0.424	2.424	
	S		18.65	47.88	0.88	0.429	2.459	
	W		18.5	37.68	0.84	0.429	2.495	
Crown								
Branch 1		10.9	6.9	5.46	NA			3.62
Branch 2		11.5	7.5	9.74				4.96

Branch 3	12.5	6.0	9.73				3.75
Remaining upper crown	12.6		102.42	0.71	466.4	2.625	31.80

Appendix 4.B: Summary statistics

Table 4.B. 1. Summary statistics of the linear models testing for the impact of cardinal orientation and daytime (day or night) on the Dykes and Unwin's chi-square statistic for sap flux density and rate across the three focal trunk locations and the three control trees (density only), as well as the impact of the cardinal orientation on the difference in cumulative water uptake between each cardinal measurement $Q^{c}_{i;q}$ *and the theoretical* $Q^{c}_{th;q}$ *for the three focal trunk locations and the three control trees. Normality and homoscedasticity were checked, and adjustments were made accordingly (see "Model specifics"). Variance was allowed to vary along a factor level ("varIdent") and transformations ("√(X+2)") were made on the dataset to meet the normality assumption. Outliers removed when necessary. N: sample size,* R^2*: coefficient of determination.*

Variable	Trunk position	Model	N	R^2	Model specifics
χ^2_{DU} **Sap flux density**	Low trunk	~Orientation x daytime	202	0.76	varIdent(~Orientation), varIdent(~daytime)
	Mid trunk		198	0.77	varIdent(~daytime)
	Upper trunk		208	0.81	varIdent(~Orientation)
	Control 1		204	0.86	varIdent(~daytime)
	Control 2		208	0.74	√(X+2), varIdent(~daytime)
	Control 3		202	0.87	
χ^2_{DU} **Sap flux rate**	Low trunk		200	0.81	varIdent(~daytime)
	Mid trunk		206	0.76	varIdent(~Orientation), varIdent(~daytime)
	Upper trunk		208	0.87	
	Low trunk	~Orientation	104	0.70	varIdent(~Orientation)

Difference from $Q^{c}_{th;q}$	Mid trunk	104	0.72	
	Upper trunk	100	0.93	
	Control 1	104	0.77	
	Control 2	104	0.71	
	Control 3	102	0.91	varIdent(~Orientation)

Table 4.B. 2. Nonlinear regression models (Weibull growth curves and asymptotic regression) testing for differences between orientations (for trunk locations) or Location (for crown models) on the relationship between the normalized hourly sap flux rate Q_i^n *and VPD with (crown only) or without the TDW (total daily water) correction factor. The variance was allowed to change as a power function of VPD to meet the models' assumptions ("Model specifics"). Outliers removed when necessary. DF: degrees of freedom; N: sample size,* R^2*: coefficient of determination.*

Trunk position	TDW correction	Model	N	R^2	Model specifics
Low trunk	No	$gnls(Q_i^n \sim Weibull(VPD), (Asymptote + Intercept \sim Orientation))$	1344	0.88	varPower(~ VPD)
Mid trunk		$gnls(Q_i^n \sim Weibull(VPD), (Asymptote + Intercept + Rate \sim Orientation))$	1344	0.88	
Upper trunk		$gnls(Q_i^n \sim Weibull(VPD), (Asymptote + Intercept + Rate \sim Orientation))$	1344	0.88	
Crown	No	$gnls(Q_i^n \sim Asymptotic\ Regression(VPD), (Asymptote + Intercept + Rate \sim Location))$	1640	0.83	varPower(~ VPD)
	Yes	$gnls(Q_i^n \sim Weibull(VPD), (Asymptote + Intercept + Rate \sim Location))$	1680	0.86	

Table 4.B. 3. Summary statistics of the linear models testing for the influence of trunk location (low, mid trunk and crown) and VPD on the absolute value of Q^{d}_{excess} *and relative to* Q^{d}*. Normality and homoscedasticity were checked, and adjustments were made accordingly (see "Model specifics"). Variance was allowed to vary along a factor level ("varIdent"). Outliers removed when necessary. DF: degrees of freedom; N: sample size,* R^2*: coefficient of determination.*

Variable	Model	N	R^2	Model specifics
$\lvert Q^{d}_{excess} \rvert$	Location x VPD	75	0.95	varIdent(~Location)
Q^{d}_{excess} **relative to** Q^{d}		72	0.81	

Table 4.B. 4. Generalized additive models for the two refilling assumptions assessing the effects of azimuth on the quarter diurnal dynamics of $Q_{storage\sim q}$ and the effects of the trunk sections (low-to-upper, low-to-mid and mid-to-upper) on the whole tree storage diurnal dynamics $Q_{storage}$. The coefficient of determination of each model (R^2) and the percentage of deviance explained are shown.

Data	Variable	Model	R^2	Deviance explained
Overnight refilling				
Low-to-upper trunk section	**Orientation**	$gam(Q_{storage\sim q} \sim Orientation + s(Time, by = Orientation, k = 12))$	0.779	78.3 %
Whole-tree	**Trunk section**	$gam(Q_{storage} \sim s(Time, by = Trunk\ section, k = 12))$	0.659	66.6 %
Long-lasting stem water deficit				
Low-to-upper trunk section	**Orientation**	$gam(Q_{storage\sim q} \sim Orientation + s(Time, by = Orientation, k = 12))$	0.704	71 %
Whole-tree	**Trunk section**	$gam(Q_{storage} \sim s(Time, by = Trunk\ section, k = 12))$	0.49	50 %

Table 4.B. 5. Details of the linear and beta regression models testing for the influence of the cardinal orientation and storage type (recharge or withdrawal) on the volume of daily storage use or percentage of daily storage use relative to total daily sap flow per cardinal direction or on the whole-tree scale under the two refilling assumptions: overnight refilling or longer-lasting stem water deficit. Normality and homoscedasticity were checked, and adjustments were made accordingly (see "Model specifics"). Variance was allowed to vary along a factor level ("varIdent") and transformations ("√X") were made on the dataset to meet the normality assumption. Outliers removed when necessary. N: sample size, R^2: coefficient of determination.

Assumption	Trunk	Variable	Model	N	R^2	Model specifics
Overnight refilling	Per cardinal direction	Percentage	~ Orientation x Type	172	0.86	√X, varIdent(~Orientation)
		Volume		170	0.94	varIdent(~Orientation), varIdent(~Type)
	Whole tree	Percentage	~1	44		Beta regression
		Volume		44		
Longer-lasting stem water deficit	Per cardinal direction	Percentage	~ Orientation x Type	173	0.73	Beta regression
		Volume		174	0.77	√X, varIdent(~Type)
	Whole tree	Percentage	~ Type	44	0.01	Beta regression
		Volume		44	< 0.01	varIdent(~Type)

Table 4.B. 6. Details of the linear models testing for the influence of the trunk section ("Height") and storage use type (recharge or withdrawal) on the relationship between the whole tree daily storage use and daily vapor pressure deficit (VPD, kPa). Normality and homoscedasticity were checked, and adjustments were made accordingly (see "Model specifics"). Variance was allowed to vary along a factor level ("varIdent") and transformations ("|X|") were made on the dataset to meet the normality assumption. Outliers removed when necessary. N: sample size, R^2: coefficient of determination.

Assumption	Variable	Type	Model	N	R^2	Model specifics
Overnight refilling	Percentage	Both	~ Height x VPD	66	0.89	
	Volume			66	0.91	
Longer-lasting stem water deficit	Percentage	Recharge	~ Height x VPD	66	0.35	
		Withdrawal	$\sim Exponential\ regression(VPD), (Intercept + Rate \sim Height)$	66	0.75	|X|, varPower(~VPD)
	Volume	Both	~ Height x Type x VPD	132	0.45	|X|, varIdent(~Height), varIdent(~Type)
Difference between the two assumptions	Q^d		~ Height x VPD	44	0.51	~ Height+VPD

Appendix 4.C: Supplementary Results

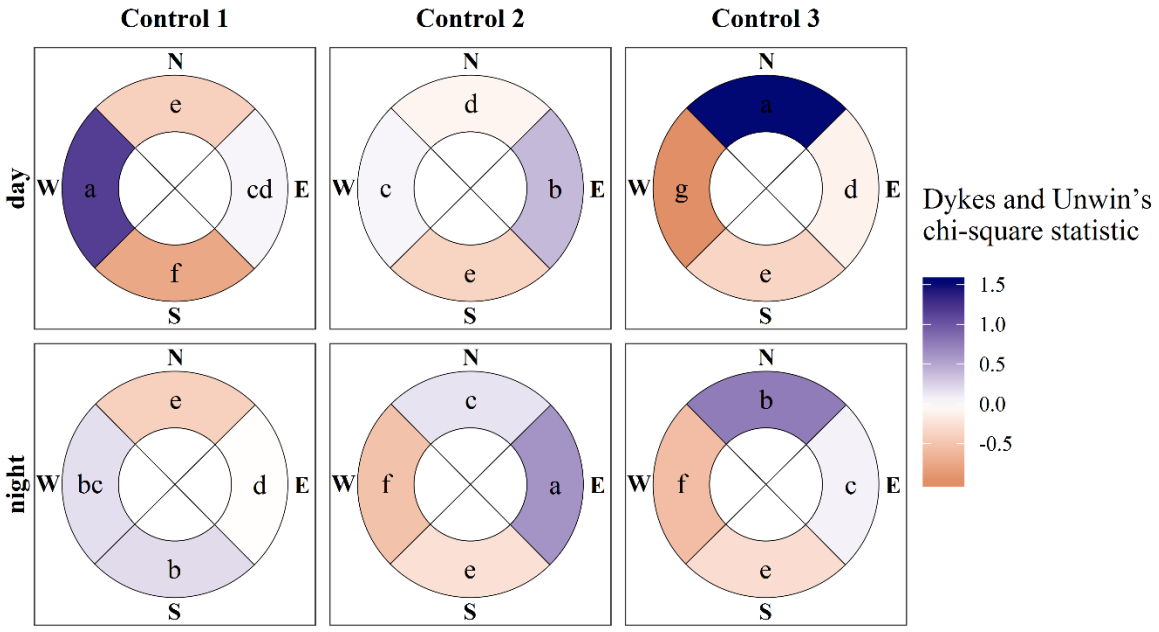

Figure 4.B. 1. Differences across azimuths between measured and theoretical sap flux density using the χ^2_{DU} statistic for the three control trees independently during the day (11:00-18:00) and night (22:00-05:00). The colored gradient varies from deep blue (positive values) to deep red (negative values). Letters indicate statistical significance ($p < 0.05$) for each control tree separately, between azimuths and daytime.

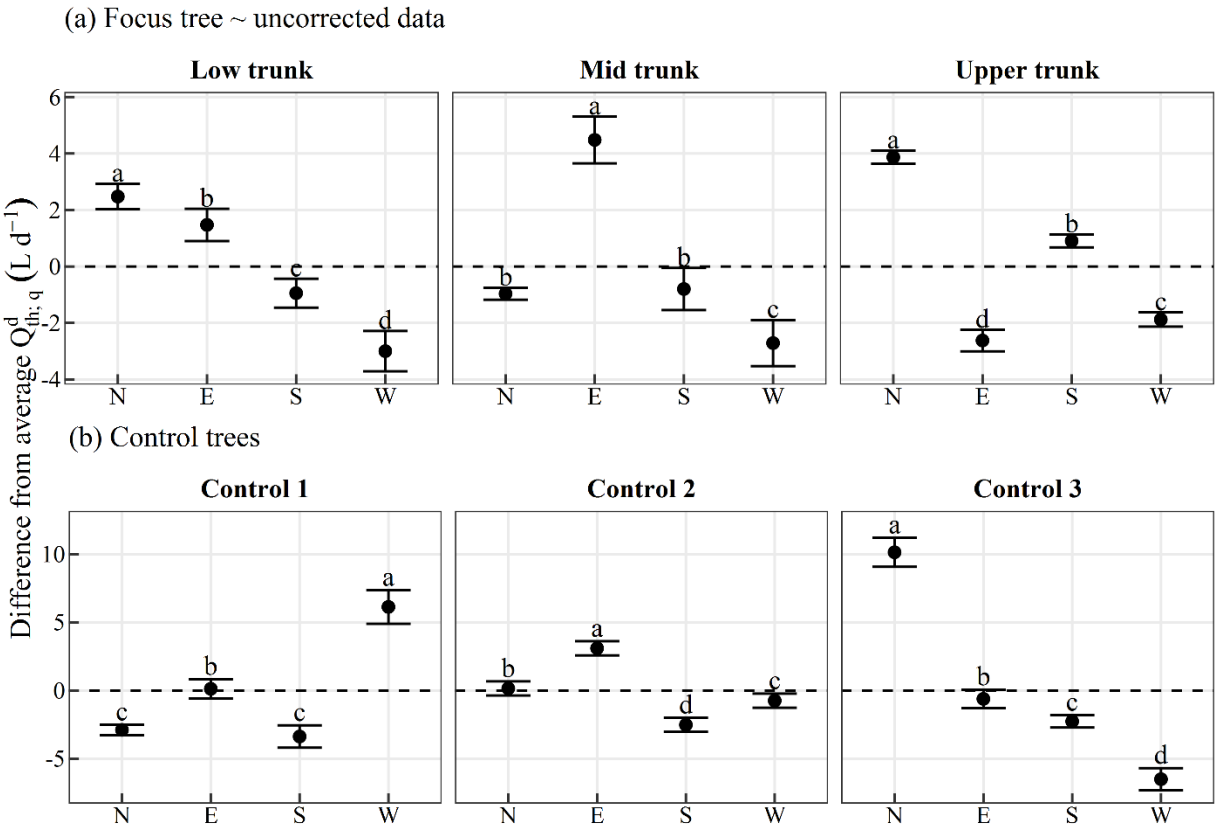

Figure 4.B. 2. Estimated marginal mean and 95 % confidence interval of the daily difference between the azimuthal sap flux and the theoretical average $Q^d_{th;q}$ (L d^{-1}) for the three trunk locations on focal tree (panel a) and the three control trees (panel b). Letters indicate statistical difference (for α=0.05) among azimuths for each of the trunk locations/control trees separately. The data was uncorrected for the TDW correction factor.

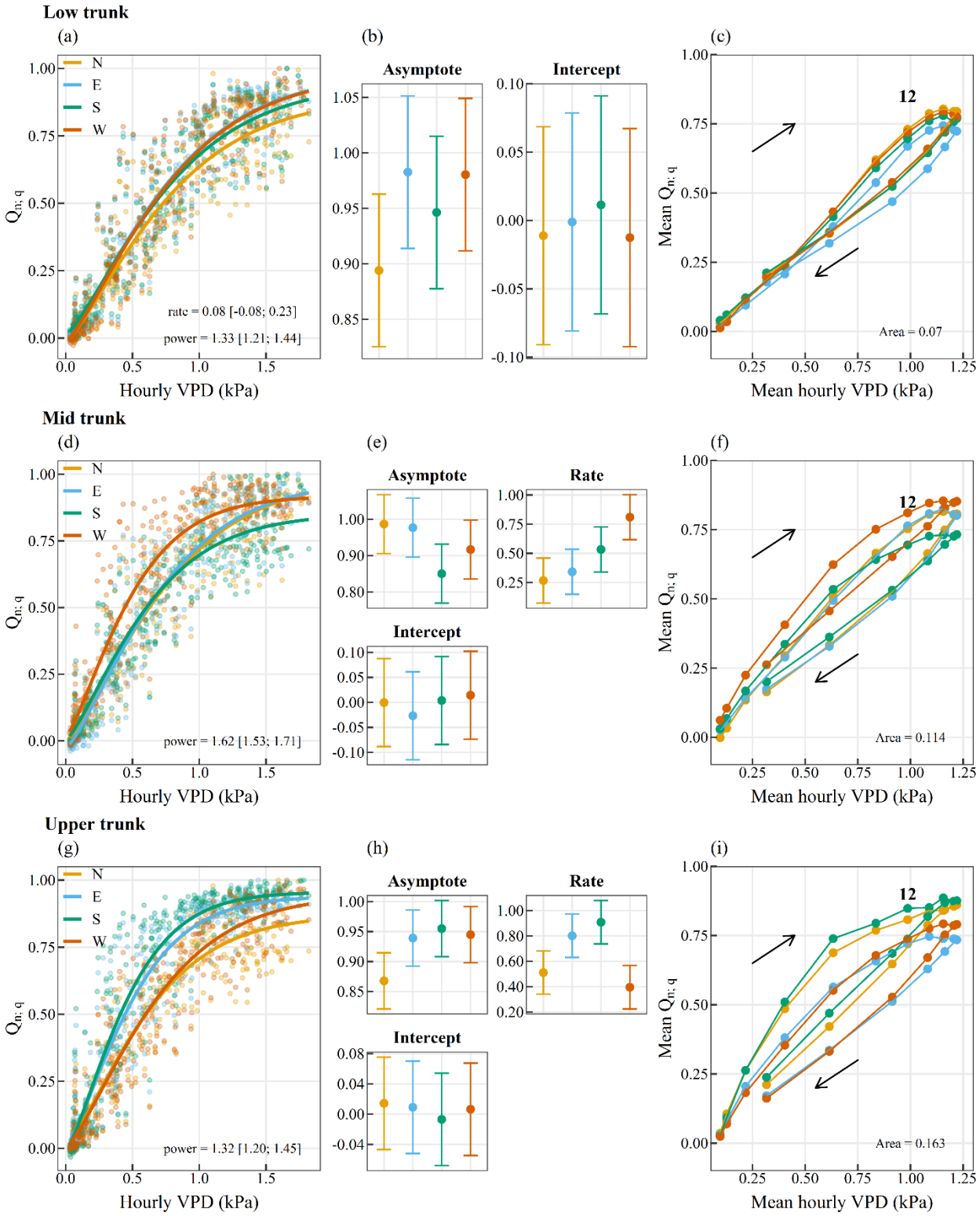

Figure 4.B. 3. Observed and modeled relationship between normalized hourly sap flux $Q_{n;\,q}$ *and atmospheric VPD (kPa) during the day for the four azimuths for the three trunk positions (low*

trunk panels a-c, mid trunk panels d-f, upper trunk panels g-i). A Weibull growth curve model was applied to model the relationship between normalized sap flux and VPD. The estimated and 95 % confidence interval for the main Weibull parameters are shown in panels b, e and h. As the power parameter of the Weibull growth curve model did not differ among azimuths for any of the trunk locations, it is simply presented as an annotation in the panels a, d and g. Similarly, the rate parameter is presented as an annotation for the low trunk position in panel a. The hysteresis between mean hourly sap flux $Q_{n;\,q}$ *and VPD is presented in panels c, f and i. Arrows indicate the direction of the hourly sap flux during the day, with noon labelled as "12".*

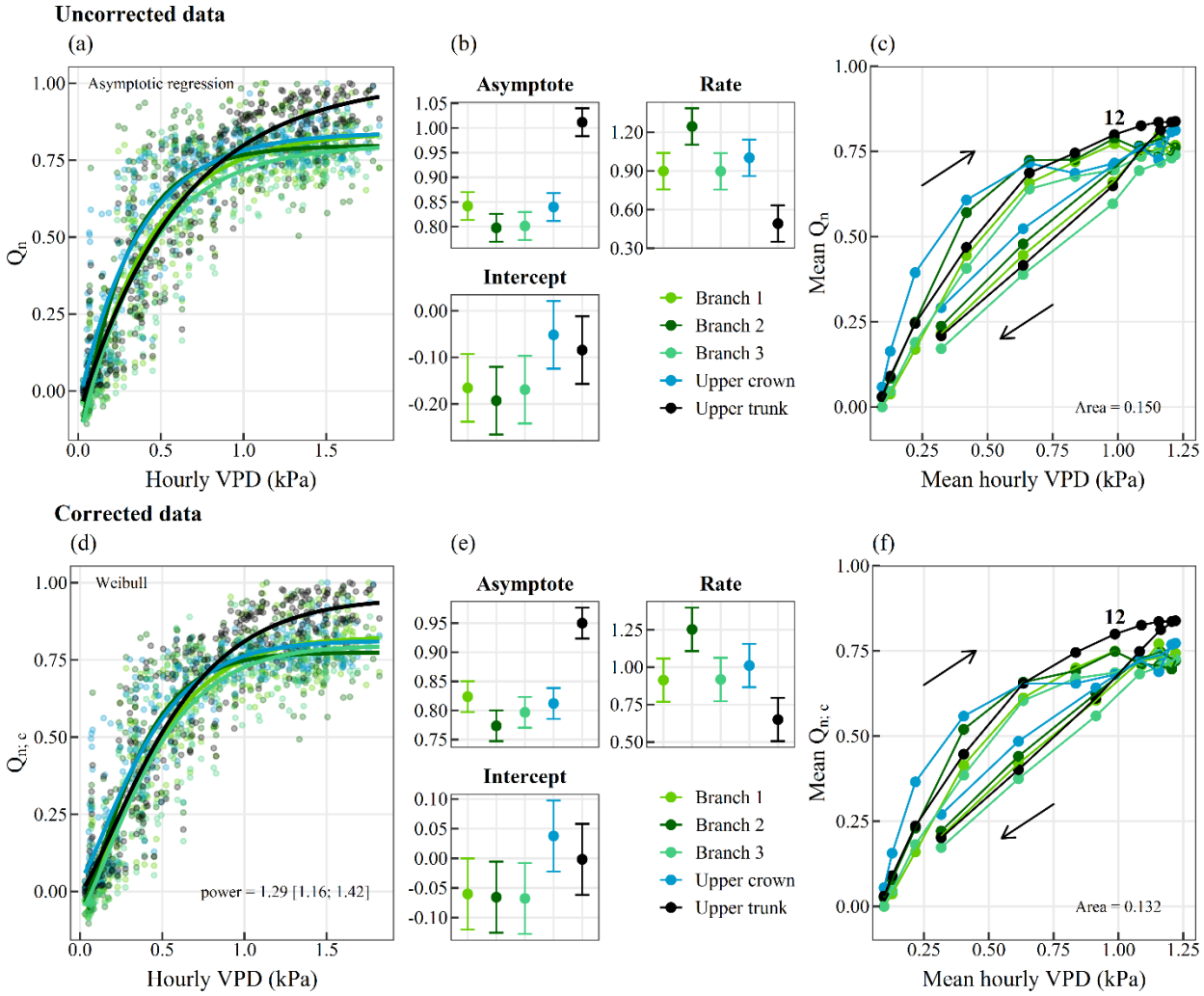

Figure 4.B. 4. Observed and modeled relationship between normalized hourly sap flux Q_n *and atmospheric VPD (kPa) during the day for the uncorrected (panels a-c) and corrected (panels d-f) datasets for the three lowest branches, the upper crown and the upper trunk. The estimated and 95 % confidence interval for the model parameters are shown in panels b and e for the four crown locations. As the power parameter of the Weibull growth curve model did not differ between crown locations, it is simply presented as an annotation in the panels d. The hysteresis between mean normalized hourly sap flux* Q_n *and VPD is presented in panels c and f. Arrows indicate the direction of the hourly sap flux during the day, with noon labelled as "12".*

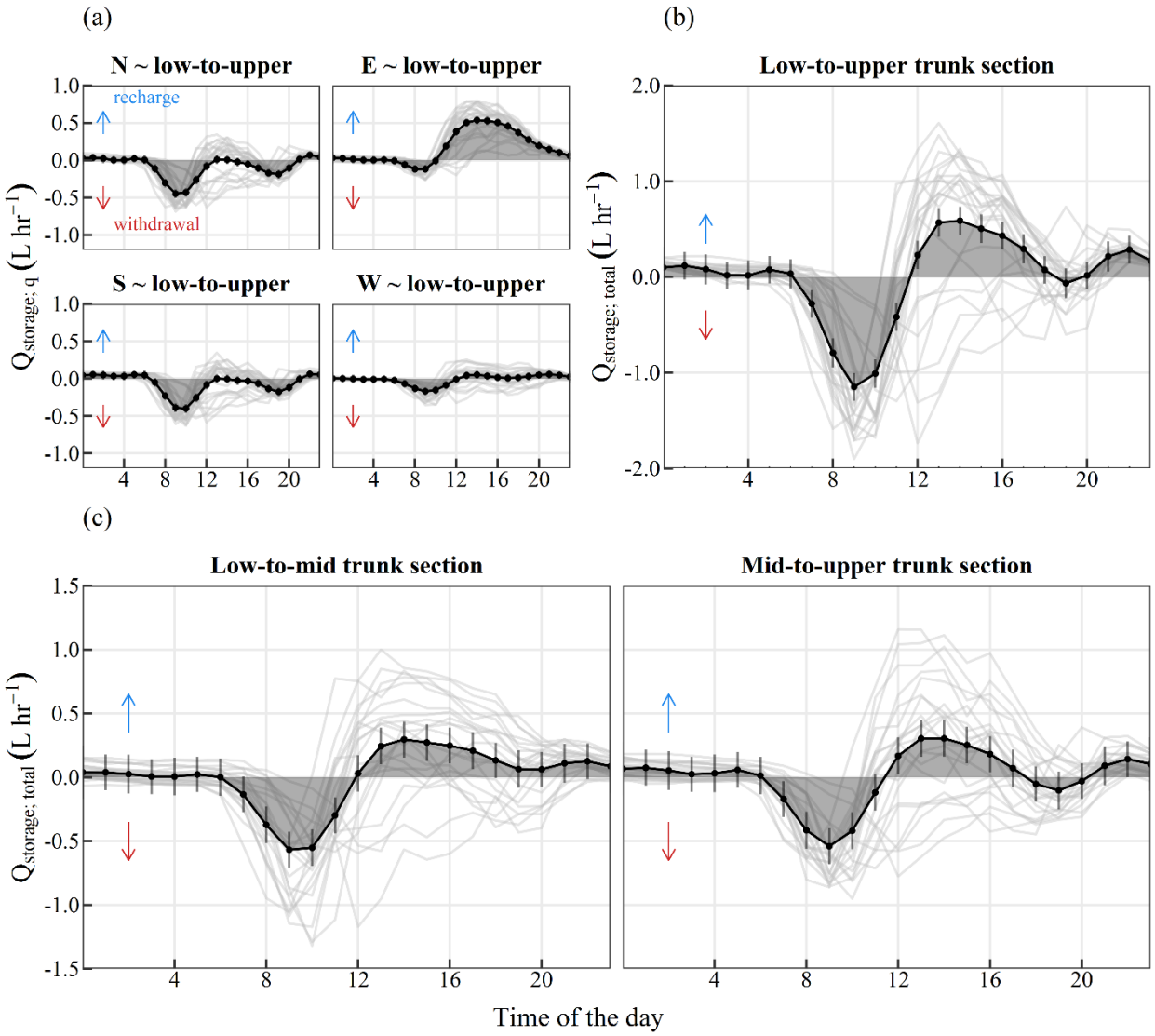

Figure 4.B. 5. Diurnal recharge and withdrawal $Q_{storage}$ *(L hr^{-1}) from the stem reservoir under the longer-lasting stem water deficit scenario (see methods for more detail) between azimuths across the entire trunk height (*$Q_{storage;\ q}$*, low-to-upper trunk section, panel a) or between trunk sections across the entire sapwood area (*$Q_{storage;\ total}$*, panels b and c). For all panels, the results from the generalized additive models fit to assess differences between azimuths (panel a) or trunk sections (panels b and c) are shown as a solid black line, and with pointwise 95% confidence intervals (error bars). The time course of stem reservoir usage for each of the 24 days of the experiment are*

shown in faded grey lines for each of the plots. Negative values indicated water withdrawal between the two trunk height locations, and positive values indicate refilling.

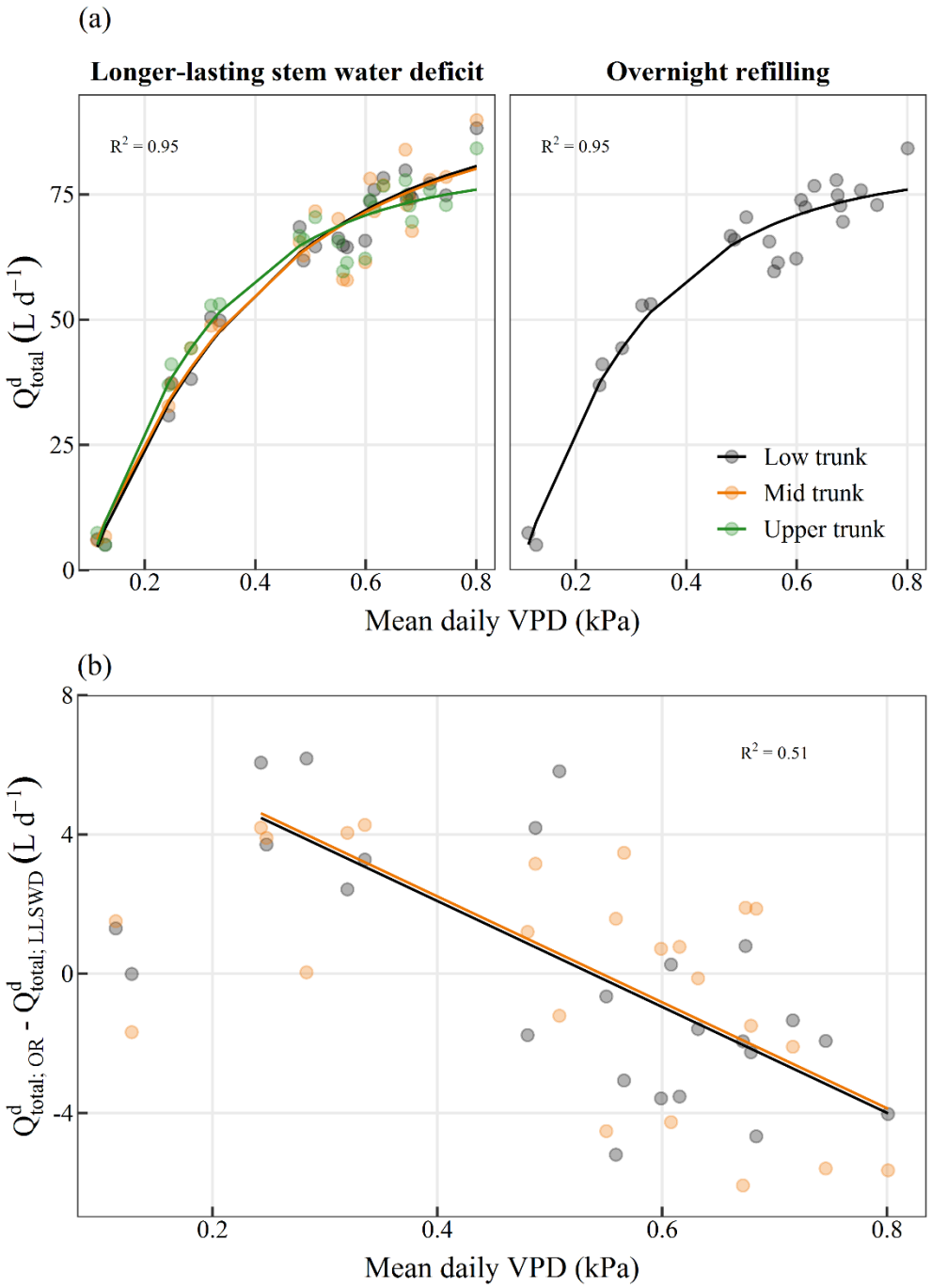

Figure 4.B. 6. Total daily flows (Q^d_{total}, L d^{-1}) under both refilling scenarios for the three trunk locations (per definition, all daily flows area equal across the trunk under the overnight refilling assumption) in relation with mean daily VPD (kPa). Panel a shows the asymptotic relationships between the two variable are shown, and their coefficient of determination (R^2). Panel b shows the

daily difference in total daily flows between the overnight refilling $Q^d_{total;OR}$ and the longer-lasting stem water deficit $Q^d_{total;LLSWD}$ scenarios for the low and mid-trunk positions in relation with mean daily VPD (kPa). The linear relationship between the two variables is shown and its coefficient of determination displayed (R^2).